Shigella triggers distinct IAM subpopulations during epithelial cell invasion to promote efficient niche establishment

Lisa Sanchez

Thèse de doctorat

Université Paris Cité

École doctorale BioSPC ED 562

Unité « Dynamique des Interactions Hôte-Pathogène », Institut Pasteur

Shigella triggers distinct IAM subpopulations during epithelial cell invasion to promote efficient niche establishment

Par Lisa SANCHEZ

Thèse de doctorat d'Infectiologie

Dirigée par Jost ENNINGA

Présentée et soutenue publiquement le 14 Novembre 2022

Rapporteurs:	Marion, Sabrina – MCU-HDR – Université de Lille
	Hilbi, Hubert – Professor - University of Zurich
Examinateurs:	King, Jason – DR - University of Sheffield
	Sauvonnet, Nathalie – DR – Université Paris-Saclay
Directeur de thèse :	Enninga, Jost – DR – Université Paris Cité

This manuscript is dedicated to me,
because in the words of a friend:
"The PhD is something that is YOUR accomplishment"
- Magdalena Gil Tarán

However, exceptionally,
I am also dedicating this work to
the overlords of my doctoral school,
because they forced me to write this.

(I am however quite proud to have written it.)

Titre : *Shigella* engendre des sous-populations distinctes d'MAIs pendant l'invasion des cellules épithéliales pour favoriser l'établissement de sa niche

Abstract (french version)

Shigella flexneri, agent responsable de la dysenterie bacillaire, est une bactérie pathogène entéro-invasive ciblant les cellules épithéliales non phagocytaires. Par l'intermédiaire d'un appareil ressemblant à une seringue, il injecte des protéines effectrices dans la cellule hôte, déclenchant des réarrangements de l'actine qui conduisant à : (i) son internalization dans une vacuole étanche appelée vacuole contenant la bactérie (VCB), et simultanément (ii) la formation de vésicules de différents diamètres entourant la BCV, appelées macropinosomes associés à l'infection (MAIs). Ensuite, *Shigella* rompt la VCB et accède au cytosol de l'hôte en se débarrassant des restes de la membrane de la VCB. Des interactions MAI-VCB se produisent avant la rupture du BCV et ont été impliquées dans cette étape ainsi que dans le décollement des restes de la VCB. Au niveau moléculaire, nous avons découvert que l'évasion bactérienne de la VCB était favorisée par des facteurs de l'hôte recrutés par les MAIs, tels que RAB11A, RAB8A et le complexe Exocyste. Malgré la découverte d'un rôle clé des MAIs dans l'infection par *Shigella*, peu est connu jusqu'à présent à leur sujet. Sur la base des résultats d'une analyse protéomique des MAIs et d'un crible fonctionnel de la rupture de la VCB, nous avons étudié de manière systématique dans le contexte de l'infection par *Shigella* l'implication d'une famille de protéines de l'hôte induisant et détectant les courbures membranaires. Les protéines de cette famille contiennent un domaine BAR, domaine de liaison à la membrane, qui a été impliqué dans la régulation des courbure membranaires. Nous avons commencé par un criblage à haut contenu à surveiller le recrutement des protéines à domaine BAR dans l'invasion par *Shigella*. Parmi les résultats les plus probants, la protéine de recyclage endosomal Sorting Nexin-8 (SNX8) est présente au niveau des MAIs où nous avons observé qu'elle induit du recyclage membranaire. La caractérisation de cette protéine par rapport aux facteurs de rupture de la VCB tels que RAB11A a révélé la présence de populations distinctes d'MAIs entourant la VCB avant sa rupture. Nous avons pu discerner une population MAI qui étnt SNX8-positive et l'autre passant de SNX8 à RAB11A. Sur la base d'analyses fonctionnelles supplémentaires, nous proposons un rôle de SNX8 comme "gardien" de l'échappement de la BCV. Ainsi, ce travail met en lumière les fonctions des MAIs dans l'échappement de la VCB de la bactérie pathogène intracellulaire *Shigella*.

Mots clés: *Shigella*, cellule hôte, macropinosomes associés à l'infection, invasion bactérienne, protéines de trafic de l'hôte, bactéries intracellulaires.

Title : *Shigella* triggers distinct IAM subpopulations during epithelial cell invasion to promote efficient niche establishment

Abstract

Shigella flexneri, the causative agent of bacillary dysentery, is an entero-invasive bacterial pathogen targeting non-phagocytic epithelial cells. Through a syringe-like apparatus, it injects effector proteins into the host cell, triggering actin rearrangements leading to: (i) its uptake within a tight vacuole called the bacterial-containing vacuole (BCV), and simultaneously (ii) the formation of vesicles with different diameters surrounding the BCV, termed infection-associated macropinosomes (IAMs). Afterwards, *Shigella* ruptures the BCV, and escapes into the host cytosol by shedding off the BCV membrane remnants. IAM-BCV interactions occur prior to BCV rupture and have been implicated in the step of BCV rupture as well as BCV remnant peeling. At the mollecular level, bacterial escape from the BCV was found to be promoted by host factors recruited to IAMs such as RAB11A, RAB8A and the Exocyst complex. Despite the discovery of a key role of IAMs in *Shigella* infection, little is known about them so far.

Based on the results of an IAM-proteomic analysis and BCV rupture functional screen, we investigated systematically the implication of a family of host proteins driving and sensing membrane curvature in the context of *Shigella* infection. Proteins within this family contain a BAR domain, a membrane binding domain which has been involved in regulating membrane curvature. We started with a high-content screen to monitor the recruitment of BAR domain proteins to the *Shigella* entry site. Among the strongest screen hits was the endosomal recycling protein Sorting Nexin-8 (SNX8) present at IAMs where we observed it induces membrane recycling. The characterization of this protein vis-à-vis BCV rupture factors such as RAB11A revealed the presence of distinct IAM populations surrounding the BCV prior to its rupture. We were able to discern one IAM population that was SNX8-positive and the other one transitioning from SNX8 to RAB11A. Based on additional functional analyses we propose a role of SNX8 as “gatekeeper” of BCV escape. Thus, this work sheds light on the functions of IAMs in BCV-escape of intracellular bacterial pathogen *Shigella*.

Key words: *Shigella*, host-cell, infection-associated macropinosomes, bacterial invasion, trafficking proteins, intracellular lifestyle.

Acknowledgements

During my PhD, I have always been told the path to the PhD defense is like a marathon. As I reach the end of this manuscript, I realize how very true this is. But reaching the end of this journey, I am very much aware that just like running a marathon, I couldn't make it without the support of my environment and several people inc particular and what I learned from them in the fields of science and life.

First, I would like to thank my PhD supervisor, Jost Enninga, who I was fortunate enough to work with since my Master 2 internship. Throughout these years, I've learned much from his approaches and views science (an angle quite different to mine when I first started) but I'm also thankful for all I've learned from you about life (e.g. to take advantage of my holidays, getting inspired from his "laisser faire" attitude and many other things). Moreover, I am thankful for his feedback on this thesis manuscript.

I would also like to thank my Master 2 internship supervisor and previous member of the Enninga lab, Candice (Yuen-Yan Chang), for her support throughout these four years and for her friendship which has meant very much to me. I am also very thankful for all she has taught me in the time she spent in our lab (I realize that not everyone is as lucky as me).

I'm also thankful for Camila Valenzuela-Montengro's mentorship and help throughout this last year of my PhD. I would particular like to express gratitude to her for reading my PhD thesis manuscript and SNX8 paper at least 100 times. Also, thanks for helping me with the cloning of my plasmids and, since I think that you inspired my curiosity for it, thank you for introducing me to the Star Wars saga.

I would also like to thank a few other current and former members of the DIHP lab. Among which, Laura Barrio-Cano, for always given excellent advice based on her objective view of the world (which was of tremendous help during conflicts) and her irreproachable scientific criticism over a beer. Magdalena Gil Tarán, for reading this thesis manuscript in its stages of preparation and for having to endure my horrible writing. I've also greatly appreciated her advice during these years of my PhD regarding life and science. Léa Swistak for being my PhD companion, her contagious optimism and company has been wonderful during the PhD marathon. Sonja Kühn for her constructive feedback during my PhD as well as her company. Jackson Luk, my "PhD desk buddy", for the interesting conversations about science and life (and the inside jokes too). Michael G. Connor for his advice and help in the science (and teaching me that I do not suck at doing PCR, since he also initially failed at cloning the pSBbi-SNX8-EGFP -just as I had). Carys Croft and

Tiziano Vignolini for their support and understanding of the challenges of the PhD writing marathon and my frustrations.

Thank you as well to all the former and current members of the DIHP lab for their company: Arthur Bienvenu, Arthur Lensen, Camille Keck, Camille Rey, Simon Blachier, Geneviève Janvier (for all the fun office gossip XD), John Berqvist, Kimi Azad, Kateryna Dotsenko, Laurent Audry (for all the office fun and always helping out when I asked for it), Margaux Bilay, Noelia López-Montero, Nora Mellouk, Patricia Latour-Lambert and Virginie Stévenin.

I would like to also thank Emmanuel Lemichez and Emmanuelle Bouveret, for their scientific input on this project and for following the progress of my thesis.

Lastly, I would also like to thank Aleix Bocquet-Pujadas (for his maths advices), Laure Blanchet, Maimouna Djamila N'Gadjaga, Maxime Mistretta, Matthew Eldridge, Samantha Smith, Simone Tazoll and Tiphaine Camarasa, and all the Young Researchers in Life Science 2021 and 2022 conferences organizers for all the fun time we spent together in Paris ☺.

And also a big thank you to my friend, Leila Dos Santos, although we don’t see each other very much, I am always very grateful for your encouragement and friendship.

Table of contents

Table of figures

Table of Tables

Abbreviations

BAR: Bin/Amphyphisin/Rvs

BCV: bacteria-containing vacuole

CCV: *Coxiella*-containg vacuole

CDC: Centers for Disease Control and Prevention

ER: endoplasmic reticulum

ERC: endosomal recycling compartment

GAP: GTPase activating protein

GDI: guanidine nucleotide dissociating inhibitor

GEF: guanidine nucleotide exchange factor

IAMs: infection-associated macropinosomes

LCV: *Legionella*-containing vacuole

M cells: microfold cells

MOI: multiplicity of infection

PAI: pathogenicity island

PI: phosphatidylinositol

PIPs: phosphatidylinositol phosphates

PI(3)P: phosphatidylinositol 3-phosphate

PI(3,4,5)P_3: phosphatidylinositol 3,4,5-trisphosphate

PI(4)P: phosphatidylinositol 4-phosphate

PI(4,5)P_2: phosphatidylinositol 4,5-bisphosphate

PI(5)P: phosphatidylinositol 5-phosphate

PMN: polymorphonuclear neutrophil

PH domain: pleckstrin homology domain

PX: Phox homology

SCV: *Salmonella*-containing vacuole

SINA: *Salmonella* INtracellular Analyzer

SNX: Sorting Nexin

SVATs: spacious vacuole-associated tubules

T3SS: type III secretion system

TCSB: trypticase casein soy broth medium

TGN: trans-Golgi network

Titre : *Shigella* engendre des sous-populations distinctes d'MAIs pendant l'invasion des cellules épithéliales pour favoriser l'établissement de sa niche

Résumé de la thèse (en Français)

Résumé de l'introduction

Shigella flexneri (ci-après nommée *Shigella*) est une bactérie Gram négative et l'agent responsable de la dysenterie bacillaire, maladie prédominant en particulier les pays en développement. Environs 600 000 décès par an sont attribuées à ce pathogène (CDC, 2019), touchant particulièrement les individus immunodéprimés (personnes âgées, jeunes enfants). Le traitement de l'infection par ce pathogène consiste à l'administration d'antibiotiques, cependant de nouvelles souches multirésitantes aux antibiotiques. L'apparition de ces souches bactérienne, pose de graves problèmes quant au traitement médical des individus atteint de la maladie. Il est donc important de comprendre au mieux l'invasion de ce pathogène afin de développer de nouveaux traitements médicaux.

Shigella est une bactérie pathogène entéro-invasive ciblant les cellules microfold, les macrophages et les cellules épithéliales non phagocytaires. Cette thèse se focalise sur l'invasion des cellules épithéliales par *Shigella*. L'invasion des cellules épithéliales de l'intestin par cet agent pathogène nécessite le transfert d'effecteurs bactériens dans la cellule cible. Pour cela, *Shigella* dispose d'une machinerie spécialisée, un complexe protéique ressemblant à une seringue nommé le système de sécrétion de type 3 (SST3). Suite au contact avec sa cellule cible, *Shigella* ancre et active le SST3 à la membrane cellulaire et injecte des protéines effectrices dans la cellule hôte. Cela déclenche des réarrangements du réseau d'actine conduisant à : (i) l'internalisation du pathogène dans une vacuole étanche appelée vacuole contenant la bactérie (VCB), et simultanément à (ii) la formation de vésicules de dMAIètre variable à proximité de la VCB, similaire en morphologie à des macropinosomes, appelées macropinosomes associés à l'infection (MAIs). Par la suite, *Shigella* rompt la VCB et se débarrasse de la membrane de la VCB pour accéder au cytosol de l'hôte. La bactérie forme par la suite une comète d'actine à l'un de ces pôles et se propage dans les cellules voisines. Les dernières études de l'équipe DIHP ont montré cependant un rôle important des MAIs dans les différentes étapes de l'infection. Préalablement à l'étape de rupture de la VCB, des interactions MAI-VCB se produisent ont étés observées et il a été montré que ces sites de contacts favorisent la rupture de la vacuole ainsi que le décollement des restes de la VCB de la bactérie (Weiner et al, 2016). Ces données montrent une contribution importante de l'hôte dans le contexte de l'infection par *Shigella*, cependant malgré la découverte d'un rôle clé des MAIs dans l'infection par *Shigella*, peu est connu jusqu'à présent à leur sujet. Au niveau moléculaire, des études précédentes de l'équipe DIHP ont démontré que l'évasion bactérienne

de la VCB était favorisée par des facteurs de l'hôte recrutés aux MAIs, tels que RAB11A, RAB8A et le complexe Exocyst (Melouk et al. 2014, Weiner et al. 2016, Chang et al. 2020). Ces trouvailles montrent une nécessité de revoir le modèle d'invasion de cette bactérie et de comprendre davantage la contribution de l'hôte dans l'infection.

Le remodelage des membranes par régulation de la courbure membrane est un processus cellulaire crucial. Ce remodelage des membranes est impliqué dans le trafic vésiculaire, la forme des organites, le recyclage de protéines. Deux facteurs sont majoritairement impliqués dans l'établissement de la courbure membranaire la composition lipidique de la membrane d'une part et d'autre part les protéines membranaires d'autre part. Parmi ces dernières, une famille de protéines est connue pour réguler la courbure membranaire : la famille des protéines à domaine Bin/Amphiphysin/Rvs (BAR). Ces protéines sont caractérisées par un domaine BAR dont le rôle est conjecturé de courber les membranes ainsi que dans la détection de courbures. Ces protéines sont impliquées dans une grande variété de processus cellulaires allant de l'endocytose, le recyclage endosomal, et bien d'autres. De part de leur participation dans de nombreux processus cellulaires, les protéines à domaine BAR sont impliqués dans l'invasion de nombreux pathogènes. Pour citer quelques exemples, la bactérie responsable de la salmonellose et apparenté à *Shigella*, *Salmonella enterica* recrute la protéine BAR SNX1 au niveau de sa vacuole lors de son invasion de cellules épithéliales grâce à l'effecteur bactérien SopB (Bujny et al, 2008). Ce recrutement de SNX1 induit la déformation de la membrane vacuolaire et la formation de tubules afin de réguler l'avenir de l'infection (Stévenin et al, 2019). Similairement, la bactérie enterohémorrhagique *E. coli*, recrute la protéine BAR IRSp53 à la membrane plasmique afin de catalyser un remodelage du réseau d'actine sous-jacent au travers des effecteurs bactérien Tir et EspFU permettant à la bactérie de former une structure nommée le « piédestal » dans lequel réside l'agent pathogène. D'autre part, deux études ont mis en évidence le détournement de la protéine à domaine BAR TOCA-1, activant la GTPase Cdc42, lors de l'invasion de la cellule hôte. Leung et al (2008) ont démontré que TOCA-1 est nécessaire à la polymérisation de l'actine à l'un des poles de ***Shigella*** afin de former la queue en comète d'actine via Cdc42 qui recrute le complexe Arp2/3. De plus, Kühn et al (2020) ont confirmé et caractérisé une structure riche en actine entourant la VCB avant sa lyse affectée le nom de cocoon d'actine et a démontré que la dynamique de cette structure dépend entre autres de TOCA-1. Cette étude a démontré la séquestration de TOCA-1 via l'effecteur IscB, une acyl transférase bactérienne, autour de la VCB ce qui entraine l'activation de Cdc42 et du complexe de nucléation d'actine Arp2/3. Ces data préliminaires mettent en lumière l'importance de la courbure membranaire dans le processus d'invasion bactérienne et suggère que les protéines à domaine BAR, de par leurs fonctions dans la cellule, sont reprogrammées par les agents pathogènes.

Résumé des résultats

Sur la base des résultats d'une analyse protéomique des MAIs (Chang et al, 2020) et d'un crible fonctionnel de la rupture de la VCB effectué par Mellouk et al (2014), nous avons étudié de manière systématique l'implication des protéines à domaine dans le contexte de l'infection par *Shigella*. Au commencement de cette thèse, pour identifier un rôle potentiel des protéines à domaine BAR, avons effectué un crible à haut contenu afin d'identifier le recrutement des protéines à domaine BAR dans l'invasion par *Shigella*. En utilisant une librairie de 66 protéines à domaine BAR fusionnées à la protéine fluorescente Enhanced Green Fluorescent Protein (EGFP), notre crible est basé sur de la microscopie à fluorescence en temps réel, permettant de visualiser les changements de localisation de chaque protéine BAR individuellement lors de l'infection. Les détails de la mise en place de ce crible est détaillé dans la publication « Time-resolved fluorescence microscopy screens on host protein subversion during bacterial cell invasion » (Sanchez et al. 2021) page 79 de ce manuscrit. Mon second manuscrit (en cours de publication) page 99 détaille la suite de mon projet de thèse et discuté par la suite. Parmi nos résultats les plus probants, nous avons observé le recrutement de la protéine de recyclage endosomale Sorting Nexin-8 (SNX8). SNX8 est une protéine BAR peu connue, localisant aux endosomes précoces dont le rôle est proposé être dans le tri et recyclage des protéines des endosomes précoces vers le Trans-Golgi (Dyve et al. 2009). L'homologue de SNX8 chez la levure Mvp1 semble également montrer un rôle de recyclage de ce facteur protéique (Suzuki et al. 2021). La surexpression de cette protéine lors de l'infection des cellules épithéliales montre le recrutement de SNX8 au niveau des MAIs environs 6 minutes avant la rupture de la VCB.. D'autre part, à une plus haute résolution temporelle, nous avons observé qu'elle induit la formation de tubules abondant en SNX8 émanant des MAIs suggérant un recyclage des protéines et lipides des MAIs par cette protéine. Dans l'ensemble ces résultats suggérent un role potentiel de la SNX8 dans la rupture et/ou désassemblage de la VCB. Suite à l'immunodétection de SNX8 (confirmant le recrutement de la protéine endogène), nous avons procédé par la caractérisation de la dynamique de recrutement de cette protéine par rapport aux facteurs précédemment identifiés aux MAIs dont RAB5A, RAB7A, RAB11A et RAB8A par microscopie a fluorescence en temps réel. Lors de l'expression de SNX8 avec les facteurs cité précédemment, nous avons observé que le recrutement de la SNX8 est couplé au recrutement de RAB5A (un marqueur précoce des macropinosomes classiques). De plus, nous avons observé lors de la surexpression de SNX8 et de RAB11A des MAIs positifs pour la SNX8 et d'autres pour RAB11A. Par ailleurs, certains des MAIs positifs pour la SNX8 viraient ensuite en RAB11 avec un comportement d'exclusion de SNX8 et RAB11A. L'ensemble de ces résultats montre que le recrutement de SNX8 est mutuellement exclusif à RAB11A au niveau des MAIs, ce qui laisse supposer l'existence de sous-ensembles d'IAM pendant l'infection par *Shigella*.

Peu est connu au sujet des MAIs et leur(s) rôle(s) dans l'invasion de *Shigella*, et en particulier il n'est pas clair si tous les MAIs ont la même composition (Mellouk et al. 2014, Weiner et al. 2016, Chang et al. 2020). De plus, le recrutement abondant de RAB11A aux MAIs rend perplexe car cette protéine RAB n'a pas été caractérisé comme constituant par défaut des macropinosomes classiques. Pour évaluer si la SNX8 localise à tous les MAIs de *Shigella*, nous avons réalisé des expériences de microscopie à temps réel de plus haute résolution spatiale couplée au rapporteur LactC2 -un senseur de phosphatidylsérine, lipide présent à la membrane plasmique- afin de suivre attentivement les MAIs depuis leur formation. Les films obtenus montrent que la SNX8 ne se localise pas à tous les MAIs formés. De plus, des infections effectuées en présence du marqueur de phase fluide fluorescent dextran (marquant les MAIs (Weiner et al. 2016)) dans les cellules HeLa transfectées par la SNX8-EGFP fixées 30 minutes suite à l'infection par *Shigella* ont confirmé que SNX8 n'est enrichi que dans une partie des MAIs formés (61%, ±4,7%). Dans l'ensemble, ces résultats révèlent la l'existence d'au moins deux sous-populations d'MAIs de composition distincte au sein d'un foyer infectieux.

Par la suite, nous avons caractérisé la localisation de la SNX8 aux MAIs. De par la présence sur la séquence protéique d'un domain PX (ayant normalement une affinité pour le phospholipide PI(3)P), nous avons surexprimé la SNX8 avec la sonde fluorescente 2xFYVE (marquant le PI(3)P). Les deux recrutements se sont produits simultanément et après la fermeture de la cupule des MAIs, de plus le recrutement de SNX8 s'est produit dans tous les MAIs marqués au 2xFYVE. Collectivement, ces résultats démontrent que l'accumulation de SNX8 se fait exclusivement dans une sous-population d'MAIs enrichis en PI(3)P. Nous avons ensuite étudié la fonction de cette sous-population nouvellement identifié d'MAIs PI(3)P+/SNX8+. Après avoir déterminé que le recrutement de SNX8 était induit par PI(3)P, nous avons évalué si PI(3)P était dépendant de la PI(3)-kinase de la cellule hôte. Ceci a été confirmé par l'utilisation de la wortmannin, un inhibiteur des PI(3)-kinases cellulaires à large spectre, qui a conduit à un arrêt du recrutement de SNX8 aux MAIs.

Le recrutement dépendant de PI(3)P de SNX8 simultanément avec celui de RAB5A, nous avons permit d'émettre l'hypothèse de l'implication de l'effecteur RAB5 de classe III PI(3)P kinase VPS34 (Vacuolar Sorting Protein 34) qui a été décrit comme étant impliqué dans les mécanismes moléculaires et la maturation de l'endosome précoce ainsi que dans la maturation macropinosome PI(3)P (Backer, 2008, Bohdanowicz et al. 2013, Spangenberg et al. 2021). Un inhibiteur spécifique de VPS34 appelé SAR405 a été décrit comme altérant la fonction de VPS34 au niveau des macropinosomes classiques (Ronan et al. 2014, Spangenberg et al. 2021). Sur la base de nos précédents résultats concernant le recrutement d'MAIs dans la VCB lors de l'endommagement de ce compartiment (Weiner et al. 2016, Chang et al. 2021), nous avons décidé d'évaluer la fonction des SNX8-MAIs dans la rupture et le désassemblage de la VCB. À cette fin, nous avons réalisé des infections en temps réel dans des cellules HeLa exprimant de transitoirement mOrange-Galectin-3 et

SNX8-eGFP avec et sans SAR405. Nous avons observé que l'ajout de SAR405 entravait le recrutement de SNX8-eGFP aux MAIs (figure 5A). L'inhibiteur a également altéré le recrutement de PI(3)P vers les MAIs (figure supplémentaire 2).

Pour suivre la rupture de la VCB et les restes de membrane, nous avons réalisé des infections en temps réel du SAR405 traité dans des cellules HeLa co-exprimant SNX8 avec le rapporteur fluorescent Galectin-3. Le temps de rupture de la VCB a été défini comme le temps entre l'éruption de la membrane et le recrutement de la Galectine-3 à la VCB. L'analyse du temps de rupture de la VCB a montré un léger retard, mais significatif, de 2 minutes en présence de l'inhibiteur SAR405 par rapport au contrôle DMSO.

Il a été démontré que l'échappement de la VCB nécessite d'abord la rupture du VCB suivie du décollement des restes de la VCB. De plus, le décollement du VCB a été décrit comme ayant un impact sur la vitesse de mobilité des bactéries (Kühn et al. 2020, Chang et al. 2020), et il est probable que l'efficacité de cet événement ait un impact sur la détection intracellulaire par xénophagie. Pour surveiller le décollement des restes de membrane de la VCB, trois phénotypes ont été décrits sur la base du mouvement de la membrane du VCB et de la rapidité du mouvement des bactéries : nous distinguons un désassemblage rapide de la VCB, un reste de la VCB lâche avec un mouvement rapide et un reste de VCB serré contre la bactérie avec un mouvement retardé des bactéries. La quantification de ces phénotypes dans l'expérience décrite a permis de valider les proportions de chaque type de désassemblage du VCB et était similaire aux phénotypes précédemment rapportés en présence de DMSO (restes de VCB serrés : 44,2%, restes de VCB lâches : 40,4%, recyclage rapide : 15,4%) (Kühn et al. 2020). Cependant, le traitement avec l'inhibiteur a provoqué une diminution du phénotype de la membrane VCB lâche en faveur d'une augmentation des bactéries qui sont connectées avec une membrane VCB serrée lors du dommage initial de la VCB. Néanmoins, aucun changement n'a été observé dans le phénotype de désassemblage rapide de la VCB en présence ou en l'absence de l'inhibiteur VPS34 (DMSO=15,4%, SAR405=16%,). Ces résultats montrent une fonction des MAIs PI(3)P-SNX8 dans la promotion d'une sortie efficace du VCB de Shigella pour atteindre le cytosol de l'hôte.

Résumé de la discussion

Par l'analyse de l'implication des protéines BAR pendant l'invasion par la bactérie pathogène *Shigella*, combinant la microscopie à fluorescence à résolution temporelle avec des sondes codées génétiquement (Sanchez et al. 2021), nous avons découvert l'existence de sous-populations distinctes de *Shigella*-MAIs. Nous avons étudié un sous-ensemble d'MAIs qui sont positifs pour PI(3)P et SNX8, montrant leur implication dans la sortie efficace de la vacuole bactérienne. Nous avons identifié le signal PI(3)P comme étant VPS34-dépendant au niveau des MAIs et montré qu'au moins une partie de ce sous-ensemble d'MAIs

a subi un switch de SNX8 vers RAB11A. Enfin, l'arrêt de la synthèse de PI(3)P aux MAIs a entraîné un retard dans la rupture de la VCB et une altération du désassemblage de la VCB.

Les étapes d'invasion de *Shigella* nécessitent un remodelage membranaire important. Par conséquent, le suivi des facteurs contenant le domaine BAR impliqués dans l'invasion de *Shigella* est apparu comme prometteur. Auparavant, il a été signalé que la protéine BAR TOCA-1 était recruté dans la cage d'actine de *Shigella* et qu'elle était crucial pour la formation de la queue d'actine (Leung et al. 2008, Baxt et Goldberg, 2014, Kühn et al. 2020), ce que nous avons également observé (données non montrées). Nous avons trouvé un enrichissement des protéines SNX-BAR, SNX8 en particulier localisé aux MAIs positifs pour le PI(3)P et y restant jusqu'aux étapes tardives de l'invasion de Shigella (Figure 2). Avec nos données, nous avons pu déterminer l'existence d'un sous-ensemble PI(3)P+/SNX8+ des MAIs de *Shigella*. De plus, il est intriguant de constater que SNX8 ne se localise que sur une partie des MAIs induits. Nos résultats s'alignent sur un rapport de Weiner et al (2016) qui a montré que les MAIs marqués au PI(3)P se co-localisent partiellement avec le dextran, marqueur de la phase fluide.

Auparavant, la macropinocytose a été proposée comme mécanisme d'entrée des pathogènes bactériens (Cossart et Sansonetti, 2004). Cependant, il a été déterminé que les MAIs de *Shigella* sont morphologiquement et compositionnellement distinctes de la vacuole bactérienne de type phagosome (Weiner et al. 2016), ce qui incite à penser que leur formation relève de mécanismes distincts. En outre, des sites de contact entre le VCB et les MAIs ont été signalés (Weiner et al. 2016) ainsi que le recrutement de facteurs de l'hôte RAB11A, RAB8A et l'exocyste (Mellouk et al. 2014, Weiner et al. 2016, Chang et al. 2020) qui ont été révélés pour favoriser la sortie de *Shigella*-VCB. Ensemble, ces données mettent en évidence les MAIs comme un compartiment distinct avec une contribution importante dans le processus d'infection. Cependant, bien qu'ils soient morphologiquement comparables aux macropinosomes canoniques, la similitude de la composition et de la formation des MAIs avec les macropinosomes "classiques" est restée obscure. Une étude récente de Spangenberg et al (2021) a montré que la maturation des macropinosomes est dépendante de VPS34, l'inhibition de VPS34 conduisant à la re-fusion des macropinosomes avec la membrane plasmique, via le recrutement de RAB10 et RAB11A. Ici, nos résultats contrastent avec ceux de Spangenberg et al, le sous-ensemble des MAIs PI(3)P+/SNX8+ médié par VPS34 se transformant en RAB11A, ce qui met en évidence la manière dont ces compartiments contrôlés par les pathogènes diffèrent des macropinosomes canoniques.

En outre, grâce à notre étude de la sous-population PI(3)P+/SNX8+ des MAIs, nous pouvons spéculer sur la ou les fonctions potentielles et la maturation des différents sous-ensembles d'MAIs. Sur la base du recrutement de RAB, nous suggérons qu'une partie de ce sous-ensemble pourrait suivre les voies de dégradation endosomale de RAB7A, les sous-ensembles SNX8+/RAB11A- d'MAIs pourraient être sujets à communiquer avec le TGN tandis que les MAIs SNX8-/RAB11A+ devenant "endosomes de recyclage"

pourraient subir un recyclage à la membrane plasmique. À l'instar de travaux antérieurs qui ont démontré une fonction des MAI dans l'accélération de la sortie de *Shigella*-VCB (Mellouk et al. 2014, Weiner et al. 2016, Chang et al. 2020) et qui mettent l'accent sur la contribution de l'hôte et de la bactérie, ces travaux montrent que le foyer de *Shigella* est constitué de sous-populations d'MAI qui mettent en évidence la subversion par la bactérie de multiples voies de l'hôte. À un niveau plus général, notre travail souligne l'importance des voies de recyclage endosomales dans les dernières étapes de l'invasion de *Shigella*. Il a été démontré que *Shigella* doit être rapidement " nue " dans le cytosol, séparée des restes de membrane du VCB (Chang et al. 2020, Kühn et al. 2020). Nous montrons dans cette étude, que conformément aux études précédentes, les MAIs jouent un rôle dans le déshabillage de la membrane du VCB de la bactérie. Cependant, nous montrons ici que *Shigella* déclenche différentes voies de maturation des MAIs jouant potentiellement différents rôles dans le processus d'infection.

Les facteurs bactériens qui dictent la diversité des MAIs pendant l'entrée de *Shigella* doivent être déterminés. Le mutant ipgD entraîne un léger retard dans l'entrée de la bactérie, cependant il abroge presque entièrement la formation des MAIs (Garza-Mayers et al. 2015, Weiner et al. 2016). Par conséquent, et également à la lumière de nos données utilisant les inhibiteurs de la PI kinase, il est très peu probable qu'IpgD soit la clé du contrôle des différents sous-ensembles d'MAI. De manière intéressante, un autre effecteur a été montré pour moduler les petites GTPases de l'hôte. IcsB est une N-acylase d’acides gras qui colle les petites GTPases aux membranes de l'hôte pendant l'invasion de *Shigella* (Liu et al. 2018). Nous avons également constaté qu'il est impliqué dans la formation du cocon d'actine, et qu'il a un impact sur l'éjection de *Shigella* de sa vacuole (Kühn et al. 2020). Par conséquent, il serait intéressant d'étudier comment le mutant icsB affecte les différentes sous-populations d'MAIs. En outre, IpaB et IpaJ ont été identifiés comme étant impliqués dans la fragmentation du Golgi, et il est possible que ces voies régulent également les différentes sous-populations de MAI (Burnaevskiy et al. 2013).

D'autres pathogènes bactériens ont également été décrits comme déclenchant des compartiments de type macropinosome lors de leur invasion. En particulier, il a été démontré que Salmonella, un agent pathogène bactérien ressemblant beaucoup à *Shigella*, forme des MCI pendant l'infection. Récemment, il a été démontré que ces MAIs de Salmonella étaient essentiels à l'établissement de la niche de Salmonella (Stévenin et al. 2019). Il a été démontré que les MAIs fusionnent avec la vacuole de Salmonella, formant ainsi la niche réplicative de Salmonella (90% des événements), tandis que l'altération de la fusion des MAIs conduit à la rupture de la vacuole de Salmonella (Perrin et al. 2004, Malik-Kale et al. 2012, Knodler et al. 2014). Par conséquent, une comparaison de la composition des MAI de Salmonella et des MAI de *Shigella* est cruciale pour comprendre l'établissement de la niche bactérienne. Cela pourrait aider à mettre en évidence les voies spécifiques exploitées par les bactéries pathogènes pour établir leur niche intracellulaire.

Chapter 1. Introduction

1.1. *Shigella flexneri*

1.1.1. *Shigella flexneri*, global impact and medical relevance

Shigella is a Gram negative facultative anaerobic bacillus responsible for bacillary dysentery (also known as shigellosis), a disease predominant in developing countries. As many as 50 serotypes of *Shigella* have been identified, which are classified into 4 species, differing in virulence levels and geographic location: *Shigella flexneri*, *Shigella sonnei*, *Shigella dysenteriae* and *Shigella boydii* (Ewing, 1949). According to the Centers for Disease Control and Prevention (CDC), the most prevalent in developing countries is *S. flexneri* whereas *S. sonnei* impact has been found to be predominant in wealthier countries (Thompson et al. 2015, Anderson et al. 2016). An estimated 80 to 165 million people are contaminated every year, primarily children under the age 5 (CDC, 2019). Of the infected, an estimated 600,000 people die from the disease mostly due to complications and lack of treatment caused by inaccessibility to healthcare (CDC, 2019).

S. flexneri infection is acquired through the fecal-oral route by the ingestion of contaminated food or water. *S. flexneri* being a highly virulent bacterium and able to resist the gastric pH, as little as 10 to 100 bacteria are sufficient to trigger the infection (Dupont et al. 1989). After reaching the small intestine and the colon, *S. flexneri* is able to cross the epithelial barrier where it infects gut cells. This elicits a massive inflammatory response which causes the symptoms of shigellosis. Symptoms of the illness then occur, the characteristics of the disease being fever, abdominal cramping, and bloody diarrhea (Jennison and Verma, 2004). However, in immuno-suppressed individuals or in infants with an incompletely developed immune system, more life-threatening acute symptoms have been reported, amongst them septicemia, seizures and toxic megacolon (Sansonetti, 2001).

Despite poverty and the low bacterial infectivity being major contributing factors of *Shigella* infection, another important pathogenicity aspect is of growing concern. The rise of antibiotic resistant *Shigella* species has complicated the treatment of shigellosis in recent years. The rapid adaptation of the bacteria to antibiotics has caused a race against time to find novel antibiotic treatments and remains today a major health threat. Initially treated using sulphonamides (Puzari, Sharma and Chetia, 2018), *Shigella* infection treatment then transitioned to tetracycline and chloramphenicol, all of which the bacteria also developed a resistance to, leading to ampicillin, co-trimoxazole and nalidixic acid use. Today, shigellosis is treated with fluoroquinolones, ceftriaxone, pivmecillinam and azithromycin (Taneja and Mewara, 2016). However, the emergence of multidrug resistant *Shigella* isolates (with *S. flexneri* often being the predominant species)

impervious to several of the current antibiotics have been reported in Korea, Pakistan, China, Indonesia, Nepal, Bangladesh and Vietnam (Mahbubur et al. 2007, Kim et al. 2008, Puzari, Sharma and Chetia, 2018). Due to the history of antibiotic adaptation of *Shigella* species and the mentioned concerning reports, there is a great need for preventative and antibiotic alternative medical care against this pathogen.

The road to a vaccine against *Shigella* has been long and hard. Due to the diversity of the different *Shigella* species and predominance in different countries/regions, two strategies have been implemented, either targeting the *Shigella*-conserved antigen among different serotypes (based on common antigens from different *Shigella* serotypes), or alternatively targeting antigens specific to individual serotypes as serotype-specific strategy (Jennison and Verma, 2004, Barry et al. 2013, Mani et al. 2016). The vaccines that are being developed based on these strategies have been under testing as they must elicit an immunological reaction, and they require to be safe and cost effective. Despite these advances several hurdles have prevented the development of *Shigella* vaccines in general, in particular the lack of reliable animal models able to replicate the shigellosis symptoms observed in humans albeit current animal model developments appear promising (Barry et al. 2013, Mitchell et al. 2020). This has hampered the characterization of the clinical efficiency and safety of vaccine candidates. Thus, the pathogenesis of *Shigella* must be further investigated in order to develop better broadly-functioning vaccine and antimicrobial strategies.

1.1.2. *Shigella flexneri* cellular pathogenesis: gut invasion and dissemination

As part of its infection cycle, *S. flexneri* (hereafter referred to as *Shigella*) crosses the epithelial cell layer to access gut cells (Figure 1.1). Numerous studies have shown that at the start of the infection the majority of bacteria do not invade enterocytes from the apical side (Mounier et al. 1992, Perdomo et al. 1994, Sansonetti et al. 1996, Rey et al. 2020). Contrasting with this, an innovative organ-on-a-chip model for the study of early epithelial-*Shigella* interactions has shown pathogen entry from the apical site into polarized epithelial cells involving peristaltic movements (Grassart et al. 2019). It will be interesting to decipher the mechanisms involved in these two different entry routes in the future. The best characterized path to bypass the epithelial barrier during *Shigella* infection takes place through the targeting of gut microfold cells (M cells) residing in the follicle-associated epithelium (Bockman and Cooper, 1973). These regions are specialized in antigen sampling from the intestinal lumen as well as their translocation to macrophages present at the sub-epithelial space. Taking advantage of the phagocytic function of M cells, *Shigella* enters them and travels either by transcytosis to the sub-epithelial space where it is endocytosed by the underlying macrophages, or it escapes the M cell vacuole to spread directly to adjacent epithelial cells (Perdomo et al.

1994, Sansonetti et al. 1996, Rey et al. 2020). In case *Shigella* is taken up by macrophages, the bacteria eliminate them inducing pyroptosis which is highlighted by the secretion of the interleukins IL-1β and IL-18 (Zychlinsky et al. 1992, Sansonetti et al. 2000, Lamkanfi and Dixit, 2010, Ashida et al., 2014, Schnupf and Sansonetti, 2019). These cytokines elicit a massive inflammatory reaction in response to the infection and to the recruitment and activation of Natural Killer (NK) immune cells to participate in effectively clearing the infection by secreting IFN- γ, thus further amplifying the inflammatory response (Way et al. 1998, Le-Barillec et al. 2005). Simultaneously to the induction of pyroptosis, *Shigellae* localized in the sub-epithelial space invade nearby epithelial cells from their basolateral side causing secretion of the chemokine interleukin-8 (IL-8) by the infected cells (Perdomo et al. 1994, Sansonetti et al. 1999). This IL-8 signal along with transcription factor NF-κB and MAP kinases JNK, ERK, and p38 propagate from the infected cells to adjacent non-infected cells and leads to their bystander activation and production of IL-8 (Kasper et al. 2010). IL-8 in turn activates polymorphonuclear neutrophils (PMNs) which cross the inter-epithelial space into the sub-epithelium (Perdomo et al. 1994, Sansonetti et al. 1999). From there, the PMNs destroy the local tissue which promotes further dissemination of the bacteria until the infection is eventually cleared by the PMNs (Perdomo et al. 1994, Sansonetti et al. 1999).

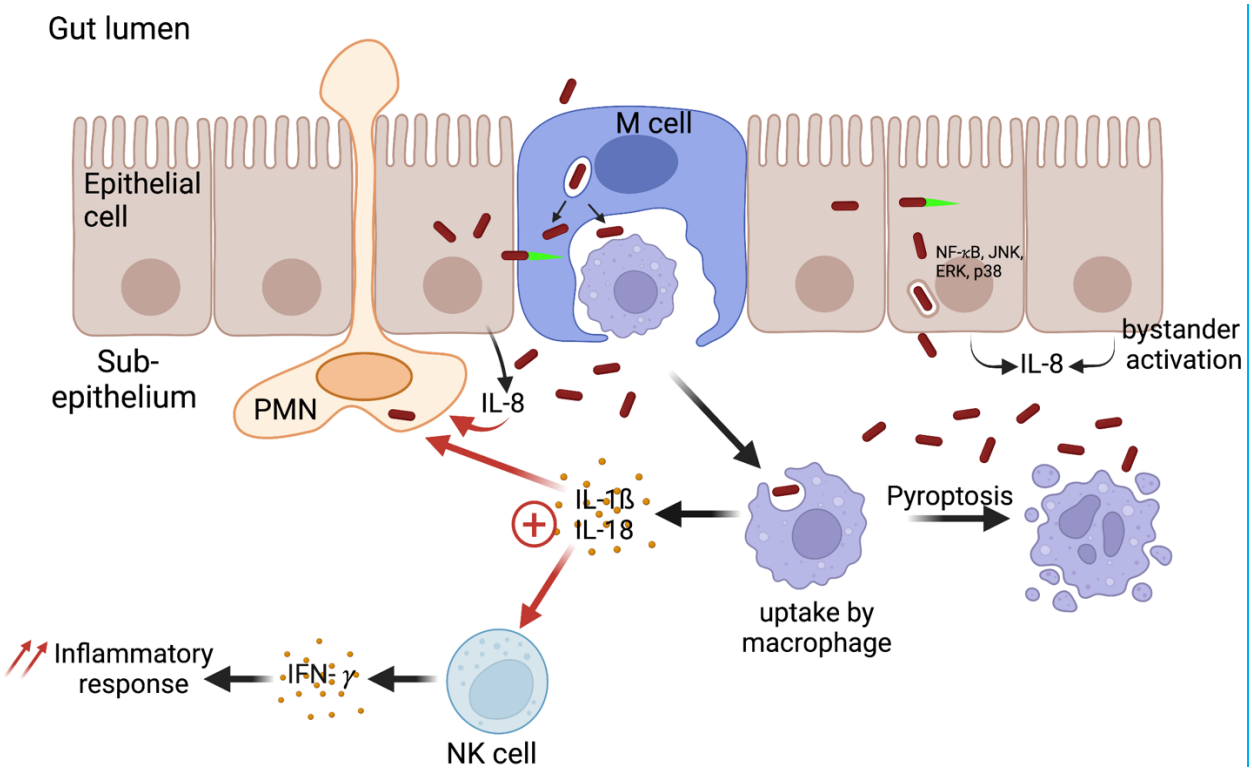

Figure 1.1. *Shigella* pathogenesis: invasion of the gut.

Created using BioRender.com

Regarding non-phagocytic epithelial cell invasion, *Shigella* uses a complex syringe-like apparatus called the type III secretion system (T3SS) which targets the plasma membrane of host cells, bridging a direct link between the host and the pathogen (Cornelis, 2006, Parsot, 2009). This apparatus, structurally similar to a syringe, allows the invading bacterium to transport effectors proteins from the bacteria cytosol to the host cytosol. These translocated effectors enable the reprogramming the host molecular pathways involved in the *Shigella* invasion steps. The following annotations are in relation to Figure 1.2. Following contact with the host cell, *Shigella* forces its entry by injecting bacterial effectors which trigger actin rearrangements leading to (1) membrane ruffling (Cossart and Sansonetti, 2004, Schroeder and Hilbi, 2008, Carayol and Van Nhieu, 2013, Valencia-Gallardo et al. 2015). This prompts (i) the uptake of *Shigella* by a phagocytosis-like mechanism within a tight vacuole termed the (2) bacteria-containing vacuole (BCV) (Cossart and Sansonetti, 2004, Weiner et al. 2016). Concomitantly, the collapse of the membrane ruffles causes (ii) the formation of vesicles of varying sizes, which we term infection-associated macropinosomes (IAMs) (Weiner et al. 2016). The IAMs are of particular importance of this thesis, and will be described in more detail below. Then, the bacterium triggers (3) the rupture of the BCV, followed by the shedding of BCV remnants away from *Shigella* (4) to escape into the cytosol where the pathogen replicates (Kühn et al. 2020, Chang et al. 2020). Having accessed the cytosol, *Shigella* avoids entrapment by the autophagy machinery and spreads to neighboring cells by (5) forming an actin comet tail at one of its poles. The bacterium penetrates the adjacent cell by (6) forming a membrane protrusion and (7) enters the target cell in a double-membraned compartment (Schroeder and Hilbi, 2008, Agaisse, 2016). Some cytosolic bacteria do not form actin tails and are entrapped within septin cages that form directly at the bacterial surface (Mostowy et al. 2009, Mostowy et al. 2010, Krokowski et al. 2018, Lobato-Márquez, 2021).

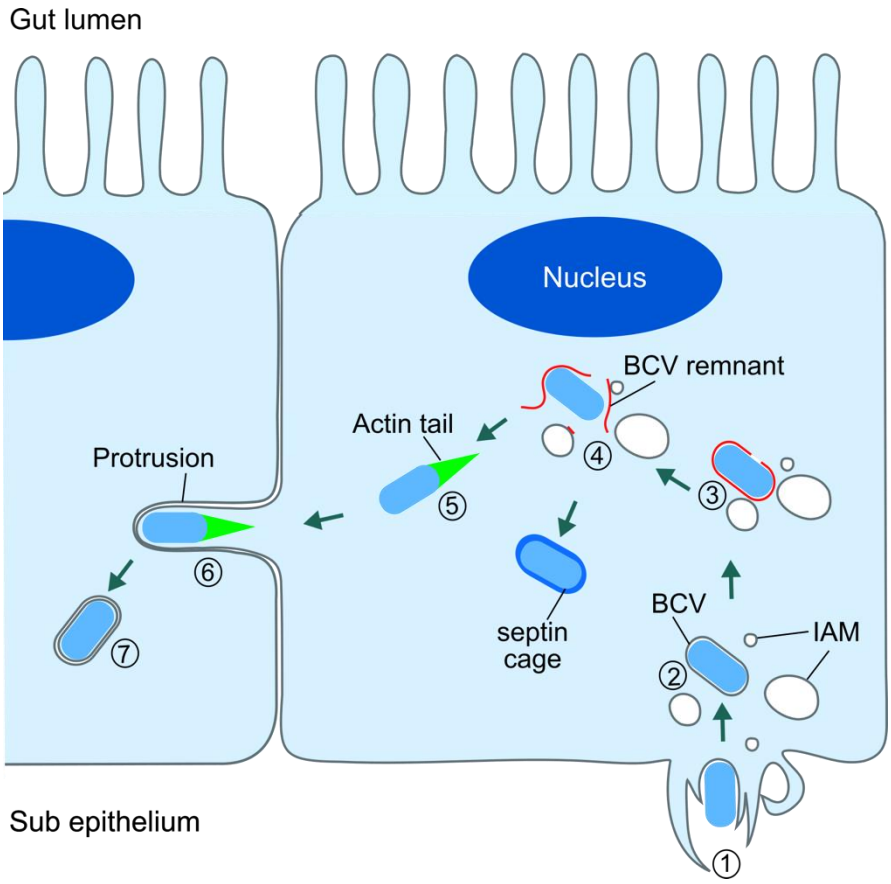

Figure 1.2. *Shigella* invasion model of non-phagocytic gut epithelial cells.

1.1.3. Molecular aspects of *Shigella* epithelial cell invasion

Genetic studies have shown the *Shigella* virulence genes are mainly encoded on a large virulence plasmid (pINV) and in chromosomal regions referred to as pathogenicity islands (PAI) (Lan et al. 2001). The pINV is a large (213 kb), single copy, non-conjugative plasmid essential for virulence and encodes the T3SS structural proteins and its bacterial effectors (Buchrieser et al. 2000, Venkatesan et al. 2001). Other PAIs also encode bacterial effectors and virulence factors such as siderophores and toxins (Mattock and Blocker, 2017).

The T3SS apparatus is key to *Shigella* virulence because it orchestrates the secretion of bacterial effectors into the cytosol of targeted cells, such as enterocytes, necessary for successful bacterial invasion and survival to the host cytosol. This evolutionarily conserved apparatus is one of the most important and sophisticated mechanisms used by *Shigella* to exploit the host (Izoré et al. 2011, Deng et al. 2017). The T3SS is a protein complex composed of roughly 50 proteins, including structural components (*e.g.* MxiG,

MxiJ, MxiI, MxiD, MxiH, MxiM), translocators (IpaB, IpaC and IpaD), chaperones (IpgA, IpgC, IpgE and Spa15), effector proteins (IpgB1, IpgB2, IcsB, IpgD, VirA, OspC1, OspC2, OspC3, see Table 1.1) and transcription activators (VirF, VirB and MxiE) (Parsot, 2009, Poraliou et al. 2016, Bajunaid et al. 2020) (see Figure 1.3). This complex apparatus is formed of several components: a basal body at the bacterial inner and outer membranes, an extracellular needle with a tip complex associated to a translocon pore binding to the host cell membrane and a cytosolic network of sorting chaperones which control the transport of bacterial effectors (Portaliou et al. 2016, Bajunaid et al. 2020). The T3SS apparatus complex's expression, assembly, activation and secretion of bacterial effectors are tightly regulated and coordinated (Parsot, 2009, Bajunaid et al. 2020). Prior to cell contact, in permissive conditions (> 32°C temperature), the *Shigella* T3SS is assembled but inactive with the translocator proteins and bacterial effectors associated to their chaperones (Parsot, 2009). The structural components of the T3SS constitute a core complex with an emanating needle that is made of polymer of the MxiH subunit (>100) (Bajunaid et al. 2020). At the tip of the needle is the translocon complex assembled of IpaB and IpaC that has been proposed to be kept closed through the IpaD protein (Blocker et al. 1999, Johnson et al. 2007, Olive et al. 2007). Upon contact with the cell plasma membrane, the T3SS is activated, the translocon complex gets inserted into the plasma membrane of targeted cell, and the premade as well as newly expressed bacterial effectors are translocated into the host cell (Menard *et al*., 1994, Enninga et al. 2005, Schroeder and Hilbi, 2008, Parsot, 2009). To access the host cell cytosol -after release by their chaperone- bacterial effectors are translocated through the needle complex. Several reports have demonstrated that given the diameter of the needle (about 20 Å), bacterial effectors need to be unfolded to pass through the needle of the T3SS (Radics et al. 2013, Dohlich et al. 2014). It is important to note that this unfolding by the bacteria complicates the study of bacterial effectors (Dohlich et al. 2014). In reaching the translocon pore, bacterial effector entry into the host cell is facilitated by the translocators and spontaneously refold in the host cell cytosol (Burkinshaw and Strynadka, 2014).

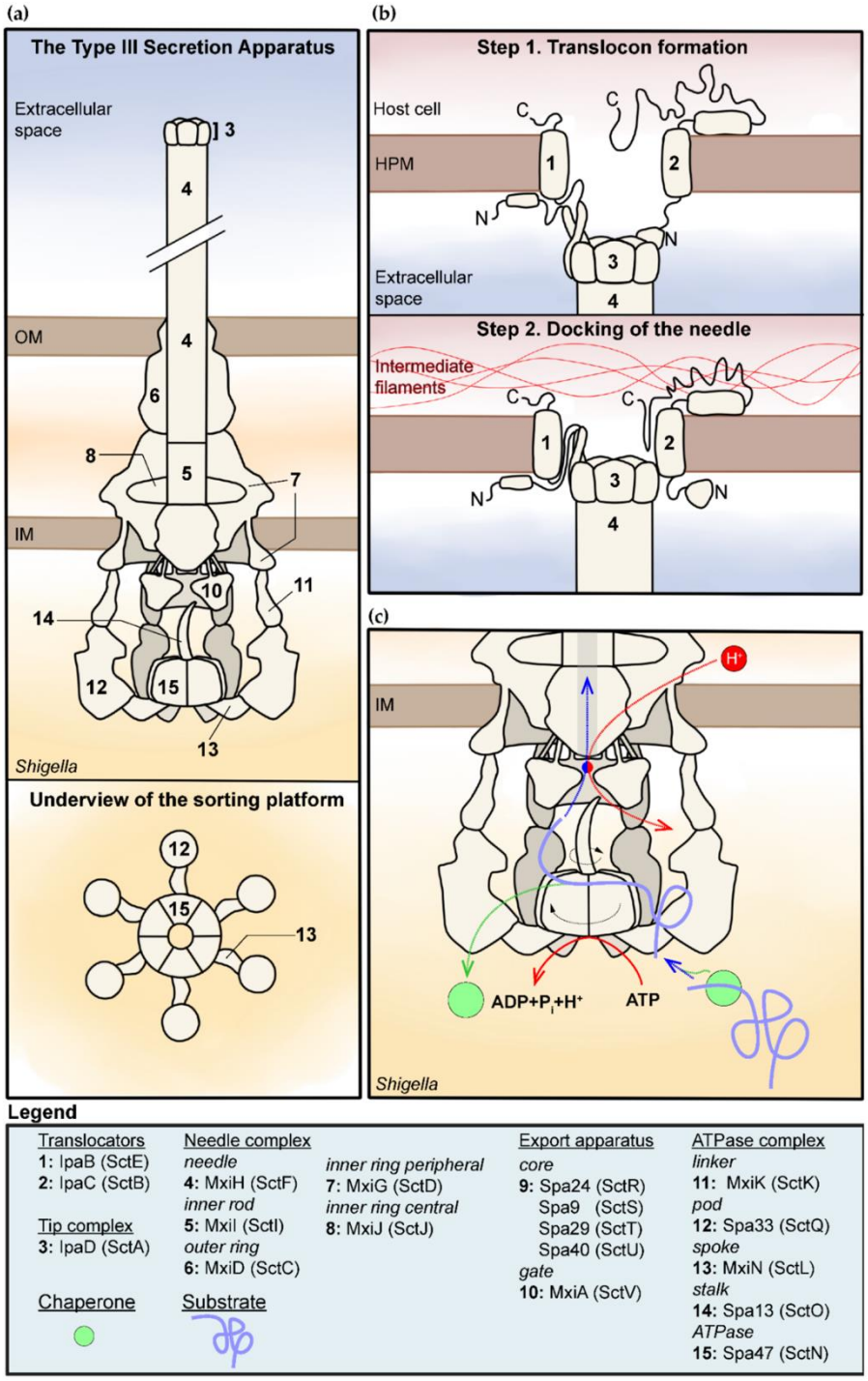

Figure 1.3. Structure of the *Shigella* type 3 secretion system (from Bajunaid et al. 2020).

(a) The T3SS secretion apparatus pre-assembled structure prior to host cell membrane contact. (b) The proposed insertion and conformational changes to the translocon pore proteins following host cell membrane contact. (c) Effector protein unfolding and transport through the T3SS basal body and needle. IM: inner membrane, OM: outer membrane, HPM: host plasma membrane.

During the initial interaction between host epithelial cells and *Shigella*, it has been shown that the bacterium can be captured by a host cell filopodia bringing it close to the cell body by filopodial retraction through the effectors IpaB and IpaD (Romero et al. 2011, Romero et al. 2012, Valencia-Gallardo et al. 2015). Moreover, the effector IcsA was reported to behave as an adhesin which facilitated contact with the host cell (Zumsteg et al. 2014). Initially, upon T3SS contact, the translocon and effector protein IpaC induces Src tyrosine kinase recruitment to the infection site followed by the activation of src signaling (Mounier et al. 2009, Carayol and Van Nhieu, 2013). Concomitantly, the T3SS-injected effector IpgB1 activates the small GTPase Rac1 by mimicking RhoG and by directly acting as a Rac1 GEF, leading to Arp2/3 recruitment (Alto et al. 2006, Handa et al. 2007). Simultaneously IpgD depletes the local plasma membrane pool of $PI(4,5)P_2$ by dephosphorylation into PI(5)P, leading to the recruitment of the Rac-1 GEF Tiam-1 (Niebuhr et al. 2002). Moreover, the phosphatase activity of IpgD also loosens the contact between the membrane and cortical actin which promotes the bacterial-driven actin network remodeling (Niebuhr et al. 2002). It should also be noted that recently, IpgD has also been reported to act as phosphotransferase resulting in elevated levels of $PI(3,4)P_2$, which has been proposed to regulate some endocytic routes such as macropinocytosis and others (Hawkins and Stephens, 2016, Walpole et al. 2022). The ensemble of these events lead to actin polymerization, formation of membrane ruffles and permit bacterial internalization (Carayol and Van Nhieu, 2013, Valencia-Gallardo et al. 2015). After ruffle formation, the bacterial effector IpaA sequesters the host cell junction proteins vinculin and β1 integrin to the infection site. IpaA simultaneously acts as a RhoA GAP leading to actin filament depolymerization and ruffle collapse (DeMali et al. 2006, Izard et al. 2006, Park et al. 2011). This leads to internalization of the bacteria by the host and IAM formation.

Once inside the BCV, the bacterium injects a second wave of effectors triggered through the activation of the T3SS and involving MxiE (of which aVirA, OspB, OspC1, OspF, IpaH1.4, IpaH4.5, IpaH7.8, IpaH9.8, OspD2/3, OspE) (Schroeder and Hilbi, 2008, Parsot, 2009, Schnupf and Sansonetti, 2019, Bajunaid et al. 2020). This wave of effectors is thought to alter host cellular immune pathways. At this stage, the bacterium forms an actin cage which was reported to occur by the recruitment of TOCA-1, a Cdc-42 GEF, to the BCV membrane via the bacterial effector IcsB (Kühn et al. 2020). After BCV disassembly, the bacterium also triggers vacuole lysis. The T3SS translocon has been proposed for a long time to be involved in membrane destabilization, and recently a role of the component IpaC has been suggested (Du et al. 2016). This T3SS-dependent damage to the BCV membrane has been hypothesized to be due to the formation of pores composed of IpaC, thus destabilizing the bacterial containing compartment. *Shigella* then sheds the BCV membrane remnants and accesses the cytosol in a process that is phenotypically very different from other BCV-damaging bacteria, such as *Salmonella* which remain in close contact with the broken BCVs (Kühn et al. 2020, Chang et al. 2020). Afterwards, the bacterial effector IcsA orchestrates actin polymerization

through the N-WASP-Arp2/3 complex leading to the formation of the so-called “actin comet tail” to one of the poles of the bacterium (Suzuki et al. 2002, Egile et al. 1999). Additionally, *Shigella* anchors TOCA-1 through IcsB to the BCV to activate N-WASP as well (Leung et al. 2008, Baxt and Goldberg, 2014). Together, these processes enable the efficient propulsion of the bacteria within the cytosol. That being said, the actin-based motility was reported to be insufficient to form the protrusion for invasion of adjacent cells. Protrusion formation requires membrane deformation and was shown to be dependent on host factors Diaphanous-related formins and Myosin X (Heindl et al. 2010, Bishai et al. 2013). Moreover, the phosphorylation of the membrane protrusion by tyrosine kinases as well as PI(3)P formation to the protrusions were shown to be important for *Shigella* dissemination (Dragoi and Agaisse, 2014, Dragoi and Agaisse, 2015, Agaisse, 2016). The role and control of the main effectors involved in the entry of *Shigella* are summarized in Table 1.1.

Bacterial effector	*Activity*	*Functions*	*Role in Shigella invasion*	*References*
IpgB1	Rac1 GEF	Actin polymerization	Membrane ruffling	Alto et al. 2006, Handa et al. 2007
IpaA	RhoA GAP, binds vinculin and β1 integrin	Actin filament depolymerization	Membrane ruffle collapse, BCV and IAM formation	DeMali et al. 2006, Izard et al. 2006, Park et al. 2011, Carayol and Van Nhieu, 2013
icsA	Adhesin	Adhesion to host cell lmembrane, F-actin recruitment	Promotes bacteria-host contact, actin tail polymerization	Bernardini et al. 1989, Egile et al. 1999, Zumsteg et al. 2014
icsB	Fatty acyltransferase?	Actin polymerization by TOCA-1 sequestration	Actin cage formation, autophagy escape	Liu et al. 2018, Kühn et al. 2020, Mostowy et al, 2010, Baxt and Goldberg, 2014
IpaB	T3SS needle translocon complex	Control secretion of bacterial effctors, BCV pore formation, Golgi fragmentation	Host cell invasion, BCV rupture, impairment of the host secretory pathway	Mounier et al. 2012, Du et al. 2016, Bajunaid et al. 2020
IpaC	T3SS needle translocon complex	Control secretion of bacterial effctors, BCV rupture, the activation of src signaling	Host cell invasion, membrane ruffling, BCV rupture	Bajunaid et al. 2020, Du et al. 2016, Mounier et al. 2009
IpgD	PI(4)-phosphatase	Actin polymerization via Rac1 , PI5P formation	Membrane ruffling, BCV maturation	Niebuhr et al. 2002

Table 1.1. Summary of the main bacterial effectors involved in *Shigella* epithelial cell invasion.

1.2. The subversion of the host trafficking machinery by intracellular bacterial pathogens

1.2.1. Phosphatidylinositol phosphates and RAB GTPases specify membrane identity

Eukaryotic cells are highly ordered structures with specific reactions occurring in well-defined membrane-enclosed structures such as the endoplasmic reticulum (ER) and the Golgi apparatus. The spatial distribution of enzymes within cellular structures testifies to the existence of specific compartment "identities" (Behnia and Munro, 2005). Even though we still lack a complete understanding of the molecular basis as to what makes up the "code" of specific compartments, several membrane trafficking events have been extensively characterized. In particular, the study of the secretory and endocytic pathways has provided insights into the molecules composing this cipher.

Vesicular trafficking is a complex, meticulously regulated process whereby a vesicle is formed, and has a very definite fate to which it matures and fuses to specific cellular compartments, leading to its recycling or degradation. This raises the questions as to how vesicles are addressed to their corresponding compartment, as to the identity of the vesicular compartments at their distinct stages of existence and as for the definition of cargo directionality (Jean and Kiger, 2012). The study of vesicular trafficking showed that cellular compartment identity is established by specific lipid and protein combinations, thus forming a "code" unique to each compartment. Main players that make up this code belong to a family of lipids called phosphatidylinositol phosphates (PIPs) and a family of small GTPases known as the RAB family (Behnia and Munro, 2005, Jean and Kiger, 2012, Schink et al. 2016).

PIPs are membrane lipids found within all membranes of eukaryotic cells formed from phosphatidylinositol (PI). In addition of containing diacylglycerol, PIPs are characterized by an inositol head group subject to modifications by phosphorylation and dephosphorylation enzymes respectively termed kinases and phosphatases (Schink et al. 2016) (see Figure 1.4). Given the spatial conformational of phosphatidylinositol, phosphatidylinositol-kinases can only modify the inositol in the 3,4 and 5 positions (Schink et al. 2016, Balla, 2013). This phosphate group addition can be reversed by phosphatase dephosphorylation. Due to the possibility of numerous modifications, a diversity of PIPs composes eukaryotic cells.

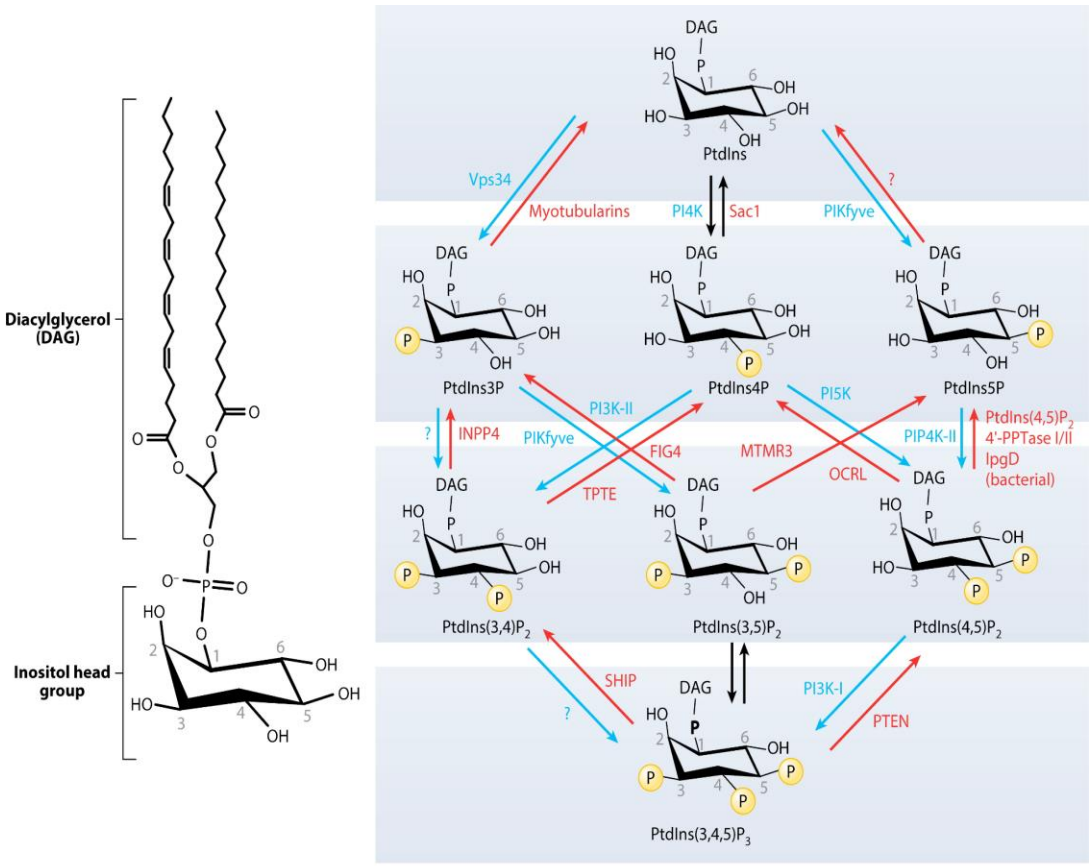

Figure 1.4. Structure of phosphatidylinositol (right) and examples of existing combinations of phosphatidylinositol phosphates (left) with their modifying kinases (in blue) and phosphatases (red) (from Schink et al. 2016).

PIPs have been shown to form microdomains within cell organelles with specific PIPs being enriched from one compartment to another. Moreover, PIP composition also varies during the maturation stages of organelles (Bala, 2013, Schink et al. 2016, Posor et al. 2022) (see Figure 1.5). As such, the plasma membrane is abundant in PI(4,5)P_2, present also in forming endocytic vesicles. Nascent endocytic vesicles, early endosomes, recycling compartments and autophagosomes have been on the other hand been found to be enriched in PI(3)P, whereas the Golgi apparatus and exocytic vesicles are characterized by PI(4)P presence (Di Paolo and De Camilli, 2006, Posor et al. 2022). These PIPs are recognized by specific proteins, thereby compartmentalizing cellular reactions. These observations led to the finding that PIPs signal the identity of cellular compartments. This spatio-temporal distribution of PIPs is governed by specific kinases and phosphatases which catalyze PIP conversion during specific cellular processes (Balla,2013, Posor et al. 2022). Exemplarily, during endocytic transport of vesicles to the endosomes, PtdIns(4,5)P 2 from the plasma membrane- derived vesicles is converted to provide an endosomal identity to this compartment by

phosphorylation through 4 and 5-phosphatases such as Synaptojanin (Saheki & De Camilli, 2012), OCRL (Bohdanowicz et al. 2012), and INPP4A/B (Boucrot et al. 2015). Suring vesicle trafficking, other kinases such as PI4-kinases (PI4K) are involved in the production of PI(4)P which has been shown to provide a secretory identity to organelle membranes such as the Golgi and the recycling endosomes and driving vesicle formation (Wang et al. 2003, Robinson and Plimp, 2014, Ketel et al. 2016, Schink et al. 2016). On the other hand, PI(3,4)P2 generation by PI3-kinases (PI3K) provides a late stage identity to forming vesicles, leading to the membrane scission by specialized proteins (Schink et al. 2016).

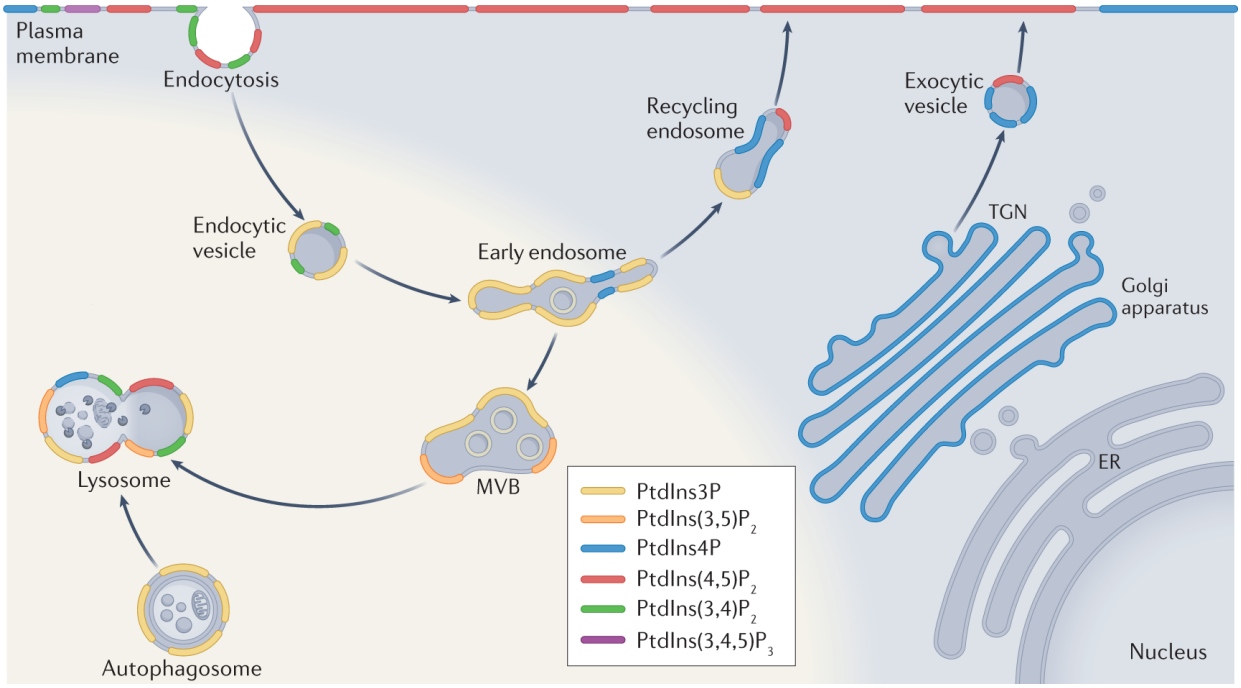

Figure 1.5. Phosphophatidylinositol phosphate spatial enrichment in the endocytic, exocytic and recycling pathways (from Posor et al. 2022).

The importance of these PIPs in membrane trafficking has come with the development of tools to modify and detect PIPs. Several approaches have been developed, of which the main one has been the development of fluorescent reporters based on PIP-detection domains from proteins specifically recognizing particular PIPs such as the pleckstrin homology domain (PH domain) or Phospholipase C**δ** which binds to PI(4,5)P_2 or the FYVE domain of HRS sensing PI(3)P (see Table 1.2 for more examples) (Posor et al. 2022). These reporters enable the visualization and the tracking of their corresponding PIPs by fluorescence microscopy. It is important to note however, that these sensors is that they often compete with other proteins binding to these lipids -thus making difficult the study of proteins binding to the same PIP as these reporters (Posor et

al. 2022). Additionally, these biosensors may not bind with the same efficiency their respective PIPs. This has prompted the development of other approaches, mainly based on mass spectrometry.

Phosphoinositide	Sensor[a]	Comments	Refs
PtdIns	*Bc*PI-PLC^{H82A}	Other lipids, including phosphatidylcholine and diacylglycerol, contribute to membrane affinity of the probe	188
PtdIns3P	2×FYVE-HRS	When purified, can be efficiently used as an antibody-like probe	7
PtdIns4P	2×P4M-SidM	Detects PtdIns4P in the Golgi complex, plasma membrane and endolysosomes	189
	PH-FAPP1	Detects only a Golgi pool of PtdIns4P and depends on ARF1 for its localization	190
PtdIns(3,4)P_2	3×cPH-TAPP1	Triplet of the cPH domain excluding other protein-binding motifs in the carboxy terminus of TAPP1 (also known as PLEKHA1)	74
PtdIns(4,5)P_2	PH-PLCδ1	The first phosphoinositide biosensor. Exclusively labels the plasma membrane but can also detect PtdIns(4,5)P_2 in other subcellular compartments	189,191,192
PtdIns(3,4,5)P_3	PH-Akt[b]	Dual PtdIns(3,4)P_2 and PtdIns(3,4,5)P_3 sensor	193,194
	PH-Btk	Specific to PtdIns(3,4,5)P_3	193,195
	2×PH-ARNO$^{2G-I303E}$	Specific to PtdIns(3,4,5)P_3; the I303E mutation eliminates binding to ARL4 GTPases	74

Table 2.2. Fluorescent reporters for different PIPs (from Posor et al. 2022).

PIPs can be reprogrammed by a set of kinases, phosphatases, phosphotransferases and phosphoisomerases that regulate the particular PIP identity of a compartment (Balla, 2013). These PIP-modulating enzymes are either expressed within any given eukaryotic cell, or such enzymes are synthesized by pathogens to reprogram host compartments (Payrastre et al. 2012, Walpole et al. 2022). The presence of PIP-modulating enzymes in bacteria highlights the coevolution between the different pathogens and the host. It should be noted that a specific identity of PIPs at a given compartment is not sufficient to explain compartment identity.

Another main factor of much importance identified as driving membrane organization are RAB GTPases (also called RAB proteins). RAB proteins are small GTP-binding proteins highly conserved in eukaryotic cells which cycle through an active GTP-bound state and an inactive GDP-bound state (Brighouse et al. 2010, Hutagalung and Novik, 2011, Pfeffer, 2013, Goody et al. 2017). These proteins are termed "molecular switches" of membrane trafficking as the act as signaling platforms regulating a variety of molecular cascades (Hutagalung and Novik, 2011, Jean and Kiger, 2012, Pfeffer, 2013, Zhen and Stenmark, 2015). Ordinarily, activated RAB proteins recruit and interact with molecular effectors involved in functions such as vesicle trafficking, membrane protein recycling and organelle quality control to name a few (Stenmark, 2009, Hutagalung and Novik, 2011). Interestingly, distinct RAB proteins are found enriched to specific compartments and to their distinct maturation stages (see Figure 1.6). In brief, for a given membrane trafficking event, the corresponding specific RAB GTPase is anchored to the membrane, and is then

activated by a cofactor called a guanine nucleotide exchange factor (GEF) which exchanges GDP for GTP in the catalytic pocket of the RAB protein (Hutagalung and Novik, 2011, Pfeffer, 2013, Goody et al. 2017). This activation leads to the recruitment of effector proteins specific to said RAB protein which in turn drive cellular processes by acting in downstream events. Afterwards, the RAB GTPase is inactivated by a GTPase activating protein (GAP) which causes the hydrolysis of GTP into GDP, and a guanidine nucleotide dissociating inhibitor (GDI) dislocates it from the membrane (Hutagalung and Novik, 2011, Pfeffer, 2013, Goody et al. 2017). Given the important functions of RAB proteins as master regulator of membrane trafficking and their specific localization with the cell architecture, together with the PIPs spatial distribution, confers an identity to cellular compartments (Hutagalung and Novik, 2011, Pfeffer, 2001). Thus, as examples early endosomes are enriched by RAB5, recycling endosomes by RAB11, the Golgi by RAB6 (see Figure 1.6). Moreover, RAB GTPases directly interact with distinct PIPs, exhibiting specific affinities for them. The current understanding of membrane trafficking is that PIPs and RABs act together to control the fate of cellular membranes (Pfeffer, 2001, Jean and Kiger, 2012).

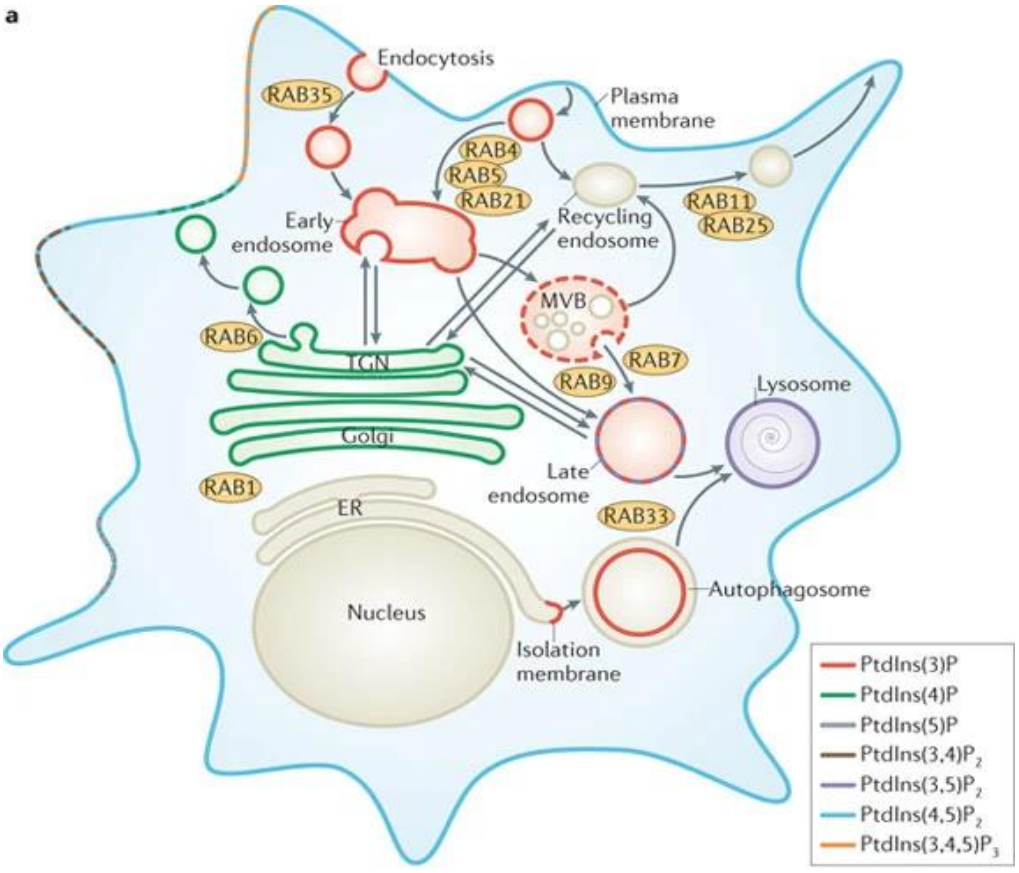

Figure 1.6. Simplified schematic of examples of RAB GTPases and PIPs enrichment to cellular compartments and stages of vesicular trafficking (from Jean and Kiger, 2012).

Out of the distinct RAB-regulated cellular pathways, the endosomal pathways are some of the best studied. Interestingly, these pathways are often found hijacked by bacterial pathogens. The endosome is a compartment specializing in the recycling and sorting of lipids and proteins from different vesicular trafficking pathways. Multiple RABs are involved in distinct functions of this compartment.

The early endosome is a compartment involved in the sorting of cargo, forming sorting tubules towards the recycling endosomes or forming intraluminal vesicles and characterized by its RAB5 recruitment, which exists in 3 isoforms: RAB5A, RAB5B, RAB5C (Chen et al. 2014, Sardana and Emr, 2021). The GEF Rabex5 is presumed to lead to RAB5 recruited to endosomes by forming a complex with the RAB5 effector Rabaptin 5 (Horiuchi et al. 1997, Mattera et al. 2006). There, RAB5 coordinates several events, of which early endosome biogenesis, sorting and maturation through its effectors, of which VPS34, APPL1, TRAP1 and tethering factors EEA1 and the CORVET complex to name a few (Langemeyer et al. 2018, Borshers et al. 2021). This recruitment of RAB5 triggers the recruitment of the CORVET complex which permits to endosome homotypic fusion with APPL1-positive endosomes (Kümmel and Ungermann, 2014, Lachmann et al. 2014, Perini et al. 2014). Rab5 also recruits the PI3-kinase VPS34 which converts PI into PI(3)P, leading to (Murray et al. 2002, Shin et al. 2005). This PI(3)P enrichment, together with RAB5 provides the identity of the early endosome compartment. This also leads to the recruitment RAB5 effectors Rabenosyn5 and tethering factor EEA1 through its FYVE domain enabling endocytic vesicle fusion with the early endosome (Simonsen et al. 1998, Nielsen et al. 2000, Kümmel and Ungermann, 2014). Following vesicle fusion, the early endosome matures towards lysosomal fusion through the switch of RAB5 for RAB7 (Poteryaev et al. 2010). VPS34-mediated PI(3)P recruitment leading to RAB5 negative regulation, and promoting RAB7 transition by recruiting the RAB7 GEF, the Mon-1-Ccz1 complex (Poteryaev et al. 2010, Cabrera et al. 2014, Lawrence et al. 2014).

At the level of recycling endosomes, RAB11 is the main RAB coordinating the sorting of membranes proteins and lipids towards the plasma membrane (Ullrich et al. 1996). Three isoforms of RAB11 have been described, RAB11A, RAB11B and RAB25 with RAB11A being ubiquitously expressed and RAB11B and RAB25 being tissue-specific (Lai et al. 1994, Goldenring et al. 1996). Whereas RAB5 coordinates endocytic trafficking, RAB11 controls membrane trafficking to the plasma membrane and is known for mediating the “slow” recycling pathway to the endosomal recycling compartment (ERC) (Grant and Donaldson, 2009). In membrane trafficking, RAB11 has been shown to regulate vesicle tethering to the plasma membrane through its interactions with Exocyst complex (Welz et al. 2014). Among the RAB11 effectors, Sec15 -a subunit of the exocyst complex- interacts with RAB11 on the endosome-derived vesicle which is thought to recruit the exocyst complex for plasma membrane tethering of the vesicle (Zhang et al.

2004, Wu et al. 2005). Other functions of RAB11 involve its recruitment of motor proteins promoting vesicle trafficking through the microtubule network of the cell. This has been proposed to occur by binding of RAB11 to protein adaptors which interact with microtubule motor proteins. A diversity of microtubule motor proteins-RAB11 complex have been described (Welz et al. 2014). Many pathogens have hijack both these pathways during their niche establishment.

1.2.2. Bacterial pathogens hijack compartment identity "codes" to establish their intracellular niche.

Bacteria have evolved over millennia together with their hosts and they have become expert at hijacking the eukaryotic cell vesicular trafficking pathways. As the PIP and RABs represent the key factors involved in the regulation of these endocytic and endocytic pathways, they are often directly or indirectly manipulated by intracellular bacteria to control their fate (Cossart and Roy, 2010, Pizarro-Cerdá et al. 2015). In particular, bacterial pathogens typically hijack the molecular machineries implicated in endocytic pathways to trigger their entry.

Endocytosis is the process of invagination of the plasma membrane leading to the uptake of an extracellular compound through the remodeling of the underlying actin network into a membrane-derived vesicle which subsequently fuses with endolysosomal compartments (Johannes et al. 2015). Multiple endocytic mechanisms coexist in the cell and are tightly regulated (Johannes et al. 2015, Thottacherry et al. 2018) (see Figure 1.7). These endocytic processes differ in their function, in the extracellular material internalized, their fate and the molecular pathways involved.

Phagocytosis is a process which enables the ingestion of large particles by professional phagocytes (e.g. neutrophils, macrophages and dendritic cells) by receptor-mediated recognition (Flannagan et al. 2012, Gordon et al. 2016). In the case of antibody-bound particles, recognition of the antibody constant region to Fc receptors on the phagocyte membrane triggers Cdc-42/N-WASP-mediated actin polymerization leading to the formation of filopodial membrane extension and subsequently Rac1-mediated particle internalization (Doherty and McMahon, 2009). The vesicle formed, termed "phagosome", is tightly wrapped around the internalized particle and undergoes acidification and the selectively fusion with lysosomes to undergo degradation (Segal et al. 1081, Tan and Russell, 2015, Gordon et al. 2016).

Macropinocytosis, is another process of large particle engulfment (>0.5µm). However, unlike phagocytosis, macropinocytosis is the non-selective uptake of extracellular particles (Thottacherry et al. 2018). Macropinocytosis has been reported to require the regulation by small GTPases ARF6 and Rac1 and additionally, the generation of PI(4,5)P2 to the plasma membrane has been shown to be necessary to macropinosome formation (West et al. 1989, Egami et al. 2014). Macropinocytosis, unlike phagocytosis which takes the shape of the engulfed particle, leads to the formation of heterogeneously sized-vesicles which are formed by the collapse of curved membrane ruffled at the plasma membrane (Egami et al. 2014).

Whereas phagocytosis and macropinocytosis endocytose large particles, smaller particles are internalized by the cells through other pathways.

Chlathrin-mediated endocytosis, mediates the endocytosis of plasma membrane receptors by recognition of a motif at the cytoplasmic tail of receptors through adaptor proteins (Brown and Goldstein, 1979, Praefcke and McMahon, 2004, Thottacherry et al. 2018). This leads to the recruitment of clathrin, a scaffolding protein for vesicle formation, to the local membrane and the formation of a clathrin-coated pit (Edeling et al. 2006). Further along, membrane bending occurs through the action of specialized proteins (FBP17, SNX9, amphiphysin) (Taylor et al. 2011). The vesicle is then excised from the plasma membrane through the dynamin-mediated fission and subsequently, clathrin-coat disassembly and endoslysosomal fusion (David el al, 1996, Kirchhausen et al. 2014).

Caveolae-mediated endocytosis, is a clathrin-independent endocytic process involved in multiple cellular functions such as mechanotransduction and membrane repair through membrane invaginations called “caveolae” (Thottacherry et al. 2018). Caveolae are formed by the association of caveolins and cavins which an ensemble of lipids in microdomains (Mayor and Pagano, 2007, Parton et al. 2019). Once formed, caveolae uptake occurs then with the pinching of the vesicle through dynamin (Henley et al. 1998).

Many other endocytic routes have been described in the cells, such as **CLIC/GEEC endocytosis**, **Flotillin-mediated endocytosis** and **Fast endophilin-mediated endocytosis** however, the molecular mechanisms involved in these pathways as well as their functions remains unclear.

These endocytic vesicles generated through these pathways present specific fates depending on their origin with some destined for fusion with the early endosomes, the recycling endosome or the lysosomes (see Figure 1.7). These fates are controlled by RAB GTPases and the PIPs. Intracellular bacterial pathogens

have developed clever strategies to manipulate these pathways through manipulation of these factors. It should be noted that pathogen uptake is different from default endocytic pathways as they require to establish pathogen-specific niches that are different from the compartments trafficked by non-pathogenic cargo (for example the lysosome or the recycling endosome).

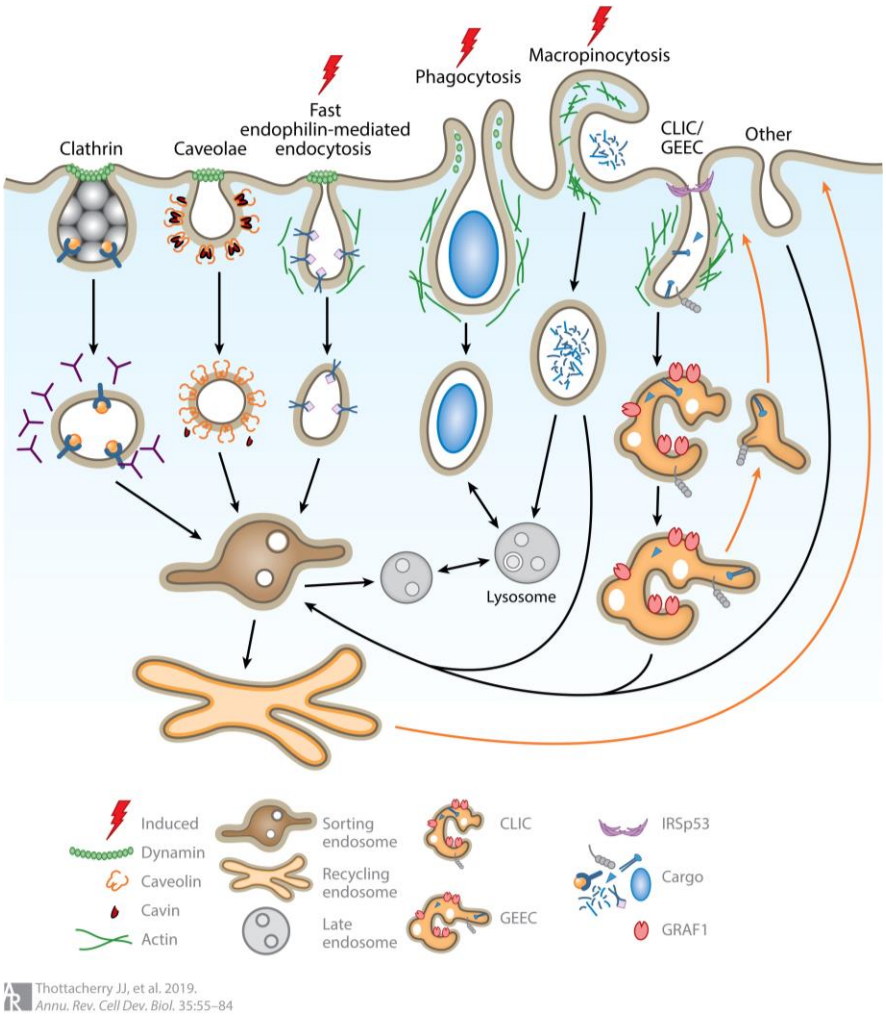

Figure 1.7. Illustration of the endocytic pathways and their interactions with cellular organelles (from Thottacherry et al. 2018)

Endocytosis requires the regulation of membrane PIPs for the displacement of the membranes. This process involves the sequential modification of PIPs through the aforementioned enzymes, with distinct PIPs recruitments depending on the endocytic pathway. This is essential to the deformation of the membrane and closure of engulfment compartments, since PIPs act as scaffolds for the molecular actin remodeling machinery usually through the recruitment of small GTPases and their corresponding effectors (Swanson, 2014). PIPs are often the target of pathogens due to their critical roles in membrane trafficking, leading to

a bacteria-driven remodeling of the actin network and subsequently their entry. Exemplarily, through the bacterial effector InlB, the cytosolic pathogen *Listeria monocytogenes* indirectly recruits the PIP kinases PI3K and PI4K through the activation of the plasma membrane receptor Met (Ireton et al. 1999, Pizarro-Cerdá et al. 2007). These kinases produce respectively PI(3,4,5)P_3 and PI(4)P which induce its entry. Some bacteria also contain specific bacterial effectors which modify phospholipids. The *Salmonella enterica* effector SopB is both a PI(4)P and PI(5)P phosphatase and catalyzes the formation of PI(3)P and PI(3,4)P_2 which is crucial for the formation of membrane ruffling, thus essential for engulfment of the bacterium (Piscatelli et al. 2016). Recently, SopB has also been found to act as phosphotransferase that generates PI(3,4)P_2 from PI(4,5)P_2 (Walpole et al. 2022).

Intracellular bacterial pathogens require a host for their survival and proliferation. The host cell cytosol being rich in nutrients and providing a safe haven from the humoral immune pathways enables intracellular bacteria to thrive. However, prior to reaching such a sanctuary, successful entry is necessary, and furthermore the pathogen requires to avoid the host cell's defense pathways that recognize invaders at different locations. Independent of the uptake pathway, all pathogens enter within membrane-enclosed compartment that is called phagosome for professional phagocytic cells, and endosomes for other cell types. The resulting vesicular compartment fuses with lysosomes or is subject to autophagy leading in both cases to the degradation of the vesicle cargo. Bacterial pathogens have adapted to avoid these degradation pathways either by (i) escaping into the cytosol where they are able to hijack the actin machinery (*Shigella, Listeria, Francisella*) or (ii) by forming a replicative niche within a modified endomembrane-bound compartment called the bacterial containing vacuole (*Salmonella, Yersinia*) (Cossart and Sansonetti, 2004). The establishment of these niches require bacteria to hijack specific host cell molecular pathways, in particular the membrane trafficking pathways (Cossart and Sansonetti, 2004).

Strategies deployed by these engulfed bacterial pathogens involve the control of membrane trafficking by both recruiting and inhibiting specific RAB GTPases and manipulating the PIPs. *Legionella pneumophila* illustrates this by recruiting RAB1 following entry in the *Legionella*-containing vacuole (LCV) through multiple bacterial factors (DrrA, LidA, LepB, SidM) by manipulating the regulation of RAB1, while at the same time sequestering the host PI(4)P to the LCV to drive the fusion of ER-derived vesicles to the LCV (Newton et al. 2010). This specific subversion of host exocytosis trafficking promotes the formation of the LCV. On the other hand, *Legionella* excludes the endocytic pathways by inhibiting fusion of the LCV to the host endocytic compartments by sequestering RAB5 and RAB22 to the endosomes, thus avoiding vacuole maturation by the endocytic pathway and lysosomal degradation (Weber and Faris, 2018, Ku et al. 2012, Lucas et al. 2014).

Inversely, pathogens often hijack the RAB/PIP pathways to prevent fusion of the bacterial vacuole to the lysosome. *Salmonella enterica* triggers the maturation of the *Salmonella*-containing vacuole (SCV) by recruiting the class III PI3-kinase VPS34 through the bacterial kinase/phosphatase SopB leading to the production of PI(3)P at the SCV. This recruits the tubule-generating protein Sorting Nexin 1 and leads to the formation of the *Salmonella*-Induced Filaments (Pizarro-Cerdá et al. 2015). Lysosome function is attenuated by sequestration of RAB9 by the bacterial effector SifA to enable survival of *Salmonella* inside the SCV while enabling lysosome fusion to the SCV to supply membranes and nutrients (McGourty et al. 2012, Jennings et al. 2017).

Bacterial pathogens also hijack the autophagy machinery to their profit (Brumell, 2012, Choy and Roy, 2013, Mostowy, 2013). *Brucella arbortu*s, a pathogen responsible for brucellosis in humans, forms a autophagosome-like compartment after internalization which acquires autophagy markers Beclin1 and ULK1 (Starr et al. 2012). This has been proposed to promote bacterial egress and spread to neighboring cells. Similarly, the *Coxiella*-containing vacuole (CCV) has been reported to be labelled with autophagy markers LC3, Beclin1 and p62 and have been conjectured to enable growth of the CCV compartment (Romano et al. 2007, Vazquez and Colombo, 2009, Winchell et al. 2014). It is important to note that *Shigella* also hijacks the autophagy machinery to prevent its degradation. Reports showed *Shigella* bypasses the autophagy degradation pathway by recruiting to the its vacuole the bacterial effectors IcsB which immobilizes TOCA-1 preventing the recruitment of autophagy markers (LC3 and others). Moreover, the bacterial effectors IcsB was shown to mask IcsA from the autophagy machinery ATG5 (Ogawa et al. 2005, Mostowy et al. 2010, Mostowy et al. 2013). Additionally, after *Shigella*-BCV rupture, the *Shigella* effector VirA has been reported to inactivate RAB1 to inhibit autophagosome formation (Dong et al. 2012).

These examples of bacterial pathogens show the versatility of intracellular bacterial pathogens with regards to the host trafficking pathways.

1.2.3. *Shigella* manipulates the host endosomal pathways to establish its niche

The contribution of the host in the case of cytosolic bacteria has remained unclear for a long time. Contrary to bacterial pathogens inhabiting an endomembrane-bound compartment as replicative niche, cytosolic bacteria must go through the critical step of escaping the bacterial vacuole and its membrane. Besides, this,

the study of *Shigella* has also provided general insights into how cytosol-residing bacteria subvert host factors to induce their entry into a compartment that can subsequently be destabilized.

As mentioned previously, *Shigella* triggers massive rearrangements of the actin network leading to large-scale membrane ruffling triggering the engulfment of the pathogen into a tight phagosome-like vacuole (the BCV) and the formation of IAMs. Similar to macropinosomes, IAMs are vesicles of varying diameter (>0.2µm-5µm) formed during this remodeling of the plasma membrane. Classically, IAMs were considered a byproduct of *Shigella* entry, however in-depth studies performed in the laboratory of this PhD thesis have shown an active role these bacteria-triggered compartments in promoting *Shigella* invasion.

In physiological conditions, macropinocytosis occurs only in some cells. A prominent example are macrophages, which form macropinosomes to sample the extracellular environment for non-self particles (such as pathogens). They are formed and mature in several steps regulated by small GTPases and PIPs (Egami et al, 2014) (see Figure 1.8). Macropinosome formation start with the ruffling of the plasma membrane triggered by the activation of the small GTPases ARF1/6 and Rac1 (see Figure 1.8) (Radhakrishna et al. 1999, Zhang et al. 1999, Fujii et al. 2013, Egami et al. 2014). It is important to note that a plethora of small GTPases have been linked to macropinocytosis formation however, many seem to be cell type-specific (Egami et al. 2014). In response to ARF6 and Rac1 activation the kinase PI4P5K which phosphorylates PI4P into $PI(4,5)P_2$, which mediates the start of membrane ruffling by recruiting the actin nucleation machinery. Afterwards, $PI(4,5)P_2$ membrane levels decrease in part by conversion into $PI(3,4,5)P_3$ by the class I PI3K kinase. $PI(3,4,5)P_3$ in turn recruits several factors (*e.g.* ARNO and Akt) which lead to actin depolymerization through actin depolymerization factors ADF/Cofilins (Rupper et al. 2001, Araki et al. 2007). Together with Rac1 deactivation, this leads to macropinosome cup closure. It is to note that afterwards $PI(3,4,5)P_3$ goes through a sequence of conversions at the membrane by other enzymes such as the 5-phosphatase SHIP into $PI(3,4)P_2$ (Egami et al. 2014). The resulting vesicle, defined as an early macropinosome, later acquires RAB5, PI(3)P and other markers such as EEA1. Recently, Spangenberg et al. (2021) reported that PI3P maturation occurs through the RAB5 effector VPS34, a PI3P kinase. In this paper, both PI3P formation and RAB5 recruitment were found to be crucial for macropinosome formation. then matures into a late macropinosome by acquiring $PI(4,5)P_2$ and RAB20, RAB21 and RAB7 (Egami et al. 2014). Afterwards macropinosomes are either recycled back to the plasma membrane or fuse with the lysosome for degradation.

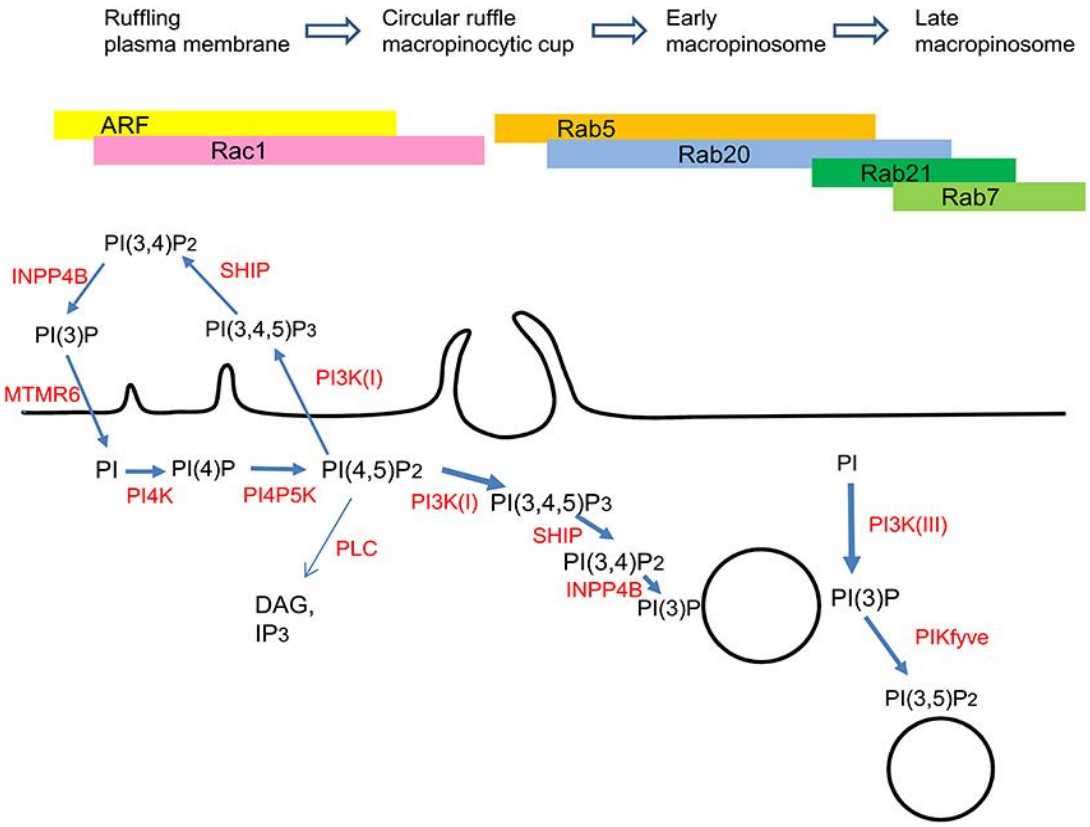

Figure 1.8. Sequential RAB small GTPases and PIP recruitment during canonical macropinosome formation and maturation (from Egami et al. 2014).

Similar in their formation to canonical macropinosomes, *Shigella*-IAMs are triggered by Rac1 activation/deactivation by the bacterium and a later acquisition of Rab5A and PI(3)P as early markers (Mellouk et al. 2014). The formation of *Shigella*-IAMs required the injection of IpgD, the *Shigella* phosphoinositide 4-phosphatase, through the T3SS. The *Shigella ipgD* mutant strain was able to enter into targeted enterocytes, however IAMs were no longer observed (Mellouk, 2014, Weiner 2016). Through this work it emerged that *Shigella*-IAMs do not play an important role for pathogen uptake, however they were found to play a key role in the subsequent intracellular niche formation (with the *ipgD* mutant affecting *Shigella*-BCV rupture). In this context, BCV-IAM contact sites were shown by Correlative Light Electron Microscopy (Weiner et al. 2016). Within the same sequence of studies, an interference RNA high-content screen revealed a role of the host factor RAB11A in promoting BCV rupture (Mellouk et al. 2014). Surprisingly, RAB11A was found absent at the *Shigella*-BCV but was enriched at the IAMs surrounding it. This was also found to be controlled by IpgD. Furthermore, recent work showed that not only does RAB11A promote efficient BCV rupture, but together with another RAB, namely RAB8A, leads to the recruitment of the exocyst complex to the IAMs (Chang et al. 2020). This pathway was shown to be hijacked

by *Shigella* to promote efficient separation between the BCV membrane remnants and the entering bacteria upon the initial damage of the BCV. Interestingly, *Shigella* was also found to form a thick actin structure surrounding the BCV prior to rupture and is thought to be triggered by the bacteria in order to prevent premature BCV rupture by the IAMs (Ehsani et al. 2012, Kühn et al. 2020). The actin cocoon is controlled by another T3SS effector named IcsB that acts as an acylase of host GTPases (Liu et al. 2018). How the actin cocoon regulates the intracellular niche formation of *Shigella* requires further investigation. Together, these results show a much more important role of IAMs during the steps after the initial *Shigella* invasion with a critical role of endosomal trafficking factors. These works also highlight the importance of studying the IAM-BCV communications and the roles of IAMs.

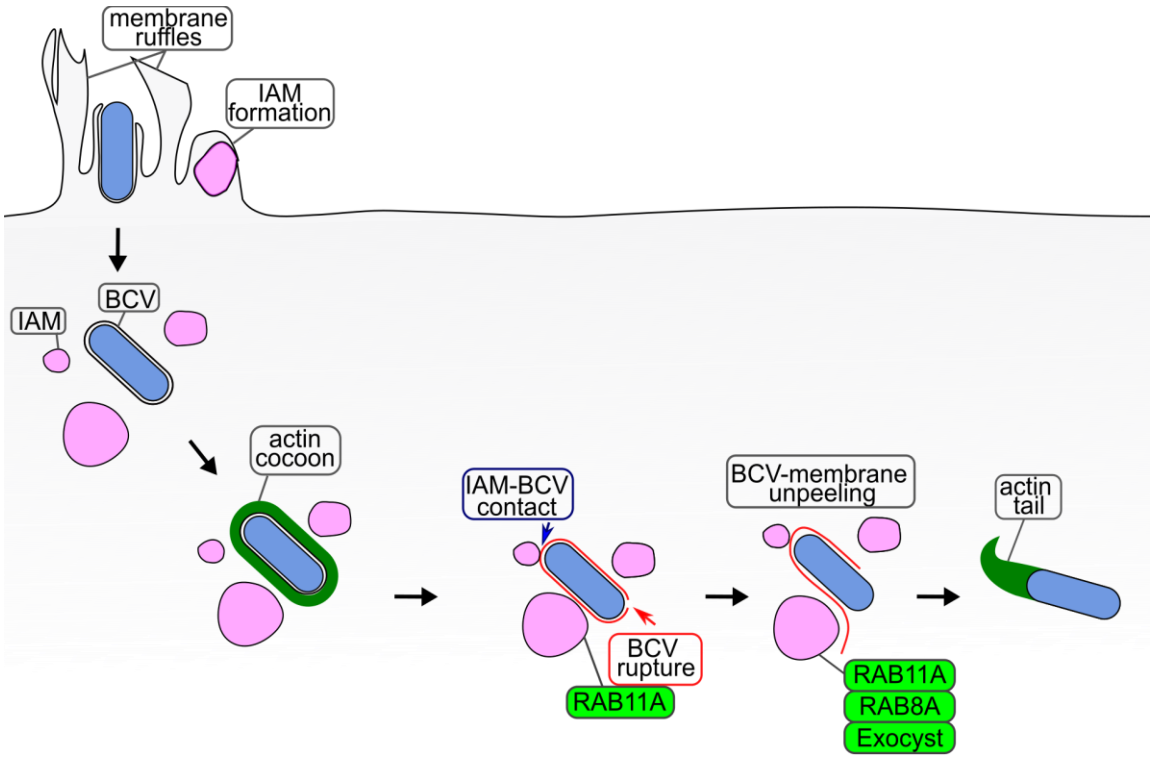

Figure 1.9. Interactions between IAMs and the BCV during *Shigella* entry

The new proposed model of *Shigella* invasion following internalization of *Shigella* within the BCV and the formation of IAMs, the bacterium subverts the actin machinery to form a thick actin structure around the BCV termed "actin cocoon", preventing early contact between IAMs and BCV. Upon disassembly of the actin cocoon, the IAM-BCV communications as well as the recruitment of the host factor RAB11A to IAMs promotes the BCV rupture. The bacterium then invades the host cell cytosol by unpeeling the BCV-membrane remnants from itself through the enrichment to IAMs of RAB11A, RAB8A and the exocyst complex. It is then free to invade neighboring cells.

1.3. Bacterial pathogens invasion requires membrane remodeling

1.3.1. Membrane remodeling as an essential cellular process and its role during bacterial invasion

Lipid membranes are the physical barriers comprising cell and organelle architecture which separate two distinct environments. Communication is essential for cell and organelle function, survival and defense, making it imperative for membranes to be rapidly deformable. Classically, membrane deformation was considered to be a passive action transpiring as a result of the underlying cellular processes. However further research showed membranes to be actively remodeled by local changes in lipid and protein composition through a series of well-orchestrated complex events and to play key functions (McMahon and Gallop, 2005, McMahon and Boucrot, 2015, Simunovic et al. 2015).

Membrane curvature can be of two forms: convex/positive curvature where the membrane curves to the outside of the compartment or a concave/negative curvature in which the membrane curves inward. One of the main mechanisms (see Figure 1.10) of membrane curvature generation and stabilization has been shown to be the shape of lipids. The size and composition of the lipid head group and acyl chain (number, length and saturation) varying from one lipid to another, this impacts the shape each lipid occupies in space (McMahon and Gallop, 2005, McMahon and Boucrot, 2015). Interestingly, membranes regulate their lipid composition (such as the PIPs for instance) and even create lipid asymmetries in the lipid with a strong impact on membrane shape and creating local membrane reshaping. Proteins have also been shown to play an important role in membrane reshaping. Transmembrane proteins have been proposed to influence membrane shape through the shape of their membrane-inserted domain or by the shape of their extramembrane domain (Unwin, 2005, Aimon et al. 2014, Copic et al. 2012, Fribourg et al. 2014). The reversible insertion of small hydrophobic motifs such as amphipathic helixes (Ford et al. 2002, Campelo et al. 2008, McMahon et al. 2010) or hydrophobic loops (Groffen et al. 2010, Plomann et al. 2010) has also been proposed to change the shape of membranes by wedging themselves to membranes. The impact of these membrane reshaping mechanisms on the membrane can be further amplified by protein clustering (e.g. transmembrane receptor crowding, the oligomerization of proteins, etc) (Copic et al. 2012, Stachowiak et al. 2012). Interestingly, cytoskeleton scaffolding can act as a platform to promote and support membrane curvature (McMahon and Gallop, 2005, McMahon and Boucrot, 2015). Such is the case for instance for filopodia and lamellipodia. Collectively, it is the synergistic action of this ensemble of mechanisms which cause membrane reshaping during cellular processes.

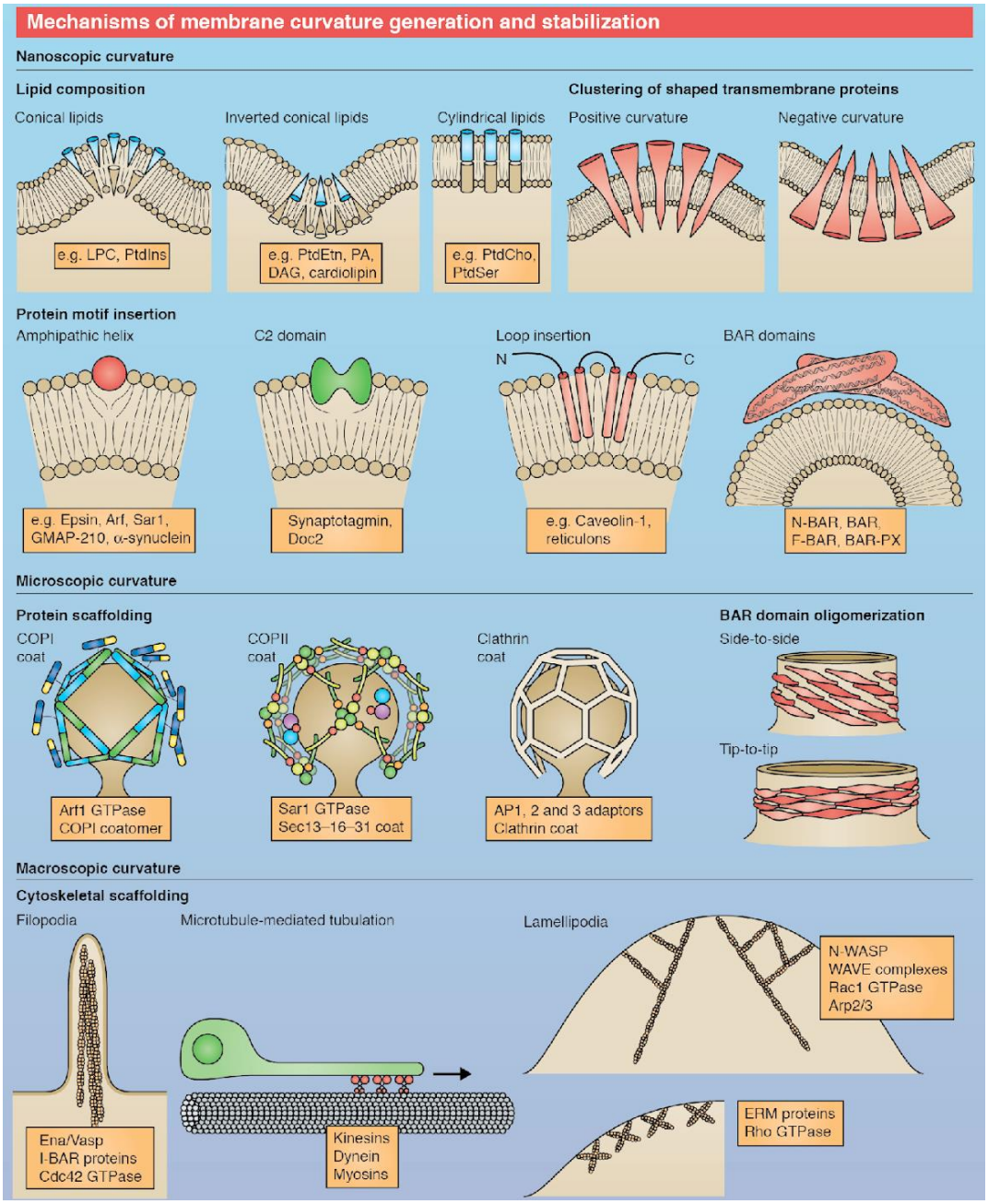

Figure 1.10. Schematic of the types of molecular mechanisms of membrane remodeling (from McMahon and Boucrot, 2015).

Membrane shaping occurs at different scales: (i) the nanoscopic scale where lipid shape (conical, inverted conical and cylindric) and membrane-bound proteins such as transmembrane proteins and hydrophobic domains (e.g. C2 domains, amphipathic helixes and loop insertions) provoke nanoscopic changes to the membrane. (ii) Protein scaffolding and oligomerization provoke a more drastic change in the membrane creating microscopic curvature changes (e.g. vesicular trafficking, endosomal recycling). (iii) Lastly, the

actin and microtubule cytoskeleton support reshaping of the membrane by acting as an underlying scaffold (e.g. filopodia, by acting as a scaffold to motor proteins or lamellipodia).

Membrane curvature is an essential mechanism to the cell, with distinct cellular processes involving and requiring reshaping of membranes. (i) Membrane curvature defines the architecture of the cell with organelles having distinctive shapes making them recognizable by electron microscopy. However, these shapes are also dynamic, changing during organelle maturation (e.g. vesicle fission and fusion) or depending on the needs of the cell (e.g. mitochondrial fission and fusion, endosomes membrane tubulation) (Shibata et al. 2009, Rafelski and Marshall, 2011) (see Figure 1.11) (ii) Another process highlighting the importance of membrane deformability is protein sorting, an essential process for the cell to regulate its signaling pathways. This event occurs at the level of the recycling endosomes and occurs by the formation of cargo-bearing tubules (Cullen and Korswagen, 2012). (ii) Interestingly, membrane curvature has been shown to be important in membrane vesicle directionality. Vesicle targeting has been shown to involve curvature sensing proteins, with proteins such as GMAP-210 in the Golgi or ATG14 in autophagosome biogenesis sensing specific curvatures (Drin et al. 2008, Fan et al. 2011). (iii) Membrane curvature is also critical for membrane fusion, with the shape of membrane vesicles trafficked due to lipid and membrane-bending protein composition has been shown to accompany SNARE fusion proteins in promote membrane fusion (Groffen et al. 2010, Snead et al. 2014). (iv) Lastly, membrane curvature may also play an important role in protein sorting. Transmembrane protein shape has been proposed to favor the organization of these proteins in microregions forming a curved region of membrane which may prime this region for vesicular trafficking (Unwin, 2005, Aimon et al. 2014). This mechanism has been further supported by the existence of curvature sensing (and inducing) sorting factors such as the ESCRT complex and Sar1 (COPII coat) (Cullen and Korswagen, 2012, Okamoto et al. 2012).

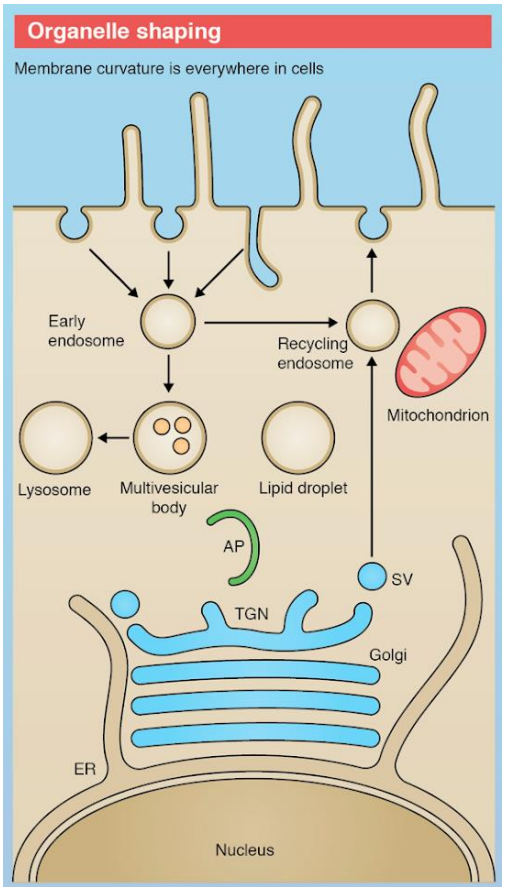

Figure 1.11. Membrane curvature-dependent cellular compartments and events. (from McMahon and Boucrot, 2015)

Interestingly, intracellular bacterial pathogens invasion involves imposing membrane curving and remodeling of the membrane during the successive entry steps. Bacteria entry requires an extensive

remodeling the plasma membrane through changes in lipid composition and remodeling the underlying actin network leading to the induction of membrane curvatures to form membrane sheet (Swanson, 2008, Cossart and Roy, 2010, Swanson, 2014, Ribet and Cossart, 2015, Buckley and King, 2017). Further curvature of these membrane sheets leads to the collapse of pathogen-induced ruffles leading to its engulfment. Such pathogens are then ingested within a vacuole curled around the bacterium which is later on extensively remodeled by the pathogen's effectors to form a replicative niche or trigger vacuole lysis (Finlay and Cossart, 1997, Gruenheid and Finlay, 2003). The pathogen-containing vacuole is also frequently remodeled and reshaped by the pathogen by the fusion of the vacuole with membrane compartments (e.g. trafficked vesicles) to form an intracellular niche for the pathogen. Some pathogens also induce the formation of membrane curved tubules in their replicative niche (Bujny et al. 2008, Stévenin et al. 2018). Collectively, these observations also highlight a function of membrane curvature in pathogen invasion.

1.3.2. The Bin/Amphyphisin/Rvs (BAR) domain-containing protein family

Many proteins are known to regulate membrane curvature in diverse ways during specific cellular processes (McLMahon and Gallop, 2005, Suetsugu et al. 2009, McMahon and Boucrot, 2015). One family of proteins has been particularly well-characterized and shown to specialize in membrane curvature reshaping and sensing (McMahon and Gallop, 2005, Allison Suarez et al. 2014, Simunovic et al. 2015). Bin/Amphyphisin/Rvs (BAR) domain-containing proteins are characterized by a banana-shaped domain called the BAR domain. This particular region has been conjectured to be involved the membrane shaping and sensing characteristic of BAR proteins, although the precise function of the BAR domain is unclear (Peter et al. 2004 Bhatia et al. 2009, Simunovic et al. 2015, Simunovic et al. 2019). BAR domains have different shapes and based on this aspect, BAR domain-containing proteins are involved in concave or convex membrane curvature processes. Often containing a PIP binding domain (*e.g.* a PX domain, PH domain) and in the case of some members, an amphipathic helix, these proteins have been shown to bind to cellular membranes (Bhatia et al. 2009, Van Weering et al. 2012). Many BAR domain-containing proteins contain protein-protein interaction domains (such as a GAP, SH3, PDZ domains) leading them to act as signaling platforms (Salzer et al. 2017, Simunovic et al. 2019). Some of these BAR domain-containing proteins have also been described as acting as scaffolds through protein clustering in diverse cellular processes (Dawson et al. 2006, Simunovic et al. 2016, Simunovic et al. 2019). Given their different varieties and the importance of membrane remodeling, they have been found to be involved in a plethora of cellular processes requiring membrane reshaping (Simunovic et al. 2015, Simunovic et al. 2019).

Although the precise function of the BAR domain-containing proteins remains elusive, BAR domain proteins function together with RAB GTPases and PIPs (Van Weering et al. 2010, Salzer et al. 2017, Simunovic et al. 2019). In many cases BAR domain-containing proteins seem to be recruited through PIPs and/or regulate RABs or be effectors of RABs. Despite their similarity in BAR domain structure, different BAR domain proteins leading to different actions, raising the questions as to how BAR domain proteins are regulated. Computational modeling has proposed that behavior of the BAR domain protein varies under some conditions (Simunovic et al. 2015). At a high density of membrane attached BAR domain proteins, BAR domain proteins would induce membrane tubulation and scaffolding whereas at low density binding, they may rather function in curvature sensing (Simunovic et al. 2015).

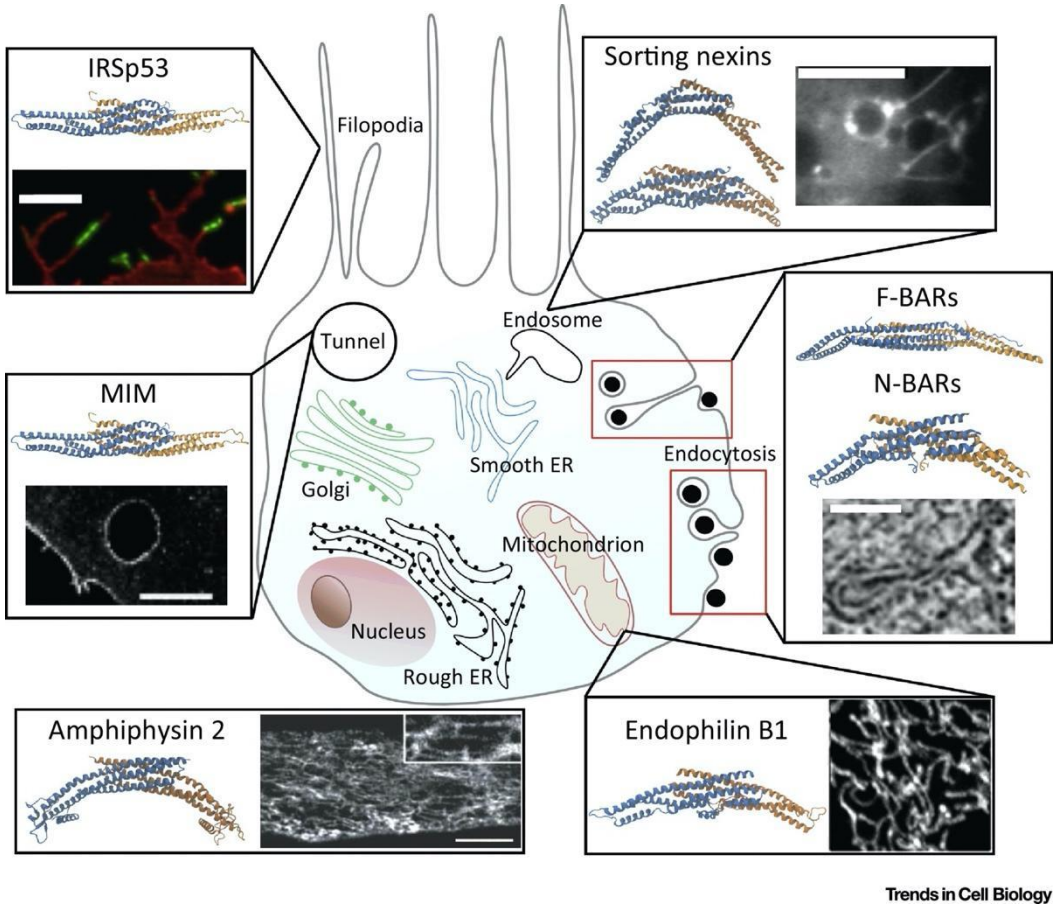

Figure 1.12. Schematic depicting examples of BAR domain-containing proteins involvement during cellular processes (from Simunovic et al. 2019).

Invasive bacteria have also been reported to exploit BAR domain proteins for their invasion and niche establishment. Bacterial pathogens often target the host actin network which they remodel for their entry or niche establishment. Some BAR domain-containing proteins interact with the actin machinery to regulate the actin network (Dawson et al. 2006, Zhao et al. 2011, Carman and Dominguez, 2018). Enterohemorrhagic *E. coli* for instance was shown to hijack I-BAR IRSp53 to the host cell membrane to trigger remodeling of the actin network leading to the formation of an actin pedestal in which reposes the bacterium (Morita-Ishihara et al. 2009, Weiss et al. 2009, Yi and Goldberg, 2009). Following cytosol access, some bacterial pathogens, such as *Shigella* or *Listeria* form an actin comet tail enabling their invasion of neighboring cells (Frischknecht and Way, 2001, Cossart and Sansonetti, 2004). To achieve this, they must traverse both the host cell and the neighbor plasma membrane forming a protrusion. *Listeria* was found to target BAR domain factor Tuba which interacts with actin regulating factors (N-WASP, etc) by its bacterial effector InlC to efficiently form such protrusions (Salazar et al. 2003, Rajabian et al. 2009, Polle *et al*., 2014). More recently, *Listeria* was also found to subvert caveolae regulating F-BAR protein PACSIN2 to neighboring cell membranes to promote its invasion into the new host (Hansen et al. 2011, Senju et al. 2011, Sanderlin et al. 2019, Dhanda et al. 2020). On the other hand, vacuolar pathogens remodel the bacterial vacuole. *Coxiella burnetii* was shown to hijack BAR domain protein FCHO2 which regulates clathrin-mediated endocytosis to promote bacterial replication through biogenesis of the bacterial vacuole (Latomanski et al. 2016).

Shigella has also been reported to reprogram at least one BAR domain protein. Following internalization, *Shigella* has been shown to form an actin cage around the BCV. This involves the immobilization of TOCA-1, a BAR protein activating actin assembly factor and small GTPase Cdc42 forming branched actin filaments, to the BCV in an icsB-dependent manner (Kühn et al. 2020). It has been proposed thata this prevents early IAM-BCV interaction and impedes early BCV-rupture. Moreover, to trigger actin tail formation, *Shigella* has also been reported to sequester TOCA-1 via IcsB (Ho et al. 2004, Leung et al. 2008, Baxt and Goldberg, 2014).

1.3.3. The particular case of SNX-BAR containing proteins and their subversion by bacterial pathogens

Endosomes are essential cellular compartments within the eukaryotic cell architecture. This key compartment mediates the intracellular fate of proteins and lipids from incoming cargo-bearing vesicles from the endocytic pathways, and further observations also point at a connection between endosomes and the secretory pathway (O'Sullivan and Lindsay, 2020). Endosomes mature throughout the course of their

interactions with trafficking vesicles by acquiring new PIP and RAB "identities" over time. Protein and lipids from incoming vesicles are sorted in this compartment, they are either further delivered to the destructive lysosomal pathway or they are recycled (Van Weering et al. 2012). Remarkably, invasive pathogens have been shown to target the host endosomal recycling pathways to establish their intracellular niche and replicate. Exemplarily, *Legionella* has been reported to inhibit retromer activity through binding of the bacterial effector RIDL to the retromer subunit VPS29 together with PI(3)P to promote intracellular replication (Finsel et al. 2013, Yao et al. 2018). Other intracellular-living bacteria such as *Salmonella enterica* serovar Typhimurium, *Chlamydia trachomatis*, *Burkholderia cenocepacia* and *Coxiella burnetii* have been reported to hijack this endosomal recycling pathways (Yong et al. 2020). Viral pathogens like the Human papillomaviruses and SARs-CoV-2 have also been shown to manipulate these pathways (Daniloski et al. 2020, Gordon et al. 2020, Yong et al. 2020, Cattin-Ortolá et al. 2021).

One particular subfamily of BAR domain-containing proteins has been shown to play an important role in endosomal recycling, the Sorting Nexin-BAR (SNX-BAR) family, and has been linked to bacterial invasion (Cullen, 2008). Composed of 12 proteins, the SNX-BAR proteins are all found in the endosomal recycling pathway and form tubules recycling endosomal membranes to the plasma membrane, the trans-Golgi network (TGN) and the endosomal recycling compartment (ERC) (Teasdale et al. 2001, Van Weering et al. 2010, Van Weering, 2014). They have been found to contain a common C-terminal BAR domain and often contain a PX domain and an amphipathic helix (Van Weering et al, 2012). They have been proposed to function in the sorting and recycling of incoming vesicles in retromer-dependent and independent endosomal recycling during clathrin-dependent and independent endocytosis (Cullen, 2008, Shortill et al. 2022). They are sequentially recruited to the endosomal recycling pathway all throughout the maturation of the endosomes. These SNX-BAR proteins are recruited during specific endosome maturation stages together with specific combinations of PIPs and RABs, in particular RAB5 and RAB7 (see Figure 1.13) (Van Weering et al. 2010, Van Weering et al. 2012). However, the PX domain lipid recognition and the BAR domain have been found to be critical for the binding of the SNX-BAR proteins to membranes (Carlton et al. 2005). Amphipathic helices have been found to play an important role in tubulation (Van Weering et al. 2012). Although much remains unclear about the molecular mechanism to their function, SNX-BAR tubule formation and scission seems to occur by coincidence-detection of a specific SNX-BAR(s) to a curved membrane enriched in its corresponding phospholipid(s) and RAB(s) leading to its binds to the membrane and subsequent hetero- or homo-dimerization through the BAR domain (Cullen, 2008, Van Weering et al. 2010). Increased binding leads to the oligomerization of the SNX-BAR protein

to the local membrane which provides the force necessary to trigger deformation of the membrane leading to tubulation (e.g. SNX1/2, SNX8) or membrane scission (e.g. SNX4) (Dawson et al. 2006, Cullen, 2008). It should be noted that most functional studies have been performed in vitro, and in vivo evidence on the action of SNX-BAR proteins requires further studies.

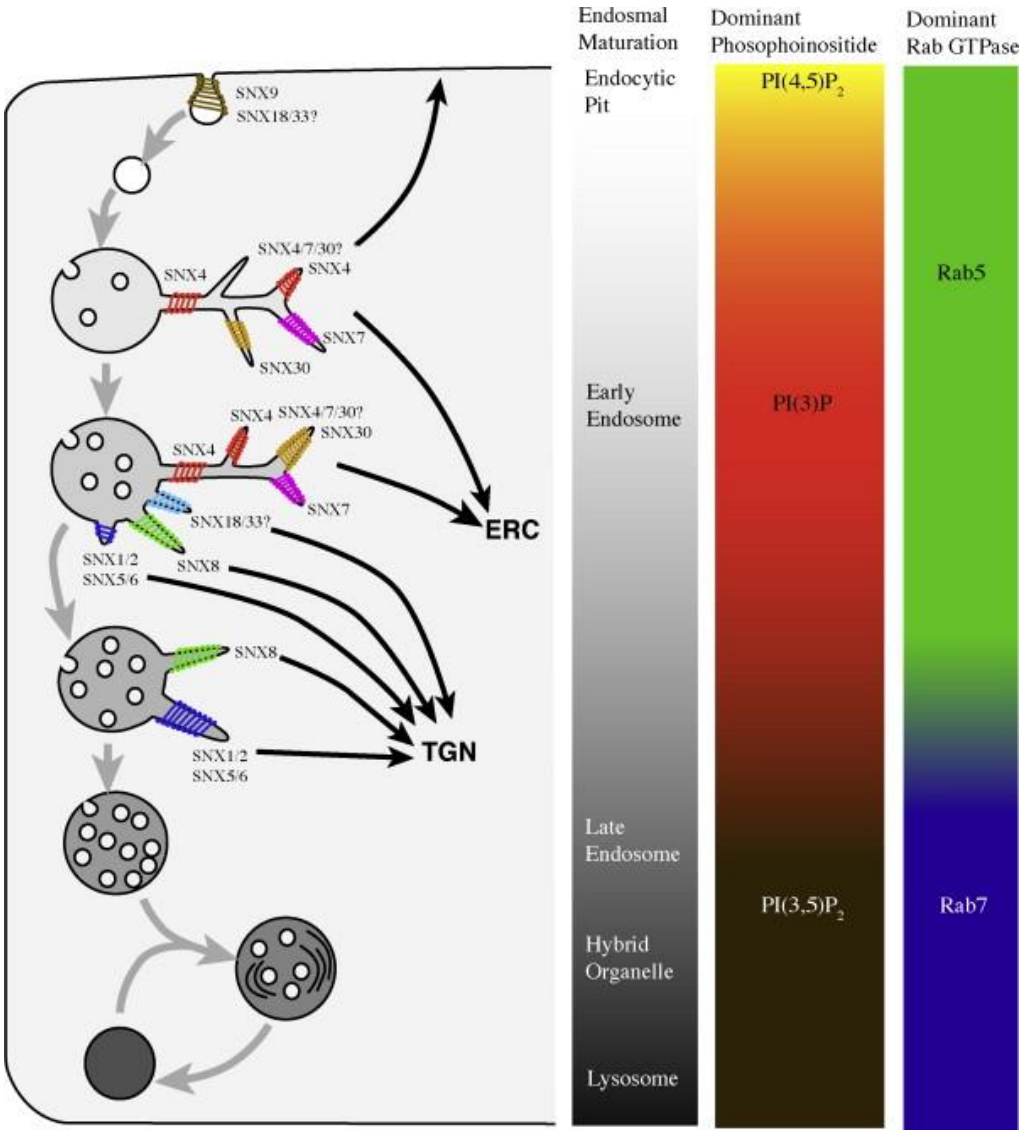

Figure 1.13. Proposed model for SNX-BAR-mediated endosomal protein sorting and recruitment together with endosomal maturation (Van Weering et al. 2010).

This figure shows the presence of diverse SNX-BAR proteins recruited to the endosome during its maturation with PIP and RAB transitions based on their affinities to these proteins. These different SNX-BAR proteins sort proteins to different compartments –the trans Golgi network (e.g. SNX8, SNX1/2), the

endocytic recycling compartment (e SNX30), the plasma membrane (SNX4)- and even catalyse the fission of membranes (SNX9).

Several intracellular bacterial pathogens have been shown to specifically hijack SNX-BAR functions. In an early study, *Chlamydia trochomatis* was shown to form a replicative niche called an "inclusion" which interacts selectively with cellular compartments (Cocchiaro and Valdivia, 2009). In this context, SNX-BAR proteins SNX5, SNX6 and SNX32 were reported as being enriched to the *Chlamydia* inclusion, forming tubules at this compartment (Mirrashidi et al. 2015). This was shown to be driven by the *Chlamydia* effector IncE which was shown to bind to the PX domain of the aforementioned SNX-BARs (Mirrashidi et al. 2015, Elwell et al. 2017) Furthermore, depletion of these SNX-BAR proteins impaired *Chlamydia* replication (Aeberhard et al. 2015, Mirrashidi et al. 2015, Elwell et al. 2017, Paul et al. 2017). *Salmonella* is another example of pathogen subverting the SNX-BAR recycling function to its profit. As in the case of *Shigella*, *Salmonella* triggers the formation of membrane ruffles to induce its internalization into a tight vacuole called the *Salmonella*-containing compartment (SCC) (Fredlung et al. 2018). SNX-18 was found recruited during Salmonella-triggered membrane ruffling by a SopB-mediated mechanism (Liebl et al. 2017). This SNX-18 recruitment was reported to promote *Salmonella* entry within the host cell. Following internalization, the early *Salmonella* containing vacuole (SCV) was also shown to form tubules enriched in the SNX-BAR SNX1 caused by SopB-mediated by PI(3)P formation (Bujny et al. 2008). This reprogramming of this SNX-BAR was shown to direct the destiny of the compartment to either rupture or formation of a *Salmonella*-replicative niche (within the SCV).

The evidence of pathogen subversion of the BAR domain-containing proteins and their importance in such a number of diverse cellular functions, highlights the potential importance of these factors in the invasion steps of intracellular pathogens. The study of the function of these factors could provide critical insights into the molecular pathways hijacked by bacterial pathogens.

1.4. Screening for host factors in the context of bacterial infection

1.4.1. The challenges of identifying bacteria-subverted host pathways

The heterogeneity of bacteria and host cells as well as the transiency of bacteria-triggered structures and invasion events poses a challenge to the identification of host factors hijacked by bacterial pathogens. Indeed, the behavior of individual bacteria and that of the different targeted host cells complexifies bacterial invasion synchronicity. As an example, implementing a homogenous invasive behavior for *Listeria* has been experimentally challenging due to the variability of individual host cell which has been reported to cause heterogeneity in bacterial adhesion and its subsequent internalization (Rengarajan et al. 2020). Additionally, bacterial events can occur very rapidly, as is the case of *Listeria* cell-to-cell spread which varies hugely among individual bacteria (Ortega et al. 2019). Similarly, *Salmonella* entry was reported to vary greatly as each individual bacterium exerts near surface swimming and assesses multiple cells before eventually deciding on invading a target cell (Misselwitz et al. 2012). Successful *Salmonella* invasion was reported to the dependent on several cellular factors unique to each cell such as cell crowding and cholesterol content and bacterial factors (Misselwitz et al. 2012, Voznica et al. 2018). Variability of the timing of infection events was also shown to depend on other factors such as the impact of bacterial cooperation on the speed of pathogen entry (Misselwitz et al. 2012, Lorkowski et al. 2014, Voznica et al. 2018). This hampers an easy interpretation of the data from assays requiring sample fixation as they do not resolve the dynamic nature of the occurring events. Adding to this complexity, in some cases bacteria adopt multiple intracellular lifestyles. *Salmonella* for one can either break the vacuole and replicate at high rates in the cytosol, it can form the *Salmonella*-containing vacuole (SCV), or remain dormant within a vacuole (Luk et al. 2021, Malik-Kale et al. 2012, Stévenin et al. 2019). This heterogeneity complicates the interpretation and data obtained from screens.

Recently, the identification of host pathways reprogrammed by bacteria has been assessed using a comprehensive proteomics-based approach of the protein content of bacteria-driven compartments (Chang, Enninga and Stévenin, 2021). This approach however, depends on the isolation of the compartments which has been an obstacle. Although these last 10 years have seen isolation techniques such as density gradient fractionation and magnetic-purification, some bacterial compartments such as the *Shigella*-BCV are not yet purifiable (Chang et al. 2020, Steinhäuser et al. 2014, Santos et al. 2015). The complexity of synchronizing bacterial pathogens and the lack of methods to properly isolate bacterial compartments emphasize the need to bypass these issues.

1.4.2. Time-lapse high-content screening to assess host-pathogen interactions

Enabling the visualization of the dynamics of specific cellular events, fluorescence time-lapse microscopy is a suitable technique. Time-lapse microcopy when coupled to fluorescence permits monitoring the behavior of host proteins localizing in their physiological environment (Lichtman and Conchello, 2005). Through the use of genetically-encoded probes, time-lapse fluorescence microscopy is a versatile technique to observe localization changes of specific factors. With regards to bacterial infection, the development of fluorescent probes has been enabling the tracking of individual intracellular bacteria. In addition, it has become possible to survey bacteria-triggered compartments and infection events, specifically during *Shigella* infection as studied in the laboratory of this PhD thesis. Exemplarily, fluorescent PI(3)P reporter 2xFYVE and fluorophore-tagged RAB5 were found to localize at early *Shigella*-IAMs, IAM maturation was observed with the recruitment of RAB11A prior to BCV rupture (Mellouk et al. 2014, Weiner et al. 2016, Kühn et al. 2017). Additionally, the cytosolic β-galactose-binding protein galectin-3 was found to mark the inside of bacterial vacuoles membranes at the precise moment of breakage (Paz et al. 2010). By enabling the simultaneous visualization of multiple specific infection events and cellular factors, fluorescence microscopy is a highly versatile technique which allows to pinpoint host factor changes during specific *Shigella* invasion steps.

In the context of epithelial cell invasion, *Shigella* is a rapidly invading pathogen. Following contact with the target cell, *Shigella* is reported to trigger actin network remodeling in as little as 200 to 400 sec (Ehsani et al. 2012). These events take place due to the rapid injection of T3SS effectors during the first minutes of contact with the host cell (Enninga et al. 2005). About 7 to 10 min after engulfment of the bacterium and formation of the IAMs, *Shigella* breaks the BCV (Ray et al. 2010). Within a range of 10 to 40 min post-entry, it forms an actin comet tail to invade neighboring cells (Ray et al. 2010). This rapid sequence of events makes investigating these steps challenging due to the heterogeneous timing of the successive infection events. In fact, the swiftness of these steps can render the observation of simultaneously occurring early and late bacterial invasion events very difficult. This hurdle emphasizes the need for high temporal resolution to explore the role of host factors in *Shigella* infection.

The acquisition of biological events occurring in the range of minutes to seconds, time-lapse fluorescence microscopy requires rapid image acquisition. The speed of image acquisition is dependent on the rapidity of the acquisition technology and should not compromise good spatial resolution. The development of several novel instruments has allowed for a gain in temporal and spatial resolution while maintaining a simplistic microscope setup. The integration of fast acquiring high-sensitivity cameras (*e.g.* EMCCD and sCMOS) together with the new generation of confocal spinning disk units (*e.g.* the Yokogawa series) and

rapid-moving stages has provided a great gain in temporal resolution with high-quality images (Sanderson et al. 2014). Furthermore, the development of new microscopes such as the Lattice Light sheet further allows further temporal resolution (Chen et al. 2014). Additionally, the use of robust systems for focus maintenance has allowed to follow events within the same z-plane. Put together, this technology enables the visualization of highly dynamic events ranging from seconds to minutes in high quality of events. Moreover, these setups enable for rapid multi-position acquisition and multiplexing with the acquisition of different conditions in parallel in real time This makes real-time fluorescence microscopy not only possible and appropriate for observing the relationship of host factors to bacterial infection events but also for dynamic candidate-based screening approach.

1.4.3. Screening using time-resolved high-content microscopy

Microscopy-based screens have been essential to identifying cellular signaling pathways and for drug discovery (Perlman et al. 2004, Botelho et al. 2015). In the field of cell biology, high-throughput fluorescence microscopy-based screening has emerged as a powerful technique. With the aim of evaluating protein function, this technique has led to the development of siRNA-based screen setups (Conrad and Gerlich, 2010, Mohr et al. 2010). Nonetheless, the complexity in setup of these screens has often demanded sample fixation, thus lacking the temporal dimension of the sequential events leading to the observed phenotype(s) (Pepperkok and Ellenberg, 2006). In the field of host-pathogen interactions, microscopy approaches to identify host and bacterial factors have been essential in the decoding of molecular pathways subverted by bacterial pathogens. In the case of *Shigella* -and also notably *Shigella*-related pathogen *Salmonella*- high-content fluorescence microscopy setups coupled the use of small inhibitor molecules and bacterial effectors have been essential for decrypting bacteria-manipulated cellular pathways (Kreibich et al. 2015, Weiner et al. 2016, Ellis et al. 2019, Kühn et al. 2020). These indirect approaches however often impact multiple signaling pathways thus making identification of precise proteins difficult. More target-specific screens such as loss-of-function assays using RNA interference and CRISPR-Cas9 have enabled a more robust identification of molecular pathways (Mellouk et al. 2014, Quereda et al. 2022). These loss-of-function screens have even been adapted to large-scale applications such as genome-wide coverage of host factors (Sönnichsen et al. 2005, Mohr et al. 2015, Conrad and Gerlich, 2010). However, the complexity of these high-throughput screens requires the need for a robust read-out to enable proper result interpretation and has often led to them being adapted for fixed experiment conditions at a given time point (Conrad and Gerlich, 2010).

By contrast, time-resolved fluorescent microscopy screens serve to view the reorganization of molecule as it occurred, and can be combined to functional assays (bacterial effector mutants, inhibitors, loss-of-function tools) (Pepperkok and Ellenberg, 2006). The combination of these assays together with microscopy automation frameworks have prompted the development of high-throughput dynamic screens (Pepperkok and Ellenberg, 2006) (see Figure 1.14). These represent a challenge as automation of nearly all steps is essential. Moreover, a significant challenge to this day in this large a screen is the automation of image analysis. Pre-processing of the obtained large data and quantification of the data with proper detection of the biological phenotype necessitate the development of complex algorithms and bio-informatic modeling which limits the feasibility of application of large time-resolved microscopy screens (Pepperkok and Ellenberg, 2006).

Medium-sized time-lapse screens of 50 to 100 proteins allow the compromise of a simple microscopy setup with minimal automation for screening protein families and reasonable spatio-temporal resolution. Moreover, although data analysis remains challenging for time-lapse fluorescence microscopy screens, data handling and processing remain reasonable given the size of the data and the data remains simple enough to be manipulated in a reasonable time. This makes it a feasible and easy to-set-up technique albeit being simply powerful method to observe protein re-localization during bacterial invasion.

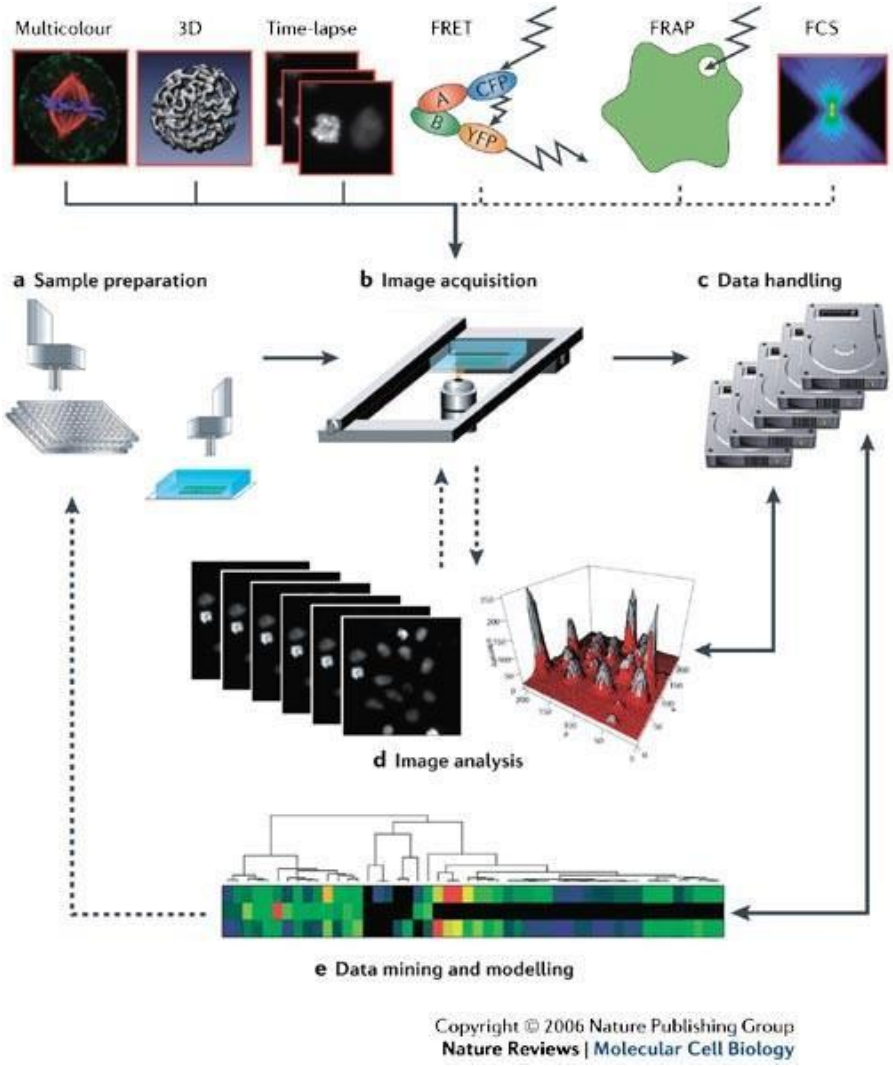

Figure 1.14. Steps and hurdles of high-throughput fluorescence microscopy screen acquisition and data analysis (from Pepperkock and Ellenberg, 2006).

High-throughput live cell microscopy screens requires automation of 5 steps. a. Sample preparation using genetically-encoded probes (use of stable cell lines, high-throughput transfections such as cell arrays). b. Acquisition using an automated microscopy setup with the possibility of multidimensional acquisition (multiple colors, three dimensions and temporality). This setup could be combined to different fluorescence techniques such as Förster Resonance Energy Transfer (FRET), Fluorescence Recovery After Photobleaching (FRAP) and fluorescence correlation spectroscopy (FCS). c. The obtained data would require special handling with appropriate dedicated hardware (hard drives, computer, etc) and software for processing. d. Automated image analysis using bioinformatic modeling (pre-processing -*e.g* noise filtering, intensity normalization-, quantitative analysis with classification of the data to the biological phenotype questioned, tracking of biological events etc). e. Data mining (data comparison) of each experimental replicate to determine robustness of the hits.

Project Rationale

Recent work these last decades from the laboratory of this PhD thesis has highlighted a need to revisit the *Shigella* invasion model, with a higher importance of the contribution of host factors, in particular the endosomal trafficking pathways playing a substantial role in infection. Moreover, IAMs' function in the invasion also deserved to be revisited for *Shigella* invasion (Weiner et al. 2016, Chang et al. 2020) in the pathogen's invasion of epithelial cells.

As previously addressed, from the formation and collapse of sheet-like extensions of the membrane to the dynamic events of the *Shigella*-triggered compartments, membrane remodeling is necessary to *Shigella* invasion for invasion. Moreover, membrane remodeling is an essential process in the shaping of organelles, protein and lipid localization and the function of host factors. BAR domain proteins playing such key roles in membrane-involved cellular processes and often reprogrammed by other bacterial pathogens (*Listeria, Salmonella*, etc.), they have a high potential in being implicated in *Shigella* pathogenesis. In this work, we investigated the contribution of host membrane remodeling factors and provide critical insight into the *Shigella*-IAM compartments, which has thus far remained poorly characterized.

Chapter 2. Material and Methods

2.1. Cell lines and cell culture

2.1.1. Cell lines, culture medium and conditions

HeLa cervical adenocarcinoma CCL2 clone from the American Type Culture Collection (ATCC) and CaCo-2 TC7 cells (ATCC) were cultured in Dulbecco's Modified Eagle Medium (DMEM High glucose with GlutaMAX^{TM} and pyruvate, Gibco) supplemented with 10% heat-inactivated Fetal Bovine Serum (FBS, Sigma Aldrich) and incubated at 37°C, 5% CO_2.

2.1.2. Cell maintenance

All cells were passed every 4 days with at a maximum of 25 passages from initial stock with the following protocol. Cells were cultured in T25 or T75 flasks (TPP). First the cells were washed once using Dulbecco's Phosphate Buffered Saline solution (DPBS without calcium and magnesium, Gibco) and detached using either 3 or 5mL Trypsin-EDTA (Sigma Aldrich). Trypsin was quenched using DMEM supplemented with 10% heat-inactivated FBS and the cells were pelleted by centrifugation at 138*g*, room temperature for 4 min.

2.1.3. Generation of LactC2-GFP and SNX8-eGFP stable cell lines using the Sleeping Beauty System (Kowarz et al. 2015).

The following protocol was used to generate LactC2-GFP and SNX8-eGFP stable cell lines. The genes of interest (the human SNX8 tagged to eGFP and the human C2 domain of Lactadherin tagged to GFP) were cloned into the Sleeping Beauty empty backbone pSBbi-Neo using the Sequence and Ligation Independent Cloning (SLIC) method (Jeong et al. 2012) (Plasmids were cloned by Michael G. Connor). Each resulting pSBbi-Neo construct (Addgene, #60525) was co-transfected with the transposase-containing vector pSB100X (Addgene, #169633) at a 100:1 ratio in HeLa cells (passage 9) seeded in a 6 well plate. Selection of the cells was performed 24 hours post-transfection using Geneticin (G418, Euromedex, #EU0601) at a concentration of 800 µg/mL and Penicillin-Streptomycin (Gibco, #15140122). Non-transfected HeLa cells were used as a positive control of the selection. The expression of the protein-of-interest was monitored by widefield microscopy and after amplification to a T75 flask, the cells were sorted by Fluorescence-Activated Cell Sorting (FACS) by level of intensity (low, medium, high). Following sorting, G418 and

PenStrep were left for two more passages before freezing the cells. They were later cultured as regular HeLa cells.

2.1.4. Seeding

Following cell passages, the detached cells were counted on a disposable hemocytometer (KOVA international). For microscopy experiments, the cells were seeded either in an optical polystyrene black 96 well plate (Greiner Bio-One, #655090) or in a 35mm glass-bottom dish (ibiDI, #81158) containing a 4-chamber silicone insert (ibiDI, #80409). For both of these supports, HeLa cells were seeded at a density of 8,000 cells per well, whereas CaCo-2 TC7 cells were seeded at a density of 5,000 cells per well. For quantitative reverse transcription Polymerase Chain Reaction (RT-qPCR) and Western Blot experiments, HeLa cells were seeded in either a 12 well plate or a 6 well plate, at a density of $8x10^4$ and $2,4x10^5$ cells respectively.

2.1.5. Transient transfections

Transient transfections were performed by lipofection using FuGENE™ HD (Promega, #E2311) as instructed by the manufacturer. Briefly, transfection complexes were prepared by diluting 2 µg of plasmid (or for co-transfections, 1µg of each plasmid) in 100µL OptiMEM (Gibco, #31985062), mixed with 4 µL of FuGENE™ HD and incubated for 10 min at room temperature. Afterwards, 5 µL of transfection mixture was added per well containing the cells seeded the previous day, the cells were then incubated 48 hours at 37°C, 5% CO_2 prior to imaging. For the complete list of plasmids transfected see table 2.6.
In the case of transfections used for generating the Sleeping Beauty stable cell lines, jetPRIME® transfection reagent (Polyplus, #101000027) was used as instructed by the manufacturer. To 200µL of JetPRIME buffer was mixed 2µg of DNA and later 4µL of JetPRIME® transfection reagent. The mixture was incubated 10 min at room temperature and the entire volume of the mix was added to the cells.

2.2. *Shigella* strains and culture preparation

2.2.1. *Shigella* strains

The following strains were used.

Shigella strains	*Modifications*	*Description*
M90T (Clerc et al. 1986)	*pBR322-AfaI*	*Wild type Shigella expressing the AfaI adhesin from uropathogenic E. coli (Nowicki et al. 1993)*
M90T AfaI ΔIpgD	*Deletion mutantM90T*	*AfaI strain with a deletion of ipgD, that encodes the inositol phosphatase effector IpgD (Niebuhr et al. 2002)*
M90T AfaI ΔIcsB	*Deletion mutantM90T*	*AfaI strain with a deletion of icsB, that encodes the Fatty Acyltransferase effector IcsB (Liu et al. 2018)*

Table 3.2. Summary of the *Shigella* strains utilized in this study.

2.2.2. Bacterial culture

Prior to infection experiments, *Shigella* strains were grown overnight at 37°C from bacteria grown on Trypticase Casein Soy Broth (TCSB) agar plates (TCSB media : 17 g/L casein (pancreatic digest), 3 g/L soya peptone (papaic digest), 5 g/L NaCl, 2.5 g/L K_2HPO_4, dextrose 2.5 g/L, pH 7.3 ± 0.2, TCSB agar: +15 g/L agar) supplemented with ampicillin at 50µg/mL and 0.01% Congo Red. Overnight cultures were prepared the day prior to the experiment by inoculating 3 colonies in 8 mL TCSB media supplemented with ampicillin at 50µg/mL and incubated at least 16h at 37°C, 220 rpm.

2.3. Infection procedures

2.3.1. Bacteria preparation

On the experiment day, a subculture is prepared by diluting the overnight culture 1:100 in 8 mL of fresh TCSB media supplemented with ampicillin 50µg/mL and incubating it for 2 hours at 37°C, 220 rpm (until the OD_{600} reaches 0.4-0.6). Then 1mL of the subculture was spun 1 min at 6000*g* and the bacteria pellet is washed twice with warm EM buffer (120 mM NaCl, 7 mM KCl, 1.8 mM $CaCl_2$, 0.8 mM $MgCl_2$, 5 mM glucose, 25 mM HEPES, pH 7.3). An inoculum was prepared by diluting the bacterial suspension in EM buffer to reach a multiplicity of infection (MOI) of 20 bacteria/cell.

2.3.2 Cell preparation and infection

Prior to the start of the infection, the cells were washed three times with EM Buffer to get rid of dead cells and 50µL of EM buffer were left in the well. For live imaging experiments, the infection was started by adding 40 µL of inoculum per well in the 37°C heated microscopy chamber. For fixed experiments, no medium was left in the well and 30 µL of inoculum (with if needed 0.5mg/mL final dextran 10 000 MW Alexa-647 (Invitrogen™, #D22914)) were added to the well, after which the samples were incubated at 20°C for 10 min to synchronize the start of the infections. The samples were then incubated 30 min or 40 min at 37°C.

2.3.3. Inhibitors

Wortmannin (Sigma Aldrich, #W1628-1MG) and SAR405 (Selleckchem, #S7682) were solubilized in DMSO and stored aliquoted at -20°C until the experiment day. For the experiments involving these inhibitors, wortmannin, SAR405 and DMSO solutions were diluted in the inoculum containing the bacteria or EM Buffer, respectively to 3.3µM and 3µM.

2.4. Immunofluorescence and stainings

2.4.1. Fixation

Samples were fixed using a freshly prepared 4% paraformaldehyde (ThermoScientific, 043368.9M) in PBS solution (KCl 200 mg/L, KH_2PO_4 200 mg/L, NaCl 8 g/L, Na_2HPO_4-$7H_2O$ 2.16 g/L) for 10 min at room

temperature. The cells were washed 3 times with PBS and later stored for up to 2 weeks in 200µL PBS 1X at 4°C.

2.4.2. Permeabilization and blocking

Samples were permeabilized using saponin diluted to 0.025% in PBS for 20 min at room temperature. Cells were washed 3 times with PBS with 1-3 min intervals were performed to rid of the saponin and blocking was performed with 2% Bovine Serum Albumin (BSA, Sigma Aldrich,#A7906-100G), 5% goat serum (Sigma Aldrich, #G9023) in PBS for 1 hour at room temperature.

2.4.3. Primary and secondary antibodies stainings

For immunofluorescence experiments, anti-SNX8 (human) (Sigma Aldrich, #HPA057296) was used as the primary antibody. The secondary antibody was a goat anti-rabbit Alexa-488 (Invitrogen™,#A11034). Both antibodies were diluted in blocking solution at a 1:250 and 1:500 dilution respectively.

2.4.4. Dyes

When needed, samples were stained 45 min with Hoechst (Invitrogen™, #1681305) and rhodamine phalloidin (Invitrogen™, #R415). Prior to image acquisition, excess dyes were washed off by three washes with PBS. Images were acquired immediately afterwards.

2.5. Microscopy and deconvolution

2.5.1. BAR domain protein screen

Time-resolved BAR domain protein screen experiments were performed in a Nikon Ti-E inverted microscope equipped with a Perfect Focus System (TI-ND6-PFS Perfect Focus Unit) using a 40X air objective (NA 0.75, WD 0.66). NIS version 5.21.02 was used.

Name	*Excitation filter (nm)*	*Emission filter (nm)*	*Fluorophores used*
FITC	*465 - 495*	*515 - 555*	*GFP, eGFP*
TRITC	*528 - 553*	*590 - 650*	*mOrange*

Table 4.3. Excitation and emission wavelengths used for the respective fluorophores.

2.5.2. High resolution spatio-temporal microscopy

High resolution time-lapses were acquired on DeltaVision Elite (Leica) using a 60X/1.42 NA oil objective and images were deconvolved using an integrated deconvolution software (Resolve3D).

Name	*Excitation filter (nm)*	*Emission filter (nm)*	*Fluorophores*
FITC	*461 - 489*	*501 - 549*	*GFP, eGFP*
TRITC	*528 - 556*	*574 - 620*	*mApple, mCherry, mOrange*

Table 5.4. Excitation and emission wavelengths used for the respective fluorophores.

2.5.3. Fixed experiments

Fixed images were acquired on a Nikon Ti-E inverted microscope equipped with a Perfect Focus System and a Yokogawa confocal spinning disk unit (CSU-W1) using a 60X/1.2 NA water objective. Images were acquired at a step-size of 0.35µm in the z-plane.

Laser (nm)	*Bandpass filter (nm)*	*Fluorophores*
405	*447/60*	*Hoechst, DAPI*
488	*525/50*	*GFP, eGFP*
561	*600/52*	*Rhodamine, mOrange, mCherry, mApple*
641	*670/30*	*Alexa-647*

Table 6.5. Excitation and emission conditions for the different fluorophores.

I designed a pipeline to automatically acquire all fixed images. Briefly, following the definition of the wells to acquire, for each well-of-interest instructions were defined to generate points in the well. Then, for each individual point of the given well, the sample was scanned once in the z-plane using brightfield to roughly identify the cellular plane. Afterwards, focus on the nucleus was performed using the Hoechst signal (excited by the 405 laser) and then 15µm around the autofocused z-plane was acquired using all four channels (and the brightfield). A more detailed description of the pipeline is shown in Figures 2.1 to 2.4.

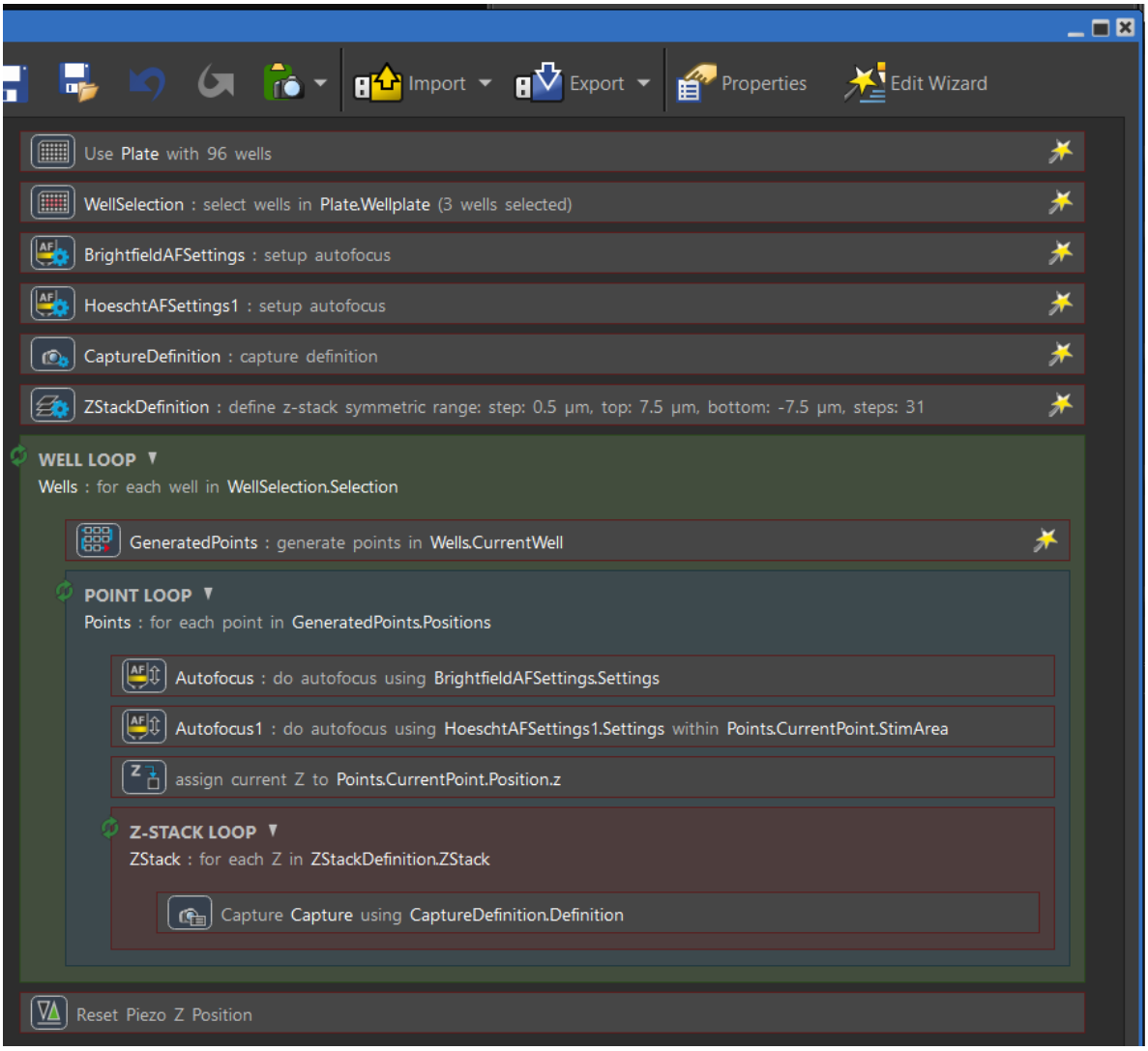

Figure 15.1. General automated acquisition pipeline for fixed samples using NIS software version 5.21.02 in a Nikon confocal spinning disk setup.

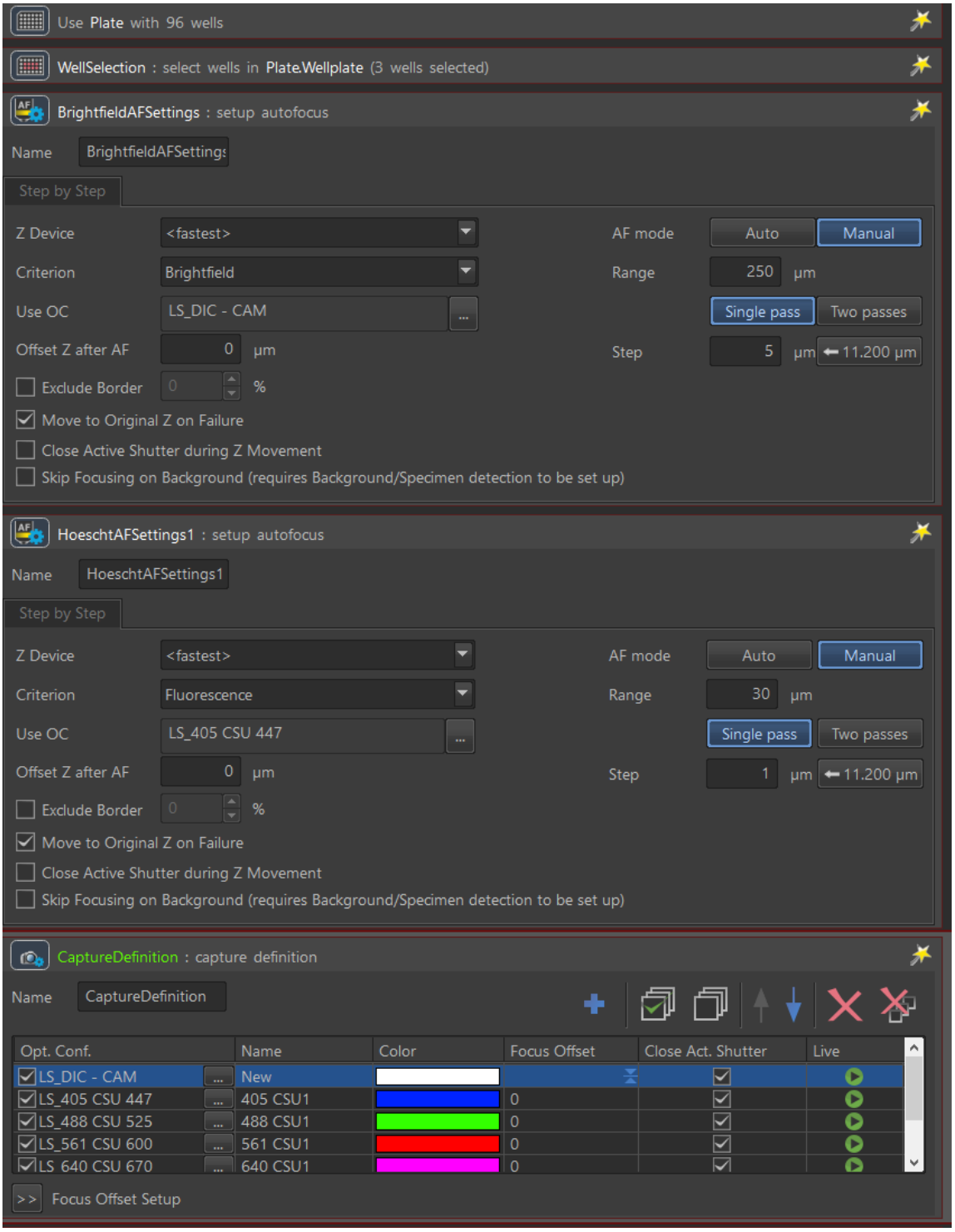

Figure 16.2. Details on brightfield autofocus, autofocus using the 405 excitation wavelength and the capture definition.

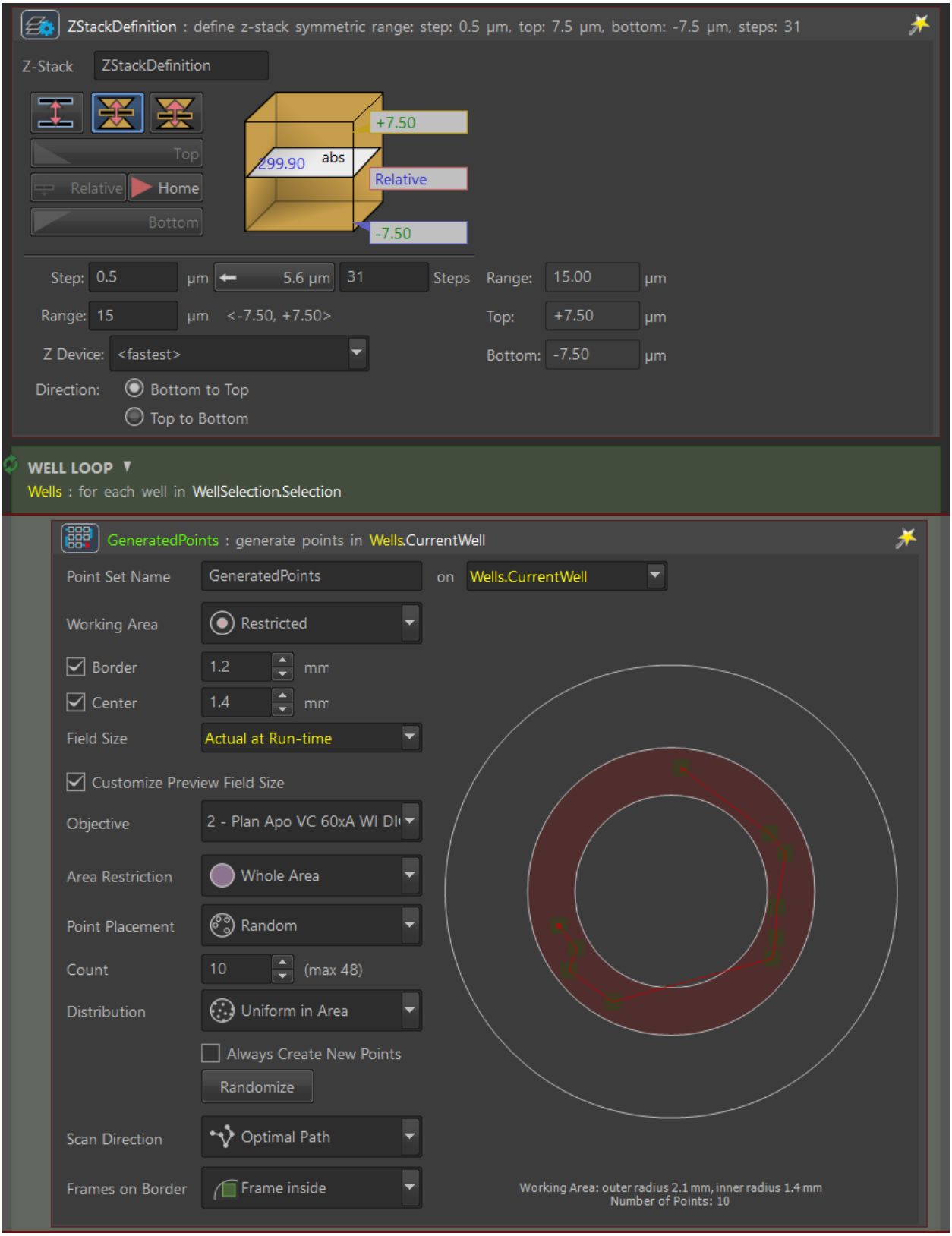

Figure 17.3. Detail of the Z-stack and the automatically generated points parameters used.

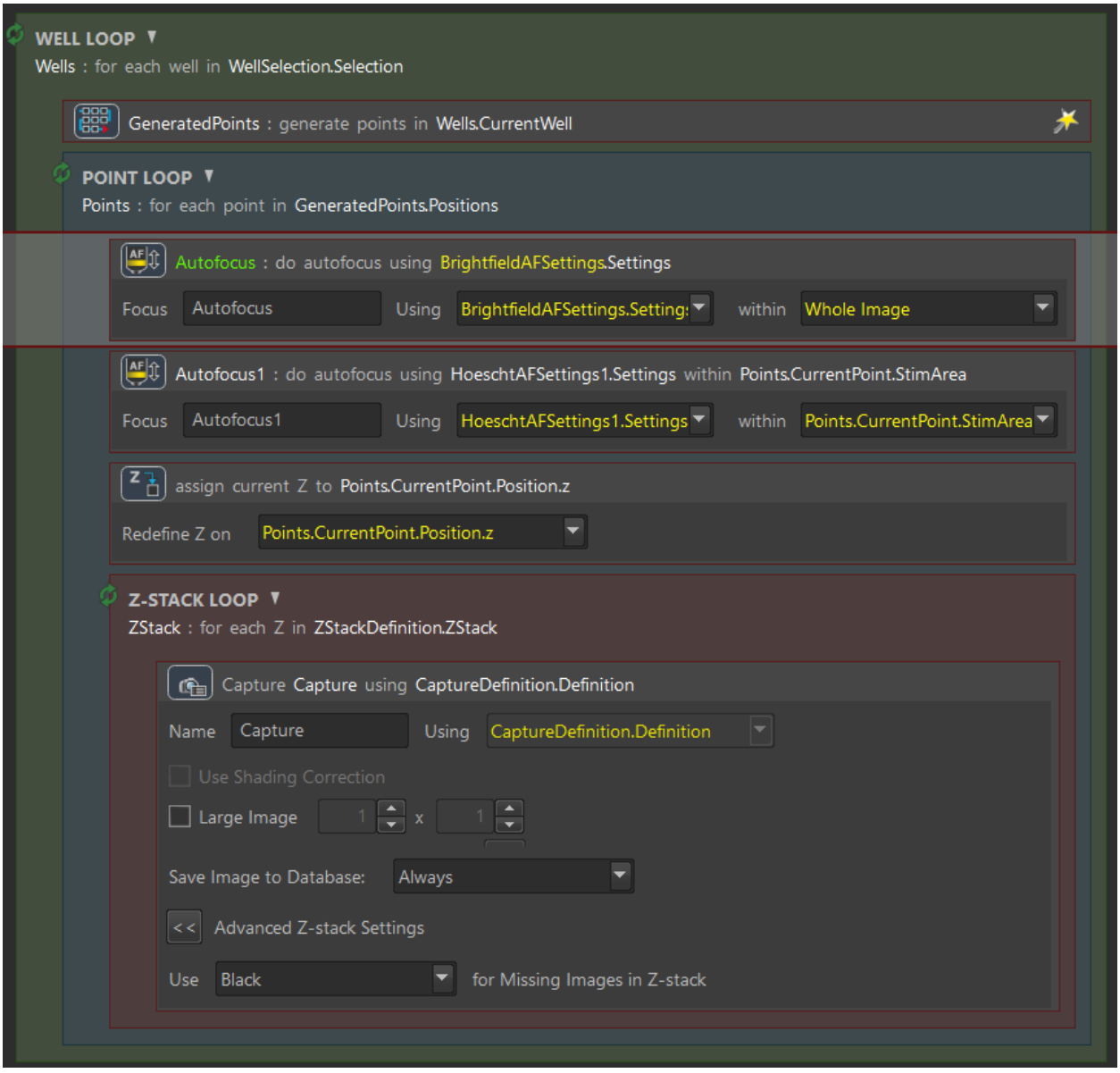

Figure 18.4. Detail of the sequential steps taking place for each generated point contained within a well. All the points in the well followed this sequence of events one after the other.

2.6. DNA manipulation

2.6.1. Construction of pDEST-SNX8-mApple

The mApple gene was amplified from a mApple-RAB11A plasmid template using Taq Polymerase (New England Biolabs, M0273S) according to the manufacturer's instructions, using primers that include the restriction sites KpnI and XbaI. The size of the amplified region was verified by gel migration in agarose 1% stained with ethidium bromide and run in TAE buffer (For 1L of 10X stock solution: Tris base 48.5g, Acetic acid 11.4mL, 0.5M EDTA (pH:8.0) 20mL, H_2O qsp 1L). Then, the mApple PCR product and the vector pSNX8-eGFP DNA were digested by KpnI (New England Biolabs, R3142S) and XbaI (New England Biolabs, R0145S) according to the manufacturer's instructions. The restriction products were separated in a 1% agarose gel stained with ethidium bromide and gel purified using the QIAquick gel extraction kit (QIAGEN, 28706X4) as instructed by the manufacturer. DNA fragments were ligated using T4 Ligase (NEB, M0202) overnight at 16°C.

2.6.2. Bacteria preparation and transformation

DH5α bacteria were streaked on a Lysogeny broth (LB) agar plate (tryptone 10 g/L, yeast extract 5 g/L, NaCl 10 g/L, Agar 15 g/L) and grown overnight, after which a subculture was grown to an OD_{600} of 0.6. Bacteria was spun at 1500*g* for 10 min at 4°C. The pellet was washed twice with cold 15% glycerol. 80µL of the remaining pellet was pipetted into an electroporation cuvette and pulsed. The bacteria were left to recover in 1mL of LB for 1 hour at 37°C and 220 rpm. 100µL of suspension was plated in LB supplemented with ampicillin at 50µg/mL and incubated overnight at 37°C.

2.6.3. Plasmid verification

The bacteria clones were selected by colony PCR using the GoTaq Flexi (Promega, #M829) according to the manufacturer's instructions. The selected colonies were used to purify plasmid for sequencing, using the Nucleospin miniPREP kit (Macherey-Nagel, #740588.50) or transfect, using the HiPure maxiPREP kit (Invitrogen™, #K210007).

2.7. Image Processing and quantification

Images were processed using ImageJ. For SAR405 experiment analysis, the background was subtracted from the image and rupture time was determined as the brightest mOrange-galectin-3 signal for the BCV rupture and entry was determined as the moment of mOrange-Galectin-3 signal from the cell volume increase at the foci site.

2.8. Statistical analysis

Statistical analysis was performed using GraphPad Prism version 9.0.0 for MacOS, GraphPad Software, San Diego, California USA, www.graphpad.com.

2.9. Plasmids

All plasmids from the BAR domain-containing library were the full-length BAR domain containing proteins and were a kind gift from Emmanuel Boucrot.

DNA Plasmid constructs

Plasmid	*Protein*	*Reference*
pArfaptin1-eGFP	*Arfaptin1-eGFP*	*Chan Wah Hak et al. 2018*
pArfaptin2-eGFP	*Arfaptin2-eGFP*	*Chan Wah Hak et al. 2018*
pICA69-eGFP	*ICA69-eGFP*	*Chan Wah Hak et al. 2018*
pICA1-like-eGFP	*ICA1-like-eGFP*	*Chan Wah Hak et al. 2018*
pPICK1-eGFP	*PICK1-eGFP*	*Chan Wah Hak et al. 2018*
pTuba-eGFP	*Tuba-eGFP*	*Chan Wah Hak et al. 2018*
pASAP1-eGFP	*ASAP1-eGFP*	*Chan Wah Hak et al. 2018*
pASAP2-eGFP	*ASAP2-eGFP*	*Chan Wah Hak et al. 2018*
pASAP3-eGFP	*ASAP3-eGFP*	*Chan Wah Hak et al. 2018*
pSH3BP1-eGFP	*SH3BP1-eGFP*	*Chan Wah Hak et al. 2018*
pAmphiphysin I-eGFP	*Amphiphysin I-eGFP*	*Chan Wah Hak et al. 2018*

pAmphiphysin II-eGFP	*Amphiphysin II-eGFP*	*Chan Wah Hak et al. 2018*
pBRAP1-eGFP	*BRAP1-eGFP*	*Chan Wah Hak et al. 2018*
pBIN3-eGFP	*BIN3-eGFP*	*Chan Wah Hak et al. 2018*
pEndophilin A1-eGFP	*Endophilin A1-eGFP*	*Chan Wah Hak et al. 2018*
pEndophilin A2-eGFP	*Endophilin A2-eGFP*	*Chan Wah Hak et al. 2018*
pEndophilin A3-eGFP	*Endophilin A3-eGFP*	*Chan Wah Hak et al. 2018*
pEndophilin B1-eGFP	*Endophilin B1-eGFP*	*Chan Wah Hak et al. 2018*
pEndophilin B2-eGFP	*Endophilin B2-eGFP*	*Chan Wah Hak et al. 2018*
pNadrin1-eGFP	*Nadrin1-eGFP*	*Chan Wah Hak et al. 2018*
pNadrin2-eGFP	*Nadrin2-eGFP*	*Chan Wah Hak et al. 2018*
pOligophrenin1-eGFP	*Oligophrenin1-eGFP*	*Chan Wah Hak et al. 2018*
peGFP-APPL1	*eGFP-APPL1*	*Chan Wah Hak et al. 2018*
peGFP-APPL2	*eGFP-APPL2*	*Chan Wah Hak et al. 2018*
pCentaurinb1-eGFP	*Centaurinb1-eGFP*	*Chan Wah Hak et al. 2018*
pCentaurinb2-eGFP	*Centaurinb2-eGFP*	*Chan Wah Hak et al. 2018*
pCentaurinb5-eGFP	*Centaurinb5-eGFP*	*Chan Wah Hak et al. 2018*
pGRAF1-eGFP	*GRAF1-eGFP*	*Chan Wah Hak et al. 2018*
pGRAF2-eGFP	*GRAF2-eGFP*	*Chan Wah Hak et al. 2018*
pSNX1-eGFP	*SNX1-eGFP*	*Chan Wah Hak et al. 2018*
pSNX2-eGFP	*SNX2-eGFP*	*Chan Wah Hak et al. 2018*
pSNX4-eGFP	*SNX4-eGFP*	*Chan Wah Hak et al. 2018*
pSNX5-eGFP	*SNX5-eGFP*	*Chan Wah Hak et al. 2018*
pSNX6-eGFP	*SNX6-eGFP*	*Chan Wah Hak et al. 2018*
pSNX7-eGFP	*SNX7-eGFP*	*Chan Wah Hak et al. 2018*
pSNX8-eGFP	*SNX8-eGFP*	*Chan Wah Hak et al. 2018*
peGFP-SNX9	*eGFP-SNX9*	*Chan Wah Hak et al. 2018*
pSNX18-eGFP	*SNX18-eGFP*	*Chan Wah Hak et al. 2018*
pSNX30-eGFP	*SNX30-eGFP*	*Chan Wah Hak et al. 2018*
pSNX32-eGFP	*SNX32-eGFP*	*Chan Wah Hak et al. 2018*
pSNX33-eGFP	*SNX33-eGFP*	*Chan Wah Hak et al. 2018*
pToca1-eGFP	*Toca1-eGFP*	*Chan Wah Hak et al. 2018*
pFBP17-eGFP	*FBP17-eGFP*	*Chan Wah Hak et al. 2018*
pCIP4-eGFP	*CIP4-eGFP*	*Chan Wah Hak et al. 2018*
pFCHo1-eGFP	*FCHo1-eGFP*	*Chan Wah Hak et al. 2018*

pFCHo2-eGFP	*FCHo2-eGFP*	*Chan Wah Hak et al. 2018*
pPSTPIP1-eGFP	*PSTPIP1-eGFP*	*Chan Wah Hak et al. 2018*
pPSTPIP2-eGFP	*PSTPIP2-eGFP*	*Chan Wah Hak et al. 2018*
pPacsin1-eGFP	*Pacsin1-eGFP*	*Chan Wah Hak et al. 2018*
pPacsin2-eGFP	*Pacsin2-eGFP*	*Chan Wah Hak et al. 2018*
pPacsin3-eGFP	*Pacsin3-eGFP*	*Chan Wah Hak et al. 2018*
pNwk1-eGFP	*Nwk1-eGFP*	*Chan Wah Hak et al. 2018*
pNwk2-eGFP	*Nwk2-eGFP*	*Chan Wah Hak et al. 2018*
psrGAP1-eGFP	*srGAP1-eGFP*	*Chan Wah Hak et al. 2018*
psrGAP2-eGFP	*srGAP2-eGFP*	*Chan Wah Hak et al. 2018*
psrGAP3-eGFP	*srGAP3-eGFP*	*Chan Wah Hak et al. 2018*
pFER-eGFP	*FER-eGFP*	*Chan Wah Hak et al. 2018*
pFES-eGFP	*FES-eGFP*	*Chan Wah Hak et al. 2018*
pNostrin-eGFP	*Nostrin-eGFP*	*Chan Wah Hak et al. 2018*
pGAS7-eGFP	*GAS7-eGFP*	*Chan Wah Hak et al. 2018*
pHMHA1-eGFP	*HMHA1-eGFP*	*Chan Wah Hak et al. 2018*
pIRSp53-eGFP	*RSp53-eGFP*	*Chan Wah Hak et al. 2018*
pMIM-eGFP	*MIM-eGFP*	*Chan Wah Hak et al. 2018*
pABBA-1-eGFP	*ABBA-1-eGFP*	*Chan Wah Hak et al. 2018*
pIRTKS1-eGFP	*IRTKS1-eGFP*	*Chan Wah Hak et al. 2018*
pIRTKS2-eGFP aka Pinkbar	*IRTKS2-eGFP*	*Chan Wah Hak et al. 2018*
pDEST-RAB5A-GFP	*RAB5A-GFP*	*Bruno Goud Lab*
pRAB7A-GFP	*RAB7A-GFP*	*Bruno Goud Lab*
pmApple-RAB8A	*mApple RAB8A*	*Chang et al. 2020*
pmApple-RAB11A	*mApple-RAB11A*	*Arnaud Echard Lab*
pmOrange-Galectin-3	*mOrange-Galectin-3*	*Ray et al., 2010*
pSNX8-mApple	*SNX8-mApple*	*This study*
p2xFYVE-mCherry	*2xFYVE-mCherry (Hrs)*	*Harald Stenmark Lab*
pSBbi-SNX8-eGFP-Neo	*SNX8-eGFP*	*Melanie Hamon Lab*
pSBbi-LactC2-GFP-Neo	*LactC2-GFP*	*Melanie Hamon Lab*

Table 7.6. List of the plasmids used.

Chapter 3. Results

During this PhD I screened and studied the role of BAR domain-containing proteins in the successive steps of *Shigella* invasion. First, I developed a high-content time-resolved screen procedure to investigate protein behavior during *Shigella* invasion. Then, I focused on researching the function of one of the screen hits, Sorting Nexin 8 (SNX8), in order to give answers to the role of IAMs in *Shigella* invasion of epithelial cells.

1. Identifying potential host factor targets in the case of bacterial pathogens remains a challenge in the host-pathogen field. Given the rapidity of bacterial invasion events and the difficulty to synchronize bacterial events, we designed a candidate-based time-resolve microscopy screen to identify potential cellular proteins targeted by invasive bacteria. During the start of my PhD, I developed a high-content fluorescence microscopy screen procedure to systematically analyze the recruitment of cellular proteins to the bacterial infection site. That work was published in June 2022 in *Methods in Molecular Biology, Effector-Triggered Immunity*. As the main author, I put in place the protocol and pipeline of acquisition. Yuen-Yan Chang participated in the conceptualization of the screen pipeline and tools. Jost Enninga and Yuen-Yan Chang co-supervised this project. Jost Enninga, together with myself wrote the manuscript which was co-edited by Nora Mellouk. Nora Mellouk also provided a data piece displayed in this manuscript.

2. My second work focuses on a hit identified by a screen using the protocol described in the first part of the results section. The identification of this protein led to the discovery of diverse IAM subpopulations co-existing around the internalized bacteria. This work sheds light on the molecular strategies used by bacterial pathogens to invade the host, and to establish their intracellular niche. Experiments and conceptualization were performed by myself. Camila Valenzuela-Montenegro participated in the supervision and conception of the project. The generation of stable cell line tools was performed by Michael G. Connor. This work was performed under the supervision of Jost Enninga.

3. An additional manuscript, joined in the appendix of this thesis manuscript, was also published in 2021 in *bioRxiv* focus on another pathogen, *Streptococcus pneumoniae*, in which I am second author. In that work, I performed confocal microscopy acquisition of experiments performed by Michael G. Connor.

3.1. Manuscript 1: Time-resolved fluorescence microscopy screens on host protein subversion during bacterial cell invasion

https://link.springer.com/protocol/10.1007/978-1-0716-2449-4_8
doi: 10.1007/978-1-0716-2449-4_8

Running head: Time-resolved bacterial invasion fluorescence microscopy screens

Lisa Sanchez[1,2], Yuen-Yan Chang[1,3], Nora Mellouk[1], Jost Enninga[1]

Affiliations :

1. Dynamics of Host-Pathogen Interactions Unit, Institut Pasteur, UMR3691 CNRS, Paris 75015, France,
2. Université de Paris, Sorbonne Paris Cite, Paris, France,
3. Division of Molecular and Cellular Biology, National Institute of Child Health and Human Development, NIH, Bethesda, Maryland,

Corresponding author: Enninga, Jost (jost.enninga@pasteur.fr).

Abstract

Intracellular bacterial pathogens have evolved a plethora of strategies to invade eukaryotic cells. By manipulating host signaling pathways, in particular vesicular trafficking, these microbes subvert host functions to promote their internalization and to establish an intracellular niche. During these events host endomembrane compartments are dynamically reorganized. *Shigella flexneri*, the causative agent of bacillary dysentery, recruits components of the host recycling and exocyst pathways of non-phagocytic enterocytes in the vicinity of its entry site to facilitate its access to the host cytosol. These factors are either dynamically tethered to *in situ* formed macropinosomes or to the bacterial containing vacuole itself. The underlying interactions cannot readily be monitored as individual bacterial infection events take place without synchronicity using cellular infection models. Therefore, time-resolved screens by fluorescence microscopy represent a powerful tool for the study of host subversion. Such screens can be performed with libraries of fluorescently tagged host factors. Using the cytosolic pathogenic agent *Shigella flexneri* as a model, we provide detailed protocols for such medium-to-high throughput multi-dimensional imaging screening of the dynamic host-pathogen cross-talk. Our workflow is designed to be easily adapted for the study of different host factor libraries and different pathogen models.

Keywords

Intracellular bacterial pathogens, membrane trafficking, high-content screening, *Shigella flexneri*, bacterial infection, BAR domain-containing proteins, Rab GTPases.

1. Introduction

Through a myriad of molecular mechanisms, bacterial pathogens invade non-phagocytic cells by injecting effector proteins using specialized secretory systems. This strategy thus enables them to survive and thrive within their host by profiting from and reprogramming host pathways. Despite bacterial invasion occurring by a variety of mechanisms, similar themes are found with regards to the subverted host components and machineries. First, following host cell contact, bacteria swiftly trigger their internalization within a vacuole. Then, the invading pathogens reach their preferred intracellular niche by either (i) triggering vacuole rupture and egress into the cytosol (*Shigella flexneri, Listeria monocytogenes*) or (ii) by reprogramming the bacterial vacuole into a specialized bacterial compartment (*Salmonella typhimurium, Yersinia pseudotuberculosis*) (1). Numerous host and pathogen factors have been identified to be involved during this crosstalk. Nevertheless, the dynamic implication of the host molecular pathways controlling the subversion of host trafficking pathways remain often unclear. Identifying at which specific step of the infection host factors are manipulated by bacterial pathogens poses a challenge. This is due to heterogenicity in the behavior of the individual bacteria and the targeted host cells, and the non-synchronous nature of the bacterial invasion process. In cellular infection models for instance, *Salmonella* entry varies greatly as individual bacteria exert near-surface swimming and "test" several cells before eventually invading a target cell (2). In the case of *Listeria* entry homogenous invasion behavior cannot be readily assessed experimentally as bacterial adhesion and its subsequent internalization reportedly dependents on the individual host cell heterogeneity (3). Moreover, the rapidity of *Listeria* cell-to-cell spread varies hugely (4). Other factors such as bacteria cooperation (e.g. *Salmonella*) and the specific bacterial load of a given experimental condition also cause variability in the timing of infection events and in the process of internalization thus hampering a straightforward interpretation of the obtained data (2,5,6). Adding to this complexity, some bacteria possess multiple intracellular lifestyles. Subsequent to its entry, *Salmonella* can either (i) break free from its vacuole and replicate at high rates inside the host cytosol, or the bacteria (ii) mature the *Salmonella*-containing vacuole, or they (iii) remain dormant within their vacuoles (7,8,9). The complexity of synchronizing bacterial infection therefore highlights the necessity of developing assays with dynamic readouts at the single cell level, and adapting them for screening for the identification of novel roles of the investigated factors.

Enabling the visualization of the highly dynamic events occurring during bacterial invasion, time-resolved imaging is an appropriate technique. Coupled with fluorescence, time-lapse microscopy allows for targeting specific "candidates" via fluorescence labeling including both, cellular and bacterial compartments. Genetically encoded fluorescent proteins, such as the Green Fluorescent Protein are widely used enabling the visualization of numerous factors with minimal functional interference. This can be applied for the

tagging of specific infection markers targeting bacterial compartments. Consequently, fluorescence time-lapse microscopy is a robust tool to decipher the molecular pathways exploited by pathogens. Current automated microscopes setups allow for time-lapse acquisitions in the range of seconds (sometimes even within milliseconds) and minutes, which suits very well the internalization dynamics of different bacterial pathogens. Equipping these systems with motorized stages piloted through a dedicated software and robust systems for maintaining the focus during automated acquisitions enables the long-term monitoring of multiple experimental conditions in parallel. These advances have been further boosted in recent years through microscope innovations, especially through the development of novel detectors that include EMCCD, sCMOS cameras, as well as Yokogawa Confocal Spinning Disk setups. More recently, lattice light-sheet microscopes, have provided the means for an ever-increasing gain in temporal resolution during image acquisition. Finally, miniaturization through patterning or microfluidics coupled with dynamic imaging is a powerful development to provide the means to increase the throughput of fluorescence microscopy.

The internalization of *Shigella* into non-phagocytic colonic epithelial cells is a rapid process triggered by the injection of effector proteins through a type 3 secretion system (T3SS) (10,11). Within a few seconds to minutes after coming into contact with the host cell *Shigella* triggers plasma membrane and actin cytoskeleton rearrangements (1,11). This leads to (i) its uptake within a tight vacuole, termed the bacterial-containing vacuole (BCV), and simultaneously (ii) the formation of large vesicles, called infection-associated macropinosomes (IAMs) (1,12). Afterwards, *Shigella* forms sometimes a dynamic actin cage around the BCV (11,13). Subsequently, within 7 to 10 min of entering, *Shigella* ruptures its vacuole and escapes into the host cytosol (14). After establishing its niche, the bacterium forms an actin comet tail around 10 to 40 min post-entry and spreads to neighboring cells (14). Investigating these invasion steps using cellular models, a large variability in the timing of the successive events is observed with cell-to-cell spreading of bacteria in some cells and early internalization events in other target cells occurring simultaneously. Therefore, approaches with high temporal resolution are key to studying the precise sequence of *Shigella* internalization.

The use of genetically-encoded fluorescent protein libraries has allowed these recent years to clarify the contribution of host trafficking factors in *Shigella* invasion. In a microscopy-based functional assay, several Rab GTPases, key regulators of vesicular trafficking, were identified as potential host factors involved in *Shigella*-containing vacuole rupture (16). Among them the Rab GTPase Rab11A, involved in endosomal recycling, was shown to be recruited to the *Shigella*-induced macropinosomes ((12,16) and **Figure 1**). Indeed, *Shigella* was found to sequester Rab11A to macropinosomes but not to the BCV through the modification of phosphatidyl-inositol phosphates by the bacterial effector IpgD, an inositol phosphatase (12,15,16). Moreover, time-lapse microscopy analysis of host factors identified by a *Shigella*-IAMs

proteomic assay, showed that the vesicular tethering exocyst complex drives the clustering of IAMs around the BCV (17). These events were found to be crucial for efficient BCV lysis and *Shigella* cytosolic escape. In addition to these trafficking factors, *Shigella* was found to subvert other endocytic factors. Indeed, shortly after internalization, by reprogramming actin signaling pathways, some *Shigella*-BCVs are surrounded by a thick dynamic structure distinct from any known cellular actin structure termed the actin cocoon (13,16). Although the function of this bacteria-driven actin structure remains to be elucidated, it is presumed to act as a gatekeeper of IAM-BCV contacts, and thus delays vacuolar rupture (13). These novel strategies of manipulation of host pathways highlight the importance of using dynamic microscopy setups in conjunction with host factor localization subversion screens to further elucidate the molecular mechanism of *Shigella* invasion.

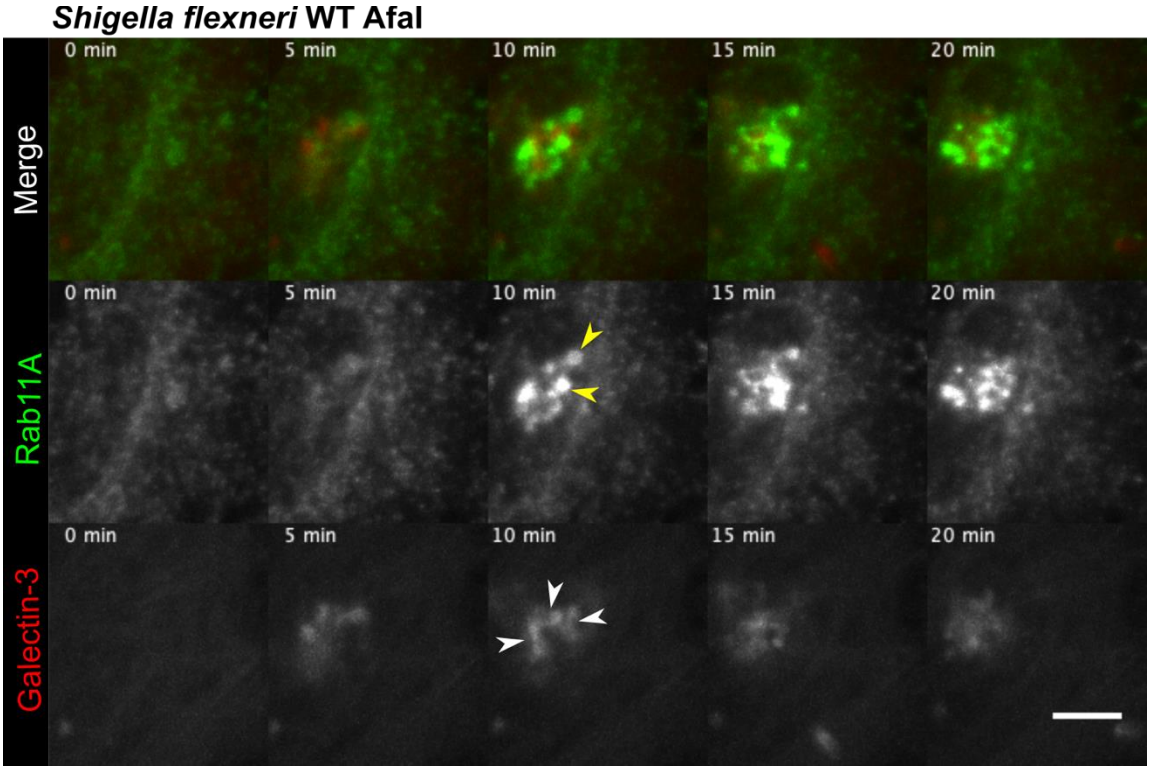

Figure 1: Re-localization of Rab11A during *Shigella* M90T AfaI infection of HeLa cells as useful tool to determine the dynamics of the bacterial invasion process. Rab11A can be distinctively observed recruited to the *Shigella*-IAMs (yellow arrowheads) during BCV rupture (white arrowheads show the galectin-3-mOrange signal around the bacteria) and remains present there during the BCV disassembly process 20 min post-infection. Scale bar is 5µm.

Fluorescence-based screens enable the observation of a protein re-localization from its physiological environment. These advantages have been essential at decoding bacteria invasion mechanism through

screening assays. The use of small inhibitor molecules (18) and bacterial effectors (12) have been crucial tools for effectively decrypting molecular pathways subverted by bacteria though screens. However, these indirect assays often impact multiple signaling pathways which may pose a challenge in identifying specific molecular pathways. More powerful and direct screens such as loss-of-function-based assays relying on RNA interference or CRISPR-Cas9 knock-out by specifically targeting host proteins may provide a clearer molecular interpretation (19). Moreover, these types of screens can be adapted for genome-wide coverage of host factors (20). These loss-of-function screens require however a robust read-out for interpretation of the results and often have been adapted for fixed experimental conditions. By contrast, dynamic screens have the advantage of allowing the direct observation of the subversion of cellular factors through the use of genetically-encoded fluorescent probes or dyes. Coupling these assays with automated microscopy has allowed the development of dynamic screens for high-throughput (21, 22). Medium-sized screens covering a chosen subset of fluorescently labeled host factors represent a compromise for live microscope as their generation and handling of these subgenomic expression vector libraries of fluorescently tagged host factors can be done relatively easily. Here, we detail an optimized protocol for a medium-sized multichannel time-lapse screen using *Shigella* as a model, but readily adaptable for numerous host-pathogen interactions or chemical insults.

2. Materials, solutions, cell lines and bacterial strains

2.1. Bacterial strains:

- *Shigella flexneri* wildtype strain M90T (23) expressing the adhesin AfaI (24) was used
- The non-invasive strains *Shigella flexneri* mutant M90T ΔmxiD (25) AfaI and the *Shigella flexneri* derivative lacking the virulence plasmid BS176 (26) AfaI were used as controls
- Chemically competent *E. coli* DH5 alpha (27)

2.2. Bacterial culture:

- Trypticase casein soy broth medium (TCSB): 17 g/L casein (pancreatic digest), 3 g/L soya peptone (papaic digest), 5 g/L NaCl, 2.5 g/L K_2HPO_4, dextrose 2.5 g/L
- TCSB agar (to the TCSB composition: 15 g/L agar; pH 7.3 ± 0.2) supplemented with 0,01 % w/v Congo Red and 50 µg/mL ampicillin
- LB medium: 10 g/L Bacto tryptone, 5 g/L Bacto yeast extract, 10 g/L NaCl, pH: 7.0 ± 0.2
- LB agar: add to the LB medium composition 15g/L agar

2.3. Cell culture:

- Dulbecco's Modified Eagle Medium (DMEM) (Gibco)
- Fetal Bovine Serum (FBS) (Sigma Aldrich)
- HeLa ATCC CCL-2
- 96-well black cell culture microplate, PS walls (Polystyrene), borosilicate bottom, F-bottom (chimney well), µCLEAR, advanced TC (Greiner Bio-One)

2.4. Plasmid library maintenance, purification and transfection:

- Plasmid stocks in sterile TE buffer (10 mM Tris, 1 mM EDTA, pH 8.0) or DNAse-free water (plasmid library)
- Glycerol 50% (v/v)
- NucleoSpin Plasmid Transfection-grade, Mini kit for ultrapure plasmid DNA (Macherey-Nagel)
- X-tremeGENE 9 DNA transfection reagent (Roche)
- Opti-MEM Reduced Serum Medium (Gibco)

2.5. Infection:

2.5.1. Bacterial infection:

- EM buffer: 120 mM NaCl, 7 mM KCl, 1.8 mM $CaCl_2$, 0.8 mM $MgCl_2$, 5 mM glucose, 25 mM HEPES, pH 7.3

2.5.2. Light microscopy:

- Multi-position, time-lapse image sequences were acquired using a Nikon Ti-E inverted epifluorescence microscope enclosed in a heating chamber with an integrated Perfect Focus System (TI-ND6-PFS Perfect Focus Unit) and equipped with the Ti-S-E motorized stage. The NIS-Elements AR (Advanced Research) microscope imaging software version 4.60 piloted the microscope, and a Nikon Plan Fluor 40X air objective (NA 0.75, WD 0.66) was used in our experimental setup. The filter cubes were: FITC (Ex: 465-495nm, Em: 515-555nm, Mirror: 505 to ∞ nm) and TRITC (Ex: 528-553nm, Em: 590-650nm, Mirror: 565 to ∞ nm).

2.6. Data Processing and Analysis:

- Fiji (Fiji Is Just ImageJ) 2.1.0/1.53c (download: https://imagej.net/Fiji/Downloads) and Icy (download: http://icy.bioimageanalysis.org/download)
- Excel 2016 (Microsoft)

3. Methods

In comparison to single-well live cell imaging, time-lapse screening requires important adjustments along with a well-designed experimental workflow. To address a specific question, key experimental parameters must be evaluated prior to proceeding to a screen. The weight of each parameter depends on the specific question to be investigated. Generally, the critical parameters to be assessed include the spatial resolution, the temporal resolution and the number of events necessary for proper interpretation of the results. Medium-sized screens are achievable by multiplexing, and the size of the screen depends on the parameters analyzed (the compartments of interest, the swiftness of the event). Pre-screen experiments are therefore important to determine the optimal experimental parameters. The following protocol was designed for *Shigella* infections and optimized for our objectives. As the subversion of Rab GTPases, such as Rab11A by *Shigella* is already well characterized, using this host factor as setup control comes very handy for experimental finetuning (**Figure 1**). Furthermore, adapting the parameters allows to perform screens with other bacterial pathogens (*see* **Note 1**).

3.1. Plasmid library preparation and handling

Our protocol has been successfully performed on a published library of expression vectors for fluorescently labeled proteins with BAR domains involved in trafficking and membrane curvature (28). This library contains 66 proteins, and it was maintained as follows.

1. 80µL of chemically competent DH5 alpha *E. coli* were transformed with each plasmid of the library. Bacterial pellets were stored at -80°C, and thawed on ice for 30min. Afterwards, 0.5 to 3µL (around 100ng) of plasmid was incubated with the bacteria on ice for 30 min prior to a 30 sec heat shock at 42°C in a water bath (or a heating block). Thereupon, the bacteria were left to recover in 950µL of LB medium for 1h at 37°C, 220 rpm (*see* **Note 2**)**.** Then, 100µL of the culture was spread into an LB agar plate and incubated at 37°C overnight.
2. An overnight culture was prepared from one of the obtained colonies (the plate can be kept for a month at 4°C if prepared freshly). A bacterial stock was prepared with 500µL of an overnight culture and 500µL of 50% glycerol (v/v) and stored at -80°C as a transformed bacteria stock.
3. The following day, 4 mL of bacterial overnight culture (from one of the obtained colonies) was miniprepped for an extraction and purification of the 66 plasmids (as described in the manufacturer's instructions). The elution was performed with 50µL of DNase-free sterile water (*see* **Note 3**).

4. The plasmid quantity obtained was then measured using a nanodrop spectrophotometer and the plasmid stock was placed at -20°C for long-term storage. A working stock was prepared at a concentration of 200 ng/L and stored at 4°C.

After plasmid library preparation, pre-screening of the following parameters was performed. Transfection efficiency and signal strength were assessed for the different library plasmids, and this was matched with the infection efficiency of the used *Shigella* strains. The pacing of the time-lapse acquisitions could be deduced from the data of data obtained from the Rab11A transfection experiments. During these experiments we co-transfected cells with a vacuolar rupture marker galectin-3 fused to mOrange (30).

3.2. Cell culture and transfection

More specifically, the localization and expression of each transfected protein "candidate" of the plasmid library as well as to the level of expression of the protein must be verified and optimized if necessary. This is critical for the microscope acquisition (*see* **Note 4**).

1. Three days prior to the experiment, cells were seeded into a black 96-well plate (*see* **Note 5, 6**). When pre-screening for the optimal number of infection events, a particular attention should be drawn to optimizing the density of cells, we recommend testing a range of 5,000 to 10,000 HeLa cells per well for this plate format. For our screen, HeLa cells were seeded at a density of 8,000 cells per well in DMEM supplemented with 10% FBS and incubated overnight at 37°C, 5% CO_2 (*see* **Note 7**). The volume of cells seeded was 100µL to ensure an adequate amount of nutrients to the cells until the experimental day.
2. The next day, the cells were transfected using X-tremeGENE 9 DNA reagent using a 3:1 transfection reagent to DNA ratio (see manufacturer's instructions). Keeping all DNA working stocks at the same concentration (200µg/µL) allows for downscaling the transfection mix and automating the transfection. After room temperature incubation, 5µL of transfection mix was added to each well followed by a 24 to 48h incubation at 37°C with 5% CO_2. The transfection can be optimized following the recommendations of the manufacturer (*see* **Note 8**). If multiple wells are to be imaged, we recommend preparing the transfection mix in sterile plastic 96-well plates. Plates were closed with sealing film before vortexing the mix. We suggest using a multi-channel pipette to prepare the mix and distributing it into each well.

3.3. Bacterial inoculum preparation

1. On the day of the transfection, the M90T AfaI strain was streaked on a TCSB agar plate supplemented with Congo red and ampicillin (50µg/mL) and incubated overnight at 37°C. The next day, three red colonies (indicative of virulent *Shigella* (29) were inoculated in TCSB broth supplemented with ampicillin (50µg/mL) and incubated overnight at 37°C in a 220 rpm shaking incubator on a 45° inclined tray.
2. Prior to starting the time-lapse experiment, a 1:100 dilution of bacterial overnight culture in ampicillin-supplemented TCSB media (50µg/mL) was prepared. The subculture was incubated for 2h at 37°C shaking at 220 rpm. During the subculture growth, the EM buffer was warmed at 37°C.
3. After 2h, the bacterial subculture optical density 600 (OD_{600}) was measured. At an OD_{600} of ≈0.4-0.7, 1mL of subculture was spun down at 6,000*g* in a tabletop centrifuge for 1 minute and the bacterial pellet was washed once with 1mL EM buffer (*see* **Note 9**).
4. 1 mL of bacteria inoculum was then prepared at a multiplicity of infection (MOI) of 20 in EM buffer for an estimated number of 64,000 cells in each well. The bacterial inoculum was kept warm at 37°C until the bacterial infection (*see* **Note 10**).

3.4. Bacterial infection

The following bacterial infection steps were optimized for a *Shigella* screen nonetheless these steps can be adapted to other pathogens. Particular attention should be drawn to the infection pre-screen. The bacteria load (MOI and volume of bacteria inoculum) should be carefully pre-screened. The following steps can be used as generic tests however we recommend testing bacterial infections at different MOIs to ensure an adequate number of infection events for the pre-determined optimal number of seeded cells.

1. The cells were washed three times with 37°C EM buffer and the medium was replaced with 50 µL of warm EM buffer (*see* **Note 11**).
2. Immediately after, the microplate was placed on a 37°C pre-warmed Nikon Ti-E microscope stage (*see* **Note 12**). Afterwards, using the NIS-Elements AR software, the sample's exposure parameters were set for an N-dimensional acquisition (ND acquisition window) using the Time-Lapse T and Multi-point XY acquisition dimensions (see part 3.5 on microscope acquisition for more details). At this point, a test run was performed to ensure sufficient time to acquire all positions (*see* **Note 13**).
3. For the time lapse screening setup, the different positions are chosen manually (*see* **Note 14**). Then, 40µL of the bacteria inoculum was added to each well (keep the well plate immobile to maintain the XY for each position), the plate was covered to prevent evaporation of the medium (to keep the

focus set on the positions) and the run was launched (*see* **Notes 15, 16**). The volume of bacteria added to the well may be adjusted to optimize the start time of the infections (*see* **Note 17**). It is noteworthy to consider that the remaining wells of the 96-wellplate can be used if (i) the plate is kept sterile or (ii) the wells are decontaminated between the runs (*see* **Note 18**).

3.5. Microscope acquisition

In the following workflow, we detail a possible setup for the image acquisition (**Figure 2**). We stress that the acquisition parameters mentioned below are to be carefully pre-determined according to the microscope that will be used for the screen. Concerning our screen, in addition to the BAR domain protein library which was eGFP-tagged, we also used galectin-3 (30), coupled to an mOrange fluorophore as used in our setup experiments with Rab11A (*see* **Figure 3**). This marker allows for the monitoring of the precise onset of the BCV rupture and the fate of the membrane remnants during the time course. Using two fluorescent reporters, attention needs to be paid to the use of proper filter cubes and the cross-talk of channels needs to be reduced to avoid a bleed-through (*see* **Note 19**).

To screen for the 66 BAR domain proteins, we divided our layout into 7 plates, each containing 10 BAR domain protein conditions each (**Figure 2**). These 7 plates were measured one after the other using FITC (eGFP-tagged library) and TRITC (galectin-3-mOrange) filter cubes (see part 2.5.2) with the parameters set as follows:

1. The exposure time and the binning of the camera settings **(***see* **Note 20**) were set respectively to 200-300ms and 1x1. It is important to test several exposure times prior to the screen as it will affect the number of positions acquired. Differences in protein expression among the screened factors need to be taken into account and should be considered when pooling the specific subsets for the successive microscope runs (*see* **Note 21**).
2. The focus was set on the cells with the PFS (Perfect Focus System) using a 40 X air objective (although higher magnification long working distance air objectives may also be used). It is important to set the focus prior to adding the bacteria otherwise the it may drift from the cells to the bacteria. Moreover, setting the focus prior to choosing the positions allows the PFS position to be recorded when selecting the positions in the NIS Elements software.
3. In our experiment, the time-lapse was set to 2 minutes for a 2 hour-long acquisition. Depending on the event-of-interest this parameter can be optimized but a compromise has to be made between the number of events to observe and the number of positions to acquired.

4. Afterwards, XY positions were selected based on brightness and phenotype using the FITC channel (the signal-of-interest). Per plate, 3 positions per well were selected manually. Each position contained multiple cells co-transfected with the protein of interest and galectin-3-mOrange (*see* **Note 22**). The order of acquisition of each well was chosen to allow the motorized stage to travel along the fastest path to minimize delays between image acquisition.

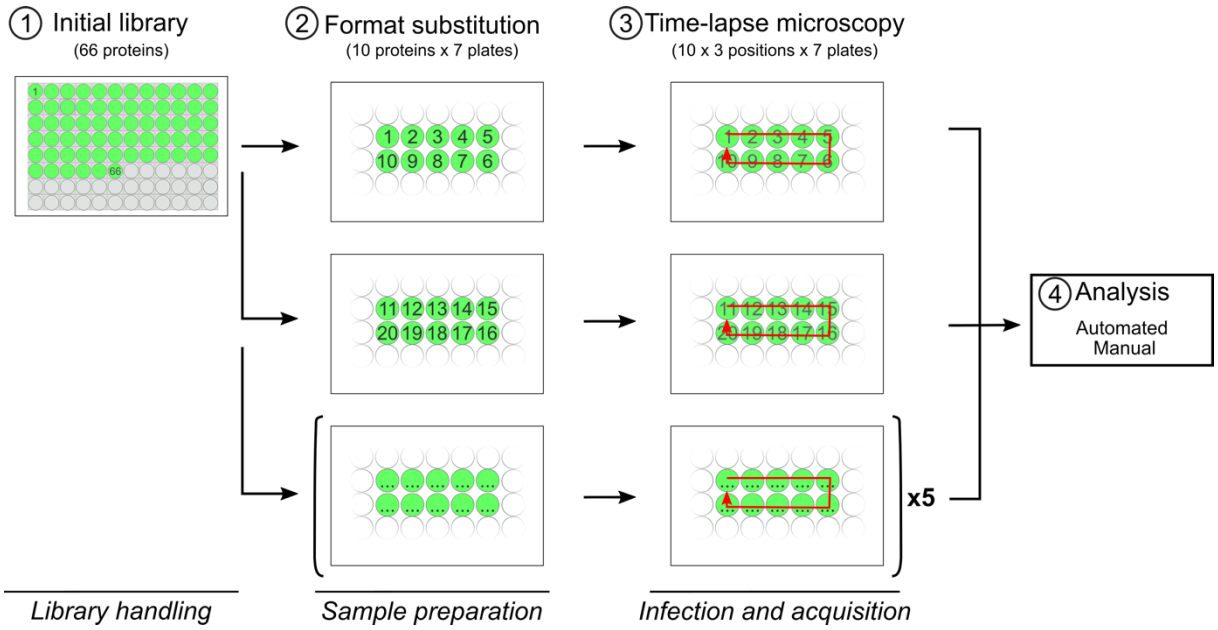

Figure 2: Workflow example of a medium-sized time-resolved screen. The initial plasmid library (66 proteins) is prepared and stored. Afterwards the samples that are prepared for imaging with the library are subdivided (the specific subdivision being determined by pre-screen experiments). Following this, the cells are infected and the protein "candidates" are screened by time-lapse microscopy following a path from well to well in an optimal way (also respecting the addition of bacteria to the wells for synchronicity).

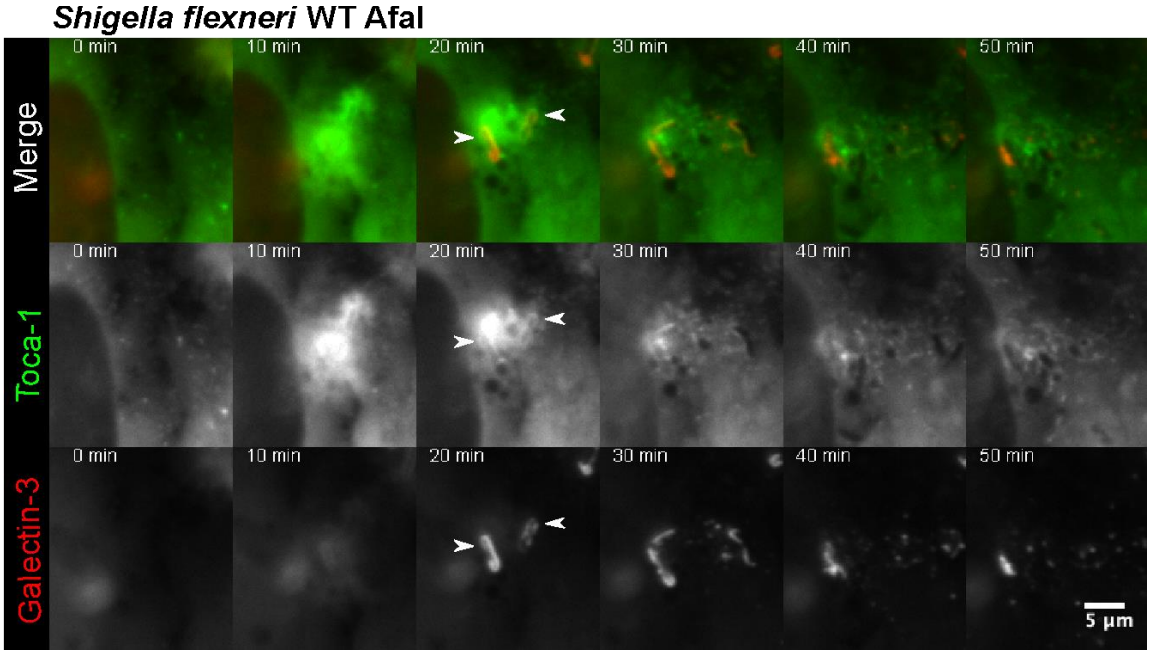

Figure 3: BAR-domain protein candidate Toca-1 (F-BAR family) enrichment to a *Shigella* M90T AfaI infection site in real-time (2 min time-lapse). Two bacteria are shown entering (signaled by the arrowheads). Both BCVs are shown ruptured at 20 min post-infection by the galectin-3-mOrange reporter. During bacterial entry, Toca-1-eGFP is recruited to the entry foci near the bacteria, the signal decreases in later time-points. The BCV membrane remnants can be seen being peeled-off after vacuolar rupture starting from the 30 min time-point.

3.6 Data analysis of bacterial infection foci and bacteria-triggered compartments

Through this *Shigella* invasion example, we present tools to analyze time-lapse imaging data for a medium-size protein screen. Nonetheless, it should be noted that a negative control for protein recruitment (such as eGFP only) and a positive control (such as the described Rab11A, **Figure 1**) are crucial for accurately identifying positive and negative hits. Non-infecting bacterial mutants, in the case of a *Shigella* screen: M90T *ΔmxiD* or BS176 strains (or other) were used as negative controls for infection to properly analyze such a large data library.

The relevant parameters we focus on including host factor recruitment to the bacteria infection site and the bacteria movement. Protein recruitment, as well as the state of bacterial compartments, are dynamic events (e.g. BCV rupture, changes in compartment size). Additionally, the physiological localization of host factors can make analysis difficult to interpret. Consequently, automated time-resolved imaging analysis is often challenging.

1. The data obtained from the Nikon NIS Elements software are generated in ND2 format (*see* **Note 23**). It can be processed using open-source software Fiji and Icy.
2. The Icy Spot Detector tool (31), detects bright spots in fluorescence images. A specific region of interest (ROI) can be analyzed which can be useful to detect the recruitment of proteins enriched at cellular structures at the invasion site or (at a higher magnification) to bacteria-triggered compartments such as macropinosomes. Size exclusion was used to avoid non-specific crosstalk.
3. Individual bacteria movements were tracked using the ImageJ plugin TrackMate (32).

Regardless, there are no direct automated methods to investigate the specific recruitment of proteins to a bacterial compartment. Hence, manual inspection remains necessary to investigate more complex phenotypes of the host factor subversion during the dynamic entry process. This is only feasible when using libraries containing up to 100 different conditions. In case of larger libraries, we recommend developing dedicated detection algorithms.

4. Notes

1. Although this screen has been optimized for *Shigella* infection, this workflow has successfully worked with *Salmonella* and other bacterial pathogens and can be combined with more complex dynamic setups (e.g., molecular inhibitors). If other pathogens are used, we recommend carefully testing the infection (infectivity, number of events, etc.) using our infection setup. For *Salmonella* infections, we suggest being very stringent with the temperature as everything must be at 37°C prior to the infection (*see* **Note 15**) and adjusting the bacteria load (MOI and inoculum volume) to optimize the infection.
2. In case transformations of plasmids were difficult, we suggest to use commercially available competent Top10 bacteria, which in our hands show a better transformation efficiency.
3. The eluted plasmids must be endotoxin-free to avoid unspecific immunogenic reactions upon transfection. Therefore, the DNA extraction kit must thus have an ethanol or isopropanol step. This step is critical for proper interpretation of the obtained data.
4. The overexpression of proteins can sometimes lead to mis-localization of the protein from its host cellular compartment. This can also lead to artifacts. Thus, verifying the localization of the protein-of-interest is necessary. The comparison to previously reported observations in online protein databases such as the Human Protein Atlas and UniProt is a quick way to confirm its proper localization. The localization of the protein can also be inspected by immunofluorescence.

Additionally, for proteins for which the expression levels strongly impact cellular mechanisms (such as GTPases), verifying gene expression is crucial. Western Blot using an anti-GFP antibody or RT-qPCR are excellent options to compare the overexpression level of the protein to the endogenous protein.

5. It is critical to use black wall glass-bottom plates when imaging fluorescence as it prevents the light from the sample exposure to contaminate the other wells. This protects the rest of the sample from photobleaching.
6. In the case of our screen, the plates we used are made from optical-grade polystyrene walls with a borosilicate bottom (175 micrometer thickness). For our experiment and microscope set-up we considered them ideal, however if a higher resolution is desired, glass bottom dishes with a thickness adjusted for high-resolution objectives should be used. A water or oil objective can provide excellent resolution, however due to the immersion media, fewer conditions can be analyzed per acquisition run. In this case a comprise must be made between the "size" of the screen and the spatial resolution desired.
7. In this screen, we have used HeLa cells. However, this protocol can be adapted for any adherent cells (optimization of cell seeding, DNA transfection, infection, and acquisition parameters may be required). At a given density, we roughly obtained 10 fluorescent cells per position with our microscope set-up. Therefore, if using different cells and for a specific microscope setup, we recommend adjusting cell seeding at satisfying density if the cell growth rate differs from HeLa cells.
8. The transfection incubation time should be optimized based on changes in cellular morphology as well as on the desired fluorescence level of the protein of interest. The DNA transfection should be tested in advance to determine the optimal transfection conditions. Also, the transfection mix preparation can be downscaled to a 5^{th} of the manufacturer's recommended 3:1 ratio reagent/DNA volumes – this may be helpful for a 96-well format. For cells that are difficult to transfect, we recommend using XtremeGENE HP (Promega).
9. *Shigella* colonies and bacterial cultures require a minimum of 16h for adequate growth. This is critical for the subculture to reach an OD_{600} of 0.4-0.7 in 2h. The agar plate can be preserved at 4°C after colony growth and is usable for infection experiments for up to 7 days.
10. If kept at 37°C, the bacteria are infectious for up to one hour after preparation. However, we recommend using it within 15 minutes of preparing them to ensure reproducibility of the results.
11. For infection performed in EM buffer, we suggest to perform time-courses up to 3h-long to remain cells in healthy conditions. In addition, washing and keeping the cells prior to the infection with

pre-warmed buffer also ensures their well-being. The addition of 37°C liquid paraffine (we recommend 12 µL/well) after bacterial infection helps further to avoid evaporation.

12. We recommend the acquisition order of the wells to follow the bacterial inoculum to each well. This ensures that the acquisition occurs with minimal delay in the wells. It is especially important if the events of interest occur early during the infection.
13. Simultaneous multicolor microscopy can be used to increase the screening throughput. This can be achieved using two cameras and a dichroic beam-splitter. This setup exposes the sample only once while capturing simultaneously two fluorescence signals thanks to the un-mixing of the signals by the beam splitter.
14. Well spread and transfected cells were selected. Additionally, the chosen cells were expressing the protein of interest at low to medium levels. This is crucial as recruitment leads to a gain of signal. If the fluorescence level is too high before infection saturation effects may occur. Moreover, a high expression of the candidate protein might lead to changes in morphology and and non-physiological behavior of the protein.
15. Bacteria should be rapidly added to each well prior to launching the acquisition, especially if the invasion process starts rapidly. In case of rapid events, multichannel pipettes help to increase synchronicity.
16. Importantly, all buffers, as well as the cells, must be pre-heated and kept at 37°C. The *Shigella* T3SS is expressed at 37°C and if the bacteria are not properly kept at this temperature, they may lose their invasion capacity. In our hands, this is even more important for other bacterial pathogens like *Salmonella*.
17. The volume of bacterial inoculum affects the time delay between the inoculum and the initial contact between the bacteria and the host cell. Testing different volumes during the pre-screening experiments is useful. For *Salmonella* infections, we recommend lowering the volume to 30 µL for a quicker invasion as otherwise infections start much later during the acquisition. It is also important to note that one must in all cases keep everything at 37°C and launch rapidly the bacterial infection.
18. Plates can be “recycled” by using the un-used wells if kept sterile.
19. To reduce bleed-though, the exposure time should be carefully set. If bleed-though is unavoidable, we recommend in this case lowering the exposure time to observe a minimal amount of cross-talk.
20. The differential expression levels of fluorescent protein candidates can hamper the proper acquisition of some of the tested proteins. Therefore, we suggest to subdivide the library of expression vectors in accordance to expression level of transfected protein, with a pooling of similarly expressed proteins in each sub-experiment.

21. It is critical for a time-lapse acquisition to adjust the exposure times and the power of the light source in a way to avoid extensive photobleaching throughout the acquisition. For a general protein recruitment screen during *Shigella* (or *Salmonella*) entry into host cells, we recommend 1 to 2-minute time-lapses for an exploratory primary screen. This setup allows a good observation of the *Shigella* invasion events.
22. The number of positions acquired should be a compromise when screening a medium-sized library. For this reason, the size of the microscope field of view and the speed of the motorized stage are important.
23. We recommend saving the acquisition files in .nd2 format as this format also records the acquisition metadata.

6. Acknowledgments

The authors of this manuscript wish to thank the entire DIHP unit and particularly the following lab members Laurent AUDRY, Laura BARRIO and Magdalena GIL for fruitful discussion, constructive criticism, technical support and mentorship during this project. The DIHP unit is supported by an ERC grant (ERC-CoG-Endosubvert), and the ANR (StopBugEntry, HBPSensing), and it is part of the two LabExes IBEID and Milieu Interieur.

7. References

1. Cossart P, Sansonetti PJ. (2004) Bacterial invasion: the paradigms of enteroinvasive pathogens. Science. doi: 10.1126/science.1090124.
2. Voznica J, Gardella C, Belotserkovsky I, Dufour A, Enninga J, Stévenin V. (2017) Identification of Parameters of Host Cell Vulnerability during Salmonella Infection by Quantitative Image Analysis and Modeling. Infect Immun. doi: 10.1128/IAI.00644-17.
3. Rengarajan M, Theriot JA. (2020) Rapidly dynamic host cell heterogeneity in bacterial adhesion governs susceptibility to infection by *Listeria monocytogenes*. Mol Biol Cell. doi: 10.1091/mbc.E19-08-0454.
4. Ortega FE, Koslover EF, Theriot JA. (2019) *Listeria monocytogenes* cell-to-cell spread in epithelia is heterogeneous and dominated by rare pioneer bacteria. Elife. doi: 10.7554/eLife.40032.

5. Lorkowski M, Felipe-López A, Danzer CA, Hansmeier N, Hensel M. (2014) Salmonella enterica invasion of polarized epithelial cells is a highly cooperative effort. Infect Immun. doi: 10.1128/IAI.00023-14.
6. Fredlund J, Santos JC, Stévenin V, Weiner A, Latour-Lambert P, Rechav K, Mallet A, Krijnse-Locker J, Elbaum M, Enninga J. (2018) The entry of Salmonella in a distinct tight compartment revealed at high temporal and ultrastructural resolution. Cell Microbiol. doi: 10.1111/cmi.12816.
7. Malik-Kale P, Winfree S, Steele-Mortimer O. (2012) The bimodal lifestyle of intracellular Salmonella in epithelial cells: replication in the cytosol obscures defects in vacuolar replication. PLoS One. doi: 10.1371/journal.pone.0038732.
8. Stévenin V, Chang YY, Le Toquin Y, Duchateau M, Gianetto QG, Luk CH, Salles A, Sohst V, Matondo M, Reiling N, Enninga J. (2019) Dynamic Growth and Shrinkage of the Salmonella-Containing Vacuole Determines the Intracellular Pathogen Niche. Cell Rep. doi: 10.1016/j.celrep.2019.11.049.
9. Luk CH, Valenzuela C, Gil M, Swistak L, Bomme P, Chang YY, Mallet A, Enninga J. (2021) Salmonella enters a dormant state within human epithelial cells for persistent infection. PLoS Pathog. doi: 10.1371/journal.ppat.1009550.
10. Schroeder GN, Hilbi H. (2008) Molecular pathogenesis of *Shigella* spp.: controlling host cell signaling, invasion, and death by type III secretion. Clin Microbiol Rev. doi: 10.1128/CMR.00032-07.
11. Ehsani S, Santos JC, Rodrigues CD, Henriques R, Audry L, Zimmer C, Sansonetti P, Tran Van Nhieu G, Enninga J. (2012) Hierarchies of host factor dynamics at the entry site of *Shigella flexneri* during host cell invasion. Infect Immun. doi: 10.1128/IAI.06391-11.
12. Weiner A, Mellouk N, Lopez-Montero N, Chang YY, Souque C, Schmitt C, Enninga J. (2016) Macropinosomes are Key Players in Early *Shigella* Invasion and Vacuolar Escape in Epithelial Cells. PLoS Pathog. doi: 10.1371/journal.ppat.1005602.
13. Kühn S, Bergqvist J, Gil M, Valenzuela C, Barrio L, Lebreton S, Zurzolo C, Enninga J. (2020) Actin Assembly around the *Shigella*-Containing Vacuole Promotes Successful Infection. Cell Rep. doi: 10.1016/j.celrep.2020.107638.
14. Ray K, Bobard A, Danckaert A, Paz-Haftel I, Clair C, Ehsani S, Tang C, Sansonetti P, Tran GV, Enninga J.(2010) Tracking the dynamic interplay between bacterial and host factors during pathogen-induced vacuole rupture in real time. Cell Microbiol. doi: 10.1111/j.1462-5822.2010.01428.x.
15. Brumell JH, Scidmore MA. (2007) Manipulation of rab GTPase function by intracellular bacterial pathogens. Microbiol Mol Biol Rev. doi: 10.1128/MMBR.00023-07.

16. Mellouk N, Weiner A, Aulner N, Schmitt C, Elbaum M, Shorte SL, Danckaert A, Enninga J. (2014) *Shigella* subverts the host recycling compartment to rupture its vacuole. Cell Host Microbe. doi: 10.1016/j.chom.2014.09.005.
17. Chang YY, Stévenin V, Duchateau M, Giai Gianetto Q, Hourdel V, Rodrigues CD, Matondo M, Reiling N, Enninga J. (2020) *Shigella* hijacks the exocyst to cluster macropinosomes for efficient vacuolar escape. PLoS Pathog. doi: 10.1371/journal.ppat.1008822.
18. Perlman ZE, Slack MD, Feng Y, Mitchison TJ, Wu LF, Altschuler SJ. (2004) Multidimensional drug profiling by automated microscopy. Science. doi: 10.1126/science.1100709.
19. Conrad C, Gerlich DW. (2010) Automated microscopy for high-content RNAi screening. J Cell Biol. doi: 10.1083/jcb.200910105.
20. Mohr S, Bakal C, Perrimon N. (2010) Genomic screening with RNAi: results and challenges. Annu Rev Biochem. doi: 10.1146/annurev-biochem-060408-092949.
21. Pepperkok R, Ellenberg J. (2006) High-throughput fluorescence microscopy for systems biology. Nat Rev Mol Cell Biol. doi: 10.1038/nrm1979.
22. Sönnichsen B, Koski LB, Walsh A, Marschall P, Neumann B, Brehm M, Alleaume AM, Artelt J, Bettencourt P, Cassin E, Hewitson M, Holz C, Khan M, Lazik S, Martin C, Nitzsche B, Ruer M, Stamford J, Winzi M, Heinkel R, Röder M, Finell J, Häntsch H, Jones SJ, Jones M, Piano F, Gunsalus KC, Oegema K, Gönczy P, Coulson A, Hyman AA, Echeverri CJ. (2005) Full-genome RNAi profiling of early embryogenesis in Caenorhabditis elegans. Nature. doi: 10.1038/nature03353.
23. Sansonetti PJ, Kopecko DJ, Formal SB. (1982) Involvement of a plasmid in the invasive ability of *Shigella flexneri*. Infect Immun. doi: 10.1128/iai.35.3.852-860.1982.
24. Nowicki B, Hart A, Coyne KE, Lublin DM, Nowicki S. (1993) Short consensus repeat-3 domain of recombinant decay-accelerating factor is recognized by Escherichia coli recombinant Dr adhesin in a model of a cell-cell interaction. J Exp Med. doi: 10.1084/jem.178.6.2115.
25. Allaoui A, Sansonetti PJ, Parsot C. (1993) MxiD, an outer membrane protein necessary for the secretion of the *Shigella flexneri* lpa invasins. Mol Microbiol. doi: 10.1111/j.1365-2958.1993.tb01097.x.
26. Sansonetti PJ, Ryter A, Clerc P, Maurelli AT, Mounier J. (1986) Multiplication of *Shigella flexneri* within HeLa cells: lysis of the phagocytic vacuole and plasmid-mediated contact hemolysis. Infect Immun. doi: 10.1128/iai.51.2.461-469.1986.
27. Chan Wah Hak L, Khan S, Di Meglio I, Law AL, Lucken-Ardjomande Häsler S, Quintaneiro LM, Ferreira APA, Krause M, McMahon HT, Boucrot E. (2018) FBP17 and CIP4 recruit SHIP2 and

lamellipodin to prime the plasma membrane for fast endophilin-mediated endocytosis. Nat Cell Biol. doi: 10.1038/s41556-018-0146-8.

28. Green MR, Sambrook J. (2018) The Hanahan Method for Preparation and Transformation of Competent *Escherichia coli*: High-Efficiency Transformation. Cold Spring Harb Protoc. doi: 10.1101/pdb.prot101188.
29. Qadri F, Hossain SA, Ciznár I, Haider K, Ljungh A, Wadstrom T, Sack DA. (1988) Congo red binding and salt aggregation as indicators of virulence in *Shigella* species. J Clin Microbiol. doi: 10.1128/jcm.26.7.1343-1348.1988.
30. Paz I, Sachse M, Dupont N, Mounier J, Cederfur C, Enninga J, Leffler H, Poirier F, Prevost MC, Lafont F, Sansonetti P. (2010) Galectin-3, a marker for vacuole lysis by invasive pathogens. Cell Microbiol. doi: 10.1111/j.1462-5822.2009.01415.x.
31. Olivo-Marin J-C. (2002) Extraction of spots in biological images using multiscale products. Pattern Recogn 35:1989–1996
32. Tinevez JY, Perry N, Schindelin J, Hoopes GM, Reynolds GD, Laplantine E, Bednarek SY, Shorte SL, Eliceiri KW. (2017) TrackMate: An open and extensible platform for single-particle tracking. Methods. doi: 10.1016/j.ymeth.2016.09.016.

3.2. Manuscript 2 - *Shigella* uses distinct IAM subpopulations during epithelial cell invasion to promote efficient intracellular niche formation

Lisa Sanchez[1,2], Camila Valenzuela-Montenegro[1], Michael G. Connor[3], Jost Enninga[1]

Affiliations :

1. Dynamics of Host-Pathogen Interactions Unit, Institut Pasteur, UMR3691 CNRS, Paris 75015, France,
2. Université de Paris, Sorbonne Paris Cité, Paris, France,
3. Chromatin and Infection Unit, Institut Pasteur, Paris 75015, France

Corresponding author: Enninga, Jost (jost.enninga@pasteur.fr).

Abstract

The intracellular bacterial pathogen *Shigella flexneri* invades non-phagocytic epithelial gut cells. Through a syringe-like apparatus called type 3 secretion system, it injects effector proteins into the host cell triggering actin rearrangements leading to (i) its uptake within a tight vacuole, termed the bacterial-containing vacuole (BCV), and simultaneously (ii) the formation of large vesicles, which we refer to as infection-associated macropinosomes (IAMs). Afterwards, *Shigella* ruptures the BCV and escapes into the host cytosol by disassembling the BCV remnants. Previously, IAMs have been shown to play a key role in *Shigella* BCV escape. Nonetheless, little is known so far on the composition and role of these IAMs. Using a microscopy-based screen, we investigated the recruitment of a family of host cell proteins involved in a variety of cellular events involving membrane curvature and sensing (e.g. endocytosis and recycling) called BAR domain proteins during *Shigella*-infection. We identified endosomal recycling protein Sorting Nexin-8 localized to IAMs in a PI(3)P-dependent manner. Further characterization showed the presence of two distinct IAM subpopulations around the BCV, either recycling back to the plasma membrane or transitioning to to become RAB11A positive "contact-IAMs" promoting BCV rupture. The IAM subpopulation duality was marked by the exclusive recruitment of either SNX8 or RAB11A. Our work sheds light on the how *Shigella* establishes its intracellular niche through selected subversion of macropinosomes.

Keywords:
Bacterial invasion, *Shigella flexneri*, BAR domain-containing protein, intracellular lifestyle, endosomal recycling.

1. Introduction

The entero-invasive bacterial pathogen *Shigella flexneri* is the causative agent of bacillary dysentery, affecting an estimated 80 to 165 million individuals (CDC, 2019). With the rise of multidrug resistant strains (Mahbubur et al. 2007, Kim et al. 2008, Puzari, Sharma and Chetia, 2018), *S. flexneri* (hereafter referred to as *Shigella*) has remained a major health threat. *Shigella* infection occurs when the bacterium traverses the gut epithelium through microfold cells and once in the sub-epithelium (Mounier et al. 1992, Perdomo et al. 1994, Sansonetti et al. 1996, Rey et al. 2020), *Shigella* uses a syringe-like apparatus, the type 3 secretion system (T3SS), to invade non-phagocytic epithelial gut cells (Schroeder and Hilbi, 2008). Upon contact with the host cell membrane, *Shigella* injects bacterial effectors into the target cell triggering massive local remodeling of the actin network (Schroeder and Hilbi, 2008, Valencia-Gallardo et al. 2014). This leads to the formation of positively shaped membranes ruffles whose collapse prompts the formation of concave membrane compartments. These enable (i) the internalization of the bacterium within a tight phagosome-like vacuole (Weiner et al. 2016) referred to as the bacteria-containing vacuole (BCV) and simultaneously (ii) the formation of vesicles heterogeneous in size that are morphologically similar to macropinosomes (Cossart and Sansonetti, 2004, Weiner et al. 2016), termed infection-associated macropinosomes (IAMs). *Shigella* then triggers BCV rupture and disassembly prompting its access to the host cell cytosol where it replicates and spreads to adjacent cells by forming an actin comet tail (Cossart and Sansonetti, 2004, Kühn et al. 2020, Chang et al. 2020).

Although the contribution of host molecular pathways subverted in the invasion and niche establishment of intravacuolar bacterial pathogens is well-defined, it remains less clear for cytosol-residing bacteria (López-Montero and Enninga, 2016, Mellouk and Enninga, 2016). While BCV rupture has been reportedly T3SS-mediated, for example through the translocator proteins IpaB and IpaC (High et al. 1982, Du et al. 2012), we previously demonstrated an impact of the endosomal recycling small GTPase RAB11A recruited to IAMs promoting BCV rupture (Mellouk et al. 2014, Weiner et al. 2016). We furthermore reported that BCV damage is followed by membrane remnant disassembly, a process indispensable for *Shigella* niche establishment (Kühn et al. 2020, Chang et al. 2020). Membrane disassembly requires RAB8A and RAB11A to be recruited to IAMs and brought in proximity of the BCV by the exocyst complex (Chang et al. 2020). These previous findings demonstrate a need to comprehensively analyze the contribution of host factors. Moreover, they decrypt IAMs not as bystander compartments but rather playing a key role in the process of *Shigella* intracellular niche formation highlighting the need to revisit and inspect in detail the *Shigella* infection process.

Membrane remodeling is actively driven by a combination of local changes in membrane lipid composition and protein-generated membrane reshaping triggering the formation of a positive or a negative curvature

necessary for a plethora of cellular processes from filopodia formation to endocytosis (McMahon and Gallop, 2005, Jarsch et al. 2016, Simunovic et al. 2019). Strikingly, the *Shigella* invasion process requires extensive membrane reshaping. Membrane ruffling is the protrusion of sheet-like extensions of the plasma membrane which subsequently curve and collapse (Swanson, 2008, Cossart and Roy, 2010, Ribet and Cossart, 2015, Buckley and King, 2017), therefore requiring curving of the local plasma membrane. Moreover, the formation of phagosomes and macropinosomes -compartments morphologically similar to the *Shigella*-triggered BCV and IAMs- has been shown to require extensive membrane reshaping (Swanson, 2008). Vesicle formation, scission and stability all require changes in lipid composition as well as protein intervention (Swanson, 2008, Swanson, 2014).

A family of membrane-binding proteins specializing in membrane reshaping and curvature sensing known as the BAR (Bin/Amphiphysin/Rvs) domain-containing proteins and involved in different cellular processes have been described (McMahon and Gallop, 2005, Allison Suarez et al. 2014, Simunovic et al. 2015, Simunovic et al. 2019). Characterized by the presence of a membrane-binding BAR domain, these proteins act in diverse cellular processes as signaling platforms (*e.g.* filopodia formation) and scaffolds (*e.g.* endosomal recycling) (Peter et al. 2004, Simunovic et al. 2015, Simunovic et al. 2019). Given their many functions in the cell, BAR domain proteins have been reportedly hijacked by invasive bacterial pathogens. *Enterohemorrhagic E. coli* was reported to reprogram negative curvature-inducing and actin remodeling factor IRSp53 to form an actin structure called the pedestal (Weiss et al. 2009, Yi and Goldberg, 2009). Endosomal recycling BAR protein SNX1 was shown to be recruited to the *Salmonella*-containing vacuole through the bacterial effector SopB to form tubular structures forming the *Salmonella* replicative niche (Bujny et al. 2008, Stévenin et al. 2019). Strikingly, *Shigella* has previously been reported to recruit BAR domain protein TOCA-1 to trigger actin rearrangements triggering actin cocoon formation and actin tail formation (Leung et al. 2008, Baxt and Goldberg, 2014, Kühn et al. 2020).

Given the essential function of BAR domain containing proteins in cellular processes and their involvement in membrane reshaping processes, we exploited a high-content multidimensional time-resolved fluorescence microscopy assay (Sanchez et al. 2021) to screen a library of the 66 BAR domain-containing proteins to comprehensively analyze the behavior of each “candidate” BAR proteins during *Shigella* invasion steps. Among host proteins being recruited at successive steps to the *Shigella* invasion site, we identified the sorting nexin family member SNX8 to be strongly present at IAMs before BCV damage and remaining there until membrane remnant disassembly. We also revealed that *Shigella* triggers the formation of several subsets of IAMs during its invasion of non-phagocytic epithelial cells with only a partial set of IAMs becoming SNX8 positive. The characterization of the SNX-positive subset showed a distinct maturation of IAMs from “canonical” macropinosomes. Furthermore, we found this subset to promote

efficient BCV egress. This diversity in IAMs reveals the *Shigella* invasion process as complex sequence of events with the bacteria hijacking multiple pathways of the endocytic and recycling pathways.

2. Materials and Methods

Bacterial strains and culture

In this study we used the *Shigella flexneri* strain M90T (Sansonetti et al. 1982) complemented with the uropathogenic *E. coli* adhesin AfaI. Prior to infection experiments, *Shigella* strains were grown overnight at 37°C from bacterial colonies grown on Trypticase Casein Soy Broth agar plates supplemented with ampicillin at 50µg/mL and 0.01% Congo Red. Experimental starters were prepared by inoculating 3 colonies in TCSB media supplemented with ampicillin 50µg/mL and incubated overnight at 37°C, 220 rpm.

Cell lines and culture conditions

HeLa cervical adenocarcinoma CCL2 clone from the American Type Culture Collection (ATCC) and CaCo-2 TC7 cells (ATCC) were cultured in Dulbecco's Modified Eagle Medium (DMEM High glucose with GlutaMAX™ and pyruvate, Gibco, #31966-021) supplemented with 10% heat-inactivated Fetal Bovine Serum (Sigma Aldrich) and incubated at 37°C, 5% CO_2.

Plasmids, cloning and cell line generation

The full list of plasmids used in this study is listed in Supplementary Table 1. The entire EGFP-tagged BAR domain plasmid library was a kind gift from Emmanuel Boucrot and is referenced in Chan Wah Hak et al. 2018. pDEST-SNX8-mApple was cloned by restriction enzyme digestion. Generation of stable HeLa cell lines was performed using the Sleeping Beauty System (Kowarz et al. 2015). In brief, pSBbi-Neo-SNX8-eGFP and pSBbi-Neo-LactC2-GFP were cloned by in vivo assembly using SLIC (Jeong et al. 2012). JetPRIME (Polyplus®, #101000027) was used to transfect plasmids into low passage HeLa cells with selection being performed using G418 at 800ng/mL (Euromedex, #EU0601) for 7 days. The cells were then collected, and serial dilution was performed in a 96 well plate with maintenance of the selection pressure. The selected cells were then amplified and sorted based on their fluorescence level using a FACS sorter.

Cell seeding and Transient transfections

Cells were seeded in either a black 96 well plate (Greiner Bio-One, #655090) or in a 35mm glass-bottom dish (ibiDI, #81158) containing a 4-chamber silicone insert (ibiDI, #80409). For both of these supports, HeLa cells were seeded at a density of 8,000 cells per well, whereas CaCo-2 TC7 cells were seeded at a density of 5,000 cells per well and transfected the following day. Transient transfections were performed by lipofection using FuGENE™ HD (Promega, #E2311) as instructed by the manufacturer. Briefly, transfection complexes were prepared by diluting 2 µg of plasmid (or for co-transfections, 1µg of each plasmid) in 100µL OptiMEM (Gibco, #31985062), mixed with 4 µL of FuGENE™ HD and incubated for 10 min at room temperature. Afterwards, 5 µL of transfection mixture was added per well containing the cells seeded the previous day, the cells were then incubated 48 hours at 37°C, 5% CO_2 prior to infection and imaging.

Infection protocol

Bacterial inoculum was prepared by diluting the starter culture to 1:100 in 8 mL of fresh TCSB media supplemented with ampicillin 50µg/mL and incubating it for 2 hours at 37°C, 220 rpm. Once the subculture OD_{600} reaches 0.4-0.6, 1mL of the subculture was spun 1 min at 6000*g* and the bacteria pellet is washed twice with warm EM buffer (120 mM NaCl, 7 mM KCl, 1.8 mM $CaCl_2$, 0.8 mM $MgCl_2$, 5 mM glucose, 25 mM HEPES, pH 7.3). An inoculum was prepared by diluting the bacterial suspension in EM buffer to reach a multiplicity of infection (MOI) of 20 bacteria/cell. For the inhibitor experiments, wortmannin (Sigma Aldrich, #W1628-1MG) and SAR405 (Selleckchem, #S7682) were dilute into the inoculum to 3.3µm and 3µM respectively from a DMSO stock solution. Prior to the infection, the cells were washed three times with EM Buffer to get rid of dead cells and 50µL of EM buffer were left in the well. For live imaging experiments, the infection was started by adding 40 µL of inoculum per well in a 37°C heated microscopy chamber. For fixed experiments, no medium was left in the well and 30 µL of inoculum with when needed 0.5mg/mL final dextran 10 000 MW Alexa-647 (Invitrogen™, #D22914) were added to the well, after which the samples were incubated at 20°C for 10 min to enable the bacteria to reach the cells. Infection was triggered by incubation at 37°C for 30min. Afterwards, samples were fixed using 4% paraformaldehyde (ThermoScientific, #043368.9M) for 10 min at room temperature and washed 3 times with PBS. DNA was stained using Hoechst (Invitrogen™, #1681305) and actin was stained by Rhodamine-Phalloidin (Invitrogen™, #R415) for 30 min prior to microscopy acquisition.

Immunofluorescence

Infections were carried out as previously described (see infection protocol). Following the fixation procedure, the cells were permeabilized using saponin diluted to 0,025% in PBS for 20 min at room temperature. Next, 3 PBS washes were performed and blocking was done with 2% Bovine Serum Albumin

(Sigma Aldrich,#A7906-100G) and 5% goat serum (Sigma Aldrich, #G9023) in PBS for 1 hour at room temperature. Afterwards, rabbit anti-SNX8 primary antibody (Sigma Aldrich, #HPA057296) diluted at 1:250 in blocking solution was incubated 1h at room temperature followed by a 45min incubation of a goat anti-rabbit Alexa-488 secondary antibody (Invitrogen, #A11034) diluted to 1:500 together with Hoechst and Rhodamine-Phalloidin. Images were acquired immediately following 3 PBS washes.

Microscopy

Time-resolved BAR domain protein screen experiments were performed in a Nikon Ti-E inverted microscope equipped with a Perfect Focus System (TI-ND6-PFS Perfect Focus Unit) using a 40X/ 0.75 NA air objective. High spatio-temporal resolution time-lapses were acquired on DeltaVision Elite (Leica) using a 60X/1.42 NA oil objective with a 0,35µm z-step and images were deconvolved using an integrated deconvolution software. Imaging of fixed experiments were acquired on a Nikon Ti-E inverted microscope equipped with a Perfect Focus System and a Yokogawa confocal spinning disk unit (CSU-W1) using a 60X/1.2 NA water objective. In this case, an automatic pipeline with autofocus using brightfield and Hoechst signal were used to define the focal plane of randomly generated points. Images were acquired at a step-size of 0.5µm in the z-plane.

Image Processing and quantification

Images were processed using Fiji (https://imagej.net/software/fiji/, version 2.1.0/1.53c). For the BAR domain screen, BAR protein TOCA-1 and EGFP were used as positive and negative controls respectively, with TOCA-1 having been shown to be recruited to the *Shigella* actin cage and actin tail (Leung et al. 2008, Kühn et al. 2020). Positive hits were counted as being enrichment of the "candidate" proteins to the infection site by comparison to the EGFP control (see Figure 1B). For the quantification of SNX8 positive IAMs, the SNX8 cytosolic fluorescence background was subtracted from the image. Cell Profiler (www.cellprofiler.org, version 4.2.1) was used to count SNX8 positive IAMs. Briefly, following removal of the cytosolic fraction of SNX8 in the SNX8 channel using Fiji, IAMs were detected using the dextran signal and the dextran-IAMs were used as a mask on the SNX8 signal. The software parameters were set to detect the upper quartile fluorescence intensity of the SNX8 to the IAMs and this was related to the detected bacteria and actin foci.

Statistical analysis

Statistical analysis was performed using GraphPad Prism version 9.0.0 for MacOS, GraphPad Software, San Diego, California USA, www.graphpad.com.

3.Results

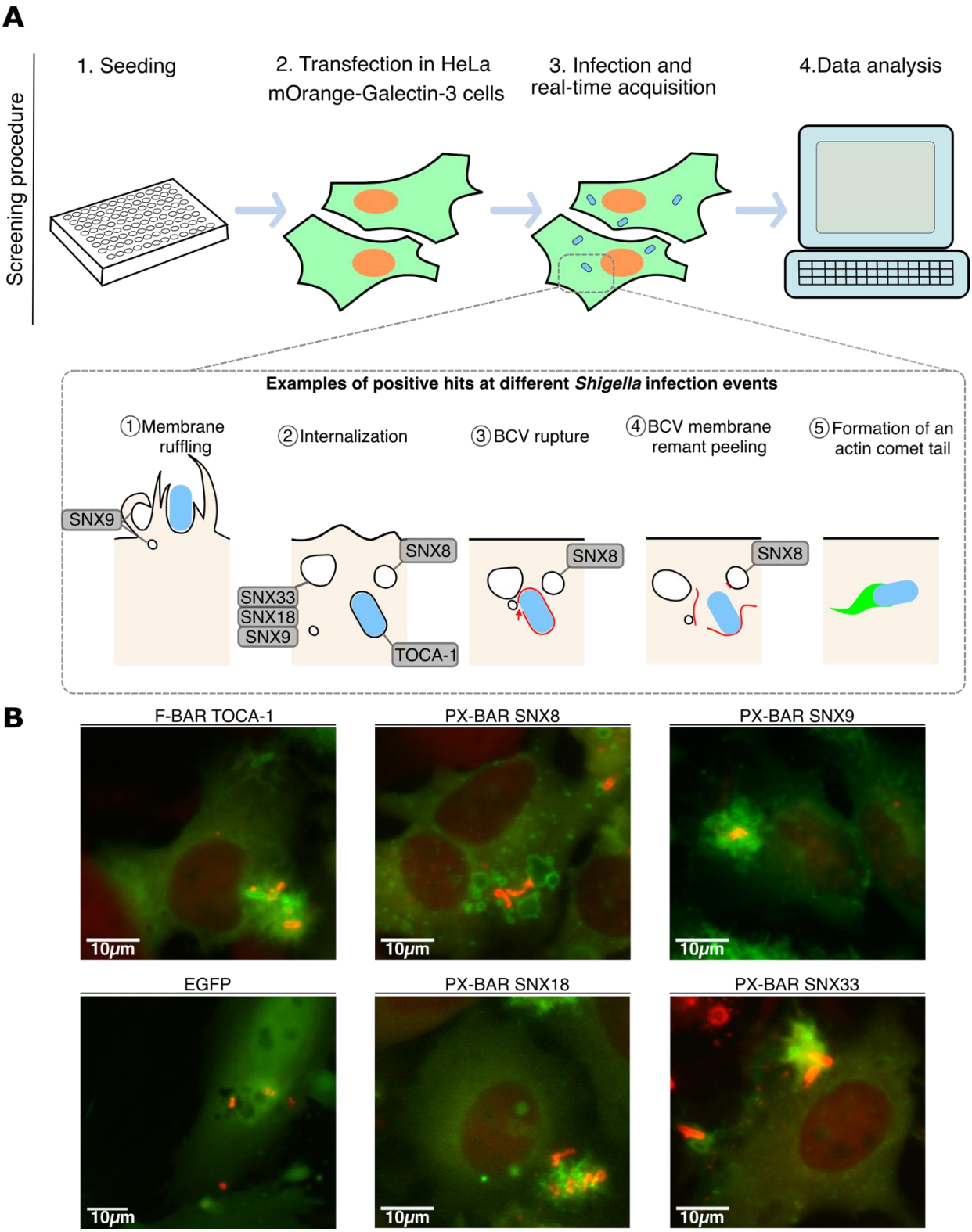

Figure 1. Time-resolved high-content screen experimental procedure and examples of positive hits of host proteins recruited to the bacterial infection foci.

A. Schematic illustration of the time-resolved screen workflow with example of positive hits and their localization during *Shigella* infection. HeLa mOrange-Galectin-3 cells were seeded, transfected with the proteins-of-interest and samples were infected with *Shigella* during microscopy acquisition. Examples of observed hit recruitment and their localization to the infection site are represented in the lower portion the figure.
B. Microscopy images of SNX-BAR family of BAR-domain containing proteins identified as positive hits. In red is shown the mOrange-Galectin-3 signal marking *Shigella*-BCV rupture and the BCV-membrane remnants, and in green the BAR-domain containing proteins included in the screen.

Identification of BAR domain-containing host factors enriched at the *Shigella flexneri* invasion focus

With the aim of identifying new molecular pathways involved in the early steps of *Shigella* infection, we carried out a high-content, time-resolved screen using a library of 66 EGFP-tagged full length BAR domain-containing proteins (see supplementary table 1 for full list) and Galectin-3, a cytosolic reporter binding the BCV membrane at the precise moment of vacuole rupture (Paz et al. 2010). In brief, a 2-minute-interval time-course of mOrange-Galectin-3 stably expressing HeLa cells transiently transfected with each BAR plasmid and infected using wildtype (WT) *Shigella* were recorded (Figure 1A). This set-up enabled simultaneously the tracking of the re-location of the "tested" protein to the infection focus and trailing of the *Shigella*-triggered membrane ruffling, BCV rupture and disassembly steps. BAR protein TOCA-1 and EGFP were used as positive and negative controls respectively, with TOCA-1 having been previously shown to be recruited to the *Shigella* actin cocoon and actin tail (Kühn et al. 2020, Leung et al. 2008). Positive hits were counted as showing enriched fluorescence of the "candidate" proteins to the infection site by comparison to the controls (Figure 1B).

After manual inspection of the data based on the behavior of the external controls, 13 BAR domain-containing proteins were identified as positive hits (see supplementary table 2). Our results revealed specific subtypes of BAR domain-containing proteins localizing to different bacterial compartments. Among the hits we found several members of the SNX-BAR family of proteins and actin nucleating factors srGAP2 and PACSINs 1, 2 and 3. We observed differential recruitments of the BAR domain proteins during the infection. Exemplarily, PACSIN recruitment was observed during membrane ruffling whereas srGAP2 was found to localize at the BCV prior to BCV rupture (data not shown). Interestingly, we observed that members of the SNX-BAR family localized to IAMs early in their formation and/or their enrichment occurred throughout *Shigella* BCV egress (Figure 1A). Among the SNX-BARs hits, we noted a significant enrichment of the early endosome sorting protein Sorting Nexin 8 (SNX8) to IAMs. This recruitment was

observed early on during the infection, and the protein remained persistently localized at the IAMs throughout the *Shigella* BCV disassembly (Figures 1A, 1B).

SNX8 localizes to IAMs and the *Shigella*-BCV prior to BCV rupture and disassembly.

SNX8 is a sorting protein localizing in the early endosome and conjectured to recycle cargo to the Trans-Golgi network (Dyve et al. 2009). Although the function of human SNX8 remains elusive, its yeast homologue MVP1 has been shown to function in retromer-independent recycling (Suzuki et al. 2021). SNX8 has also been linked to several pathologies involving endosomal recycling defects such as Alzheimer's (Xie et al. 2019, Vanzo et al. 2014).

Following the identification of SNX8 as a hit in our screen, we proceeded to comprehensively characterize SNX8 recruitment to IAMs. To observe the totality of plasma membrane-derived IAMs, we employed previously described the phosphatidylserine-specific biosensor LactC2 (Yeung et al. 2008, Vecchio and Stahelin 2018). Furthermore, we first evaluated the presence of endogenous SNX8 to IAMs by immunodetection using an anti-SNX8 antibody. Confocal microscopy analysis confirmed the presence of endogenous SNX8 to LactC2-marked vesicles in proximity of *Shigella* (Figure 2A). We then monitored SNX8 behavior in relation to the ruptured BCV membrane. Temporal analysis of images from higher spatial resolution live-cell imaging of HeLa and CaCo-2 cells transiently co-expressing SNX8-EGFP and mOrange-Galectin-3 showed the recruitment of SNX8 to *Shigella*-IAMs occurred prior to BCV rupture and remained at the IAMs until *Shigella*-BCV remnant unpeeling (Figures 2B and 2C). Quantification of SNX8 recruitment to the *Shigella* entry focus emphasized the presence of SNX8 at the onset of BCV rupture roughly 6 min prior and throughout BCV disassembly (occurring on average 20min post-infection according to our previous work (Chang et al. 2020)) (Figure 2D). Moreover, SNX8 time-lapses showed SNX8 positive tubules emanating from IAMs (Figure 2B), as previously described for SNX-BARs by Van Weering et al (2010). We also observed the BCV to be transiently enriched in SNX8 prior to BCV rupture (Figure 2B). Together, these results suggest a potential involvement of SNX8 in the steps of BCV rupture and/or disassembly.

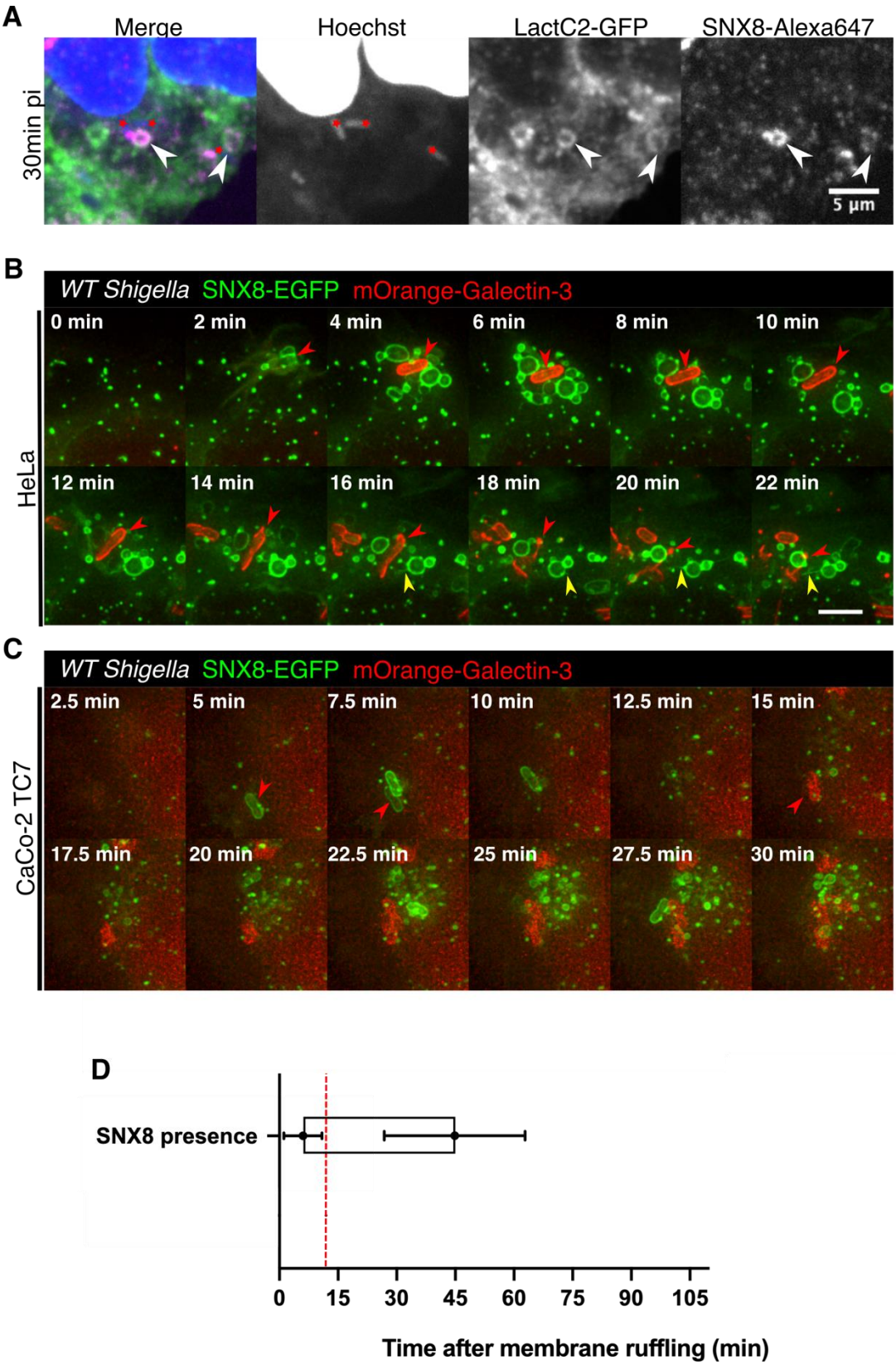

Figure 2. SNX8 is recruited to IAMs and BCV prior to *Shigella*-BCV egress.

A. Fixed microscopy of LactC2-GFP stably expressing HeLa cells (in green) infected with *Shigella* for 30 min and stained for endogenous SNX8 (in magenta). The bacteria and cell nucleus were marked with Hoechst (in blue). White arrowheads and red stars represent individual IAMs and bacteria respectively. Scale bar: 5µm.

B, C. Time-lapse microscopy images of HeLa cells (B) and CaCo-2 cells (C) transfected with mOrange-Galectin-3 (in red) and SNX8-EGFP (in green) infected with *Shigella*. Red arrows point to an entering bacterium and yellow arrows point to SNX8-rich tubules emanating from SNX8-IAMs. Scale bar: 3µm.

D. Quantitative analysis of SNX8-EGFP temporal recruitment sequence to the infection focus. SNX8 presence is shown as a box with the average start of the recruitment at 6min and dissipation at 44.8min. Infection foci from duplicate experiments were analyzed (n>60). Standard deviation of the data for SNX8 recruitment start and end are shown. The red bar represents the average BCV rupture time point (11.9min).

Characterization of SNX8 behavior during IAMs maturation

Previously, several small RAB GTPases were shown recruited during *Shigella*-IAM maturation with several of these playing a role in promoting the invasion steps (RAB8A, RAB11A), marking an importance of IAMs-recruited factors (Mellouk et al. 2014, Weiner et al. 2016, Chang et al. 2020). Following the spatio-temporal characterization of SNX8 to the infection focus, we aimed to comprehensively analyze the relationship between SNX8 and IAM-recruited RAB proteins by examining the behavior of these factors. For this, 35 sec time-courses allowed sufficient temporal resolution to distinguish the precise moment of recruitment of all factors. Infections of HeLa cells co-transfected with SNX8 and RAB5A, RAB7A, RAB8A or RAB11A were carried out. Canonical macropinosome maturation has previously been reported to involve the early marker RAB5A and late marker RAB7A (Egami et al. 2014, Buckley and King, 2017). We confirmed the recruitment of RAB5A to IAMs early on during the *Shigella* infection as previously reported by Mellouk et al (2014) (Figure 3A). Microscopy time-lapse images showed SNX8 recruitment occurs simultaneously with RAB5A recruitment to IAMs (Figure 3A). Furthermore, temporal analysis of SNX8 and RAB5A fluorescence intensity to individual IAMs further emphasized this observation (Figure 3E). Microscopic analysis also revealed SNX8 recruitment to IAMs occurred prior to RAB7A accumulation and decreased with RAB7A presence (Figure 3B). Moreover, nearly all SNX8-IAMs acquired RAB7A and we observed the formation of SNX8-negative RAB7A-labeled tubules suggesting distinct recycling pathways of RAB7 and SNX8. These results show SNX8 recruitment to occur in “canonical macropinosome”-like maturing IAMs as soon as the early stage of IAMs maturation and ends in the late stage.

RAB11A and RAB8A enrichment to IAMs was found to promote efficient BCV rupture and egress and to be recruited during those events (Weiner et al. 2016, Chang et al. 2020), this is similar to our observation of SNX8 recruitment. Analysis of the time-lapse images showed that in the case of RAB11A and RAB8A overexpression, SNX8 only partially recruited to the formed IAMs (Figures 3C, 3D). We distinguished in both cases 3 distinct recruitments: (i) the recruitment of both proteins overexpressed, (i) only RAB protein recruitment and (iii) only SNX8 recruitment. In IAMs recruiting both factors, we observed RAB8A recruitment to IAM occurred prior to SNX8 recruitment (Figure 3C) but these factors did not seem to overlap at the monitored IAMs. When co-expressing RAB11A and SNX8, SNX8 was recruited first to IAMs and either was replaced by RAB11A or remained at the IAM without any later RAB11A recruitment (Figure 3D). Analysis of individual IAMs also showed this switch (Figure 3F). Together, these results show SNX8 recruitment is mutually exclusive to RAB11A and RAB8A at IAMs and this hints at the existence of IAM subsets during *Shigella* infection.

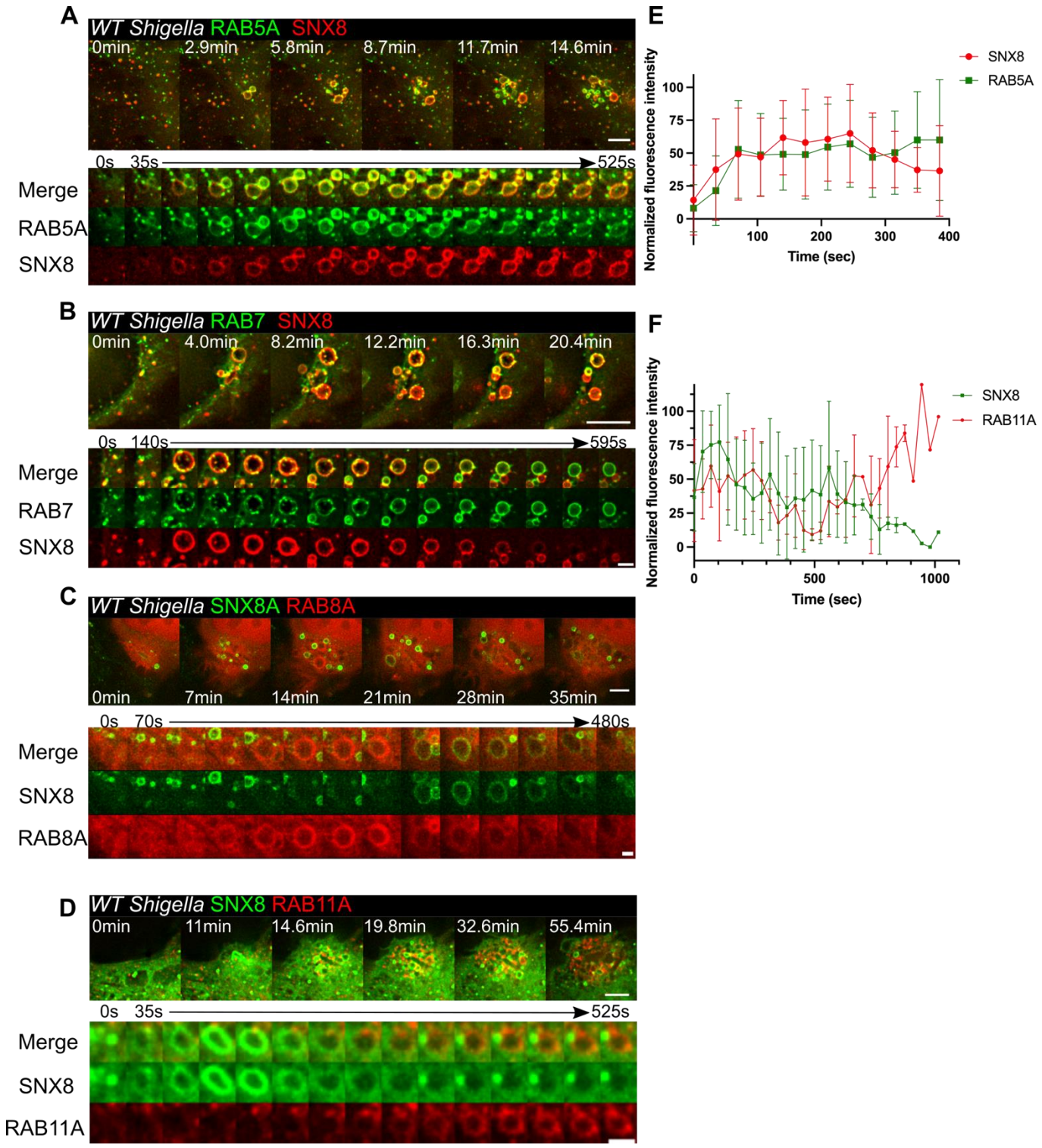

Figure 3. Characterization of the maturation of SNX8-IAMs to RAB GTPases.

A, B, C, D. Live cell 35sec time-lapse microscopy images of HeLa cells co-expressing RAB GTPases and SNX8 and infected with *Shigella*: A.RAB5A-GFP/SNX8-mApple, B.RAB7A-GFP/SNX8-mApple,

C.SNX8-EGFP/RAB8A-mApple, D.SNX8-EGFP/RAB11A-mApple. The infection foci and a zoom on a macropinosome of the infection site are shown together. Scale bars are respectively 5µm and 1,5µm.
E. Fluorescence intensity of SNX8-mApple and RAB5A-GFP to individual IAMs. Fluorescence intensity was normalized to the maximum and minimum intensities measured for each individual IAM (n=8 events).
F. Fluorescence intensity of SNX8-SNX8 and RAB511-mApple to individual IAMs. Fluorescence intensity was normalized to the maximum and minimum intensities measured for each individual IAM (n=8 events).

SNX8 is recruited to a PI(3)P positive subpopulation of IAMs

Little is known about IAMs and their role(s) in *Shigella* invasion, and in particular it is unknown whether all IAMs are of the same composition (Mellouk et al. 2014, Weiner et al. 2016, Chang et al. 2020). Furthermore, the strong recruitment of RAB11A to IAMs has been puzzling as this Rab has not been characterized as default constituent of macropinosomes. To assess whether SNX8 localizes to all *Shigella*-IAMs, we first performed time-lapse microscopy experiments at higher spatial resolution using the LactC2 reporter to carefully monitor IAMs. In brief, 1-minute-interval time-course experiments were performed of SNX8-mApple transiently transfected LactC2-GFP stable HeLa cells infected with *Shigella*. Image analysis confirmed IAMs were LactC2-labelled throughout their lifetime and the localization of SNX8 to IAMs in the vicinity of the bacteria (Figure 4A). Moreover, we also remarked SNX8 recruitment to IAMs begins shortly after IAM cup closure. However, we noticed SNX8 did not localize to all IAMs formed (see Figure 4A). Additionally, infections were fixed at the 30 min time point for staining with the fluorescent fluid phase marker dextran to label IAMs (Weiner et al. 2016) in SNX8-EGFP transiently transfected HeLa cells. This further confirmed SNX8 to be enriched only to a part of the IAMs formed with just over half of IAMs being SNX8 positive (61%, ±4,7%) (Figures 4B, 4C). Together, these results reveal the co-existence of at least two subsets of IAMs of distinct composition within an infection focus.

SNX8 was reported to contain a PX domain binding to PI(3)P (Van Weering et al. 2012) and we previously showed that IAMs produced during *Shigella* infections mature by recruiting PI(3)P (Weiner et al. 2016). To establish a causal link between SNX8 recruitment and PI(3)P presence to IAMs, we utilized the previously described PI(3)P binding probe 2xFYVE (HRS) (Stenmark et al. 1996). We performed 1min time-lapse *Shigella* infections of SNX8-EGFP and a mCherry-2xFYVE transiently co-transfected HeLa cells. This first confirmed the localization of 2xFYVE to IAMs, and we also noted that SNX8 enrichment occurred simultaneously with 2xFYVE labelling of the IAMs. Both recruitments occurred simultaneously after IAM cup closure, moreover SNX8 recruitment occurred to all 2xFYVE-labelled IAMs (see Figure 4C). Collectively, these results demonstrate the accumulation of SNX8 is exclusively to a subpopulation of PI(3)P-enriched IAMs.

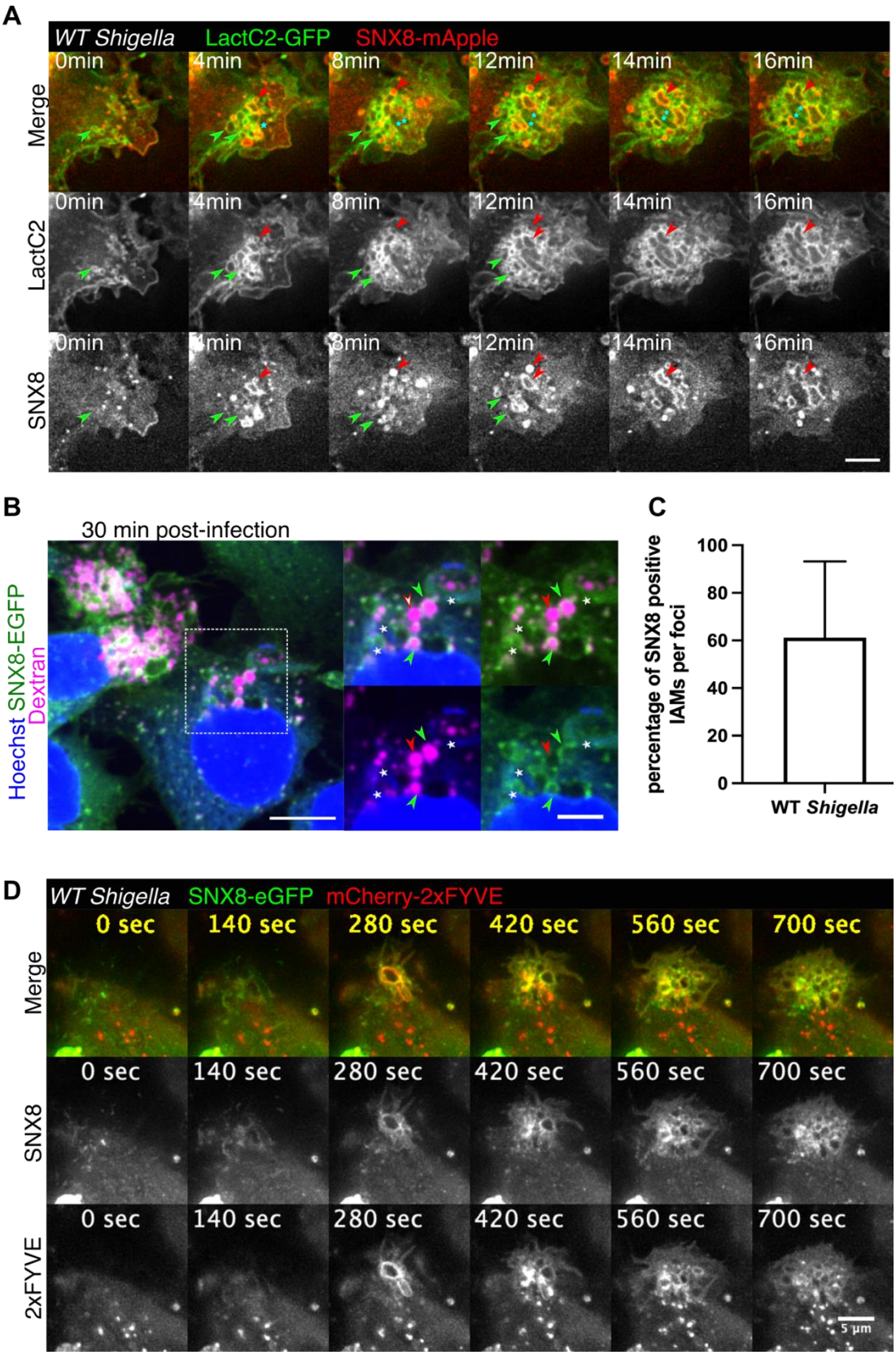

Figure 4. SNX8 is heterogeneously recruited to IAMs in a PI(3)P-dependent manner.

A. Time-lapse microscopic analysis of SNX8 distribution at IAMs in LactC2-GFP-expressing HeLa cells transfected with SNX8-mApple. Entering bacteria are tracked with blue stars. Red and green arrows highlight SNX8 positive and negative IAMs respectively. Scale bar is 5µm.

B. Fixed confocal image of HeLa cells expressing SNX8-EGFP were infected with *Shigella* together with dextran-Alexa647 at 30min post-infection. SNX8 signal is in green and dextran-containing IAMs are in magenta. Green arrowheads show SNX8 positive-IAMs, red arrowheads show SNX8 negative IAMs and stars show the bacteria. Scale bars are 10µm and 5µm.

C. Quantification of dextran-labelled IAMs recruiting SNX8-EGFP following 30 min incubation with wildtype *Shigella*. The average percentage of IAMs recruiting SNX8 per infection foci is shown. Automated analysis was performed on duplicate experiments (n>90 infection foci per experiment).

D. Time-lapse microscopy images of mCherry-2xFYVE and SNX8-EGFP-expressing HeLa cells infected with *Shigella*. Scale bar is 5µm.

SNX8/PI(3)P impairment to IAMs hampered *Shigella* BCV egress

We proceeded to investigate the function of the newly identified subset of PI(3)P+/SNX8+ IAMs. Having determined the recruitment of SNX8 to be PI(3)P-driven, we assessed whether PI(3)P was host-cell PI(3)-kinase-dependent. This was confirmed by using the broad spectrum PI(3)-kinase inhibitor wortmannin (see supplementary Figure 1), which led to an arrest of SNX8 recruitment to IAMs. We remarked however that SNX8 recruitment to the BCV remained, implying a PI(3)-kinase independent recruitment to this compartment.

Given the PI(3)P-dependent recruitment of SNX8 together with RAB5A, we hypothesized the involvement of the RAB5 effector class III PI(3)P kinase VPS34 (Vacuolar Sorting Protein 34) which has been reported to be involved in the early endosome and macropinosome PI(3)P maturation (Backer, 2008, Bohdanowicz et al. 2013, Spangenberg et al. 2021). Interestingly, a VPS34-specific inhibitor called SAR405 has been described to impair VPS34 function in canonical macropinosomes (Ronan et al. 2014, Spangenberg et al. 2021). Based on our previous findings of IAM recruitment to the BCV during the damage of this compartment, we decided to assess the function of SNX8-IAMs in BCV rupture and unpeeling. To this end, we performed real-time infections in HeLa cells transiently expressing mOrange-Galectin-3 and SNX8-eGFP with and without SAR405. We observed that addition of SAR405 hampered the recruitment of SNX8-eGFP to IAMs (Figure 5A). The inhibitor also impaired PI(3)P-recruitment to IAMs (supplementary Figure 2).

From the dynamics SNX8 recruitment and due to the anticipated relevance of IAMs in the events of *Shigella* intracellular niche formation, we investigated SNX8-IAMs function in BCV rupture and unpeeling. To track the BCV rupture and membrane remnants, we performed real-time infections of SAR405 treated in

HeLa cells co-expressing SNX8 together with the fluorescent reporter Galectin-3. BCV rupture time was defined as the time in between membrane ruffling and Galectin-3 recruitment to the BCV (see illustration in Figure 5B). Analysis of the BCV rupture time showed a slight, yet significant delay of 2 min in the presence of the SAR405 inhibitor compared to the DMSO control (Figure 5B).

BCV egress, has been shown to require first BCV rupture followed by the unpeeling of the BCV remnants. Furthermore, BCV unpeeling has been described as impacting the speed of bacteria mobility (Kühn et al. 2020, Chang et al. 2020), and it is likely that the efficiency of this events impact on intracellular detection by xenophagy. To monitor unpeeling of BCV membrane remnants, three phenotypes have been described on the basis of BCV membrane movement and the swiftness of bacteria movement: we distinguish a quick BCV disassembly, loose BCV remnant with quick movement and a tight BCV remnants with delayed bacteria movement (Figure 5C). Quantification of these phenotypes in the aforementioned experiment validated the proportions of each type of BCV-unpeeling was similar to the phenotypes previously reported in the presence of DMSO (tight BCV remnants:44,2%, Loose BCV remnants:40,4%, Quick recycling: 15,4%) (Figure 5D) (Kühn et al. 2020). However, treatment with the inhibitor caused a decrease of the loose BCV membrane phenotype in favor of an increase in bacteria that are connected with a tight BCV membrane upon initial BCV damage (Figure 5D). Nonetheless, no change occurred in the quick BCV disassembly phenotype in the presence of absence of VPS34 inhibitor (DMSO=15,4%, SAR405=16%,). These results show a function of PI(3)P-SNX8 IAMs in promoting efficient *Shigella* BCV egress to reach the host cytosol.

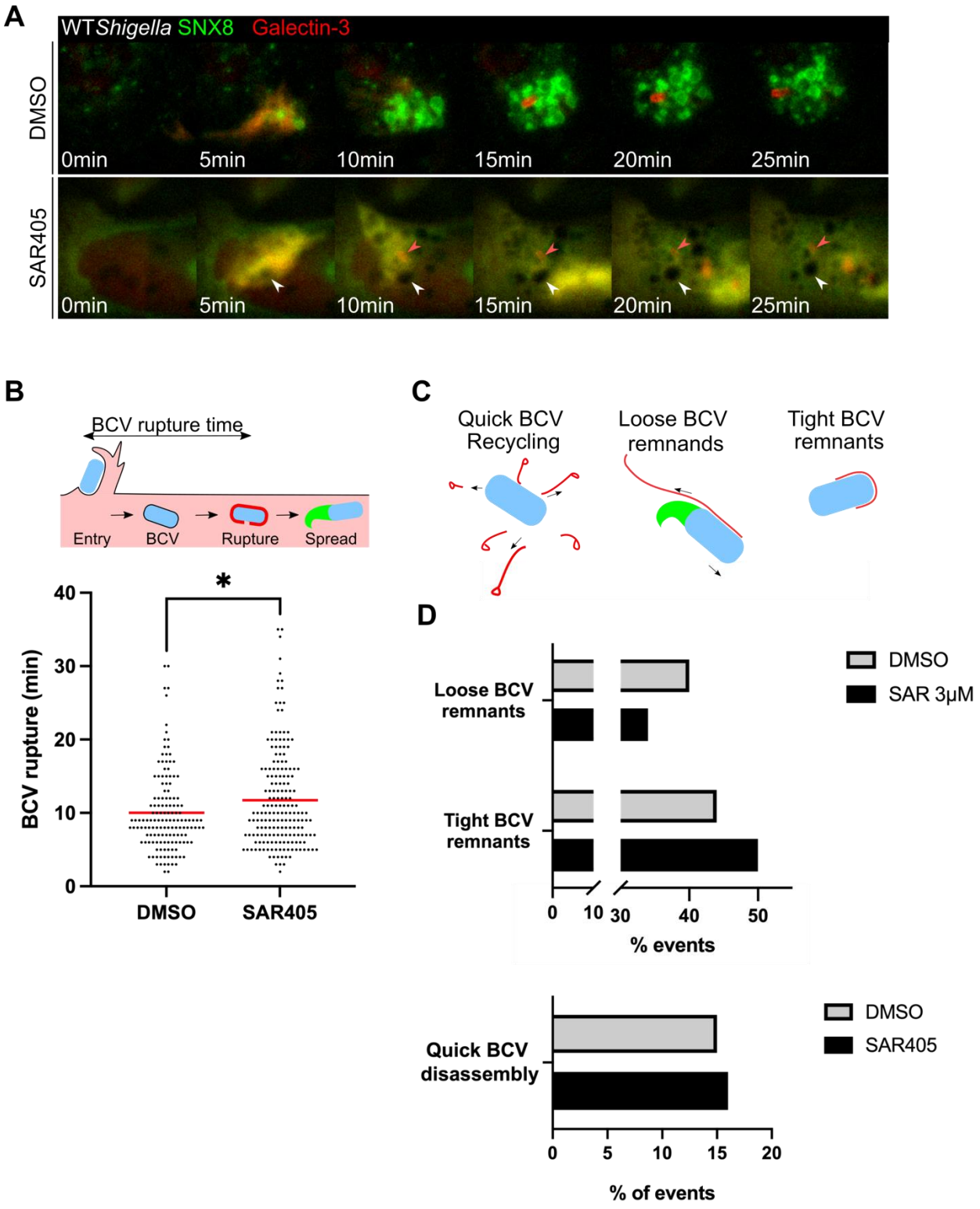

Figure 5. SNX8-PI(3)P IAMs promote BCV rupture and bacteria rapid escape from the BCV.

A. Time-lapse images of *Shigella* infections in SNX8-eGFP/mOrange-Galectin-3 transiently transfected HeLa cells in the presence of DMSO or SAR405 inhibitor. Red arrow follows the ruptured bacterium and white arrow tracks an individual IAM from its formation.

B. BCV rupture time of the first 3 bacteria entering a bacterial focus in WT *Shigella* infected cells in the presence of DMSO or SAR405 (n>140 events for each condition). Statistical analysis was performed using a Mann and Whitney (*p<0.05).

C. Schematic illustration of BCV unpeeling phenotypes: quick BCV disassembly, tight BCV remnants with delayed bacteria movement and loose BCV remnants with bacteria movement.

D. Quantification of BCV unpeeling events in SNX8-EGFP and mOrange-Galectin-3 expressing HeLa cells treated with SAR405 or DMSO (nDMSO=233, nSAR405=289).

Discussion

Following a comprehensive screen of the involvement of BAR proteins during *Shigella* invasion combining time-resolved fluorescence microscopy with genetically-encoded probes (Sanchez et al. 2021), we discovered the existence of distinct *Shigella*-IAM subpopulations. We studied a subset of IAMs which are PI(3)P and SNX8 positive showing their implication in efficient bacterial vacuole egress. We identified the PI(3)P signal to be VPS34-dependent and showed at least part of this subset of IAMs underwent a RAB11A switch. Lastly, PI(3)P synthesis arrest to these IAMs led to delayed BCV rupture and impairment of BCV disassembly.

Shigella invasion steps require extensive membrane remodeling. Hence, monitoring BAR domain-containing factors involved in *Shigella* invasion appeared as promising. Previously, TOCA-1 was reported to be recruited to the *Shigella* actin cage and to be crucial for actin-tail formation (Leung et al. 2008, Baxt and Goldberg, 2014, Kühn et al. 2020) which we also observed (data not shown). We found an enrichment of SNX-BAR proteins, SNX8 in particular localized to PI(3)P positive IAMs and staying there until the late *Shigella* invasion steps (Figure 2). With our data, we could determine the existence of a PI(3)P+/SNX8+ subset of *Shigella*-IAMs. Additionally, it was intriguing that SNX8 localized only to part of the induced IAMs (Figure 3). Our results align with a report from Weiner et al (2016) which showed PI(3)P-labelled IAMs partially co-localizing with the fluid phase marker dextran.

Previously, macropinocytosis was proposed as the entry mechanism for bacterial pathogens (Cossart and Sansonetti, 2004). However, *Shigella*-IAMs were determined to be distinct morphologically and in composition from the bacterial phagosome-like vacuole (Weiner et al. 2016) prompting their formation as being driven by separate mechanisms. Furthermore, contact sites between BCV and IAMs were reported (Weiner et al. 2016) as well as the recruitment of host factors RAB11A, RAB8A and exocyst (Mellouk et

al. 2014, Weiner et al. 2016, Chang et al. 2020) which were revealed to promote *Shigella*-BCV egress. Together these data highlight IAMs as a separate compartment with an important contribution in the infection process. However, although morphologically comparable to canonical macropinosomes, the similarity in composition and formation of IAMs to "classical" macropinosomes has remained unclear. A recent study from Spangenberg et al (2021) found macropinosome maturation to be VPS34-dependent with inhibition of VPS34 leading to the refusion of macropinosomes with the plasma membrane, via RAB10 and RAB11A recruitment. Here, our results contrasted with those of Spangenberg et al with the VPS34-mediated PI(3)P+/SNX8+ IAMs subset maturing to RAB11A, highlighting how these pathogen-controlled compartments differ from canonical macropinosomes.

Apart from that, through our study of the PI(3)P+/SNX8+ subpopulation of IAMs, we can speculate about the potential function(s) and maturation of the different subsets of IAMs. Based on RAB recruitment, we suggest that some of this subset may follow the RAB7A endosomal degradation pathways, SNX8+/RAB11A- subsets of IAMs may be subject to communicate with the TGN whereas SNX8-/RAB11A+ IAMs becoming "recycling endosome-like" could undergo recycling at the plasma membrane. Similar to previous work which demonstrated a function of IAMs in accelerating *Shigella*-BCV egress (Mellouk et al. 2014, Weiner et al. 2016, Chang et al. 2020) and emphasizing both a contribution of the host and the bacteria, this work showcases the *Shigella* focus as being comprised of subpopulations of IAMs evidencing the subversion by the bacterium of multiple host pathways. At a more general level, our work highlights the importance of the endosomal recycling pathways in the later steps of *Shigella* invasion. *Shigella* has been shown to need to be rapidly "naked" within the cytosol separated from the BCV membrane remnants (Chang et al. 2020, Kühn et al. 2020). We show in this study, that in accordance with previous studies, IAMs play a role in the disrobing of the BCV membrane from the bacteria. However, we show here that *Shigella* triggers different maturation pathways of IAMs potentially playing different roles in the infection process.

The bacterial factors that dictate the diversity of IAMs during *Shigella* entry need to be determined. The *ipgD* mutant leads to a slight delay in bacterial entry, however it almost entirely abrogated the formation of IAMs (Garza-Mayers et al. 2015, Weiner et al. 2016). Therefore, and also in light of our data using the PI kinase inhibitors, it is very unlikely that IpgD is key to control the different IAM subsets. Interestingly, another effector has been shown to modulate small host GTPases. IcsB is an N-fatty acylase that glues small GTPases to host membranes during *Shigella* invasion (Liu et al. 2018). We have also found that it is involved in the formation of the actin cocoon, and it has an impact on egress of *Shigella* from its vacuole (Kühn et al. 2020). Therefore, it would be interesting to study how the icsB mutant affects the different subpopulations of IAMs. Furthermore, IpaB and IpaJ have been identified to be involved in Golgi

fragmentation, and it is possible that these pathways also regulate the different subsets of IAMs (Burnaevskiy et al. 2013).

Other bacterial pathogens have also been described to trigger macropinosome-like compartments during their invasion. In particular, *Salmonella* -a bacterial pathogen closely resembling *Shigella*- has been shown to form IAMs during infection. Recently, these *Salmonella*-IAMs were shown to be critical for *Salmonella* niche establishment (Stévenin et al. 2019). IAMs were shown to fuse to the *Salmonella* vacuole, forming the *Salmonella* replicative niche (90% of events), whereas impairment of IAM fusion lead to rupture of the *Salmonella* vacuole (Perrin et al. 2004, Malik-Kale et al. 2012, Knodler et al. 2014). Hence, a comparison of the composition of *Salmonella*-IAMs and *Shigella*-IAMs is crucial to understanding bacteria niche establishment. This could help to highlight specific pathways exploited by bacterial pathogens to establish their intracellular niche.

Authors contribution and acknowledgments

Conceived and designed all experiments: LS, CVM and JE. Performed and analyzed data for all experiments: LS with specific contributions from MGC (pSBbi-SNX8-EGFP and SNX8-EGFP HeLa cell line). LS, CMV and JE edited and reviewed this manuscript. JE supervised the research and secured funding. We would also like to thank Magdalena Gil-Taran for feedback on this manuscript and Yuen-Yan Chang, Laura Barrio-Cano and Sonja Kühn for fruitful discussion on this project. Lastly, we would like to thank Laurent Audry for technical support.

Bibliography

Buckley, C.M. and King, J.S., 2017. Drinking problems: mechanisms of macropinosome formation and maturation. *The FEBS journal*, *284*(22), pp.3778-3790.

Bujny, M.V., Ewels, P.A., Humphrey, S., Attar, N., Jepson, M.A. and Cullen, P.J., 2008. Sorting nexin-1 defines an early phase of *Salmonella*-containing vacuole-remodeling during Salmonella infection. *Journal of cell science*, *121*(12), pp.2027-2036.

Burnaevskiy, N., Fox, T.G., Plymire, D.A., Ertelt, J.M., Weigele, B.A., Selyunin, A.S., Way, S.S., Patrie, S.M. and Alto, N.M., 2013. Proteolytic elimination of N-myristoyl modifications by the *Shigella* virulence factor IpaJ. *Nature*, *496*(7443), pp.106-109.

Centers for Disease Control and Prevention. Yellow Book [http://wwwnc.cdc.gov/travel/yellowbook/2016/infectious-diseases-related-to-travel/shigellosis] Accessed 5 Oct 2022.

Chan Wah Hak, L., Khan, S., Di Meglio, I., Law, A.L., Lucken-Ardjomande Häsler, S., Quintaneiro, L.M., Ferreira, A., Krause, M., McMahon, H.T. and Boucrot, E., 2018. FBP17 and CIP4 recruit SHIP2 and lamellipodin to prime the plasma membrane for fast endophilin-mediated endocytosis. *Nature cell biology*, *20*(9), pp.1023-1031.

Chang, Y.Y., Stévenin, V., Duchateau, M., Giai Gianetto, Q., Hourdel, V., Rodrigues, C.D., Matondo, M., Reiling, N. and Enninga, J., 2020. *Shigella* hijacks the exocyst to cluster macropinosomes for efficient vacuolar escape. *PLoS pathogens*, *16*(8), p.e1008822.

Cossart, P. and Sansonetti, P.J., 2004. Bacterial invasion: the paradigms of enteroinvasive pathogens. *Science*, *304*(5668), pp.242-248.

Cossart, P. and Roy, C.R., 2010. Manipulation of host membrane machinery by bacterial pathogens. *Current opinion in cell biology*, *22*(4), pp.547-554.

Du, J., Reeves, A.Z., Klein, J.A., Twedt, D.J., Knodler, L.A. and Lesser, C.F., 2016. The type III secretion system apparatus determines the intracellular niche of bacterial pathogens. *Proceedings of the National Academy of Sciences*, *113*(17), pp.4794-4799.

Dyve, A.B., Bergan, J., Utskarpen, A. and Sandvig, K., 2009. Sorting nexin 8 regulates endosome-to-Golgi transport. *Biochemical and biophysical research communications*, *390*(1), pp.109-114.

Garza-Mayers, A.C., Miller, K.A., Russo, B.C., Nagda, D.V. and Goldberg, M.B., 2015. *Shigella flexneri* regulation of ARF6 activation during bacterial entry via an IpgD-mediated positive feedback loop. *MBio*, *6*(2), pp.e02584-14.

High, N., Mounier, J., Prevost, M.C. and Sansonetti, P.J., 1992. IpaB of *Shigella flexneri* causes entry into epithelial cells and escape from the phagocytic vacuole. *The EMBO journal*, *11*(5), pp.1991-1999.

Jarsch, I.K., Daste, F. and Gallop, J.L., 2016. Membrane curvature in cell biology: An integration of molecular mechanisms. *Journal of Cell Biology*, *214*(4), pp.375-387.

Jeong, J.Y., Yim, H.S., Ryu, J.Y., Lee, H.S., Lee, J.H., Seen, D.S. and Kang, S.G., 2012. One-step sequence-and ligation-independent cloning as a rapid and versatile cloning method for functional genomics studies. *Applied and environmental microbiology*, *78*(15), pp.5440-5443.

Kim, J.Y., Kim, S.H., Jeon, S.M., Park, M.S., Rhie, H.G. and Lee, B.K., 2008. Resistance to fluoroquinolones by the combination of target site mutations and enhanced expression of genes for efflux pumps in *Shigella flexneri* and *Shigella sonnei* strains isolated in Korea. *Clinical Microbiology and Infection*, *14*(8), pp.760-765.

Kowarz, E., Löscher, D. and Marschalek, R., 2015. Optimized Sleeping Beauty transposons rapidly generate stable transgenic cell lines. *Biotechnology journal*, *10*(4), pp.647-653.

Kühn, S., Bergqvist, J., Gil, M., Valenzuela, C., Barrio, L., Lebreton, S., Zurzolo, C. and Enninga, J., 2020. Actin assembly around the *Shigella*-containing vacuole promotes successful infection. *Cell reports*, *31*(6), p.107638.

Leung, Y., Ally, S. and Goldberg, M.B., 2008. Bacterial actin assembly requires toca-1 to relieve N-wasp autoinhibition. *Cell host & microbe*, *3*(1), pp.39-47.

Liu, W., Zhou, Y., Peng, T., Zhou, P., Ding, X., Li, Z., Zhong, H., Xu, Y., Chen, S., Hang, H.C. and Shao, F., 2018. Nε-fatty acylation of multiple membrane-associated proteins by *Shigella* IcsB effector to modulate host function. *Nature microbiology*, *3*(9), pp.996-1009.

López-Montero, N. and Enninga, J., 2018. Diverted recycling—*Shigella* subversion of Rabs. *Small GTPases*, *9*(5), pp.365-374.

Mahbubur, R., Shoma, S., Rashid, H., El Arifeen, S., Baqui, A.H., Siddique, A.K., Nair, G.B. and Sack, D.A., 2007. Increasing spectrum in antimicrobial resistance of *Shigella* isolates in Bangladesh: resistance to azithromycin and ceftriaxone and decreased susceptibility to ciprofloxacin. *Journal of health, population, and nutrition*, *25*(2), p.158.

McMahon, H.T. and Gallop, J.L., 2005. Membrane curvature and mechanisms of dynamic cell membrane remodeling. *Nature*, *438*(7068), pp.590-596.

Mellouk, N., Weiner, A., Aulner, N., Schmitt, C., Elbaum, M., Shorte, S.L., Danckaert, A. and Enninga, J., 2014. *Shigella* subverts the host recycling compartment to rupture its vacuole. *Cell host & microbe*, *16*(4), pp.517-530.

Mellouk, N. and Enninga, J., 2016. Cytosolic access of intracellular bacterial pathogens: the *Shigella* paradigm. *Frontiers in cellular and infection microbiology*, *6*, p.35.

Mounier, J., Vasselon, T., Hellio, R., Lesourd, M. and Sansonetti, P.J., 1992. *Shigella flexneri* enters human colonic Caco-2 epithelial cells through the basolateral pole. *Infection and immunity*, *60*(1), pp.237-248.

Mounier, J., Boncompain, G., Senerovic, L., Lagache, T., Chrétien, F., Perez, F., Kolbe, M., Olivo-Marin, J.C., Sansonetti, P.J. and Sauvonnet, N., 2012. *Shigella* effector IpaB-induced cholesterol relocation disrupts the Golgi complex and recycling network to inhibit host cell secretion. *Cell Host & Microbe*, *12*(3), pp.381-389.

Paz, I., Sachse, M., Dupont, N., Mounier, J., Cederfur, C., Enninga, J., Leffler, H., Poirier, F., Prevost, M.C., Lafont, F. and Sansonetti, P., 2010. Galectin-3, a marker for vacuole lysis by invasive pathogens. *Cellular microbiology*, *12*(4), pp.530-544.

Perdomo, O.J., Cavaillon, J.M., Huerre, M., Ohayon, H., Gounon, P. and Sansonetti, P.J., 1994. Acute inflammation causes epithelial invasion and mucosal destruction in experimental shigellosis. *The Journal of experimental medicine*, *180*(4), pp.1307-1319.

Peter, B.J., Kent, H.M., Mills, I.G., Vallis, Y., Butler, P.J.G., Evans, P.R. and McMahon, H.T., 2004. BAR domains as sensors of membrane curvature: the amphiphysin BAR structure. *Science*, *303*(5657), pp.495-499.

Puzari, M., Sharma, M. and Chetia, P., 2018. Emergence of antibiotic resistant *Shigella* species: A matter of concern. *Journal of infection and public health*, *11*(4), pp.451-454.

Rey, C., Chang, Y.Y., Latour-Lambert, P., Varet, H., Proux, C., Legendre, R., Coppée, J.Y. and Enninga, J., 2020. Transcytosis subversion by M cell-to-enterocyte spread promotes *Shigella flexneri* and *Listeria monocytogenes* intracellular bacterial dissemination. *PLoS pathogens*, *16*(4), p.e1008446.

Ribet, D. and Cossart, P., 2015. How bacterial pathogens colonize their hosts and invade deeper tissues. *Microbes and infection*, *17*(3), pp.173-183. doi: 10.1016/j.micinf.2015.01.004

Sanchez, L., Chang, Y.Y., Mellouk, N. and Enninga, J., 2022. Time-resolved fluorescence microscopy screens on host protein subversion during bacterial cell invasion. In *Effector-Triggered Immunity* (pp. 113-131). Humana, New York, NY.

Sansonetti PJ, Kopecko DJ, Formal SB. (1982) Involvement of a plasmid in the invasive ability of *Shigella flexneri*. Infect Immun. doi: 10.1128/iai.35.3.852-860.1982.

Sansonetti, P.J., Arondel, J., Cantey, J.R., Prévost, M.C. and Huerre, M., 1996. Infection of rabbit Peyer's patches by *Shigella flexneri*: effect of adhesive or invasive bacterial phenotypes on follicle-associated epithelium. *Infection and immunity*, *64*(7), pp.2752-2764.

Schroeder, G.N. and Hilbi, H., 2008. Molecular pathogenesis of *Shigella* spp.: controlling host cell signaling, invasion, and death by type III secretion. *Clinical microbiology reviews*, *21*(1), pp.134-156.

Simunovic, M., Voth, G.A., Callan-Jones, A. and Bassereau, P., 2015. When physics takes over: BAR proteins and membrane curvature. *Trends in cell biology*, *25*(12), pp.780-792.

Simunovic, M., Evergren, E., Callan-Jones, A. and Bassereau, P., 2019. Curving cells inside and out: roles of BAR domain proteins in membrane shaping and its cellular implications. *Annual review of cell and developmental biology*, *35*, pp.111-129.

Spangenberg, H., Sneeggen, M., Tortola, M.M., Valenzuela, C., Chang, Y.Y., Stenmark, H., Raiborg, C. and Schink, K.O., 2021. A phosphoinositide and RAB switch controls early macropinocytosis. *bioRxiv*.

Stévenin, V., Chang, Y.Y., Le Toquin, Y., Duchateau, M., Gianetto, Q.G., Luk, C.H., Salles, A., Sohst, V., Matondo, M., Reiling, N. and Enninga, J., 2019. Dynamic growth and shrinkage of the Salmonella-containing vacuole determines the intracellular pathogen niche. *Cell reports*, *29*(12), pp.3958-3973.

Suarez, A., Ueno, T., Huebner, R., McCaffery, J.M. and Inoue, T., 2014. Bin/Amphiphysin/Rvs (BAR) family members bend membranes in cells. *Scientific reports*, *4*(1), pp.1-6.

Suzuki, S.W., Oishi, A., Nikulin, N., Jorgensen, J.R., Baile, M.G. and Emr, S.D., 2021. A PX-BAR protein Mvp1/SNX8 and a dynamin-like GTPase Vps1 drive endosomal recycling. *Elife*, *10*, p.e69883.

Swanson, J.A., 2008. Shaping cups into phagosomes and macropinosomes. *Nature reviews Molecular cell biology*, *9*(8), pp.639-649.

Swanson, J.A., 2014. Phosphoinositides and engulfment. *Cellular microbiology*, *16*(10), pp.1473-1483. doi: 10.1111/cmi.12334

Valencia-Gallardo, C.M., Carayol, N. and Tran Van Nhieu, G., 2015. Cytoskeletal mechanics during *Shigella* invasion and dissemination in epithelial cells. *Cellular microbiology*, *17*(2), pp.174-182.

Vanzo, R.J., Martin, M.M., Sdano, M.R., Teta, K., Aggarwal, V. and South, S.T., 2014. SNX8: A candidate gene for 7p22 cardiac malformations including tetralogy of fallot. *Am. J. Med. Genet. A*, *164*, pp.554-556.

Weiner, A., Mellouk, N., Lopez-Montero, N., Chang, Y.Y., Souque, C., Schmitt, C. and Enninga, J., 2016. Macropinosomes are key players in early *Shigella* invasion and vacuolar escape in epithelial cells. *PLoS pathogens*, *12*(5), p.e1005602.

Weiss, S.M., Ladwein, M., Schmidt, D., Ehinger, J., Lommel, S., Städing, K., Beutling, U., Disanza, A., Frank, R., Jänsch, L. and Scita, G., 2009. IRSp53 links the enterohemorrhagic *E. coli* effectors Tir and EspFU for actin pedestal formation. *Cell host & microbe*, *5*(3), pp.244-258.

Xie, Y., Niu, M., Ji, C., Huang, T.Y., Zhang, C., Tian, Y., Shi, Z., Wang, C., Zhao, Y., Luo, H. and Can, D., 2019. SNX8 Enhances Non-amyloidogenic APP Trafficking and Attenuates Aβ Accumulation and Memory Deficits in an AD Mouse. *Frontiers in Cellular Neuroscience*, *13*, p.410.

Yi, C.R. and Goldberg, M.B., 2009. Enterohemorrhagic *Escherichia coli* raises the I-BAR. *Proceedings of the National Academy of Sciences*, *106*(16), pp.6431-6432.

Supplementary data

Supplementary table 1. List of DNA plasmid constructs used.

Plasmid name	*Full length protein*	*Reference*
pArfaptin1-eGFP	*Arfaptin1-eGFP*	*Chan Wah Hak et al. 2018*
pArfaptin2-eGFP	*Arfaptin2-eGFP*	*Chan Wah Hak et al. 2018*
pICA69-eGFP	*ICA69-eGFP*	*Chan Wah Hak et al. 2018*
pICA1-like-eGFP	*ICA1-like-eGFP*	*Chan Wah Hak et al. 2018*
pPICK1-eGFP	*PICK1-eGFP*	*Chan Wah Hak et al. 2018*
pTuba-eGFP	*Tuba-eGFP*	*Chan Wah Hak et al. 2018*
pASAP1-eGFP	*ASAP1-eGFP*	*Chan Wah Hak et al. 2018*
pASAP2-eGFP	*ASAP2-eGFP*	*Chan Wah Hak et al. 2018*
pASAP3-eGFP	*ASAP3-eGFP*	*Chan Wah Hak et al. 2018*
pSH3BP1-eGFP	*SH3BP1-eGFP*	*Chan Wah Hak et al. 2018*
pAmphiphysin I-eGFP	*Amphiphysin I-eGFP*	*Chan Wah Hak et al. 2018*
pAmphiphysin II-eGFP	*Amphiphysin II-eGFP*	*Chan Wah Hak et al. 2018*
pBRAP1-eGFP	*BRAP1-eGFP*	*Chan Wah Hak et al. 2018*
pBIN3-eGFP	*BIN3-eGFP*	*Chan Wah Hak et al. 2018*
pEndophilin A1-eGFP	*Endophilin A1-eGFP*	*Chan Wah Hak et al. 2018*
pEndophilin A2-eGFP	*Endophilin A2-eGFP*	*Chan Wah Hak et al. 2018*
pEndophilin A3-eGFP	*Endophilin A3-eGFP*	*Chan Wah Hak et al. 2018*
pEndophilin B1-eGFP	*Endophilin B1-eGFP*	*Chan Wah Hak et al. 2018*
pEndophilin B2-eGFP	*Endophilin B2-eGFP*	*Chan Wah Hak et al. 2018*
pNadrin1-eGFP	*Nadrin1-eGFP*	*Chan Wah Hak et al. 2018*
pNadrin2-eGFP	*Nadrin2-eGFP*	*Chan Wah Hak et al. 2018*
pOligophrenin1-eGFP	*Oligophrenin1-eGFP*	*Chan Wah Hak et al. 2018*
peGFP-APPL1	*eGFP-APPL1*	*Chan Wah Hak et al. 2018*
peGFP-APPL2	*eGFP-APPL2*	*Chan Wah Hak et al. 2018*
pCentaurinb1-eGFP	*Centaurinb1-eGFP*	*Chan Wah Hak et al. 2018*
pCentaurinb2-eGFP	*Centaurinb2-eGFP*	*Chan Wah Hak et al. 2018*
pCentaurinb5-eGFP	*Centaurinb5-eGFP*	*Chan Wah Hak et al. 2018*
pGRAF1-eGFP	*GRAF1-eGFP*	*Chan Wah Hak et al. 2018*
pGRAF2-eGFP	*GRAF2-eGFP*	*Chan Wah Hak et al. 2018*

pSNX1-eGFP	*SNX1-eGFP*	*Chan Wah Hak et al. 2018*
pSNX2-eGFP	*SNX2-eGFP*	*Chan Wah Hak et al. 2018*
pSNX4-eGFP	*SNX4-eGFP*	*Chan Wah Hak et al. 2018*
pSNX5-eGFP	*SNX5-eGFP*	*Chan Wah Hak et al. 2018*
pSNX6-eGFP	*SNX6-eGFP*	*Chan Wah Hak et al. 2018*
pSNX7-eGFP	*SNX7-eGFP*	*Chan Wah Hak et al. 2018*
pSNX8-eGFP	*SNX8-eGFP*	*Chan Wah Hak et al. 2018*
peGFP-SNX9	*eGFP-SNX9*	*Chan Wah Hak et al. 2018*
pSNX18-eGFP	*SNX18-eGFP*	*Chan Wah Hak et al. 2018*
pSNX30-eGFP	*SNX30-eGFP*	*Chan Wah Hak et al. 2018*
pSNX32-eGFP	*SNX32-eGFP*	*Chan Wah Hak et al. 2018*
pSNX33-eGFP	*SNX33-eGFP*	*Chan Wah Hak et al. 2018*
pToca1-eGFP	*Toca1-eGFP*	*Chan Wah Hak et al. 2018*
pFBP17-eGFP	*FBP17-eGFP*	*Chan Wah Hak et al. 2018*
pCIP4-eGFP	*CIP4-eGFP*	*Chan Wah Hak et al. 2018*
pFCHo1-eGFP	*FCHo1-eGFP*	*Chan Wah Hak et al. 2018*
pFCHo2-eGFP	*FCHo2-eGFP*	*Chan Wah Hak et al. 2018*
pPSTPIP1-eGFP	*PSTPIP1-eGFP*	*Chan Wah Hak et al. 2018*
pPSTPIP2-eGFP	*PSTPIP2-eGFP*	*Chan Wah Hak et al. 2018*
pPacsin1-eGFP	*Pacsin1-eGFP*	*Chan Wah Hak et al. 2018*
pPacsin2-eGFP	*Pacsin2-eGFP*	*Chan Wah Hak et al. 2018*
pPacsin3-eGFP	*Pacsin3-eGFP*	*Chan Wah Hak et al. 2018*
pNwk1-eGFP	*Nwk1-eGFP*	*Chan Wah Hak et al. 2018*
pNwk2-eGFP	*Nwk2-eGFP*	*Chan Wah Hak et al. 2018*
psrGAP1-eGFP	*srGAP1-eGFP*	*Chan Wah Hak et al. 2018*
psrGAP2-eGFP	*srGAP2-eGFP*	*Chan Wah Hak et al. 2018*
psrGAP3-eGFP	*srGAP3-eGFP*	*Chan Wah Hak et al. 2018*
pFER-eGFP	*FER-eGFP*	*Chan Wah Hak et al. 2018*
pFES-eGFP	*FES-eGFP*	*Chan Wah Hak et al. 2018*
pNostrin-eGFP	*Nostrin-eGFP*	*Chan Wah Hak et al. 2018*
pGAS7-eGFP	*GAS7-eGFP*	*Chan Wah Hak et al. 2018*
pHMHA1-eGFP	*HMHA1-eGFP*	*Chan Wah Hak et al. 2018*
pIRSp53-eGFP	*RSp53-eGFP*	*Chan Wah Hak et al. 2018*
pMIM-eGFP	*MIM-eGFP*	*Chan Wah Hak et al. 2018*

pABBA-1-eGFP	*ABBA-1-eGFP*	*Chan Wah Hak et al. 2018*
pIRTKS1-eGFP	*IRTKS1-eGFP*	*Chan Wah Hak et al. 2018*
pIRTKS2-eGFP aka Pinkbar	*IRTKS2-eGFP*	*Chan Wah Hak et al. 2018*
pDEST-RAB5A-GFP	*RAB5A-GFP*	*Bruno Goud Lab*
pRAB7A-GFP	*RAB7A-GFP*	*Bruno Goud Lab*
pmApple-RAB8A	*mApple RAB8A*	*Chang et al. 2020*
pmApple-RAB11A-7	*mApple-RAB11A*	*Arnaud Echard Lab*
pmOrange-Galectin-3	*mOrange-Galectin-3*	*Ray et al., 2010*
SNX8-mApple	*SNX8-mApple*	*This study*
2xFYVE-mCherry	*2xFYVE-mCherry (Hrs)*	*Harald Stenmark Lab*
pSBbi-SNX8-eGFP-Neo	*SNX8-eGFP*	*Melanie Hamon Lab*
pSBbi-LactC2-GFP-Neo	*LactC2-GFP*	*Melanie Hamon Lab*

Supplementary Table 2. Summary of the BAR domain-containing protein screen results.

ID	BAR Protein	Family	Result
1	Arfaptin1	Classical	Negative
2	Arfaptin2	Classical	Negative
3	ICA69	Classical	Negative
4	ICA1-like	Classical	Positive
5	PICK1	Classical	Negative
6	Tuba	Classical	Negative
7	ASAP1	N-BAR	Unclear
8	ASAP2	N-BAR	Negative
9	ASAP3	N-BAR	Negative
10	SH3BP1	N-BAR	Negative
11	Amphiphysin I	N-BAR	Positive
12	Amphiphysin II	N-BAR	Unclear
13	BRAP1	N-BAR	Unclear
14	BIN3	N-BAR	Unclear
15	Endophilin A1	N-BAR	Negative
16	Endophilin A2	N-BAR	Negative
17	Endophilin A3	N-BAR	Negative
18	Endophilin B1	N-BAR	Negative
19	Endophilin B2	N-BAR	Negative
20	Nadrin1	N-BAR	Negative
21	Nadrin2	N-BAR	Negative
22	Oligophrenin 1	BAR-PH	Positive
23	APPL1	BAR-PH	Negative
24	APPL2	BAR-PH	Negative
25	Centaurinß1	BAR-PH	Negative
26	Centaurinß2	BAR-PH	Negative
27	Centaurinß5	BAR-PH	Negative
28	GRAF1	BAR-PH	Negative
29	GRAF2	BAR-PH	Positive
30	SNX1	PX-BAR	Negative
31	SNX2	PX-BAR	Negative
32	SNX4	PX-BAR	Positive
33	SNX5	PX-BAR	Positive

ID	Protein	Family	Result
34	SNX6	PX-BAR	Negative
35	SNX7	PX-BAR	Negative
36	SNX8	PX-BAR	Positive
37	SNX9	PX-BAR	Positive
38	SNX18	PX-BAR	Positive
39	SNX30	PX-BAR	Unclear
40	SNX32	PX-BAR	Negative
41	SNX33	PX-BAR	Positive
42	Toca1	F-BAR	Positive
43	FBP17	F-BAR	Unclear
44	CIP4	F-BAR	Unclear
45	FCHo1	F-BAR	Negative
46	FCHo2	F-BAR	Unclear
47	PSTPIP1	F-BAR	Unclear
48	PSTPIP2	F-BAR	Negative
49	Pacsin1	F-BAR	Positive
50	Pacsin2	F-BAR	Positive
51	Pacsin3	F-BAR	Positive
52	Nwk1	F-BAR	Negative
53	Nwk2	F-BAR	Negative
54	srGAP1	F-BAR	Unclear
55	srGAP2	F-BAR	Positive
56	srGAP3	F-BAR	Negative
57	FER	F-BAR	Negative
58	FES	F-BAR	Negative
59	Nostrin	F-BAR	Negative
60	GAS7	F-BAR	Negative
61	HMHA1	F-BAR	Negative
62	IRSp53	I-BAR	Negative
63	MIM	I-BAR	Negative
64	ABBA-1	I-BAR	Positive
65	IRTKS1	I-BAR	Negative
66	IRTKS2	I-BAR	Negative

The results shown are a summary of 3 independent experiments on each candidate protein. Positive hits were counted as being observed to the infection site at least twice, negatives being all 3 tries showed no visible recruitment and unclear being that recruitment was observed only once.

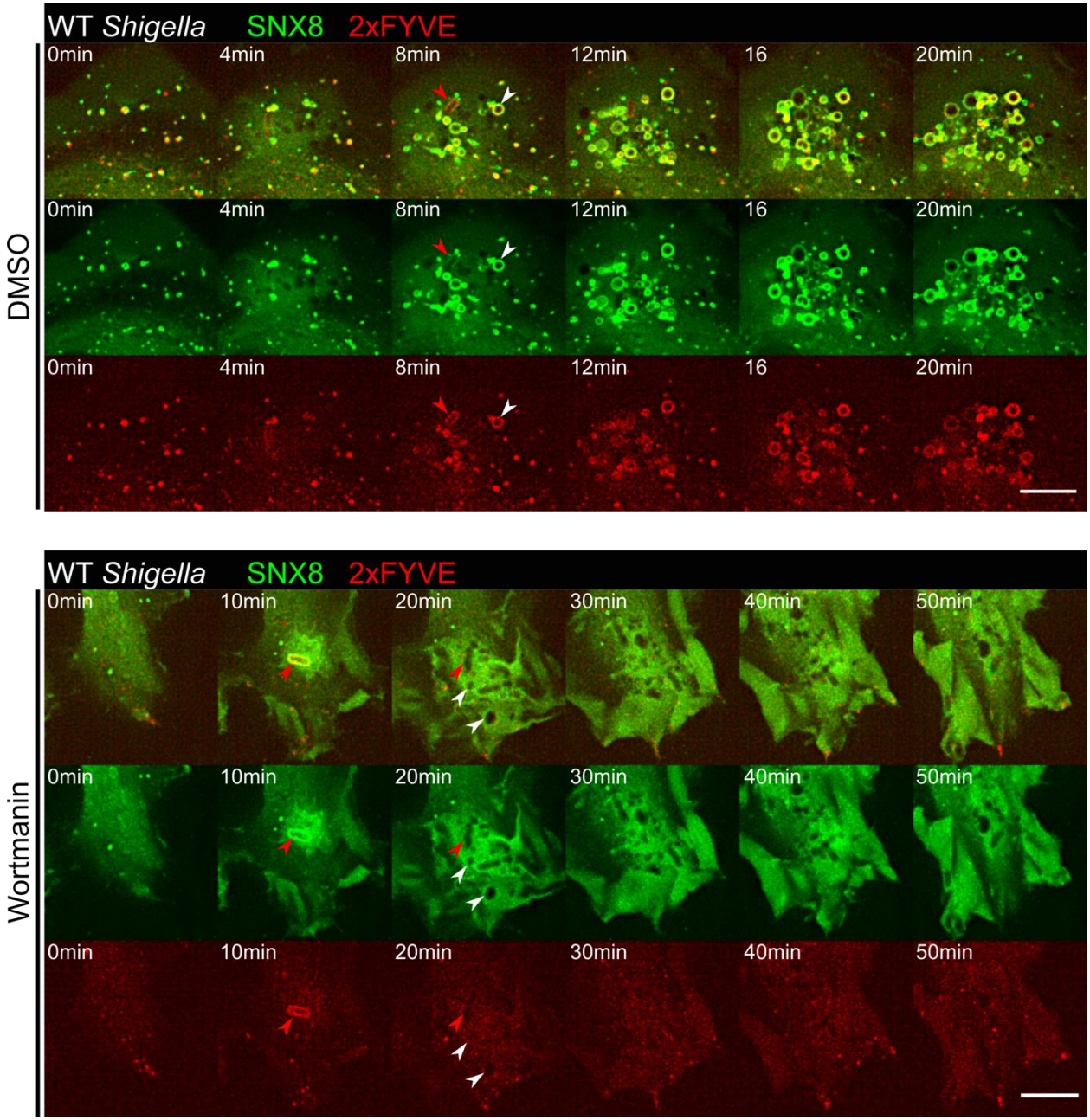

Supplementary figure 1. Wortmannin inhibition of PI(3)P *de novo* synthesis leads to arrest of SNX8 recruitment to IAMs

HeLa mOrange-Galectin-3 were transfected with SNX8 and infected with wildtype *Shigella* together with wortmannin (0,44µM final). Red arrowheads show an example of entering bacteria. White arrowheads show examples of formed IAMs. Scale bar is 5µm.

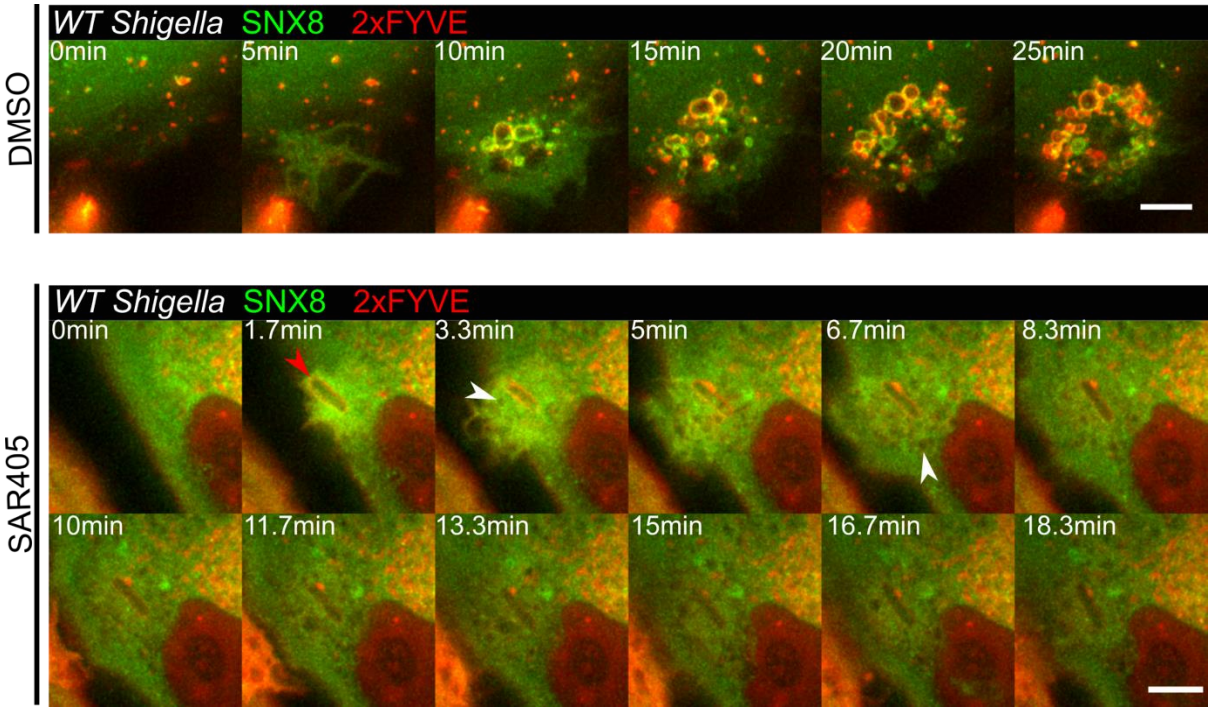

Supplementary figure 2: Effect of SAR405 on PI(3)P presence at the *Shigella* infection focus.
Microscopy images of HeLa cells co-transfected with SNX8-eGFP and 2xFYVE-mCherry infected with wildtype *Shigella* treated with DMSO or PI(3)-kinase VPS34 inhibitor SAR405. Red and white arrows show an entering the bacterium and a formed macropinosome, respectively. Scale bar is 5µm.

Chapter 4. Discussion

Research summary

In this work, I developed a method to comprehensively screen using candidate-based approach a medium-size library of BAR domain-containing proteins with the aim of identifying host pathways implicated in *Shigella* invasion. Upon characterization of the main hit of my screen, I discovered the existence of multiple IAM subsets triggered by *Shigella*. The study of one of these subsets showed non-typical behavior distinct from canonical macropinosomes, and furthermore we showed this IAM-subpopulation to promote the escape of *Shigella* from the BCV. These data provide a better understanding of the invasion steps of *Shigella flexneri* and highlights the multitude of host-pathways hijacked by the bacterium.

Implications of my research and future directions

Screening for host pathways subverted by *Shigella flexneri* and other pathogens

To identify molecular pathways reprogrammed by *Shigella* upon non-phagocytic epithelial cell invasion, we implemented a workflow for the systematic analysis of host factors based on a candidate approach. Classically, systematic screening approaches in the host-pathogen interaction field are performed with a candidate-based approach or an unbiased analysis obtaining the inventory of compartments involved in the host-pathogen interaction (Chang et al. 2020). Candidate-based screening have been performed in most cases in fixed samples at chosen time-points, and they pose the problem of bacterial invasion synchronicity and the speed of invasion events, particularly in the case of cytosolic bacteria. Therefore, sample fixation results in an important drawback providing only a snapshot of the involvement or protein behavior of the chosen "candidates" (Mellouk et al. 2014). Similarly, unbiased approaches -which consist of proteomic detection of the full protein content of bacterial compartments- also require infection synchronization (Santos et al. 2012, Chang et al. 2020, Stévenin et al. 2019). Furthermore, isolation of given compartments involved in the host-pathogen crosstalk is a requirement, but often represents a significant challenge despite the development of novel innovative isolation strategies (Steinhäuser et al. 2014, Chang et al. 2020). Moreover, sample preparation is delicate.

Therefore, we decided to use an alternative approach, and we designed a workflow using genetically-encoded reporters coupled to multidimensional time-lapse microscopy to comprehensively analyze the behavior of host factors during bacterial infection (*see* manuscript 1). By labelling specific cellular compartments and using a simple experimental workflow and setup, we can observe re-localization of proteins to test as it occurs in the infection compartments. The workflow elaborated in this work provides information on one specific factor with temporal and spatial information. We chose the family of BAR proteins as target as *Shigella* imposes a variety of host membrane rearrangements during its entry into target cells.

Interestingly, functional screens using fluorescence microscopy have been largely contributed to the study of host-pathogen interactions (Prudêncio and Lehmann, 2009). However, in addition to being performed on fixed samples, the robustness of these screens depends on a "scoring" of the results implicating the need for proper data normalization (Birmingham et al. 2009, Mellouk et al. 2014). Additionally, finding the proper read-out can be challenging. This complicates the screen setup. Our candidate-based setup provides a rapid, straightforward and simple method (with standard equipment requirements typically present in a given cell biology laboratory) yielding readily analyzable results. The simplicity of our workflow additionally enabled the scaling of the screen to a library of medium size (50-100 protein candidates) as well as making it versatile for a primary screen which can be adapted to the use of inhibitor molecules, different cell lines, or other microscope equipment (with increased spatiotemporal resolution) for instance.

Even though proteins strongly enriched to the infection site can be easily uncovered with our screen, low intensity signals of the tested proteins at the infection site may make identification less straight forward and lead to false negatives. Therefore, the sensitivity of this type of screen is dependent of the microscopy equipment. Ultra-sensitive cameras (sCMOS, EMCCD) and background-rejecting microscopes (e.g. spinning disk confocal microscopes) coupled to rapidly moving stages are crucial if high sensitivity and good throughput is required. Moreover, although a time-resolved screen enables the labelling of cellular and/or bacterial elements, the temporal scale of the screen may limit the use of fluorescent reporters or of the number of proteins "candidates" screened per experiment. In the case of *Shigella*, the swiftness of infection events (Ehsani et al. 2012) limited the use of fluorophores to two in order to screen for 10 proteins at a time. Lastly, candidate-based approaches requiring the overexpression of recombinant proteins can lead to the generation of artefacts such as protein aggregates and mislocalizations. Therefore, transfection optimization or the generation of stables cell lines expressing the proteins-of-interest at a low level, as well as the validation of the recruitment through immunodetection are a must before delving on to the investigation of a host molecular pathway. Another possibility to improve the screening is to modulate the support on which the experiments are done. For example, micropatterning or microfluidics are tools to minimize the areas or support size, so screening can be accelerated, or larger libraries can be screened (Kobel et al. 2009, Gobaa et al. 2011, Kim et al. 2019).

Identification of *Shigella*-IAM subpopulations

Using the aforementioned workflow combining multidimensional time-lapse imaging and genetically-encoded fluorescent probes to comprehensively screen for membrane remodeling factors enriched to the

Shigella infection focus, we uncovered the recruitment of the endosomal recycling factor SNX8 to a subpopulation of *Shigella*-IAMs involved in promoting BCV rupture and disassembly. The results from this study provide clarity to discrepancies surrounding the contribution of host factors in *Shigella* invasion. Based on our results, we hypothesize that *Shigella* subverts several host molecular pathways to IAMs discriminating between distinct IAM subpopulations to promote its latter invasion steps upon bacterial uptake.

Out of our hits, we observed a strong enrichment of the endosomal sorting protein SNX8 to *Shigella*- IAMs and transiently to the BCV rapidly upon infection and persisting throughout it. Furthermore, we found that SNX8 recruitment was driven by PI(3)P positive IAMs. Upon characterization of SNX8 recruitment, we discovered that SNX8 localizes only to a subset of the formed IAMs around the invading bacterium. This finding is similar to previouos work on IAMs formed in HeLa cells, were PI(3)P reporter 2xFYVE was reported to partially co-localize to IAMs (Weiner et al. 2016). Nevertheless, the previous study to not investigate the compartmental heterogeneity of the IAMs, and speculated whether the partial co-localization was simplly due to a "kinetic" effect with IAMs maturing from one composition to another. My time-lapse based approach could clear differentiate such a maturation phenotype from a phenotype that takes into account different subpopulations.
Strikingly, we also discovered that PI(3)P *de novo* synthesis hindrance by inhibition of the PI(3) kinase VPS34 did not alter SNX8 recruitment to the BCV suggesting PI(3)P synthesis to the IAMs is driven by a distinct mechanism. These results support the findings of our lab as to the BCV being of distinct formation and maturation as the IAMs (Weiner et al. 2016). Moreover, given the previously observed role in *Salmonella* of spacious vacuole-associated tubules (SVATs) (Bujny et al. 2008) and the recently proposed role of the SNX8 yeast homologue MVP1 as a retromer-independent driver of endosomal recycling (Suzuki et al. 2021), *Shigella* may trigger the recruitment of SNX8 and recycling factors to the BCV to remove excess membrane from BCV, priming the vacuole for disruption by the T3SS-mediated pore formation (Du et al. 2016). Nevertheless, it remains unclear whether such membranes can be carried away through the thick forming actin cocoon (Kühn et al. 2020).

Based on the aforementioned findings, we aimed to characterize the subset of PI(3)P+/SNX8+ IAMs that we identified in our analysis. Although termed "infection-associated macropinosomes" from their phenotypical similarity to "macropinosomes" -they are large vesicles (>0,5µm) formed from the collapse of membrane ruffles in some cell types- their resemblance in composition and maturation to canonical macropinosomes remains unclear. Similar in formation to canonical macropinosomes, we reported in this work the initial presence of the marker RAB5A to IAMs and from the impact of the VPS34 inhibitor

SAR405, the RAB5A effector VPS34-driven PI(3)P synthesis (Spangenberg et al. 2021). As depicted by Spangenberg et al. we also found RAB8A localizing to macropinosomes prior to SNX8 (and therefore PI(3)P) recruitment. These results therefore show a "canonical macropinosome"-like initial maturation of IAMs. However, contrary to findings from Spangenberg et al. we observed a shift of SNX8-IAMs to the endosomal recycling marker RAB11A in the absence of VPS34 inhibition (Figure 4D). We also observed the formation of multiple subpopulations of IAMs negative for SNX8 positive for all the analyzed RAB proteins (Figure 4). Together these results highlight the presence of multiple IAM subsets at the *Shigella* infection focus, suggesting different molecular pathways hijacked by this pathogen and possibly a larger role of IAMs in the infection process than previously described.

Interestingly, disruption of the maturation of the PI(3)P+/SNX8+ IAM subpopulation by inhibition of VPS34 caused a delay in the initial BCV rupture and more importantly in the egress from the BCV (Figure 5B). Under this condition, we also noted a shift in BCV disassembly phenotypes. Previous studies from our lab showed the existence of three phenotypes that characterize swiftness *Shigella*-BCV escape upon its initial damage with the (i) "sticky" and (ii) "quick recycling" phenotypes leading to a rapid escape of the bacterium and the (iii) "capped" phenotype leading to a delay in bacteria mobility (Kühn et al. 2020, Chang et al. 2020). Our results showed that impairment of PI(3)P+/SNX8+ IAM subset maturation lead to a shift from a "sticky" BCV disassembly to "capped". Previously, RAB11A (Mellouk et al. 2014, Weiner et al. 2016, Chang et al. 2020) present at IAMs were shown to promote BCV rupture and disassembly. Having found a shift from SNX8 to RAB11A in the maturation of this IAM subset, we presume that VPS34 inhibition may impair the RAB11A shift in the PI(3)P+/SNX8+ subset maturation. This in turn would then cause a delay in BCV rupture and an imbalance in BCV unpeeling phenotypes leading to a delayed unpeeling of the BCV membrane and cytosolic access.

Other pathogens also form macropinosome-like vesicles during their invasion. *Salmonella enterica*, a bacterium closely-related to *Shigella* has recently been shown to modulate its intracellular lifestyle through IAMs. Fusion of IAMs to the BCV was shown to lead to the formation of the *Salmonella* replicative vacuole whereas the absence of fusion triggers *Salmonella* vacuole rupture upon formation of vacuole-destabilizing tubules (SVATs) prompting access of the bacteria to the cytosol (Bujny et al. 2008, Stévenin et al. 2019). This dual lifestyle has not been observed in *Shigella*. Moreover, proteomic analysis of IAMs showed differences in composition between the two pathogens (Stévenin et al. 2019, Chang et al. 2020). In *Shigella,* the results from our study together with the aforementioned findings on IAM composition suggest a different role of IAMs from *Salmonella*-IAMs. It will be interesting whether there are entirely different populations during *Shigella* and *Salmonella* entry, or whether it is the balance between different IAM

subpopulations that lead to the different phenotypes. Here, it will be interesting to take into account similarities and differences of the injected T3SS effectors. Some, such as IpgD and SopB can be found in both bacteria, however there is no homologue of the *Shigella* effector IcsB in *Salmonella*. Unfortunately, it is not possibly to simply express an effector from one bacterium in the other, as the T3SS signal sequences that allow secretion are not really compatible (communication with Leigh Knodler, and our own data). Together with previous work in our lab, this study suggests a complex function of IAMs of promoting the later steps of *Shigella* infection, possibly through the reprogramming of multiple endosomal recycling pathways.

References

Agaisse, H., 2016. Molecular and cellular mechanisms of *Shigella flexneri* dissemination. *Frontiers in cellular and infection microbiology*, *6*, p.29. doi: 10.3389/fcimb.2016.00029

Aeberhard, L., Banhart, S., Fischer, M., Jehmlich, N., Rose, L., Koch, S., Laue, M., Renard, B.Y., Schmidt, F. and Heuer, D., 2015. The proteome of the isolated *Chlamydia trachomatis* containing vacuole reveals a complex trafficking platform enriched for retromer components. *PLoS pathogens*, *11*(6), p.e1004883. doi: 10.1371/journal.ppat.1004883

Aimon, S., Callan-Jones, A., Berthaud, A., Pinot, M., Toombes, G.E. and Bassereau, P., 2014. Membrane shape modulates transmembrane protein distribution. *Developmental cell*, *28*(2), pp.212-218. doi: 10.1016/j.devcel.2013.12.012

Alto, N.M., Shao, F., Lazar, C.S., Brost, R.L., Chua, G., Mattoo, S., McMahon, S.A., Ghosh, P., Hughes, T.R., Boone, C. and Dixon, J.E., 2006. Identification of a bacterial type III effector family with G protein mimicry functions. *Cell*, *124*(1), pp.133-145. doi: 10.1016/j.cell.2005.10.031

Anderson, M., Sansonetti, P.J. and Marteyn, B.S., 2016. *Shigella* diversity and changing landscape: insights for the twenty-first century. *Frontiers in cellular and infection microbiology*, *6*, p.45. doi: 10.3389/fcimb.2016.00045 doi: 10.3389/fcimb.2016.00045

Ashida, H., Kim, M. and Sasakawa, C., 2014. Manipulation of the host cell death pathway by *Shigella*. Cellular Microbiology, 16(12), pp.1757-1766. doi: 10.1111/cmi.12367

Araki, N., Egami, Y., Watanabe, Y. and Hatae, T., 2007. Phosphoinositide metabolism during membrane ruffling and macropinosome formation in EGF-stimulated A431 cells. *Experimental cell research*, *313*(7), pp.1496-1507. doi: 10.1016/j.yexcr.2007.02.012

Bajunaid, W., Haidar-Ahmad, N., Kottarampatel, A.H., Ourida Manigat, F., Silué, N., F. Tchagang, C., Tomaro, K. and Campbell-Valois, F.X., 2020. The T3SS of *Shigella*: expression, structure, function, and role in vacuole escape. *Microorganisms*, *8*(12), p.1933. doi: 10.3390/microorganisms8121933

Balla, T., 2013. Phosphoinositides: tiny lipids with giant impact on cell regulation. *Physiological reviews*, *93*(3), pp.1019-1137. doi: 10.1152/physrev.00028.201

Barry, E.M., Pasetti, M.F., Sztein, M.B., Fasano, A., Kotloff, K.L. and Levine, M.M., 2013. Progress and pitfalls in *Shigella* vaccine research. *Nature reviews Gastroenterology & hepatology*, *10*(4), pp.245-255. doi: 10.1038/nrgastro.2013.12

Baxt, L.A. and Goldberg, M.B., 2014. Host and bacterial proteins that repress recruitment of LC3 to *Shigella* early during infection. *PloS one*, *9*(4), p.e94653. doi: 10.1371/journal.pone.0094653

Behnia, R. and Munro, S., 2005. Organelle identity and the signposts for membrane traffic. *Nature*, *438*(7068), pp.597-604. doi: 10.1038/nature04397

Bernardini, M.L., Mounier, J., d'Hauteville, H., Coquis-Rondon, M. and Sansonetti, P.J., 1989. Identification of icsA, a plasmid locus of *Shigella flexneri* that governs bacterial intra-and intercellular spread through interaction with F-actin. *Proceedings of the National Academy of Sciences*, *86*(10), pp.3867-3871. doi: 10.1073/pnas.86.10.3867

Bhatia, V.K., Madsen, K.L., Bolinger, P.Y., Kunding, A., Hedegård, P., Gether, U. and Stamou, D., 2009. Amphipathic motifs in BAR domains are essential for membrane curvature sensing. *The EMBO journal*, *28*(21), pp.3303-3314. doi: 10.1038/emboj.2009.261

Bishai, E.A., Sidhu, G.S., Li, W., Dhillon, J., Bohil, A.B., Cheney, R.E., Hartwig, J.H. and Southwick, F.S., 2013. Myosin-X facilitates *Shigella*-induced membrane protrusions and cell-to-cell spread. Cellular microbiology, 15(3), pp.353-367. doi: 10.1111/cmi.12051

Blocker, A., Gounon, P., Larquet, E., Niebuhr, K., Cabiaux, V., Parsot, C. and Sansonetti, P., 1999. The tripartite type III secreton of *Shigella flexneri* inserts IpaB and IpaC into host membranes. *The Journal of cell biology*, *147*(3), pp.683-693. doi: 10.1083/jcb.147.3.683

Bockman, D.E. and Cooper, M.D., 1973. Pinocytosis by epithelium associated with lymphoid follicles in the bursa of Fabricius, appendix, and Peyer's patches. An electron microscopic study. American journal of Anatomy, 136(4), pp.455-477. doi: 10.1002/aja.1001360406

Bohdanowicz, M., Balkin, D.M., De Camilli, P. and Grinstein, S., 2012. Recruitment of OCRL and Inpp5B to phagosomes by Rab5 and APPL1 depletes phosphoinositides and attenuates Akt signaling. *Molecular biology of the cell*, *23*(1), pp.176-187. doi: 10.1091/mbc.E11-06-0489

Borchers, A.C., Langemeyer, L. and Ungermann, C., 2021. Who's in control? Principles of Rab GTPase activation in endolysosomal membrane trafficking and beyond. *Journal of Cell Biology*, *220*(9), p.e202105120. doi: 10.1083/jcb.202105120

Botelho, H.M., Uliyakina, I., Awatade, N.T., Proença, M.C., Tischer, C., Sirianant, L., Kunzelmann, K., Pepperkok, R. and Amaral, M.D., 2015. Protein traffic disorders: an effective high-throughput fluorescence microscopy pipeline for drug discovery. *Scientific reports*, *5*(1), pp.1-8. doi: 10.1038/srep09038

Boucrot, E., Ferreira, A., Almeida-Souza, L., Debard, S., Vallis, Y., Howard, G., Bertot, L., Sauvonnet, N. and McMahon, H.T., 2015. Endophilin marks and controls a clathrin-independent endocytic pathway. *Nature*, *517*(7535), pp.460-465. doi: 10.1038/nature14067

Brighouse, A., Dacks, J.B. and Field, M.C., 2010. Rab protein evolution and the history of the eukaryotic endomembrane system. *Cellular and molecular life sciences*, *67*(20), pp.3449-3465. doi: 10.1007/s00018-010-0436-1

Brown, M.S. and Goldstein, J.L., 1979. Receptor-mediated endocytosis: insights from the lipoprotein receptor system. *Proceedings of the National Academy of Sciences*, *76*(7), pp.3330-3337. doi: 10.1073/pnas.76.7.3330

Brumell, J.H., 2012. *Brucella* "hitches a ride" with autophagy. Cell Host & Microbe, 11(1), pp.2-4. doi: 10.1016/j.chom.2012.01.003

Buchrieser, C., Glaser, P., Rusniok, C., Nedjari, H., d'Hauteville, H., Kunst, F., Sansonetti, P. and Parsot, C., 2000. The virulence plasmid pWR100 and the repertoire of proteins secreted by the type III secretion apparatus of *Shigella flexneri*. Molecular microbiology, 38(4), pp.760-771. doi: 10.1046/j.1365-2958.2000.02179.x

Buckley, C.M. and King, J.S., 2017. Drinking problems: mechanisms of macropinosome formation and maturation. *The FEBS journal*, *284*(22), pp.3778-3790. doi: 10.1111/febs.14115

Bujny, M.V., Ewels, P.A., Humphrey, S., Attar, N., Jepson, M.A. and Cullen, P.J., 2008. Sorting nexin-1 defines an early phase of Salmonella-containing vacuole-remodeling during Salmonella infection. *Journal of cell science*, *121*(12), pp.2027-2036. doi: 10.1242/jcs.018432

Burkinshaw, B.J. and Strynadka, N.C., 2014. Assembly and structure of the T3SS. *Biochimica et Biophysica Acta (BBA)-Molecular Cell Research*, *1843*(8), pp.1649-1663. doi: 10.1016/j.bbamcr.2014.01.035

Cabrera, M., Nordmann, M., Perz, A., Schmedt, D., Gerondopoulos, A., Barr, F., Piehler, J., Engelbrecht-Vandré, S. and Ungermann, C., 2014. The Mon1–Ccz1 GEF activates the Rab7 GTPase Ypt7 via a longin-fold–Rab interface and association with PI(3)P-positive membranes. *Journal of cell science*, *127*(5), pp.1043-1051. doi: 10.1242/jcs.140921

Campelo, F., McMahon, H.T. and Kozlov, M.M., 2008. The hydrophobic insertion mechanism of membrane curvature generation by proteins. *Biophysical journal*, *95*(5), pp.2325-2339. doi: 10.1529/biophysj.108.133173

Carayol, N. and Van Nhieu, G.T., 2013. Tips and tricks about *Shigella* invasion of epithelial cells. Current opinion in microbiology, 16(1), pp.32-37. doi: 10.1016/j.mib.2012.11.010

Cattin-Ortolá, J., Welch, L.G., Maslen, S.L., Papa, G., James, L.C. and Munro, S., 2021. Sequences in the cytoplasmic tail of SARS-CoV-2 Spike facilitate expression at the cell surface and syncytia formation. *Nature communications*, *12*(1), pp.1-11. doi: 10.1038/s41467-021-25589-1

Carlton, J., Bujny, M., Rutherford, A. and Cullen, P., 2005. Sorting nexins–unifying trends and new perspectives. *Traffic*, *6*(2), pp.75-82. doi: 10.1111/j.1600-0854.2005.00260.x

Carman, P.J. and Dominguez, R., 2018. BAR domain proteins—a linkage between cellular membranes, signaling pathways, and the actin cytoskeleton. *Biophysical reviews*, *10*(6), pp.1587-1604. doi: 10.1007/s12551-018-0467-7

Centers for Disease Control and Prevention. *Yellow Book* [http://wwwnc.cdc.gov/travel/yellowbook/2016/infectious-diseases-related-to-travel/shigellosis] Accessed 5 Oct 2022.

Chan Wah Hak, L., Khan, S., Di Meglio, I., Law, A.L., Lucken-Ardjomande Häsler, S., Quintaneiro, L.M., Ferreira, A., Krause, M., McMahon, H.T. and Boucrot, E., 2018. FBP17 and CIP4 recruit SHIP2 and lamellipodin to prime the plasma membrane for fast endophilin-mediated endocytosis. *Nature cell biology*, *20*(9), pp.1023-1031. doi: 10.1038/s41556-018-0146-8.

Chang, Y.Y., Stévenin, V., Duchateau, M., Giai Gianetto, Q., Hourdel, V., Rodrigues, C.D., Matondo, M., Reiling, N. and Enninga, J., 2020. *Shigella* hijacks the exocyst to cluster macropinosomes for efficient vacuolar escape. *PLoS pathogens*, *16*(8), p.e1008822. doi: https://doi.org/10.1371/journal.ppat.1008822

Chen, B.C., Legant, W.R., Wang, K., Shao, L., Milkie, D.E., Davidson, M.W., Janetopoulos, C., Wu, X.S., Hammer III, J.A., Liu, Z. and English, B.P., 2014. Lattice light-sheet microscopy: imaging molecules to embryos at high spatiotemporal resolution. *Science*, 346(6208), p.1257998. doi : 10.1126/science.1257998

Choy, A. and Roy, C.R., 2013. Autophagy and bacterial infection: an evolving arms race. *Trends in microbiology*, 21(9), pp.451-456. doi: 10.1016/j.tim.2013.06.009

Clerc, P.L., Ryter, A., Mounier, J. and Sansonetti, P.J., 1987. Plasmid-mediated early killing of eucaryotic cells by *Shigella flexneri* as studied by infection of J774 macrophages. *Infection and immunity*, *55*(3), pp.521-527. doi: 10.1128/iai.55.3.521-527.1987

Cocchiaro, J.L. and Valdivia, R.H., 2009. New insights into *Chlamydia* intracellular survival mechanisms. *Cellular microbiology*, *11*(11), pp.1571-1578. doi: 10.1111/j.1462-5822.2009.01364.x

Conrad, C. and Gerlich, D.W., 2010. Automated microscopy for high-content RNAi screening. *Journal of Cell Biology*, *188*(4), pp.453-461. doi: 10.1083/jcb.200910105.

Čopič, A., Latham, C.F., Horlbeck, M.A., D'Arcangelo, J.G. and Miller, E.A., 2012. ER cargo properties specify a requirement for COPII coat rigidity mediated by Sec13p. *Science*, *335*(6074), pp.1359-1362. doi: 10.1126/science.1215909

Cornelis, G.R., 2006. The type III secretion injectisome. *Nature Reviews Microbiology*, 4(11), pp.811-825. doi: 10.1038/nrmicro1526

Cossart, P. and Sansonetti, P.J., 2004. Bacterial invasion: the paradigms of enteroinvasive pathogens. *Science*, *304*(5668), pp.242-248. doi: 10.1126/science.1090124

Cossart, P. and Roy, C.R., 2010. Manipulation of host membrane machinery by bacterial pathogens. *Current opinion in cell biology*, *22*(4), pp.547-554. doi: 10.1016/j.ceb.2010.05.006

Cullen, P.J., 2008. Endosomal sorting and signalling: an emerging role for sorting nexins. *Nature reviews Molecular cell biology*, *9*(7), pp.574-582. doi: 10.1038/nrm2427

Cullen, P.J. and Korswagen, H.C., 2012. Sorting nexins provide diversity for retromer-dependent trafficking events. *Nature cell biology*, *14*(1), pp.29-37. doi: 10.1038/ncb2374

Daniloski, Z., Jordan, T.X., Wessels, H.H., Hoagland, D.A., Kasela, S., Legut, M., Maniatis, S., Mimitou, E.P., Lu, L., Geller, E. and Danziger, O., 2021. Identification of required host factors for SARS-CoV-2 infection in human cells. *Cell*, *184*(1), pp.92-105. doi: 10.1016/j.cell.2020.10.030

Dawson, J.C., Legg, J.A. and Machesky, L.M., 2006. Bar domain proteins: a role in tubulation, scission and actin assembly in clathrin-mediated endocytosis. *Trends in cell biology*, *16*(10), pp.493-498. doi: 10.1016/j.tcb.2006.08.004

David, C., McPherson, P.S., Mundigl, O. and De Camilli, P., 1996. A role of amphiphysin in synaptic vesicle endocytosis suggested by its binding to dynamin in nerve terminals. *Proceedings of the National Academy of Sciences*, *93*(1), pp.331-335. doi: 10.1073/pnas.93.1.331

Del Vecchio, K. and Stahelin, R.V., 2018. Investigation of the phosphatidylserine binding properties of the lipid biosensor, Lactadherin C2 (LactC2), in different membrane environments. *Journal of bioenergetics and biomembranes*, *50*(1), pp.1-10. doi: 10.1007/s10863-018-9745-0

DeMali, K.A., Jue, A.L. and Burridge, K., 2006. IpaA targets β1 integrins and rho to promote actin cytoskeleton rearrangements necessary for *Shigella* entry. *Journal of Biological Chemistry*, *281*(51), pp.39534-39541. doi: 10.1074/jbc.M605939200

Deng, W., Marshall, N.C., Rowland, J.L., McCoy, J.M., Worrall, L.J., Santos, A.S., Strynadka, N.C. and Finlay, B.B., 2017. Assembly, structure, function and regulation of type III secretion systems. *Nature Reviews Microbiology*, *15*(6), pp.323-337. doi: 10.1038/nrmicro.2017.20

Dhanda, A.S., Yu, C., Lulic, K.T., Vogl, A.W., Rausch, V., Yang, D., Nichols, B.J., Kim, S.H., Polo, S., Hansen, C.G. and Guttman, J.A., 2020. *Listeria monocytogenes* exploits host caveolin for cell-to-cell spreading. *Mbio*, *11*(1), pp.e02857-19. doi: 10.1128/mBio.02857-19

Di Paolo, G. and De Camilli, P., 2006. Phosphoinositides in cell regulation and membrane dynamics. *Nature*, *443*(7112), pp.651-657. doi: 10.1038/nature05185

Dohlich, K., Zumsteg, A.B., Goosmann, C. and Kolbe, M., 2014. A substrate-fusion protein is trapped inside the type III secretion system channel in *Shigella flexneri*. *PLoS pathogens*, *10*(1), p.e1003881. doi: 10.1371/journal.ppat.1003881

Doherty, G.J. and McMahon, H.T., 2009. Mechanisms of endocytosis. *Annual review of biochemistry*, *78*(1), pp.857-902. doi: 10.1146/annurev.biochem.78.081307.110540

Dong, N., Zhu, Y., Lu, Q., Hu, L., Zheng, Y. and Shao, F., 2012. Structurally distinct bacterial TBC-like GAPs link Arf GTPase to Rab1 inactivation to counteract host defenses. *Cell*, *150*(5), pp.1029-1041. doi: 10.1016/j.cell.2012.06.050

Dragoi, A.M. and Agaisse, H., 2014. The serine/threonine kinase STK11 promotes *Shigella flexneri* dissemination through establishment of cell-cell contacts competent for tyrosine kinase signaling. *Infection and immunity*, *82*(11), pp.4447-4457. doi: 10.1128/IAI.02078-14

Dragoi, A.M. and Agaisse, H., 2015. The class II phosphatidylinositol 3-phosphate kinase PIK3C2A promotes *Shigella flexneri* dissemination through formation of vacuole-like protrusions. *Infection and immunity*, *83*(4), pp.1695-1704. doi: 10.1128/IAI.03138-14

Drin, G., Morello, V., Casella, J.F., Gounon, P. and Antonny, B., 2008. Asymmetric tethering of flat and curved lipid membranes by a golgin. *Science*, *320*(5876), pp.670-673. doi: 10.1126/science.1155821

Du, J., Reeves, A.Z., Klein, J.A., Twedt, D.J., Knodler, L.A. and Lesser, C.F., 2016. The type III secretion system apparatus determines the intracellular niche of bacterial pathogens. *Proceedings of the National Academy of Sciences*, *113*(17), pp.4794-4799. doi: 10.1073/pnas.1520699113

DuPont, H.L., Levine, M.M., Hornick, R.B. and Formal, S.B., 1989. Inoculum size in shigellosis and implications for expected mode of transmission. *The Journal of infectious diseases*, 159(6), pp.1126-1128. doi: 10.1093/infdis/159.6.1126

Edeling, M.A., Smith, C. and Owen, D., 2006. Life of a clathrin coat: insights from clathrin and AP structures. *Nature reviews Molecular cell biology*, *7*(1), pp.32-44. doi: 10.1038/nrm1786

Egami, Y., Taguchi, T., Maekawa, M., Arai, H. and Araki, N., 2014. Small GTPases and phosphoinositides in the regulatory mechanisms of macropinosome formation and maturation. *Frontiers in physiology*, *5*, p.374. doi: 10.3389/fphys.2014.00374

Egile, C., Loisel, T.P., Laurent, V., Li, R., Pantaloni, D., Sansonetti, P.J. and Carlier, M.F., 1999. Activation of the CDC42 effector N-WASP by the *Shigella flexneri* IcsA protein promotes actin nucleation by Arp2/3 complex and bacterial actin-based motility. *The Journal of cell biology*, *146*(6), pp.1319-1332. doi: 10.1083/jcb.146.6.1319

Ellis, M.J., Tsai, C.N., Johnson, J.W., French, S., Elhenawy, W., Porwollik, S., Andrews-Polymenis, H., McClelland, M., Magolan, J., Coombes, B.K. and Brown, E.D., 2019. A macrophage-based screen identifies antibacterial compounds selective for intracellular Salmonella Typhimurium. *Nature communications*, *10*(1), pp.1-14. doi: 10.1038/s41467-018-08190-x

Elwell, C.A., Czudnochowski, N., von Dollen, J., Johnson, J.R., Nakagawa, R., Mirrashidi, K., Krogan, N.J., Engel, J.N. and Rosenberg, O.S., 2017. *Chlamydia* interfere with an interaction between the mannose-6-phosphate receptor and sorting nexins to counteract host restriction. *Elife*, *6*, p.e22709. doi: 10.7554/eLife.22709.

Ehsani, S., Santos, J.C., Rodrigues, C.D., Henriques, R., Audry, L., Zimmer, C., Sansonetti, P., Tran Van Nhieu, G. and Enninga, J., 2012. Hierarchies of host factor dynamics at the entry site of *Shigella flexneri* during host cell invasion. *Infection and immunity*, *80*(7), pp.2548-2557. doi: 10.1128/IAI.06391-11

Enninga, J., Mounier, J., Sansonetti, P. and Nhieu, G.T.V., 2005. Secretion of type III effectors into host cells in real time. *Nature methods*, *2*(12), pp.959-965. doi: 10.1038/nmeth804

Ewing, W.H., 1949. *Shigella* nomenclature. *Journal of bacteriology*, 57(6), pp.633-638. doi: 10.1128/jb.57.6.633-638.1949

Fan, W., Nassiri, A. and Zhong, Q., 2011. Autophagosome targeting and membrane curvature sensing by Barkor/Atg14 (L). *Proceedings of the National Academy of Sciences*, *108*(19), pp.7769-7774. doi: 10.1073/pnas.1016472108

Finlay, B.B. and Cossart, P., 1997. Exploitation of mammalian host cell functions by bacterial pathogens. *Science*, *276*(5313), pp.718-725. doi: 10.1126/science.276.5313.718

Finsel, I., Ragaz, C., Hoffmann, C., Harrison, C.F., Weber, S., van Rahden, V.A., Johannes, L. and Hilbi, H., 2013. The Legionella effector RidL inhibits retrograde trafficking to promote intracellular replication. *Cell host & microbe*, *14*(1), pp.38-50. doi: 10.1016/j.chom.2013.06.001

Flannagan, R.S., Jaumouillé, V. and Grinstein, S., 2012. The cell biology of phagocytosis. *Annual Review of Pathology: Mechanisms of Disease*, *7*, pp.61-98. doi: 10.1146/annurev-pathol-011811-132445

Fredlund, J., Santos, J.C., Stévenin, V., Weiner, A., Latour-Lambert, P., Rechav, K., Mallet, A., Krijnse-Locker, J., Elbaum, M. and Enninga, J., 2018. The entry of Salmonella in a distinct tight compartment

revealed at high temporal and ultrastructural resolution. *Cellular Microbiology*, *20*(4), p.e12816. doi: 10.1111/cmi.12816

Fribourg, P.F., Chami, M., Sorzano, C.O.S., Gubellini, F., Marabini, R., Marco, S., Jault, J.M. and Lévy, D., 2014. 3D cryo-electron reconstruction of BmrA, a bacterial multidrug ABC transporter in an inward-facing conformation and in a lipidic environment. *Journal of molecular biology*, *426*(10), pp.2059-2069. doi: 10.1016/j.jmb.2014.03.002.

Frischknecht, F. and Way, M., 2001. Surfing pathogens and the lessons learned for actin polymerization. *Trends in cell biology*, *11*(1), pp.30-38. doi: 10.1016/s0962-8924(00)01871-7.

Ford, M.G., Mills, I.G., Peter, B.J., Vallis, Y., Praefcke, G.J., Evans, P.R. and McMahon, H.T., 2002. Curvature of clathrin-coated pits driven by epsin. *Nature*, *419*(6905), pp.361-366. doi: 10.1038/nature01020

Fujii, M., Kawai, K., Egami, Y. and Araki, N., 2013. Dissecting the roles of Rac1 activation and deactivation in macropinocytosis using microscopic photo-manipulation. *Scientific reports*, *3*(1), pp.1-10. doi: 10.1038/srep02385

Gobaa, S., Hoehnel, S., Roccio, M., Negro, A., Kobel, S. and Lutolf, M.P., 2011. Artificial niche microarrays for probing single stem cell fate in high throughput. *Nature methods*, *8*(11), pp.949-955. doi: 10.1038/nmeth.1732

Goldenring, J.R., Smith, J., Vaughan, H.D., Cameron, P., Hawkins, W. and Navarre, J., 1996. Rab11 is an apically located small GTP-binding protein in epithelial tissues. *American Journal of Physiology-Gastrointestinal and Liver Physiology*, *270*(3), pp.G515-G525. doi: 10.1152/ajpgi.1996.270.3.G515

Gordon, S., 2016. Phagocytosis: an immunobiologic process. *Immunity*, *44*(3), pp.463-475. doi: 10.1016/j.immuni.2016.02.026

Gordon, D.E., Jang, G.M., Bouhaddou, M., Xu, J., Obernier, K., White, K.M., O'Meara, M.J., Rezelj, V.V., Guo, J.Z., Swaney, D.L. and Tummino, T.A., 2020. A SARS-CoV-2 protein interaction map reveals targets for drug repurposing. *Nature*, *583*(7816), pp.459-468. doi: 10.1038/s41586-020-2286-9

Goody, R.S., Müller, M.P. and Wu, Y.W., 2017. Mechanisms of action of Rab proteins, key regulators of intracellular vesicular transport. *Biological chemistry*, *398*(5-6), pp.565-575. doi: 10.1515/hsz-2016-0274

Grant, B.D. and Donaldson, J.G., 2009. Pathways and mechanisms of endocytic recycling. *Nature reviews Molecular cell biology*, *10*(9), pp.597-608. doi: 10.1038/nrm2755

Grassart, A., Malardé, V., Gobaa, S., Sartori-Rupp, A., Kerns, J., Karalis, K., Marteyn, B., Sansonetti, P. and Sauvonnet, N., 2019. Bioengineered human organ-on-chip reveals intestinal microenvironment and mechanical forces impacting *Shigella* infection. *Cell host & microbe*, 26(3), pp.435-444. doi: 10.1016/j.chom.2019.08.007

Groffen, A.J., Martens, S., Arazola, R.D., Cornelisse, L.N., Lozovaya, N., de Jong, A.P., Goriounova, N.A., Habets, R.L., Takai, Y., Borst, J.G. and Brose, N., 2010. Doc2b is a high-affinity Ca2+ sensor for spontaneous neurotransmitter release. *Science*, *327*(5973), pp.1614-1618. doi: 10.1126/science.1183765

Gruenheid, S. and Finlay, B.B., 2003. Microbial pathogenesis and cytoskeletal function. *Nature*, *422*(6933), pp.775-781. doi: 10.1038/nature01603

Handa, Y., Suzuki, M., Ohya, K., Iwai, H., Ishijima, N., Koleske, A.J., Fukui, Y. and Sasakawa, C., 2007. *Shigella* IpgB1 promotes bacterial entry through the ELMO–Dock180 machinery. *Nature cell biology*, *9*(1), pp.121-128. doi: 10.1038/ncb1526

Hansen, C.G., Howard, G. and Nichols, B.J., 2011. Pacsin 2 is recruited to caveolae and functions in caveolar biogenesis. *Journal of cell science*, *124*(16), pp.2777-2785. doi: 10.1242/jcs.084319

Hawkins, P.T. and Stephens, L.R., 2016. Emerging evidence of signalling roles for PI (3, 4) P 2 in class I and II PI(3)K-regulated pathways. *Biochemical Society Transactions*, *44*(1), pp.307-314. doi: 10.1042/BST20150248

Heindl, J.E., Saran, I., Yi, C.R., Lesser, C.F. and Goldberg, M.B., 2010. Requirement for formin-induced actin polymerization during spread of *Shigella flexneri*. *Infection and immunity*, 78(1), pp.193-203. doi: 10.1128/IAI.00252-09

Henley, J.R., Krueger, E.W., Oswald, B.J. and McNiven, M.A., 1998. Dynamin-mediated internalization of caveolae. *The Journal of cell biology*, *141*(1), pp.85-99. doi: 10.1083/jcb.141.1.85

Ho, H.Y.H., Rohatgi, R., Lebensohn, A.M., Ma, L., Li, J., Gygi, S.P. and Kirschner, M.W., 2004. Toca-1 mediates Cdc42-dependent actin nucleation by activating the N-WASP-WIP complex. *Cell*, *118*(2), pp.203-216. doi: 10.1016/j.cell.2004.06.027

Horiuchi, H., Lippé, R., McBride, H.M., Rubino, M., Woodman, P., Stenmark, H., Rybin, V., Wilm, M., Ashman, K., Mann, M. and Zerial, M., 1997. A novel Rab5 GDP/GTP exchange factor complexed to Rabaptin-5 links nucleotide exchange to effector recruitment and function. *Cell*, *90*(6), pp.1149-1159. doi: 10.1016/s0092-8674(00)80380-3

Hutagalung, A.H. and Novick, P.J., 2011. Role of Rab GTPases in membrane traffic and cell physiology. *Physiological reviews*, *91*(1), pp.119-149. doi: 10.1152/physrev.00059.2009

Ireton, K., Payrastre, B. and Cossart, P., 1999. The *Listeria monocytogenes* protein InlB is an agonist of mammalian phosphoinositide 3-kinase. *Journal of Biological Chemistry*, *274*(24), pp.17025-17032. doi: 10.1074/jbc.274.24.17025

Izard, T., Tran Van Nhieu, G. and Bois, P.R., 2006. *Shigella* applies molecular mimicry to subvert vinculin and invade host cells. *The Journal of cell biology*, 175(3), pp.465-475. doi: 10.1083/jcb.200605091

Izore, T., Job, V. and Dessen, A., 2011. Biogenesis, regulation, and targeting of the type III secretion system. *Structure*, *19*(5), pp.603-612. doi: 10.1016/j.str.2011.03.015

Jean, S. and Kiger, A.A., 2012. Coordination between RAB GTPase and phosphoinositide regulation and functions. *Nature reviews Molecular cell biology*, *13*(7), pp.463-470. doi: 10.1038/nrm3379

Jennings, E., Thurston, T.L. and Holden, D.W., 2017. *Salmonella* SPI-2 type III secretion system effectors: molecular mechanisms and physiological consequences. *Cell Host & Microbe*, *22*(2), pp.217-231. doi: 10.1016/j.chom.2017.07.009

Jennison, A.V. and Verma, N.K., 2004. *Shigella flexneri* infection: pathogenesis and vaccine development. *FEMS microbiology reviews*, *28*(1), pp.43-58. doi: 10.1016/j.femsre.2003.07.002

Jeong, J.Y., Yim, H.S., Ryu, J.Y., Lee, H.S., Lee, J.H., Seen, D.S. and Kang, S.G., 2012. One-step sequence-and ligation-independent cloning as a rapid and versatile cloning method for functional genomics studies. *Applied and environmental microbiology*, *78*(15), pp.5440-5443. doi: 10.1128/AEM.00844-12

Johannes, L., Parton, R.G., Bassereau, P. and Mayor, S., 2015. Building endocytic pits without clathrin. *Nature reviews Molecular cell biology*, *16*(5), pp.311-321. doi: 10.1038/nrm3968

Johnson, S., Roversi, P., Espina, M., Olive, A., Deane, J.E., Birket, S., Field, T., Picking, W.D., Blocker, A.J., Galyov, E.E. and Picking, W.L., 2007. Self-chaperoning of the type III secretion system needle tip proteins IpaD and BipD. *Journal of Biological Chemistry*, *282*(6), pp.4035-4044. doi: 10.1074/jbc.M607945200

Kasper, C.A., Sorg, I., Schmutz, C., Tschon, T., Wischnewski, H., Kim, M.L. and Arrieumerlou, C., 2010. Cell-cell propagation of NF-κB transcription factor and MAP kinase activation amplifies innate immunity against bacterial infection. *Immunity*, 33(5), pp.804-816. doi: 10.1016/j.immuni.2010.10.015

Ketel, K., Krauss, M., Nicot, A.S., Puchkov, D., Wieffer, M., Müller, R., Subramanian, D., Schultz, C., Laporte, J. and Haucke, V., 2016. A phosphoinositide conversion mechanism for exit from endosomes. *Nature*, *529*(7586), pp.408-412. doi: 10.1038/nature16516

Kim, J.Y., Kim, S.H., Jeon, S.M., Park, M.S., Rhie, H.G. and Lee, B.K., 2008. Resistance to fluoroquinolones by the combination of target site mutations and enhanced expression of genes for efflux pumps in *Shigella flexneri* and *Shigella sonnei* strains isolated in Korea. *Clinical Microbiology and Infection*, *14*(8), pp.760-765. doi: 10.1111/j.1469-0691.2008.02033.x

Kim, J.A., Hong, S. and Rhee, W.J., 2019. Microfluidic three-dimensional cell culture of stem cells for high-throughput analysis. *World Journal of Stem Cells*, *11*(10), p.803. doi: 10.4252/wjsc.v11.i10.803

Kirchhausen, T., Owen, D. and Harrison, S.C., 2014. Molecular structure, function, and dynamics of clathrin-mediated membrane traffic. *Cold Spring Harbor perspectives in biology*, *6*(5), p.a016725. doi: 10.1101/cshperspect.a016725

Kobel, S., Limacher, M., Gobaa, S., Laroche, T. and Lutolf, M.P., 2009. Micropatterning of hydrogels by soft embossing. *Langmuir*, *25*(15), pp.8774-8779. doi: 10.1021/la9002115

Kreibich, S. and Hardt, W.D., 2015. Experimental approaches to phenotypic diversity in infection. *Current opinion in microbiology*, *27*, pp.25-36. doi: 10.1038/nrm1979.

Krokowski, S., Lobato-Márquez, D., Chastanet, A., Pereira, P.M., Angelis, D., Galea, D., Larrouy-Maumus, G., Henriques, R., Spiliotis, E.T., Carballido-López, R. and Mostowy, S., 2018. Septins recognize and entrap dividing bacterial cells for delivery to lysosomes. *Cell host & microbe*, 24(6), pp.866-874. doi: 10.1016/j.chom.2018.11.005

Ku, B., Lee, K.H., Park, W.S., Yang, C.S., Ge, J., Lee, S.G., Cha, S.S., Shao, F., Heo, W.D., Jung, J.U. and Oh, B.H., 2012. VipD of *Legionella pneumophila* targets activated Rab5 and Rab22 to interfere with endosomal trafficking in macrophages. *PLoS pathogens*, *8*(12), p.e1003082. doi: 10.1371/journal.ppat.1003082

Kühn, S., Lopez-Montero, N., Chang, Y.Y., Sartori-Rupp, A. and Enninga, J., 2017. Imaging macropinosomes during *Shigella* infections. *Methods*, *127*, pp.12-22. doi: 10.1016/j.ymeth.2017.05.007

Kühn, S., Bergqvist, J., Gil, M., Valenzuela, C., Barrio, L., Lebreton, S., Zurzolo, C. and Enninga, J., 2020. Actin assembly around the *Shigella*-containing vacuole promotes successful infection. *Cell reports*, *31*(6), p.107638. doi: 10.1016/j.celrep.2020.107638

Kümmel, D. and Ungermann, C., 2014. Principles of membrane tethering and fusion in endosome and lysosome biogenesis. *Current opinion in cell biology*, *29*, pp.61-66. doi: 10.1016/j.ceb.2014.04.007.

Kowarz, E., Löscher, D. and Marschalek, R., 2015. Optimized Sleeping Beauty transposons rapidly generate stable transgenic cell lines. *Biotechnology journal*, *10*(4), pp.647-653. doi: 10.1002/biot.201400821

Lachmann, J., Glaubke, E., Moore, P.S. and Ungermann, C., 2014. The Vps39-like TRAP1 is an effector of Rab5 and likely the missing Vps3 subunit of human CORVET. *Cellular logistics*, *4*(4), p.e970840. doi: 10.4161/21592780.2014.970840

Lai, F., Stubbs, L. and Artzt, K., 1994. Molecular analysis of mouse Rab11b: a new type of mammalian YPT/Rab protein. *Genomics*, *22*(3), pp.610-616. doi: 10.1006/geno.1994.1434

Lamkanfi, M. and Dixit, V.M., 2010. Manipulation of host cell death pathways during microbial infections. *Cell host & microbe*, 8(1), pp.44-54. doi: 10.1016/j.chom.2010.06.007

Lan, R., Lumb, B., Ryan, D. and Reeves, P.R., 2001. Molecular evolution of large virulence plasmid in *Shigella* clones and enteroinvasive *Escherichia coli*. *Infection and immunity*, *69*(10), pp.6303-6309. doi: 10.1128/IAI.69.10.6303-6309.2001

Langemeyer, L., Fröhlich, F. and Ungermann, C., 2018. Rab GTPase function in endosome and lysosome biogenesis. *Trends in cell biology*, *28*(11), pp.957-970. doi: 10.1016/j.tcb.2018.06.007

Latomanski, E.A., Newton, P., Khoo, C.A. and Newton, H.J., 2016. The effector Cig57 hijacks FCHO-mediated vesicular trafficking to facilitate intracellular replication of *Coxiella burnetii*. *PLoS pathogens*, *12*(12), p.e1006101. doi: 10.1371/journal.ppat.1006101

Lawrence, G., Brown, C.C., Flood, B.A., Karunakaran, S., Cabrera, M., Nordmann, M., Ungermann, C. and Fratti, R.A., 2014. Dynamic association of the PI3P-interacting Mon1-Ccz1 GEF with vacuoles is controlled through its phosphorylation by the type 1 casein kinase Yck3. *Molecular biology of the cell*, *25*(10), pp.1608-1619. doi: 10.1091/mbc.E13-08-0460

Le-Barillec, K., Magalhaes, J.G., Corcuff, E., Thuizat, A., Sansonetti, P.J., Phalipon, A. and Di Santo, J.P., 2005. Roles for T and NK cells in the innate immune response to *Shigella flexneri*. *The Journal of Immunology*, 175(3), pp.1735-1740. doi: 10.4049/jimmunol.175.3.1735

Leung, Y., Ally, S. and Goldberg, M.B., 2008. Bacterial actin assembly requires toca-1 to relieve N-wasp autoinhibition. *Cell host & microbe*, *3*(1), pp.39-47. doi: 10.1016/j.chom.2007.10.011

Li, L., Wan, T., Wan, M., Liu, B., Cheng, R. and Zhang, R., 2015. The effect of the size of fluorescent dextran on its endocytic pathway. Cell biology international, 39(5), pp.531-539. doi: 10.1002/cbin.10424

Lichtman, J.W. and Conchello, J.A., 2005. Fluorescence microscopy. *Nature methods*, *2*(12), pp.910-919. doi: 10.1038/nmeth817

Liebl, D., Qi, X., Zhe, Y., Barnett, T.C. and Teasdale, R.D., 2017. SopB-mediated recruitment of SNX18 facilitates Salmonella Typhimurium internalization by the host cell. *Frontiers in cellular and infection microbiology*, *7*, p.257. doi: 10.3389/fcimb.2017.00257

Liu, W., Zhou, Y., Peng, T., Zhou, P., Ding, X., Li, Z., Zhong, H., Xu, Y., Chen, S., Hang, H.C. and Shao, F., 2018. Nε-fatty acylation of multiple membrane-associated proteins by *Shigella* IcsB effector to modulate host function. *Nature microbiology*, *3*(9), pp.996-1009. doi: 10.1038/s41564-018-0215-6

Lobato-Márquez, D., Xu, J., Güler, G.Ö., Ojiakor, A., Pilhofer, M. and Mostowy, S., 2021. Mechanistic insight into bacterial entrapment by septin cage reconstitution. *Nature communications*, 12(1), pp.1-14. doi: 10.1038/s41467-021-24721-5

Lorkowski, M., Felipe-López, A., Danzer, C.A., Hansmeier, N. and Hensel, M., 2014. *Salmonella enterica* invasion of polarized epithelial cells is a highly cooperative effort. *Infection and Immunity*, *82*(6), pp.2657-2667. doi: 10.1128/IAI.00023-14

Lucas, M., Gaspar, A.H., Pallara, C., Rojas, A.L., Fernández-Recio, J., Machner, M.P. and Hierro, A., 2014. Structural basis for the recruitment and activation of the *Legionella* phospholipase VipD by the host GTPase Rab5. *Proceedings of the National Academy of Sciences*, *111*(34), pp.E3514-E3523. doi: 10.1073/pnas.1405391111

Luk, C.H., Valenzuela, C., Gil, M., Swistak, L., Bomme, P., Chang, Y.Y., Mallet, A. and Enninga, J., 2021. *Salmonella* enters a dormant state within human epithelial cells for persistent infection. *PLoS pathogens*, *17*(4), p.e1009550. doi: 10.1371/journal.ppat.1009550

Mahbubur, R., Shoma, S., Rashid, H., El Arifeen, S., Baqui, A.H., Siddique, A.K., Nair, G.B. and Sack, D.A., 2007. Increasing spectrum in antimicrobial resistance of *Shigella* isolates in Bangladesh: resistance to azithromycin and ceftriaxone and decreased susceptibility to ciprofloxacin. *Journal of health, population, and nutrition*, *25*(2), p.158.

Malik-Kale, P., Winfree, S. and Steele-Mortimer, O., 2012. The bimodal lifestyle of intracellular *Salmonella* in epithelial cells: replication in the cytosol obscures defects in vacuolar replication. *PloS one*, *7*(6), p.e38732. doi: 10.1371/journal.pone.0038732

Mani, S., Wierzba, T. and Walker, R.I., 2016. Status of vaccine research and development for *Shigella*. *Vaccine*, 34(26), pp.2887-2894. doi: 10.1016/j.vaccine.2016.02.075

Mattera, R., Tsai, Y.C., Weissman, A.M. and Bonifacino, J.S., 2006. The Rab5 guanine nucleotide exchange factor Rabex-5 binds ubiquitin (Ub) and functions as a Ub ligase through an atypical Ub-interacting motif and a zinc finger domain. *Journal of Biological Chemistry*, *281*(10), pp.6874-6883. doi: 10.1074/jbc.M509939200

Mattock, E. and Blocker, A.J., 2017. How do the virulence factors of *Shigella* work together to cause disease?. *Frontiers in cellular and infection microbiology*, *7*, p.64. doi: 10.3389/fcimb.2017.00064

Mayor, S. and Pagano, R.E., 2007. Pathways of clathrin-independent endocytosis. *Nature reviews Molecular cell biology*, *8*(8), pp.603-612. doi: 10.1038/nrm2216

McGourty, K., Thurston, T.L., Matthews, S.A., Pinaud, L., Mota, L.J. and Holden, D.W., 2012. *Salmonella* inhibits retrograde trafficking of mannose-6-phosphate receptors and lysosome function. *Science*, *338*(6109), pp.963-967. doi: 10.1126/science.1227037

McMahon, H.T. and Gallop, J.L., 2005. Membrane curvature and mechanisms of dynamic cell membrane remodelling. *Nature*, *438*(7068), pp.590-596. doi: 10.1038/nature04396

McMahon, H.T., Kozlov, M.M. and Martens, S., 2010. Membrane curvature in synaptic vesicle fusion and beyond. *Cell*, *140*(5), pp.601-605. doi: 10.1016/j.cell.2010.02.017

McMahon, H.T. and Boucrot, E., 2015. Membrane curvature at a glance. *Journal of cell science*, *128*(6), pp.1065-1070. doi: 10.1242/jcs.114454

Mellouk, N., Weiner, A., Aulner, N., Schmitt, C., Elbaum, M., Shorte, S.L., Danckaert, A. and Enninga, J., 2014. *Shigella* subverts the host recycling compartment to rupture its vacuole. *Cell host & microbe*, *16*(4), pp.517-530.doi: https://doi.org/10.1016/j.chom.2014.09.005

Menard, R., Sansonetti, P. and Parsot, C., 1994. The secretion of the *Shigella flexneri* Ipa invasins is activated by epithelial cells and controlled by IpaB and IpaD. *The EMBO journal*, *13*(22), pp.5293-5302. doi: 10.1002/j.1460-2075.1994.tb06863.x

Mirrashidi, K.M., Elwell, C.A., Verschueren, E., Johnson, J.R., Frando, A., Von Dollen, J., Rosenberg, O., Gulbahce, N., Jang, G., Johnson, T. and Jäger, S., 2015. Global mapping of the Inc-human interactome reveals that retromer restricts *Chlamydia* infection. *Cell host & microbe*, *18*(1), pp.109-121. doi: 10.1016/j.chom.2015.06.004

Misselwitz, B., Barrett, N., Kreibich, S., Vonaesch, P., Andritschke, D., Rout, S., Weidner, K., Sormaz, M., Songhet, P., Horvath, P. and Chabria, M., 2012. Near surface swimming of Salmonella Typhimurium explains target-site selection and cooperative invasion. *PLoS pathogens*, *8*(7), p.e1002810. doi: 10.1371/journal.ppat.1002810

Mitchell, P.S., Roncaioli, J.L., Turcotte, E.A., Goers, L., Chavez, R.A., Lee, A.Y., Lesser, C.F., Rauch, I. and Vance, R.E., 2020. NAIP–NLRC4-deficient mice are susceptible to shigellosis. *Elife*, 9, p.e59022. doi: 10.7554/eLife.59022

Mohr, S., Bakal, C. and Perrimon, N., 2010. Genomic screening with RNAi: results and challenges. *Annual review of biochemistry*, *79*, p.37. doi: 10.1146/annurev-biochem-060408-092949

Morita-Ishihara, T., Terajima, J., Watanabe, H. and Izumiya, H., 2009. Interaction between enterohemorrhagic *Escherichia coli* O157: H7 EspFu and IRSp53 induces dynamic membrane remodeling in epithelial cells. *Jpn J Infect Dis*, *62*, pp.351-355.

Mostowy, S., Nam Tham, T., Danckaert, A., Guadagnini, S., Boisson-Dupuis, S., Pizarro-Cerdá, J. and Cossart, P., 2009. Septins regulate bacterial entry into host cells. *PloS one*, 4(1), p.e4196. doi: 10.1371/journal.pone.0004196

Mostowy, S., Bonazzi, M., Hamon, M.A., Tham, T.N., Mallet, A., Lelek, M., Gouin, E., Demangel, C., Brosch, R., Zimmer, C. and Sartori, A., 2010. Entrapment of intracytosolic bacteria by septin cage-like structures. *Cell host & microbe*, 8(5), pp.433-444. doi: 10.1016/j.chom.2010.10.009

Mostowy, S., 2013. Autophagy and bacterial clearance: a not so clear picture. Cellular microbiology, 15(3), pp.395-402. doi: 10.1111/cmi.12063.

Mounier, J., Vasselon, T., Hellio, R., Lesourd, M. and Sansonetti, P.J., 1992. *Shigella flexneri* enters human colonic Caco-2 epithelial cells through the basolateral pole. Infection and immunity, 60(1), pp.237-248. doi: 10.1128/iai.60.1.237-248.1992

Mounier, J., Popoff, M.R., Enninga, J., Frame, M.C., Sansonetti, P.J. and Van Nhieu, G.T., 2009. The IpaC carboxyterminal effector domain mediates Src-dependent actin polymerization during *Shigella* invasion of epithelial cells. *PLoS pathogens*, *5*(1), p.e1000271. doi: 10.1371/journal.ppat.1000271

Mounier, J., Boncompain, G., Senerovic, L., Lagache, T., Chrétien, F., Perez, F., Kolbe, M., Olivo-Marin, J.C., Sansonetti, P.J. and Sauvonnet, N., 2012. *Shigella* effector IpaB-induced cholesterol relocation disrupts the Golgi complex and recycling network to inhibit host cell secretion. *Cell Host & Microbe*, *12*(3), pp.381-389. doi: 10.1016/j.chom.2012.07.010

Murray, J.T., Panaretou, C., Stenmark, H., Miaczynska, M. and Backer, J.M., 2002. Role of Rab5 in the recruitment of hVps34/p150 to the early endosome. *Traffic*, *3*(6), pp.416-427. doi: 10.1034/j.1600-0854.2002.30605.x

Newton, H.J., Ang, D.K., Van Driel, I.R. and Hartland, E.L., 2010. Molecular pathogenesis of infections caused by *Legionella pneumophila*. *Clinical microbiology reviews*, *23*(2), pp.274-298. doi: 10.1128/CMR.00052-09

Niebuhr, K., Giuriato, S., Pedron, T., Philpott, D.J., Gaits, F., Sable, J., Sheetz, M.P., Parsot, C., Sansonetti, P.J. and Payrastre, B., 2002. Conversion of PtdIns (4, 5) P2 into PtdIns (5) P by the *S. flexneri* effector IpgD reorganizes host cell morphology. *The EMBO journal*, *21*(19), pp.5069-5078. doi: 10.1093/emboj/cdf522

Nielsen, E., Christoforidis, S., Uttenweiler-Joseph, S., Miaczynska, M., Dewitte, F., Wilm, M., Hoflack, B. and Zerial, M., 2000. Rabenosyn-5, a novel Rab5 effector, is complexed with hVPS45 and recruited to endosomes through a FYVE finger domain. *The Journal of cell biology*, *151*(3), pp.601-612. doi: 10.1083/jcb.151.3.601

Nowicki, B., Hart, A., Coyne, K.E., Lublin, D.M. and Nowicki, S., 1993. Short consensus repeat-3 domain of recombinant decay-accelerating factor is recognized by Escherichia coli recombinant Dr adhesin in a model of a cell-cell interaction. *The Journal of experimental medicine*, *178*(6), pp.2115-2121. doi: 10.1084/jem.178.6.2115

O'Sullivan, M.J. and Lindsay, A.J., 2020. The endosomal recycling pathway—at the crossroads of the cell. *International Journal of Molecular Sciences*, *21*(17), p.6074. doi: 10.3390/ijms21176074

Okamoto, M., Kurokawa, K., Matsuura-Tokita, K., Saito, C., Hirata, R. and Nakano, A., 2012. High-curvature domains of the ER are important for the organization of ER exit sites in Saccharomyces cerevisiae. *Journal of cell science*, *125*(14), pp.3412-3420. doi: 10.1242/jcs.100065

Olive, A.J., Kenjale, R., Espina, M., Moore, D.S., Picking, W.L. and Picking, W.D., 2007. Bile salts stimulate recruitment of IpaB to the *Shigella flexneri* surface, where it colocalizes with IpaD at the tip of the type III secretion needle. *Infection and immunity*, *75*(5), pp.2626-2629. doi: 10.1128/IAI.01599-06

Ortega, F.E., Koslover, E.F. and Theriot, J.A., 2019. *Listeria monocytogenes* cell-to-cell spread in epithelia is heterogeneous and dominated by rare pioneer bacteria. *Elife*, *8*, p.e40032. doi: 10.7554/eLife.40032

Ogawa, M., Yoshimori, T., Suzuki, T., Sagara, H., Mizushima, N. and Sasakawa, C., 2005. Escape of intracellular *Shigella* from autophagy. *Science*, *307*(5710), pp.727-731. doi: 10.1126/science.1106036

Park, H., Valencia-Gallardo, C., Sharff, A., Van Nhieu, G.T. and Izard, T., 2011. Novel Vinculin Binding Site of the IpaA Invasin of *Shigella**♦. *Journal of Biological Chemistry*, *286*(26), pp.23214-23221.

Parsot, C., 2009. *Shigella* type III secretion effectors: how, where, when, for what purposes? *Current opinion in microbiology*, *12*(1), pp.110-116. doi: 10.1016/j.mib.2008.12.002

Paul, B., Kim, H.S., Kerr, M.C., Huston, W.M., Teasdale, R.D. and Collins, B.M., 2017. Structural basis for the hijacking of endosomal sorting nexin proteins by *Chlamydia trachomatis*. *Elife*, *6*, p.e22311. doi: 10.7554/eLife.22311

Payrastre, B., Gaits-Iacovoni, F., Sansonetti, P. and Tronchère, H., 2012. Phosphoinositides and cellular pathogens. *Phosphoinositides II: the diverse biological functions*, pp.363-388. doi: 10.1007/978-94-007-3015-1_12

Paz, I., Sachse, M., Dupont, N., Mounier, J., Cederfur, C., Enninga, J., Leffler, H., Poirier, F., Prevost, M.C., Lafont, F. and Sansonetti, P., 2010. Galectin-3, a marker for vacuole lysis by invasive pathogens. *Cellular microbiology*, *12*(4), pp.530-544. doi: 10.1016/j.celrep.2020.107638

Perdomo, O.J., Cavaillon, J.M., Huerre, M., Ohayon, H., Gounon, P. and Sansonetti, P.J., 1994. Acute inflammation causes epithelial invasion and mucosal destruction in experimental shigellosis. *The Journal of experimental medicine*, *180*(4), pp.1307-1319. doi: 10.1084/jem.180.4.1307

Perdomo, J.J., Gounon, P. and Sansonetti, P.J., 1994. Polymorphonuclear leukocyte transmigration promotes invasion of colonic epithelial monolayer by *Shigella flexneri*. The Journal of clinical investigation, 93(2), pp.633-643. doi: 10.1172/JCI117015

Perini, E.D., Schaefer, R., Stöter, M., Kalaidzidis, Y. and Zerial, M., 2014. Mammalian CORVET is required for fusion and conversion of distinct early endosome subpopulations. *Traffic*, *15*(12), pp.1366-1389. doi: 10.1111/tra.12232

Perlman, Z.E., Slack, M.D., Feng, Y., Mitchison, T.J., Wu, L.F. and Altschuler, S.J., 2004. Multidimensional drug profiling by automated microscopy. Science, 306(5699), pp.1194-1198. doi: 10.1126/science.1100709

Peter, B.J., Kent, H.M., Mills, I.G., Vallis, Y., Butler, P.J.G., Evans, P.R. and McMahon, H.T., 2004. BAR domains as sensors of membrane curvature: the amphiphysin BAR structure. *Science*, *303*(5657), pp.495-499. doi: 10.1126/science.1092586

Pepperkok, R. and Ellenberg, J., 2006. High-throughput fluorescence microscopy for systems biology. *Nature reviews Molecular cell biology*, *7*(9), pp.690-696. doi: 10.1038/nrm1979

Pfeffer, S.R., 2001. Rab GTPases: specifying and deciphering organelle identity and function. *Trends in cell biology*, *11*(12), pp.487-491. doi: 10.1016/s0962-8924(01)02147-x

Pfeffer, S.R., 2013. Rab GTPase regulation of membrane identity. *Current opinion in cell biology*, *25*(4), pp.414-419. doi: 10.1016/j.ceb.2013.04.002

Piscatelli, H.L., Li, M. and Zhou, D., 2016. Dual 4‐and 5‐phosphatase activities regulate SopB‐dependent phosphoinositide dynamics to promote bacterial entry. *Cellular microbiology*, *18*(5), pp.705-719. doi: 10.1111/cmi.12542

Pizarro‐Cerdá, J., Payrastre, B., Wang, Y.J., Veiga, E., Yin, H.L. and Cossart, P., 2007. Type II phosphatidylinositol 4‐kinases promote *Listeria monocytogenes* entry into target cells. *Cellular microbiology*, *9*(10), pp.2381-2390. doi: 10.1111/j.1462-5822.2007.00967.x

Pizarro-Cerdá, J., Kühbacher, A. and Cossart, P., 2015. Phosphoinositides and host–pathogen interactions. *Biochimica et Biophysica Acta (BBA)-Molecular and Cell Biology of Lipids*, *1851*(6), pp.911-918. doi: 10.1016/j.bbalip.2014.09.011

Plomann, M., Wittmann, J.G. and Rudolph, M.G., 2010. A hinge in the distal end of the PACSIN 2 F-BAR domain may contribute to membrane-curvature sensing. *Journal of molecular biology*, *400*(2), pp.129-136. doi: 10.1016/j.jmb.2010.05.008

Polle, L., Rigano, L.A., Julian, R., Ireton, K. and Schubert, W.D., 2014. Structural details of human tuba recruitment by InlC of *Listeria monocytogenes* elucidate bacterial cell-cell spreading. *Structure*, *22*(2), pp.304-314. doi: 10.1016/j.str.2013.10.017

Portaliou, A.G., Tsolis, K.C., Loos, M.S., Zorzini, V. and Economou, A., 2016. Type III secretion: building and operating a remarkable nanomachine. *Trends in biochemical sciences*, *41*(2), pp.175-189. doi: 10.1016/j.tibs.2015.09.005

Posor, Y., Jang, W. and Haucke, V., 2022. Phosphoinositides as membrane organizers. *Nature Reviews Molecular Cell Biology*, pp.1-20. doi: 10.1038/s41580-022-00490-x

Poteryaev, D., Datta, S., Ackema, K., Zerial, M. and Spang, A., 2010. Identification of the switch in early-to-late endosome transition. *cell*, *141*(3), pp.497-508. doi: 10.1016/j.cell.2010.03.011

Praefcke, G.J. and McMahon, H.T., 2004. The dynamin superfamily: universal membrane tubulation and fission molecules?. *Nature reviews Molecular cell biology*, *5*(2), pp.133-147. doi: 10.1038/nrm1313

Puzari, M., Sharma, M. and Chetia, P., 2018. Emergence of antibiotic resistant *Shigella* species: A matter of concern. *Journal of infection and public health*, *11*(4), pp.451-454. doi: 10.1016/j.jiph.2017.09.025

Quereda, J.J., Morel, C., Lopez-Montero, N., Ziveri, J., Rolland, S., Grenier, T., Aulner, N., Danckaert, A., Charbit, A., Enninga, J. and Cossart, P., 2022. A role for Taok2 in *Listeria monocytogenes* vacuolar escape. *The Journal of infectious diseases*, *225*(6), pp.1005-1010. doi: 10.1093/infdis/jiaa367

Radics, J., Königsmaier, L. and Marlovits, T.C., 2014. Structure of a pathogenic type 3 secretion system in action. *Nature structural & molecular biology*, *21*(1), pp.82-87. doi: 10.1038/nsmb.2722

Radhakrishna, H., Al-Awar, O., Khachikian, Z. and Donaldson, J.G., 1999. ARF6 requirement for Rac ruffling suggests a role for membrane trafficking in cortical actin rearrangements. *Journal of cell science*, *112*(6), pp.855-866. doi: 10.1242/jcs.112.6.855

Rafelski, S.M. and Marshall, W.F., 2008. Building the cell: design principles of cellular architecture. *Nature Reviews Molecular Cell Biology*, *9*(8), pp.593-602. doi: 10.1038/nrm2460

Rajabian, T., Gavicherla, B., Heisig, M., Müller-Altrock, S., Goebel, W., Gray-Owen, S.D. and Ireton, K., 2009. The bacterial virulence factor InlC perturbs apical cell junctions and promotes cell-to-cell spread of *Listeria*. *Nature cell biology*, *11*(10), pp.1212-1218. doi: 10.1038/ncb1964

Ray, K., Bobard, A., Danckaert, A., Paz‐Haftel, I., Clair, C., Ehsani, S., Tang, C., Sansonetti, P., Van Nhieu, G.T. and Enninga, J., 2010. Tracking the dynamic interplay between bacterial and host factors during pathogen‐induced vacuole rupture in real time. *Cellular microbiology*, *12*(4), pp.545-556. doi: 10.1111/j.1462-5822.2010.01428.x

Rengarajan, M. and Theriot, J.A., 2020. Rapidly dynamic host cell heterogeneity in bacterial adhesion governs susceptibility to infection by *Listeria monocytogenes*. *Molecular biology of the cell*, *31*(19), pp.2097-2106. doi: 10.1091/mbc.E19-08-0454

Rey, C., Chang, Y.Y., Latour-Lambert, P., Varet, H., Proux, C., Legendre, R., Coppée, J.Y. and Enninga, J., 2020. Transcytosis subversion by M cell-to-enterocyte spread promotes *Shigella flexneri* and *Listeria monocytogenes* intracellular bacterial dissemination. *PLoS pathogens*, *16*(4), p.e1008446. doi: 10.1371/journal.ppat.1008446

Ribet, D. and Cossart, P., 2015. How bacterial pathogens colonize their hosts and invade deeper tissues. *Microbes and infection*, *17*(3), pp.173-183. doi: 10.1016/j.micinf.2015.01.004

Robinson, D.G. and Pimpl, P., 2014. Clathrin and post-Golgi trafficking: a very complicated issue. *Trends in plant science*, *19*(3), pp.134-139. doi: 10.1016/j.tplants.2013.10.008

Romano, P.S., Gutierrez, M.G., Berón, W., Rabinovitch, M. and Colombo, M.I., 2007. The autophagic pathway is actively modulated by phase II *Coxiella burnetii* to efficiently replicate in the host cell. *Cellular microbiology*, *9*(4), pp.891-909. doi: 10.1111/j.1462-5822.2006.00838.x

Romero, S., Grompone, G., Carayol, N., Mounier, J., Guadagnini, S., Prevost, M.C., Sansonetti, P.J. and Van Nhieu, G.T., 2011. ATP-mediated Erk1/2 activation stimulates bacterial capture by filopodia, which precedes *Shigella* invasion of epithelial cells. *Cell host & microbe*, *9*(6), pp.508-519. doi: 10.1016/j.chom.2011.05.005

Romero, S., Quatela, A., Bornschlögl, T., Guadagnini, S., Bassereau, P. and Tran Van Nhieu, G., 2012. Filopodium retraction is controlled by adhesion to its tip. *Journal of cell science*, *125*(21), pp.4999-5004. doi: 10.1242/jcs.104778

Ronan, B., Flamand, O., Vescovi, L., Dureuil, C., Durand, L., Fassy, F., Bachelot, M.F., Lamberton, A., Mathieu, M., Bertrand, T. and Marquette, J.P., 2014. A highly potent and selective Vps34 inhibitor alters vesicle trafficking and autophagy. *Nature chemical biology*, *10*(12), pp.1013-1019. doi: 10.1038/nchembio.1681

Rupper, A., Lee, K., Knecht, D. and Cardelli, J., 2001. Sequential activities of phosphoinositide 3-kinase, PKB/Akt, and Rab7 during macropinosome formation in Dictyostelium. *Molecular biology of the cell*, *12*(9), pp.2813-2824. doi: 10.1091/mbc.12.9.2813

Saheki, Y. and De Camilli, P., 2012. Synaptic vesicle endocytosis. *Cold Spring Harbor perspectives in biology*, *4*(9), p.a005645. doi: 10.1101/cshperspect.a005645

Salazar, M.A., Kwiatkowski, A.V., Pellegrini, L., Cestra, G., Butler, M.H., Rossman, K.L., Serna, D.M., Sondek, J., Gertler, F.B. and De Camilli, P., 2003. Tuba, a novel protein containing bin/amphiphysin/Rvs and Dbl homology domains, links dynamin to regulation of the actin cytoskeleton. *Journal of Biological Chemistry*, *278*(49), pp.49031-49043. doi: 10.1074/jbc.M308104200

Salzer, U., Kostan, J. and Djinović-Carugo, K., 2017. Deciphering the BAR code of membrane modulators. *Cellular and Molecular Life Sciences*, *74*(13), pp.2413-2438. doi: 10.1007/s00018-017-2478-0

Sanderlin, A.G., Vondrak, C., Scricco, A.J., Fedrigo, I., Ahyong, V. and Lamason, R.L., 2019. RNAi screen reveals a role for PACSIN2 and caveolins during bacterial cell-to-cell spread. *Molecular biology of the cell*, *30*(17), pp.2124-2133. doi: 10.1091/mbc.E19-04-0197

Sanderson, M.J., Smith, I., Parker, I. and Bootman, M.D., 2014. Fluorescence microscopy. Cold Spring Harbor Protocols, 2014(10), pp.pdb-top071795. doi, 10.1101/pdb.top071795

Sansonetti, P.J., Arondel, J., Cantey, J.R., Prévost, M.C. and Huerre, M., 1996. Infection of rabbit Peyer's patches by *Shigella flexneri*: effect of adhesive or invasive bacterial phenotypes on follicle-associated epithelium. *Infection and immunity*, *64*(7), pp.2752-2764. doi: 10.1128/iai.64.7.2752-2764.1996

Sansonetti, P.J., Arondel, J., Huerre, M., Harada, A. and Matsushima, K., 1999. Interleukin-8 controls bacterial transepithelial translocation at the cost of epithelial destruction in experimental shigellosis. Infection and immunity, 67(3), pp.1471-1480. doi: 10.1128/IAI.67.3.1471-1480.1999

Sansonetti, P.J., Phalipon, A., Arondel, J., Thirumalai, K., Banerjee, S., Akira, S., Takeda, K. and Zychlinsky, A., 2000. Caspase-1 activation of IL-1β and IL-18 are essential for *Shigella flexneri*–induced inflammation. *Immunity,* 12(5), pp.581-590. doi: 10.1016/s1074-7613(00)80209-5

Sansonetti, P.J., 2001. III. Shigellosis: from symptoms to molecular pathogenesis. American Journal of Physiology-Gastrointestinal and Liver Physiology, 280(3), pp.G319-G323. doi: 10.1152/ajpgi.2001.280.3.G319

Santos, J.C., Duchateau, M., Fredlund, J., Weiner, A., Mallet, A., Schmitt, C., Matondo, M., Hourdel, V., Chamot-Rooke, J. and Enninga, J., 2015. The COPII complex and lysosomal VAMP 7 determine intracellular *Salmonella* localization and growth. Cellular Microbiology, 17(12), pp.1699-1720. doi: 10.1111/cmi.12475

Sardana, R. and Emr, S.D., 2021. Membrane protein quality control mechanisms in the endo-lysosome system. *Trends in Cell Biology*, *31*(4), pp.269-283. doi: 10.1016/j.tcb.2020.11.011

Schink, K.O., Tan, K.W. and Stenmark, H., 2016. Phosphoinositides in control of membrane dynamics. *Annual review of cell and developmental biology*, *32*, pp.143-171. doi: 10.1146/annurev-cellbio-111315-125349

Schnupf, P. and Sansonetti, P.J., 2019. *Shigella* pathogenesis: new insights through advanced methodologies. *Microbiology spectrum*, 7(2), pp.7-2. doi: 10.1128/microbiolspec.BAI-0023-2019

Schroeder, G.N. and Hilbi, H., 2008. Molecular pathogenesis of *Shigella* spp.: controlling host cell signaling, invasion, and death by type III secretion. *Clinical microbiology reviews*, *21*(1), pp.134-156. doi: 10.1128/CMR.00032-07

Segal, A.W., Geisow, M., Garcia, R., Harper, A. and Miller, R., 1981. The respiratory burst of phagocytic cells is associated with a rise in vacuolar pH. *Nature*, *290*(5805), pp.406-409. doi: 10.1038/290406a0

Senju, Y., Itoh, Y., Takano, K., Hamada, S. and Suetsugu, S., 2011. Essential role of PACSIN2/syndapin-II in caveolae membrane sculpting. *Journal of cell science*, *124*(12), pp.2032-2040. doi: 10.1242/jcs.086264

Shibata, Y., Hu, J., Kozlov, M.M. and Rapoport, T.A., 2009. Mechanisms shaping the membranes of cellular organelles. *Annual Review of Cell and Developmental*, *25*, pp.329-354. doi: 10.1146/annurev.cellbio.042308.113324

Shin, H.W., Hayashi, M., Christoforidis, S., Lacas-Gervais, S., Hoepfner, S., Wenk, M.R., Modregger, J., Uttenweiler-Joseph, S., Wilm, M., Nystuen, A. and Frankel, W.N., 2005. An enzymatic cascade of Rab5 effectors regulates phosphoinositide turnover in the endocytic pathway. *The Journal of cell biology*, *170*(4), pp.607-618. doi: 10.1128/microbiolspec.BAI-0023-2019

Simonsen, A., Lippe, R., Christoforidis, S., Gaullier, J.M., Brech, A., Callaghan, J., Toh, B.H., Murphy, C., Zerial, M. and Stenmark, H., 1998. EEA1 links PI (3) K function to Rab5 regulation of endosome fusion. *Nature*, *394*(6692), pp.494-498. doi: 10.1038/28879

Simunovic, M., Voth, G.A., Callan-Jones, A. and Bassereau, P., 2015. When physics takes over: BAR proteins and membrane curvature. *Trends in cell biology*, *25*(12), pp.780-792. doi:10.1016/j.tcb.2015.09.005

Simunovic, M., Evergren, E., Golushko, I., Prévost, C., Renard, H.F., Johannes, L., McMahon, H.T., Lorman, V., Voth, G.A. and Bassereau, P., 2016. How curvature-generating proteins build scaffolds on membrane nanotubes. *Proceedings of the National Academy of Sciences*, *113*(40), pp.11226-11231. doi: 10.1073/pnas.1606943113

Simunovic, M., Evergren, E., Callan-Jones, A. and Bassereau, P., 2019. Curving the cells inside and out: Roles of BAR-domain proteins in intracellular trafficking, shaping organelles, and cancer. *Annual Review of Cell and Developmental Biology*. doi: 10.1146/annurev-cellbio-100617-060558

Snead, D., Wragg, R.T., Dittman, J.S. and Eliezer, D., 2014. Membrane curvature sensing by the C-terminal domain of complexin. *Nature communications*, *5*(1), pp.1-10. doi: 10.1038/ncomms5955

Spangenberg, H., Sneeggen, M., Tortola, M.M., Valenzuela, C., Chang, Y.Y., Stenmark, H., Raiborg, C. and Schink, K.O., 2021. A phosphoinositide and RAB switch controls early macropinocytosis. *bioRxiv*. doi: https://doi.org/10.1101/2021.11.03.467145

Sönnichsen, B., Koski, L.B., Walsh, A., Marschall, P., Neumann, B., Brehm, M., Alleaume, A.M., Artelt, J., Bettencourt, P., Cassin, E. and Hewitson, M., 2005. Full-genome RNAi profiling of early embryogenesis in Caenorhabditis elegans. *Nature*, *434*(7032), pp.462-469. doi: 10.1038/nature03353

Starr, T., Child, R., Wehrly, T.D., Hansen, B., Hwang, S., López-Otin, C., Virgin, H.W. and Celli, J., 2012. Selective subversion of autophagy complexes facilitates completion of the Brucella intracellular cycle. Cell host & microbe, 11(1), pp.33-45. doi: 10.1016/j.chom.2011.12.002

Stachowiak, J.C., Schmid, E.M., Ryan, C.J., Ann, H.S., Sasaki, D.Y., Sherman, M.B., Geissler, P.L., Fletcher, D.A. and Hayden, C.C., 2012. Membrane bending by protein–protein crowding. *Nature cell biology*, *14*(9), pp.944-949. doi: 10.1038/ncb2561

Stenmark, H., 2009. Rab GTPases as coordinators of vesicle traffic. *Nature reviews Molecular cell biology*, *10*(8), pp.513-525. doi: 10.1038/nrm2728

Stévenin, V., Chang, Y.Y., Le Toquin, Y., Duchateau, M., Gianetto, Q.G., Luk, C.H., Salles, A., Sohst, V., Matondo, M., Reiling, N. and Enninga, J., 2019. Dynamic growth and shrinkage of the *Salmonella*-containing vacuole determines the intracellular pathogen niche. *Cell reports*, *29*(12), pp.3958-3973. doi: 10.1016/j.celrep.2019.11.049

Steinhäuser, C., Dallenga, T., Tchikov, V., Schaible, U.E., Schütze, S. and Reiling, N., 2014. Immunomagnetic isolation of pathogen-containing phagosomes and apoptotic blebs from primary phagocytes. Current protocols in immunology, 105(1), pp.14-36. doi: 10.1002/0471142735.im1436s105

Suarez, A., Ueno, T., Huebner, R., McCaffery, J.M. and Inoue, T., 2014. Bin/Amphiphysin/Rvs (BAR) family members bend membranes in cells. *Scientific reports*, *4*(1), pp.1-6. doi: 10.1038/srep04693

Suetsugu, S., Toyooka, K. and Senju, Y., 2010, June. Subcellular membrane curvature mediated by the BAR domain superfamily proteins. In *Seminars in cell & developmental biology* (Vol. 21, No. 4, pp. 340-349). Academic Press. doi: 10.1016/j.semcdb.2009.12.002

Suzuki, T., Mimuro, H., Suetsugu, S., Miki, H., Takenawa, T. and Sasakawa, C., 2002. Neural Wiskott–Aldrich syndrome protein (N-WASP) is the specific ligand for *Shigella* VirG among the WASP family and determines the host cell type allowing actin-based spreading. *Cellular microbiology*, *4*(4), pp.223-233. doi: 10.1046/j.1462-5822.2002.00185.x

Swanson, J.A., 2008. Shaping cups into phagosomes and macropinosomes. *Nature reviews Molecular cell biology*, *9*(8), pp.639-649. doi: 10.1038/nrm2447.

Swanson, J.A., 2014. Phosphoinositides and engulfment. *Cellular microbiology*, *16*(10), pp.1473-1483. doi: 10.1111/cmi.12334

Tan, S. and Russell, D.G., 2015. Trans-species communication in the *Mycobacterium tuberculosis*-infected macrophage. *Immunological reviews*, *264*(1), pp.233-248. doi: 10.1111/imr.12254

Taneja, N. and Mewara, A., 2016. Shigellosis: epidemiology in India. *The Indian journal of medical research*, 143(5), p.565. doi: 10.4103/0971-5916.187104

Taylor, M.J., Perrais, D. and Merrifield, C.J., 2011. A high precision survey of the molecular dynamics of mammalian clathrin-mediated endocytosis. *PLoS biology*, *9*(3), p.e1000604. doi: 10.1371/journal.pbio.1000604

Teasdale, R.D., Loci, D., Houghton, F., Karlsson, L. and Gleeson, P.A., 2001. A large family of endosome-localized proteins related to sorting nexin 1. *Biochemical Journal*, *358*(1), pp.7-16. doi: 10.1042/0264-6021:3580007

Thompson, C.N., Duy, P.T. and Baker, S., 2015. The rising dominance of *Shigella sonnei*: an intercontinental shift in the etiology of bacillary dysentery. *PLoS neglected tropical diseases*, 9(6), p.e0003708. doi: 10.1371/journal.pntd.0003708

Thottacherry, J.J., Sathe, M., Prabhakara, C. and Mayor, S., 2019. Spoilt for choice: Diverse endocytic pathways function at the cell surface. *Annual review of cell and developmental biology*, *35*, p.55. doi: 10.1146/annurev-cellbio-100617-062710

Ullrich, O., Reinsch, S., Urbé, S., Zerial, M. and Parton, R.G., 1996. Rab11 regulates recycling through the pericentriolar recycling endosome. *The Journal of cell biology*, *135*(4), pp.913-924. doi: 10.1083/jcb.135.4.913

Unwin, N., 2005. Refined structure of the nicotinic acetylcholine receptor at 4 Å resolution. *Journal of molecular biology*, *346*(4), pp.967-989. doi: 10.1016/j.jmb.2004.12.031

Valencia-Gallardo, C.M., Carayol, N. and Tran Van Nhieu, G., 2015. Cytoskeletal mechanics during S higella invasion and dissemination in epithelial cells. Cellular microbiology, 17(2), pp.174-182. doi: 10.1111/cmi.12400

Van Weering, J.R., Verkade, P. and Cullen, P.J., 2010, June. SNX–BAR proteins in phosphoinositide-mediated, tubular-based endosomal sorting. In *Seminars in cell & developmental biology* (Vol. 21, No. 4, pp. 371-380). Academic Press. doi: 10.1016/j.semcdb.2009.11.009

Van Weering, J.R., Verkade, P. and Cullen, P.J., 2012. SNX–BAR‐Mediated Endosome Tubulation is Co‐ordinated with Endosome Maturation. *Traffic*, *13*(1), pp.94-107. doi: 10.1111/j.1600-0854.2011.01297.x

Van Weering, J.R., Sessions, R.B., Traer, C.J., Kloer, D.P., Bhatia, V.K., Stamou, D., Carlsson, S.R., Hurley, J.H. and Cullen, P.J., 2012. Molecular basis for SNX‐BAR‐mediated assembly of distinct endosomal sorting tubules. *The EMBO journal*, *31*(23), pp.4466-4480. doi: 10.1038/emboj.2012.283

Vazquez, C.L. and Colombo, M.I., 2010. Coxiella burnetii modulates Beclin 1 and Bcl-2, preventing host cell apoptosis to generate a persistent bacterial infection. *Cell Death & Differentiation*, *17*(3), pp.421-438. doi: 10.1038/cdd.2009.129

Venkatesan, M.M., Goldberg, M.B., Rose, D.J., Grotbeck, E.J., Burland, V. and Blattner, F.R., 2001. Complete DNA sequence and analysis of the large virulence plasmid of *Shigella flexneri*. *Infection and immunity*, *69*(5), pp.3271-3285. doi: 10.1128/IAI.69.5.3271-3285.2001

Voznica, J., Gardella, C., Belotserkovsky, I., Dufour, A., Enninga, J. and Stévenin, V., 2017. Identification of parameters of host cell vulnerability during Salmonella infection by quantitative image analysis and modeling. *Infection and immunity*, *86*(1), pp.e00644-17. doi: 10.1128/IAI.00644-17

Walpole, G.F., Pacheco, J., Chauhan, N., Clark, J., Anderson, K.E., Abbas, Y.M., Brabant-Kirwan, D., Montaño-Rendón, F., Liu, Z., Zhu, H. and Brumell, J.H., 2022. Kinase-independent synthesis of 3-phosphorylated phosphoinositides by a phosphotransferase. *Nature Cell Biology*, 24(5), pp.708-722. doi: 10.1038/s41556-022-00895-y

Wang, Y.J., Wang, J., Sun, H.Q., Martinez, M., Sun, Y.X., Macia, E., Kirchhausen, T., Albanesi, J.P., Roth, M.G. and Yin, H.L., 2003. Phosphatidylinositol 4 phosphate regulates targeting of clathrin adaptor AP-1 complexes to the Golgi. *Cell*, *114*(3), pp.299-310. doi: 10.1016/s0092-8674(03)00603-2

Way, S.S., Borczuk, A.C., Dominitz, R. and Goldberg, M.B., 1998. An essential role for gamma interferon in innate resistance to *Shigella flexneri* infection. Infection and immunity, 66(4), pp.1342-1348. doi: 10.1128/IAI.66.4.1342-1348.1998

Weber, M.M. and Faris, R., 2018. Subversion of the endocytic and secretory pathways by bacterial effector proteins. *Frontiers in cell and developmental biology*, *6*, p.1. doi: 10.3389/fcell.2018.00001

Weiner, A., Mellouk, N., Lopez-Montero, N., Chang, Y.Y., Souque, C., Schmitt, C. and Enninga, J., 2016. Macropinosomes are key players in early *Shigella* invasion and vacuolar escape in epithelial cells. *PLoS pathogens*, *12*(5), p.e1005602. doi: https://doi.org/10.1371/journal.ppat.1005602

Weiss, S.M., Ladwein, M., Schmidt, D., Ehinger, J., Lommel, S., Städing, K., Beutling, U., Disanza, A., Frank, R., Jänsch, L. and Scita, G., 2009. IRSp53 links the enterohemorrhagic E. coli effectors Tir and EspFU for actin pedestal formation. *Cell host & microbe*, *5*(3), pp.244-258. doi: 10.1016/j.chom.2009.02.003

Welz, T., Wellbourne-Wood, J. and Kerkhoff, E., 2014. Orchestration of cell surface proteins by Rab11. *Trends in cell biology*, *24*(7), pp.407-415. doi: 10.1016/j.tcb.2014.02.004

Winchell, C.G., Graham, J.G., Kurten, R.C. and Voth, D.E., 2014. Coxiella burnetii type IV secretion-dependent recruitment of macrophage autophagosomes. *Infection and immunity*, *82*(6), pp.2229-2238. doi: 10.1128/IAI.01236-13

Wu, S., Mehta, S.Q., Pichaud, F., Bellen, H.J. and Quiocho, F.A., 2005. Sec15 interacts with Rab11 via a novel domain and affects Rab11 localization in vivo. *Nature structural & molecular biology*, *12*(10), pp.879-885. doi: 10.1038/nsmb987

Yao, J., Yang, F., Sun, X., Wang, S., Gan, N., Liu, Q., Liu, D., Zhang, X., Niu, D., Wei, Y. and Ma, C., 2018. Mechanism of inhibition of retromer transport by the bacterial effector RidL. *Proceedings of the National Academy of Sciences*, *115*(7), pp.E1446-E1454. doi: 10.1073/pnas.1717383115

Yi, C.R. and Goldberg, M.B., 2009. Putting enterohemorrhagic *E. coli* on a pedestal. *Cell Host & Microbe*, *5*(3), pp.215-217. doi: 10.1016/j.chom.2009.03.002

Yong, X., Mao, L., Shen, X., Zhang, Z., Billadeau, D.D. and Jia, D., 2021. Targeting endosomal recycling pathways by bacterial and viral pathogens. *Frontiers in Cell and Developmental Biology*, *9*, p.648024. doi: 10.3389/fcell.2021.648024

Zhang, Q., Calafat, J., Janssen, H. and Greenberg, S., 1999. ARF6 is required for growth factor-and rac-mediated membrane ruffling in macrophages at a stage distal to rac membrane targeting. *Molecular and cellular biology*, *19*(12), pp.8158-8168. doi: 10.1128/MCB.19.12.8158

Zhang, X.M., Ellis, S., Sriratana, A., Mitchell, C.A. and Rowe, T., 2004. Sec15 is an effector for the Rab11 GTPase in mammalian cells. *Journal of Biological Chemistry*, *279*(41), pp.43027-43034. doi: 10.1074/jbc.M402264200

Zhao, H., Pykäläinen, A. and Lappalainen, P., 2011. I-BAR domain proteins: linking actin and plasma membrane dynamics. *Current opinion in cell biology*, *23*(1), pp.14-21. doi: 10.1016/j.ceb.2010.10.005

Zhen, Y. and Stenmark, H., 2015. Cellular functions of Rab GTPases at a glance. *Journal of cell science*, *128*(17), pp.3171-3176. doi: 10.1242/jcs.166074

Zumsteg, A.B., Goosmann, C., Brinkmann, V., Morona, R. and Zychlinsky, A., 2014. IcsA is a *Shigella flexneri* adhesin regulated by the type III secretion system and required for pathogenesis. *Cell host & microbe*, *15*(4), pp.435-445. doi: 10.1016/j.chom.2014.03.001

Zychlinsky, A., Prevost, M.C. and Sansonetti, P.J., 1992. *Shigella flexneri* induces apoptosis in infected macrophages. Nature, 358(6382), pp.167-169. doi: 10.1038/358167a0

Appendix

Supplementary Manuscript: Pneumococcus triggers NFkB degradation in COMMD2 aggresome-like bodies

https://www.biorxiv.org/content/10.1101/2022.04.08.487599v1.full

doi: https://doi.org/10.1101/2022.04.08.487599

Pneumococcus triggers NFkB degradation in COMMD2 aggresome-like bodies

Michael G. Connor[1*], Lisa Sanchez[2], Christine Chevalier[1], Filipe Carvalho[3], Matthew G. Eldridge[1], Thibault Chaze[4], Mariette Matondo[4], Caroline M. Weight[5], Robert S. Heyderman[5], Jost Enninga[2], Melanie A. Hamon[1*].

Affliations:

1. Chromatin and Infection, Institut Pasteur, Paris, France.

2. Dynamics of Host–Pathogen, Interactions Unit, Institut Pasteur, & UMR CNRS, Paris, France.

3. Institut MICALIS (UMR 1319) INRAE, AgroParisTech, Université Paris-Saclay

4. Institut Pasteur, Université de Paris Cité, CNRS UAR2024, Proteomics Platform, Mass Spectrometry. for Biology Unit, 75015 Paris, France.

5. Division of Infection and Immunity, University College London, London, UK.

*Correspondence:

Michael G. Connor (mconnor@pasteur.fr) & Melanie A. Hamon (melanie.hamon@pasteur.fr)

Abstract

NF-kB driven cellular immunity is essential for both pro- and anti-inflammatory responses to microbes, which makes it one of the most frequently targeted pathways by bacteria during pathogenesis. How NF-kB tunes the epithelial response to *Streptococcus pneumoniae* across the spectrum of commensal to pathogenic host phenotypic outcomes is not fully understood. In this study, we compare a commensal-like 6B ST90 strain to an invasive TIGR4 isolate and demonstrate that TIGR4 both blunts and antagonizes NF-kB activation. We identified, through comparative mass spectrometry of the p65 interactome, that the 6B ST90 isolate drives a non-canonical NF-kB RelB cascade, whereas TIGR4 induces p65 degradation though aggrephagy. Mechanistically, we show that during TIGR4 challenge a novel interaction of COMMD2 with p65 and p62 is established to mediate degradation of p65. With these results, we establish a role for COMMD2 in negative NF-kB regulation, and present a paradigm for diverging NF-kB responses to pneumococcus. Thus, our studies reveal for the first time a new bacterial pathogenesis mechanism to repress host inflammatory response though COMMD2 mediated turnover of p65.

Introduction

The eukaryotic NF-kappaB family of transcriptional regulators are well documented for their potent ability to drive both pro- and anti-inflammatory cellular immune responses during microbe-host interaction [1-3]. As such, it is also one of the most frequently targeted host pathways during pathogenic infection. Of the three main documented NF-kB activation pathways - canonical, non-canonical and atypical- the canonical cascade is the most frequently documented as triggered and targeted for exploitation by bacteria [4-7].

The canonical pathway consists of NF-kB subunit heterodimers of p65/p50 or homodimers of p65/p65 bound to an inhibitory protein, such as IkBa. NF-kB subunits are normally sequestered in the cytoplasm in an inactive state [8]. Upon sensing of inflammatory molecules, such as cytokines (IL-1β or TNFα), pathogen-associated molecular patterns (PAMPs; i.e. lipopolysaccharide), and danger-associated molecular patterns (DAMPs; i.e. IL-1α or nuclear protein HMGB1) NF-kB subunits are rapidly activated by phosphorylation on serine residues (S536 and S276). Simultaneously, NF-kB dimers are released from their inhibitory IkB proteins and translocated to the nucleus of the cell for additional modification. Ultimately, this process leads to the binding of activated dimers to cognate NF-kB DNA motifs, thereby inducing NF-kB dependent gene transcription. NF-kB activation is tightly controlled for precise and rapid induction, but also for prompt repression. NF-kB dimers can be repressed through extraction, sequestration, and degradation from within the nucleus, while in parallel blocking cytoplasmic activation and promoting transcription of negative regulators [4,5,7,9-13]. However, in contrast to the myriad of studies on activators only a few negative regulators of NF-kB and their pathways have been documented.

COMMD (copper metabolism gene MURR1 domain)[14] proteins are among the select few negative regulators of NF-kB [12,14-19]. There are ten members of the COMMD family, all of which, interact with NF-kB to regulate signaling. The best-studied architype member, COMMD1, upon stimulation by TNF will lead to extraction of p65 from chromatin, followed by ubiquitination and proteasomal degradation. This process, functions independently of NF-kB nuclear translocation and IkBa, but through association with Cullin proteins, is able to terminate NF-kB signaling [12,14,16-22]. For the other COMMD proteins, however, neither their functional activity, their mechanism of NF-kB repression, or their interacting partners, outside of cullins, are known.

Unsurprisingly many bacterial species actively target the NF-kB pathway to repress the innate immune defenses of the host and support their survival. To date, all bacterial processes either coopt NF-kB repressors or directly target NF-kB pathway proteins using virulence factors (general review [3,23]). We and others have shown the obligate human pathobiont, *Streptococcus pneumoniae* (the pneumococcus), fine-tunes NF-kB signaling to support its interaction with the host, across the spectrum of commensal to pathogenic outcomes [24-30]. Surprisingly, we showed that a pathogenic *S. pneumoniae* strain showed very little NF-kB signaling

compared to a colonizing, asymptomatic strain. This observation raised the possibility that pneumococcus could subvert NF-kB signaling, which has not yet been documented.

Here, we demonstrate that a pathogenic TIGR4 pneumococcal strain [24], in contrast to a commensal-like 6B ST90 isolate [24], represses phosphorylation and activation of NF-kB p65. In fact, TIGR4 infection leads to specific degradation of p65 in airway epithelial cells, even upon stimulation with a strong inflammatory agonist, IL-1β. We performed an interactome of p65 and show that each pneumococcal strain interacts with diverging p65 interacting partners, revealing an original aggrephagy mechanism involving COMMD2 and p62. Therefore, we report a novel mechanism of pathogenesis to degrade p65 and repress the host response, specifically induced by TIGR4.

Results

TIGR4 antagonizes NF-kB p65 activation

Previously we showed a commensal-like 6B ST90 pneumococcal strain activated p65 to drive a unique inflammatory signature in comparison to a disease causing TIGR4 strain [24]. We showed that challenge with an invasive TIGR4 strain resulted in decreased transcriptional activation of several inflammatory cytokines [24,31], which suggested that NF-kB p65 activation was being disrupted by TIGR4. To directly measure NF-kB activation, we challenged A549 cells with either TIGR4 or 6B ST90 alone, or in combination with IL-1β, a pro-inflammatory stimulus known to drive p65 activation, by phosphorylation of the key serine residues 536 and 276 (review [10]). Cells were collected 2hr post-challenge for immunoblotting and the total levels of p65 were determined. Interestingly, upon infection with TIGR4, p65 levels significantly decreased compared to uninfected or 6B infected cells (Fig. 1A & B). It is important to note that p65 levels decreased even in the presence of IL-1β, which normally drives p65 activation.

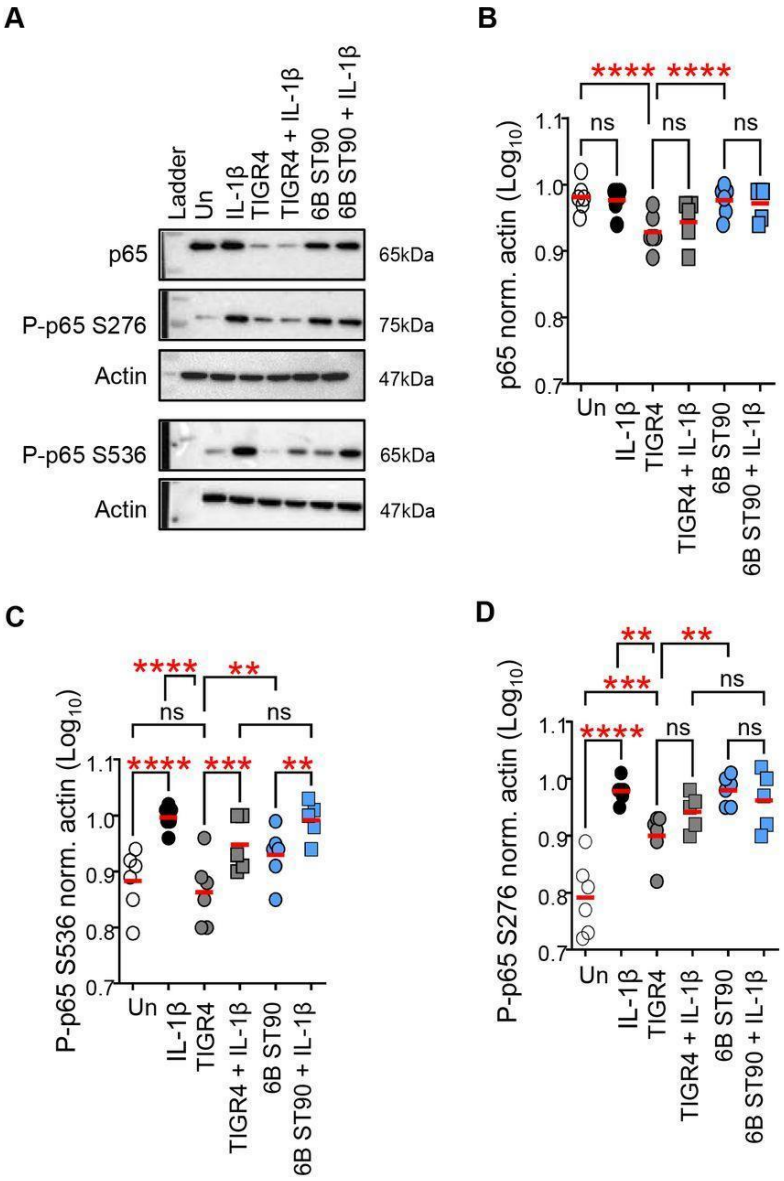

Figure 1: TIGR4 antagonizes p65 activation.

Immunoblot of A549 human airway epithelial cells 2 hrs post-challenge with either IL-1β (10 ng/ml), TIGR4 (MOI 20) or 6B ST90 (MOI 20) (+/- IL-1β; 10 ng/ml). Whole cell lysates probed for p65, phosphorylated p65 at Serine 276, phosphorylated p65 at Serine 536 or Actin. A) Representative image of immunoblot. Actin normalized B) total p65, C) phosphorylated p65 at Serine 276 and D) phosphorylated p65 at Serine 536 (n=11 biological replicates). Dot blot with mean (red line). One-way ANOVA with repeated measures with mixed-effects analysis comparing all means with Tukey's multiple comparison post-hoc test. **P ≤ 0.01, ***P ≤ 0.001, ****P ≤ 0.0001. Full blots provided in Supplementary Information 1.

Regardless of the total level of p65, we also evaluated the activity level of p65 by measuring phosphorylation at S536 and S276, under all conditions. TIGR4 was able to induce phosphorylation at S276, albeit at levels significantly lower than IL-1β alone, or 6B infection, but not at S536 (Fig. 1A, C, D). Importantly, time course monitoring of S536 phoshorylation, reveals that at no time point during infection, do the levels increase above uninfected levels (Sup. Fig. 1A). Taken together, these results show that TIGR4 is a poor activator of p65 in comparison to the 6B ST90 strain. Remarkably, the addition of IL-1β during TIGR4 infection did not restore phosphorylation of S536 or S276 to levels comparable to IL-1β alone, suggesting that infection with this strain of pneumococcus is actively antagonizing NF-kB signaling.

S. pneumoniae is an opportunistic respiratory pathogen. As such upper airway epithelial cells among the first to be encountered, which in turn triggers initial host responses. Therefore, we studied p65 levels and phosphorylation in primary human nasal epithelial cells (Sup. Fig. 1A) and nasopharyngeal Detroit 562 cells (Sup. Fig. 1B). Importantly, both of these cell types display the same blunting of NF-kB activation.

We further evaluated nuclear translocation of p65 by immunofluorescence, as this is a hallmark of p65 activation. Nuclear p65 intensity was quantified and normalized to the nuclear area by segmenting on the DAPI nuclear strain for TIGR4 (+/- IL-1β) against uninfected and IL-1β controls (Fig. 2A & B). In comparison to uninfected conditions, TIGR4 challenge caused slight nuclear recruitment of p65, but remained significantly lower ($pV \leq 0.001$) in comparison to IL-1β alone. Unexpectedly, there was a significant increase in nuclear p65 between TIGR4 + IL-1β and IL-1β alone (Fig. 2A & B), establishing that p65 is translocated in the TIGR4 + IL-1β condition even though phosphorylation levels are aberrant. It should be noted that this increase could be overestimated due to the cellular nucleus shrinking upon infection.

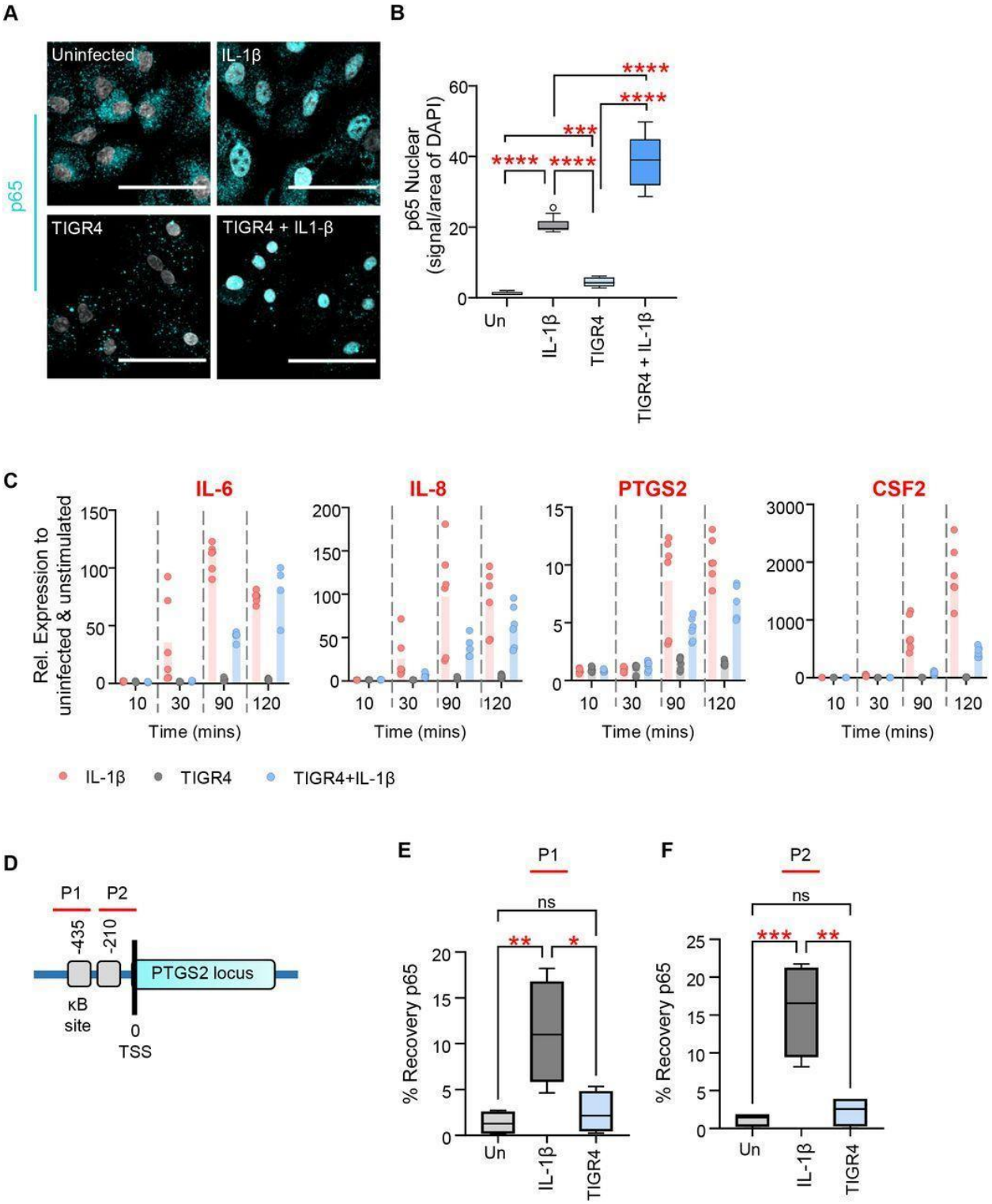

Figure 2: TIGR4 represses p65 dependent transcription.

Immunofluorescence confocal microscopy of paraformaldehyde fixed A549 cells 2 h post-challenge with either IL-1β (10 ng/ml) or TIGR4 (+/- IL-1β 10 ng/ml; MOI 20) stained for p65 (cyan) and nucleus (DAPI; gray). Scale bar = 100μm. B) Quantification of nuclear p65 normalized to the nuclei (n = 3 biological

replicates with total nuclei counts for Uninfected n= 636, IL-1β n= 801, TIGR4 n=633, TIGR4 + IL-1β n=516). Tukey box and whisker plot with defined box boundaries being the upper and lower interquartile range (IQR), 'whiskers' (fences) being ± 1.5 times IQR and the median depicted by the middle solid line. Dots represent outliers. Two-way ANOVA comparing all means with Tukey's multiple comparison post-hoc test. ****P ≤ 0.0001. C) RT-qPCR IL-6, IL-8, PTGS2 & CSF2 transcript profiles of A549 cells over a 2 hr time course challenged with either IL-1β or TIGR4 (+/- IL-1β 10 ng/ml; MOI 20). Graphed as the relative expression of each indicated transcript to matched uninfected/unstimulated control per time point (n = 3 biological replicates; 2 technicals per replicate). Displayed as a dot plot with each data point and a bar representing the mean. Chromatin was obtained from A549 cells either untreated (light gray), IL- 1β treated (10 ng/ml; dark gray) or 2 hrs post-challenge with TIGR4 (light blue; MOI 20). D) Schematic representation of PTGS2 promoter with ChIP-qPCR primer locations (P1 & P2) and NF-κB sites [63]. E & F) ChIP-qPCR represented as % recovery against input of p65 at indicated NF-κB sites. Tukey box and whisker plot with defined box boundaries being the upper and lower interquartile range (IQR), 'whiskers' (fences) being ± 1.5 times IQR and the median depicted by the middle solid line (n=3 biological replicates with 2 technicals per replicate). One-way ANOVA comparing all means with Tukey's multiple comparison post-hoc test. *P ≤ 0.05, **P ≤ 0.01, ***P ≤ 0.001.

We then tested if aberrant activation and low translocation influenced downstream effector functions, namely transcription of p65 dependent genes. Total RNA was collected from A549 cells at 10, 30, 90, and 120 minutes post challenge with TIGR4 (+/- IL-1β) and IL-1β alone. Relative expression was determined for IL-6, IL-8, CFS2 and PTGS2 (COX-2) against uninfected/untreated controls at each time point. Surprisingly, TIGR4 infection alone did not lead to activation of any of the genes tested up to 2h post challenge, in comparison to IL-1β alone (Fig. 2C). Furthermore, under conditions where IL-1β was added during TIGR4 challenge, there was both a delay and a repression of these transcripts in comparison to IL-1β alone. This was corroborated with the diminished p65 phosphorylation at S536 at the protein level at the same time points (Sup. Fig. 1A).

Transcriptional activation by p65 requires its binding to cognate kappa-biding sites at the chromatin level. Therefore, we evaluated levels of chromatin bound p65 at the locus of the NF-kB dependent gene *PTGS2*. Herein, chromatin was collected from A549 cells 2 hrs post-challenge with TIGR4 and the recovery of p65 quantified against uninfected and IL-1β controls by ChIP-qPCR targeting the two kappa-binding sites upstream of the *PTGS2* transcriptional start site (Fig. 2D). At both sites in TIGR4 challenged cells, there was less than 5% recovery of p65. This stands in contrast to the three-fold higher p65 recovery in IL-1β

alone (Fig. 2E & F). Therefore, the lack of p65 driven transcription under TIGR4 challenge is intrinsically due to the absence of p65 at the chromatin.

Altogether, these data show the TIGR4 pneumococcal strain antagonizes p65 activation even in the presence of the pro-inflammatory cytokine, IL-1β. This creates a dysfunctional p65 signaling cascade leading to poor downstream activation of p65 dependent transcription.

A divergent NF-kB p65 interactome supports TIGR4 driven p65 degradation

To begin to understand the NF-kB p65 activation differences between the two pneumococcal isolates we performed mass spectrometry of NF-kB p65 (Fig. 3A). Herein, an A549 GFP-p65 cell line was challenged with either TIGR4 or 6B ST90 and 2 hrs post-challenge GFP-p65 was immunoprecipitated with a matched A549 GFP alone control for mass spectrometry interactome analysis. From the analysis we identified p65 posttranslational modifications, as well as proteins interacting with p65 under the different conditions tested (Sup. Table 1).

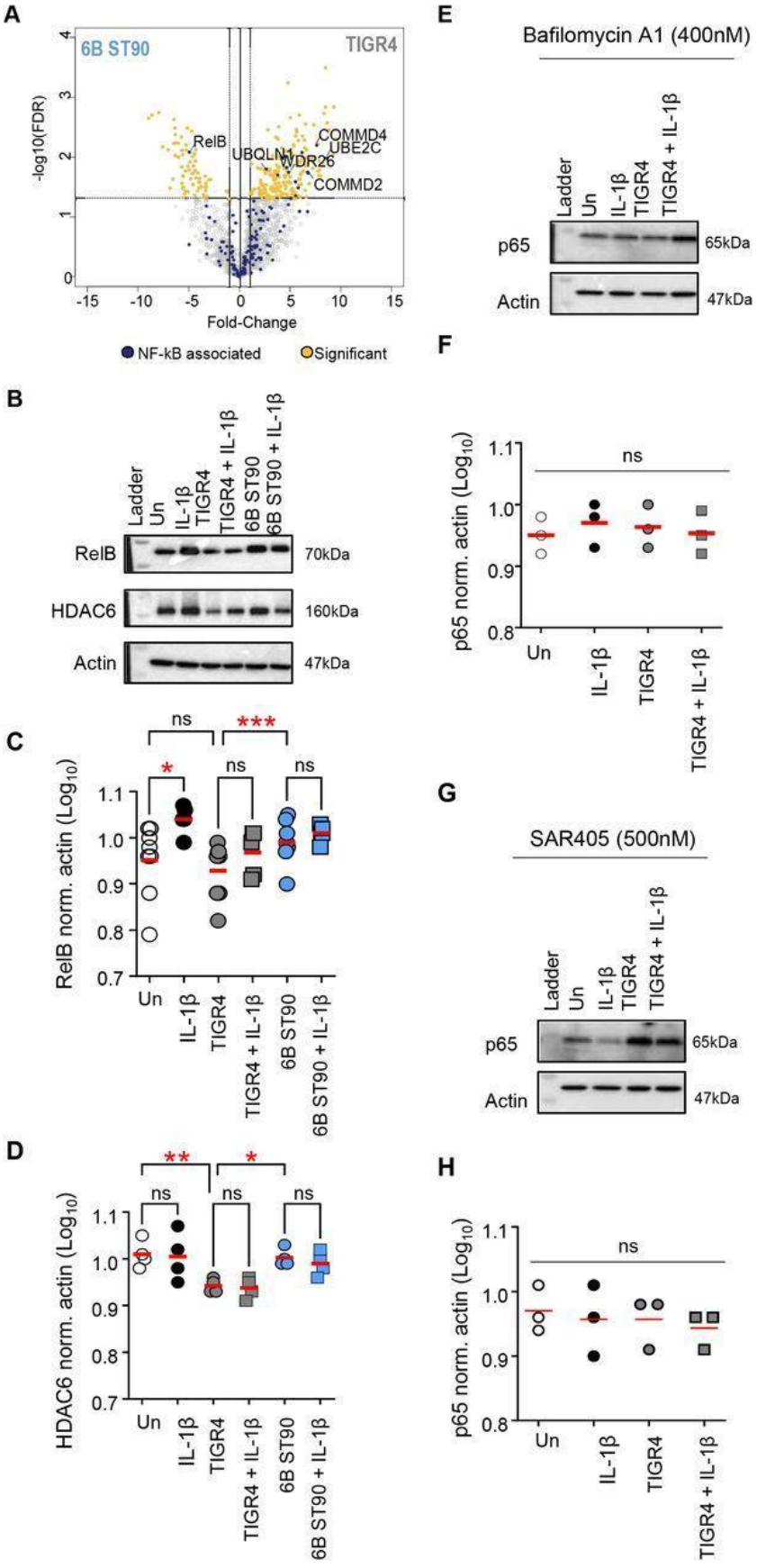
A
6B ST90
TIGR4
-log10(FDR)
RelB
UBQLN1
WDR26
COMMD4
UBE2C
COMMD2
Fold-Change
NF-kB associated
Significant
B
Ladder
Un
IL-1β
TIGR4
TIGR4 + IL-1β
6B ST90
6B ST90 + IL-1β
RelB
70kDa
HDAC6
160kDa
Actin
47kDa
C
RelB norm. actin (Log10)
ns
***
*
ns
ns
Un
IL-1β
TIGR4
TIGR4 + IL-1β
6B ST90
6B ST90 + IL-1β
D
HDAC6 norm. actin (Log10)
**
*
ns
ns
ns
E
Bafilomycin A1 (400nM)
p65
65kDa
Actin
47kDa
F
p65 norm. actin (Log10)
ns
G
SAR405 (500nM)
H

Figure 3: TIGR4 induces a divergent p65 interactome leading to NF-kB p65 turnover by aggrephagy. Mass-spectrometry interactome (n=4 biological replicates per condition) of immunoprecipitated GFP-p65 from a stable A549 GFP-p65 cell line (1×10^7 cells total) 2 hrs post challenge with either 6B ST90 (MOI 20) or TIGR4 (MOI 20). A) Volcano plot of identified interacting partners with known NF-kB p65 partners in blue and general significant targets in yellow. Lines represent FDR and fold-change cutoffs with targets of interested denoted. B) Representative immunoblot of A549 whole cell lysates 2 hrs post-challenge with either IL-1β (10 ng/ml), TIGR4 (MOI 20) or 6B ST90 (MOI 20) (+/- IL-1β; 10 ng/ml) probed for RelB, HDAC6, or Actin. C & D) Quantification of RelB or HDAC6 levels normalized to Actin (n=4 biological replicates). Displayed as a dot blot with mean (red line). One-way ANOVA with repeated measures with mixed-effects analysis comparing all means. *P ≤ 0.05, **P ≤ 0.01, ***P ≤ 0.001. Whole cell lysates from A549 cells 2 hrs post-challenge with either IL-1β (10 ng/ml) or TIGR4 (MOI 20; +/- IL-1β; 10 ng/ml) from E) Bafilomycin A1 (400nM) or G) SAR405 (500nM) pretreated cells (both 3 hrs) and immunoblots probed for p65 or actin (n=3 biological replicates). Quantified levels of total p65 normalized to actin from F) Bafilomycin A1 (400nM) or H) SAR405 (500nM). Dot blot with mean (red line). One-way ANOVA with repeated measures with mixed-effects analysis comparing all means. ns = not significant. Full blots provided in Supplementary Information 2

The interactome data for 6B ST90 showed the sole NF-kB associated target was RelB, a major component of the non-canonical NF-kB pathway. Using whole cell lysates obtained from A549 cells 2 hrs post challenge with either 6B ST90 (+/- IL-1β) or TIGR4 (+/- IL-1β) we confirmed that RelB was significantly (pV ≤ 0.001) elevated during challenge with 6B ST90 (+/- IL-1β) in comparison to both uninfected and TIGR4 (+/- IL-1β; Fig. 3B & C) and associated with p65 by co-immunoprecipitation (Sup. Fig. 2C).

In contrast, the TIGR4 challenged p65 mass spectrometry dataset enriched for different NF-kB associated targets. Gene Ontology and KEGG pathway analysis enriched for protein degradation pathways, including proteins such as HDAC6, a p62, and ubiquitin (Sup. Table 1) [32]. Indeed, p62 is a classical receptor of autophagy, HDAC6 an ubiquitin-binding histone deacetylase known to be important in modulating autophagy, and together have been shown to degrade protein aggregates through a process termed aggrephagy [32-34]. Therefore, our proteomic data suggested that p65 could be targeted for degradation through an aggrephagy pathway under TIRG4 infection conditions. To begin testing this hypothesis we probed whole cell lysates obtained from A549 cells 2 hrs post challenge with either 6B ST90 (+/- IL-1β) or TIGR4 (+/- IL-1β) for HDAC6 levels, as HDAC6 is degraded along with its cargo during aggrephagy (Fig. 3B & D). Indeed, only during TIGR4 challenge conditions did total HDAC6 levels decrease in comparison

to uninfected, IL-1β alone and 6B ST90 groups. We then tested this hypothesis further using known chemical inhibitors to either proteasome or aggrephagy/lysosomal pathways. We treated cells with MG132 (10μM) [35], a general proteasome inhibitor, with Bafilomycin A1 (400nM) [36-38], an inhibitor of the terminal vATPase assembly during aggrephagy/lysosome fusion, or with SAR405 (500nM) [38,39], a PI3K inhibitor of the initiation of aggrephagy pathway, and assessed the levels of p65. Bafilomycin A1 and SAR405 treatments restored levels of p65 during TIGR4 challenge (+/- IL-1β) to comparable levels of uninfected and IL-1β alone (Fig. 3C), while MG132 had no effect in restoring p65 levels during TIGR4 challenge (Sup. Fig. 2A). The same trend for Bafilomycin A1 upon p65 levels 2 hrs post-challenge with TIGR4 was observed in primary human nasal epithelial cells (Sup. Fig. 2B). These data, along with the identification of HDAC6 and p62 in the p65 interactome strongly suggest that TIGR4 is inducing degradation of p65 through an aggrephagy pathway.

We further determined if degradation was restricted to only the p65 subunit or was also impacting the levels p50, which in a heterodimer with p65 is the primary translocated unit to the nucleus [5]. We immunoprecipitated endogenous p65 from A549 cells challenged with 6B ST90 or TIGR4 against uninfected and IL-1β and probed for the p50 subunit. Already in the input, the levels of p50 is lower upon infection with TIGR4 compared to 6B ST90, which is also noticeable from the immunoprecipitation (Sup. Fig. 2C). This observation further supports that TIGR4 challenge is targeting NF-kB p65 complex as a whole.

Overall, these data demonstrate TIGR4, in contrast to 6B ST90, induces diverging NF-kB p65 signaling cascade that results in: 1) differential protein binding, 2) degradation of p65 through aggrephagy.

COMMD2 associates with both p65 and p62 and translocates to the nucleus

The COMMD1 protein has previously been shown to terminate NF-kB signaling through proteasomal degradation [16,17,19,21,40]. Our interactome identified COMMD2 and COMMD4 as among the most highly enriched proteins associating to p65 under TIGR4 infection conditions compared to 6B ST90. COMMD2 and COMMD4 were previously shown to associate with p65 and NFkB1 [14], and other members of this protein family have a repressive role in NFkB signaling [12,16-18,20,22]. Therefore, we hypothesized that COMMD2 and COMMD4, through their association with p65, could be involved in p65 turnover through a similar aggrephagy pathway.

With no robust COMMD2 antibody commercially available for co-immunoprecipitation or immunoblot, we generated an A549 GFP-COMMD2 ectopic expression stable cell line, from which GFP-COMMD2 was immunoprecipitated from lysates 2 hrs post-challenge with either 6B ST90 (+/- IL-1β), TIGR4 (+/- IL-1β) or from our uninfected and IL-1β controls. Samples were probed for p65 or p62 to detect interaction

with COMMD2. Our results show that only under TIGR4 challenge conditions do p65 and p62 interact with COMMD2 (Fig. 4A & B). Furthermore, upon addition of IL1β, p65 interacts with COMMD2 to even higher levels. Therefore, COMMD2 is a new infection specific interacting partner of p65, making a complex of p65-COMMD2-p62.

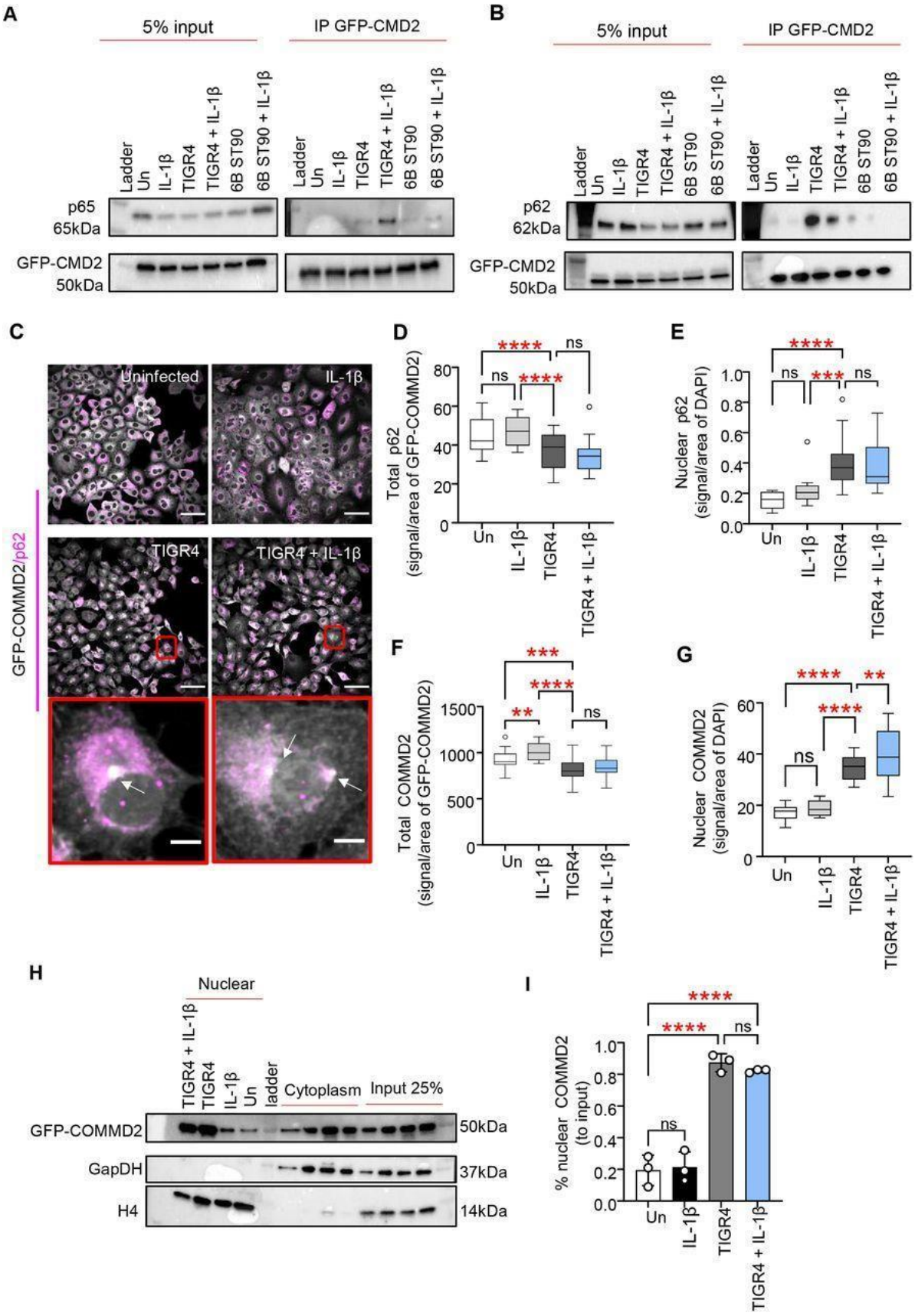
A
5% input
IP GFP-CMD2
Ladder
Un
IL-1β
TIGR4
TIGR4 + IL-1β
6B ST90
6B ST90 + IL-1β
p65
65kDa
GFP-CMD2
50kDa
B
5% input
IP GFP-CMD2
p62
62kDa
GFP-CMD2
50kDa
C
Uninfected
IL-1β
TIGR4
TIGR4 + IL-1β
GFP-COMMD2/p62
D
Total p62
(signal/area of GFP-COMMD2)
E
Nuclear p62
(signal/area of DAPI)
F
Total COMMD2
(signal/area of GFP-COMMD2)
G
Nuclear COMMD2
(signal/area of DAPI)
H
Nuclear
Cytoplasm
Input 25%
GFP-COMMD2
GapDH
H4
50kDa
37kDa
14kDa
I
% nuclear COMMD2
(to input)
ns

Figure 4: TIGR4 drives NF-kB p65 interaction with COMMD2 and p62 (SQSTM1) and nuclear translocation.

Immunoprecipitates using GFP-Trap agarose beads were collected from a stable A549 GFP-COMMD2 cell line 2 hrs post-challenge with either IL-1β (10 ng/ml) or TIGR4 (MOI 20; +/- IL-1β; 10 ng/ml). A) A single representative immunoblot from 3 biological replicates of GFP-COMMD2 immunoprecipitation lysates (input & IP) probed for p65 or GFP.. B) Representative immunoblot from 3 biological replicates of GFP-COMMD2 immunoprecipitation lysates (input & IP) probed for p62 or GFP.. Full blots provided in Supplementary Information 3. C) Immunofluorescence confocal microscopy of stable A549 GFP-COMMD2 cells 2 h post-challenge with either IL-1β (10 ng/ml) or TIGR4 (+/- IL-1β 10 ng/ml; MOI 20) stained for p62 (magenta) against GFP-COMMD2 (gray). Scale bar = 100 µm. Red inset images of single cell highlighting (white arrow) perinuclear punta. Inset scale bar 10 µm. Quantification of total cellular p62 D) normalized to cell area (GFP-COMMD2 signal) and nuclear p62 E) normalized to the area of the nucleus (DAPI signal; n = 3 biological replicates with total cell counts for Uninfected n= 548, IL-1β n= 670, TIGR4 n=356, TIGR4 + IL-1β n=271). Quantification of total cellular COMMD2 F) normalized to cell area (GFP-COMMD2 signal) and nuclear COMMD2 G) normalized to the area of the nucleus (DAP I signal; n = 3 biological replicates with total cell counts for Uninfected n= 864, IL-1β n= 1068, TIGR4 n=596, TIGR4 + IL-1β n=534). Tukey box and whisker plot with defined box boundaries being the upper and lower interquartile range (IQR), 'whiskers' (fences) being ± 1.5 times IQR and the median depicted by the middle solid line. Dots represent outliers. Two-way ANOVA comparing all means with Tukey's multiple comparison post-hoc test. **P ≤ 0.01, ***P ≤ 0.001, ****P ≤ 0.0001. H) Cell fractions from a stable A549 GFP-COMMD2 cell line 2 hrs post-challenge with either IL-1β (10 ng/ml) or TIGR4 (MOI 20; +/- IL-1β; 10 ng/ml). Representative immunoblot probed for GFP (COMMD2) enrichment across cellular compartments. GapDH or histone H4 (H4) used to determine fraction purity. Full blots provided in Supplementary Information 3. I) Percent nuclear COMMD2 levels normalized to input (n=3 biological replicates). Graphed as mean ± STD with dots representing individual biological replicates. One-way ANOVA with repeated measures with mixed-effects analysis comparing all means with Tukey's multiple comparison post-hoc test. ****P ≤ 0.0001.

Although infection with TIGR4 leads to p65 degradation, the small amount left in the cell is nuclear (Fig. 1E). Therefore, to evaluate the cellular localization of the p65-COMMD2-p62 we performed immunofluorescence experiments using the GFP-COMMD2 A549 cell line. Using this cell line, we further determined infection induced effect on p62. The GFP-COMMD2 A549 cell line was challenged with

TIGR4 (+/- IL-1β) and compared to uninfected and IL-1β controls, followed by paraformaldehyde fixation and probing for p62. Total p62 levels in the nucleus were determined per cell, by segmentation on the GFP-COMMD2 signal for the cellular cell boundaries and DAPI for the nucleus (Fig. 4C). There was a significant ($pV \leq 0.001$) decrease in total p62 levels for TIGR4 challenged cells (+/- IL-1β) in comparison to both uninfected and IL-1β alone (Fig. 4D), which is expected upon activation of protein degradation pathways. Interestingly, there is a reciprocal increase in the nuclear levels of p62 (Fig. 4E), showing that during TIGR4 challenge there is movement of p62 between the cytoplasm and nuclear compartments in addition to degradation. Moreover, we noticed COMMD2, an otherwise cytoplasmic protein was translocated in the nucleus of cells challenged with TIGR4 (+/- IL-1β) (Fig. 4C). Similarly to p62, there was a decrease in total COMMD2 levels, indicative of protein turnover, and an increase of COMMD2 in the nucleus (Fig. 4F & G).

We confirmed our microscopy observation by performing cell fractionations. We immunoblotted cell fractions obtained from the GFP-COMMD2 stable cell line 2 hrs post-challenge with TIGR4 (+/- IL-1β) as well as from uninfected and IL-1β controls (Fig. 4H & I). Whereas cells treated with IL-1β alone displayed 20% COMMD2 in the nucleus, similar to untreated/uninfected cells, TIGR4 (+/- IL-1β) challenge conditions had 80% of COMMD2 consistently nuclear (Fig. 4I). The levels of cytoplasmic COMMD2 under TIGR4 (+/- IL-1β) challenge conditions correspondingly decreased, demonstrating a relocalization of COMMD2. Finally, we tested if the commensal-like strain 6B ST90 could also induce COMMD2. Using cellular fractionation and immunoblotting, we show that 6B ST90 was incapable of triggering nuclear localization of COMMD2 (Sup. Fig.3A), which demonstrates relocalization is TIGR4 specific. Strikingly, upon challenge with TIGR4, we observed perinuclear COMMD2 puncta formation. Such puncta of protein aggregates, along with a decrease in p62 levels have previously been described [41-45] and further support our findings that TIGR4 is activating aggrephagy during infection.

To further test if inhibiting terminal stages of aggrephagy would restore p62 levels, we treated cells with Bafilomycin A1 (400nM) and collected whole cell lysates 2 hrs post-challenge with either IL-1β alone or TIGR4 (MOI 20). Samples were immunoblotted for p62 and actin for quantification. The results showed Bafilomycin A1 treatment blocked p62 degradation during TIGR4 challenge restoring it to comparable uninfected levels (Sup. Fig. 3A), further demonstrating that TIGR4 challenge triggers p65 turnover through an infection induced p65-COMMD2-p62 complex.

TIGR4 mediated COMMD2 nuclear translocation is dependent on Ply

Our data show a strain specific degradation of p65 and relocalization of COMMD2, suggesting intrinsic factors to TIGR4 challenge were responsible for these effects. Thus, we tested TIGR4 mutants of

Pneumolysin (Ply) and Pyruvate oxidase (SpxB), two major pneumococcal virulence factors we have previously shown to affect host cell signaling at the nuclear level [46-48]. A549 GFP-COMMD2 stable cell line was challenged for 2 hrs with either wildtype TIGR4, TIGR4Δply or TIGR4ΔspxB and the nuclear levels of COMMD2 quantified against uninfected and IL-1β alone. Nuclear COMMD2 levels were measured by deconvoluted epifluorescence, and quantified by measuring signal intensity normalized by nuclear area by segmenting the nucleus using DAPI stain (Fig. 5A & B). These data show COMMD2 was found primarily within the cytoplasm of uninfected and IL-β treated cells, and translocated to the nucleus upon TIGR4 challenge. Similar levels of nuclear translocation were obtained with the *ΔspxB* mutant, indicating that pneumococcal pyruvate oxidase and peroxide production is not necessary for COMMD2 localization. However, deletion of the PLY toxin completely abrogated nuclear translocation, indicating that this bacterial factor is essential (Fig. 5B). Since the 6B ST90 strain does not lead to nuclear translocation of COMMD2 (Sup. Fig.3A), we concluded that although Pneumolysin is essential, it is not sufficient, since 6B ST90 produces the same amount of this toxin as TIGR4 [24].

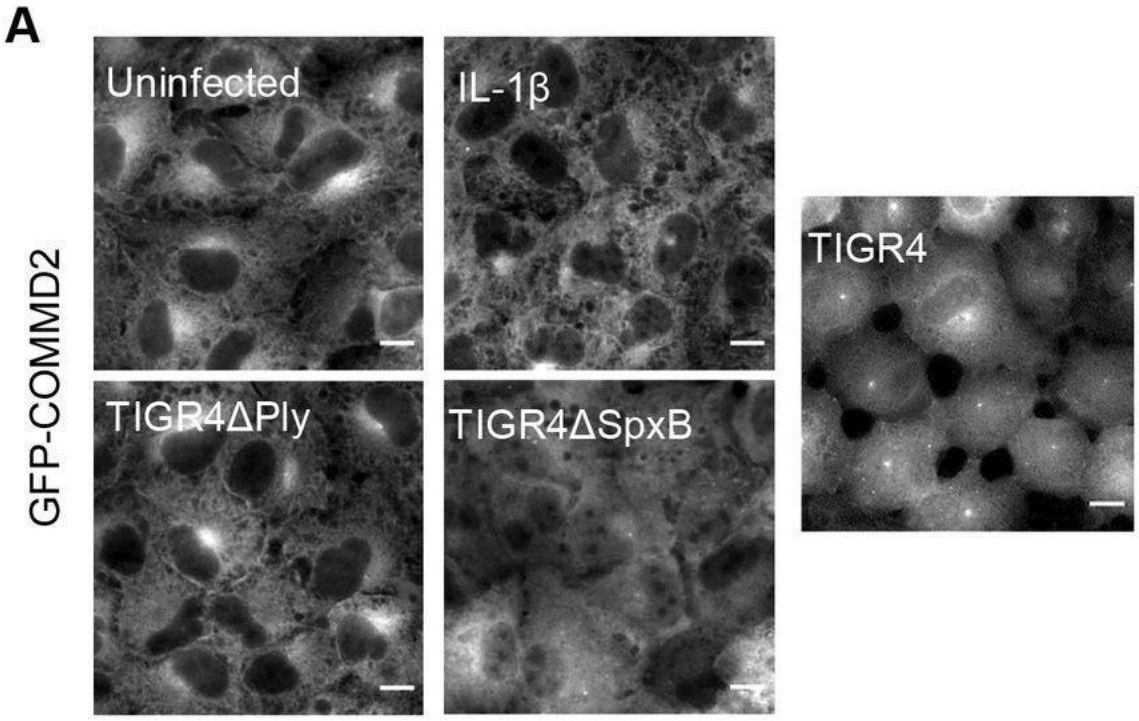
A
GFP-COMMD2
Uninfected
IL-1β
TIGR4
TIGR4ΔPly
TIGR4ΔSpxB

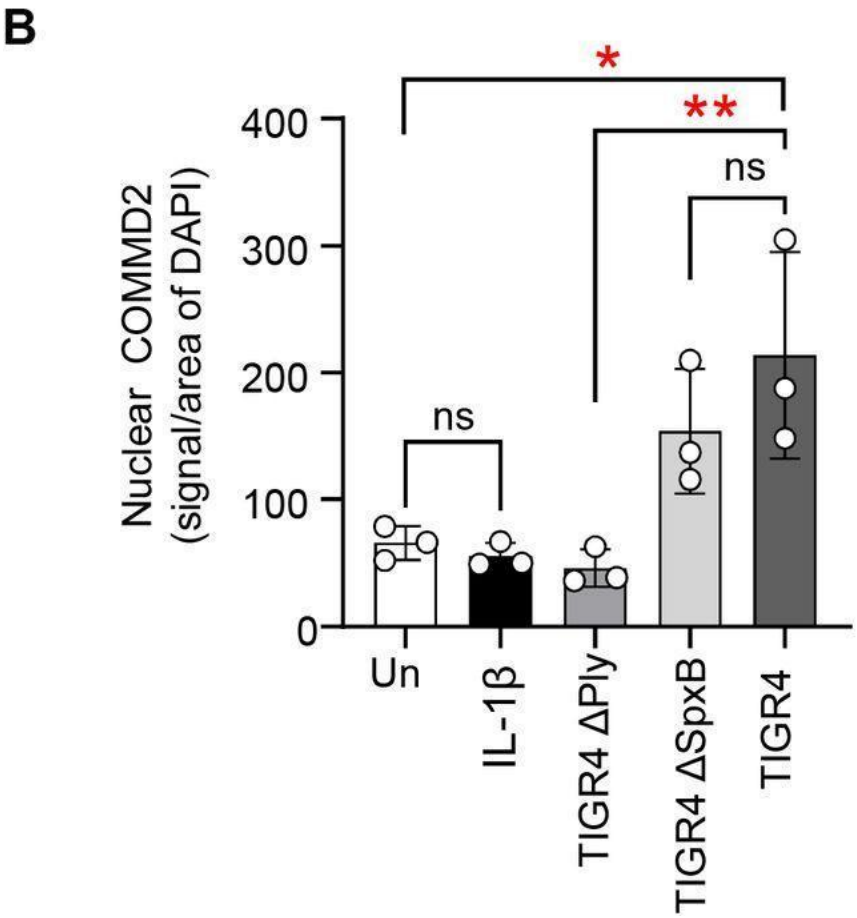
B
Nuclear COMMD2
(signal/area of DAPI)
400
300
200
100
0
*
**
ns
ns
Un
IL-1β
TIGR4 ΔPly
TIGR4 ΔSpxB
TIGR4

Figure 5: TIGR4 challenge triggers COMMD2 nuclear localization in a Ply dependent manner.
A) Immunofluorescence deconvolution epifluorescence microscopy of paraformaldehyde fixed stable A549 GFP-COMMD2 cells 2 h post-challenge with either IL-1β (10 ng/ml), TIGR4 wildtype (MOI 20), TIGR4 *Δply* (MOI 20), or TIGR4 *ΔspxB* (MOI 20) with GFP-COMMD2 (gray). Scale bar = 10µm. B) Quantification of nuclear GFP-COMMD2 normalized to the segmented nuclei using DAPI signal (omitted in representative images for phenotype clarity; n = 3 biological replicates with total nuclei counts for Uninfected n= 6292, IL-1β n= 6579, TIGR4 n=5061, TIGR4 ΔPly n=7607, TIGR4 ΔSpxB n=6566). Graphed as mean ± STD with dots representing individual biological replicates. One-way ANOVA comparing all means with Tukey's multiple comparison post-hoc test. *P ≤ 0.05, **P ≤ 0.01.

COMMD2 exports p65 for lysosomal degradation

COMMD2 has two nuclear export signal domains and no predicted nuclear localization signal domains, suggesting a function for this protein in the cytoplasm, where aggrephagy degradation has been shown to occur [33,34,49]. Thus, we postulated COMMD2 was involved with nuclear export of aberrantly phosphorylated p65 under TIGR4 challenge. This mechanism of action would be similar to the architype family member COMMD1, which binds NF-kB in the nucleus and exports it through CRM1 for degradation [12,22]. Therefore, we tested whether COMMD2 was exported through CRM1 by using the Leptomycin B inhibitor [50]. GFP-COMMD2 cells were treated with Leptomycin B (10 nM), and immunofluorescence was used to image p62 and p65. Strikingly, by blocking nuclear export we observed that COMMD2 was now localized to the nucleus in uninfected and IL-1β treated cells. Similarly, p62 and p65 are relocalized to the nucleus. In fact, COMMD2 and p62 were detected in puncta in the nucleus (Fig. 6A), where p65 was localized (Fig. 6B). Notably, our IL-1β positive pro-inflammatory stimulus control, known to drive nuclear translocation of p65, had a significant (pV ≤ 0.0001) increase in the nuclear level of COMMD2 and p62 in comparison to uninfected cells (Fig. 6C & D). These surprising data suggest that under nuclear export stress, COMMD2 and p62 are naturally recruited to the nucleus at specific puncta through a defined process.

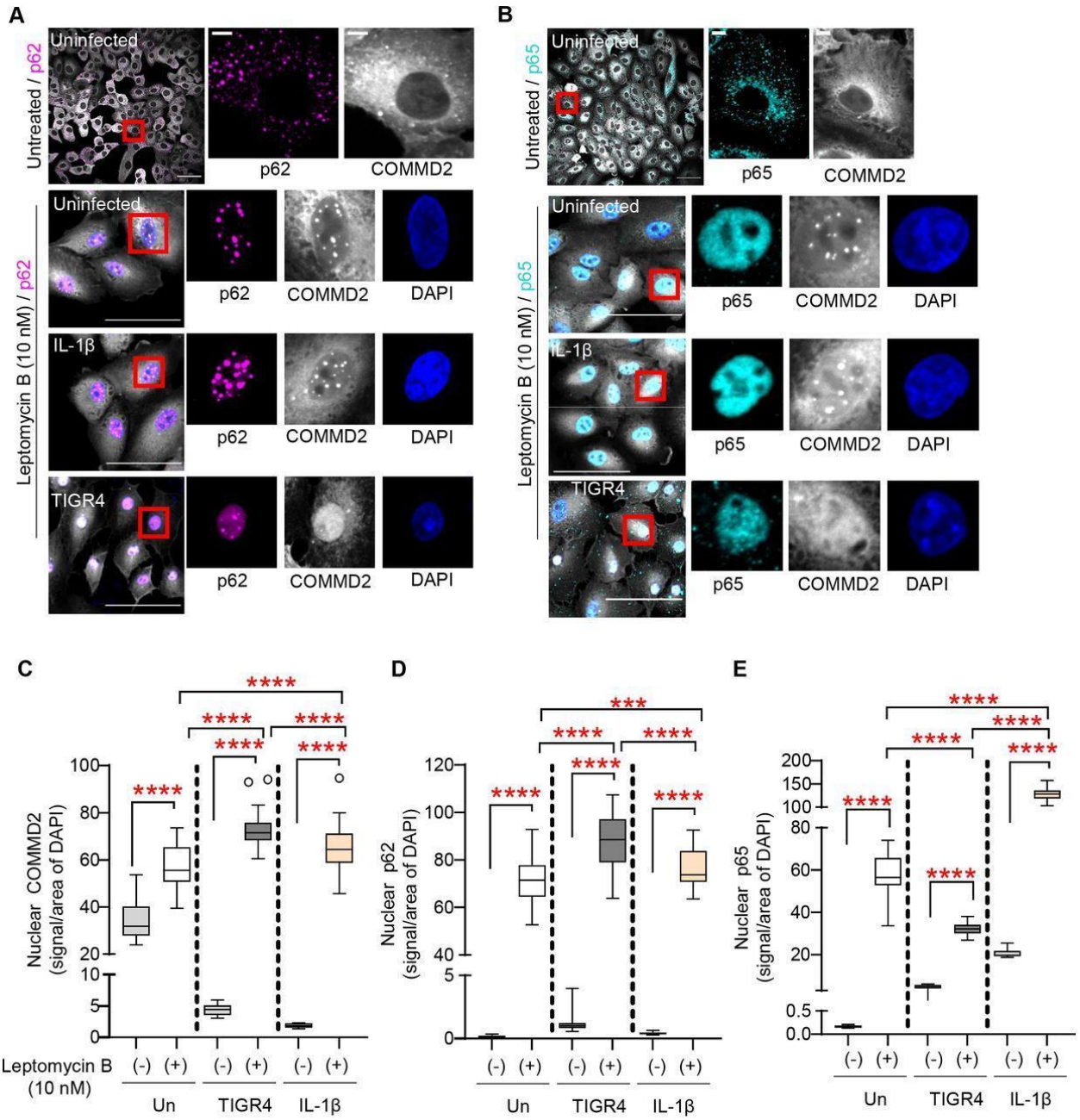

Figure 6: COMMD2-p65-p62 is exported from nucleus through CRM1.

Immunofluorescence confocal microscopy of stable A549 GFP-COMMD2 pretreated for 3 hrs with Leptomycin B (10 nM) prior to 2 hr challenge with either IL-1β (10 ng/ml) or TIGR4 (MOI 20). Paraformaldehyde fixed cells stained for p62 (magenta), or B) p65 (cyan) against GFP-COMMD2 (gray) and nuclei (DAPI; blue). Scale bar = 100 µm or 10 µm for uninfected and untreated single cell inserts. Nuclear levels of C) GFP-COMMD2 or D) p62 normalized to the segmented nuclei using DAPI signal (n = 3 biological replicates with total nuclei counts for Uninfected (-) n=1664, Uninfected n= 742, IL-1β (-) n=1068, IL-1β n= 920, TIGR4 (-) n=585, TIGR4 n=798). E) Nuclear levels of p65 normalized to the

segmented nuclei using DAPI signal (n = 3 biological replicates with total nuclei counts for Uninfected (-) n=489, Uninfected n= 1492, IL-1β (-) n=576 IL-1β n= 1658, TIGR4 (-) n=680, TIGR4 n=1514). Tukey box and whisker plot with defined box boundaries being the upper and lower interquartile range (IQR), 'whiskers' (fences) being ± 1.5 times IQR and the median depicted by the middle solid line. Dots represent outliers. Two-way ANOVA comparing all means with Tukey's multiple comparison post-hoc test. ***P ≤ 0.001, ****P ≤ 0.0001.

Interestingly, upon challenge with TIGR4, Leptomycin B treated cells displayed higher levels of COMMD2 and p62 accumulation in the nucleus than without treatment (Fig. 6A, C & D). Thus, upon inhibiting nuclear export of COMMD2 and p62, these proteins are no longer being degraded upon infection and accumulate in the nucleus. Similarly, Leptomycin B inhibition also increased the nuclear p65 levels in all conditions compared to untreated cells (Fig. 6E), and even restored p65 levels to those of cells stimulated with IL-1β alone. Although COMMD2 puncta are observed upon addition of Leptomycin B, the substantial amount of p65 trapped within the nucleus of these cells rendered definitive scoring of puncta and colocalization difficult and was not done. Furthermore, under conditions of TIGR4+ IL-1β and Leptomycin B inhibition, we observed a significant (pV ≤ 0.0001) increase in p62 puncta compared to TIGR4 alone (Fig. 7A & B). These data therefore show that without Leptomycin B inhibition TIGR4 challenge leads to an active CRM1 dependent export of p65. Altogether, these results imply that p65 is exported from the nucleus via COMMD2 – p62 dependent process upon challenge with TIGR4.

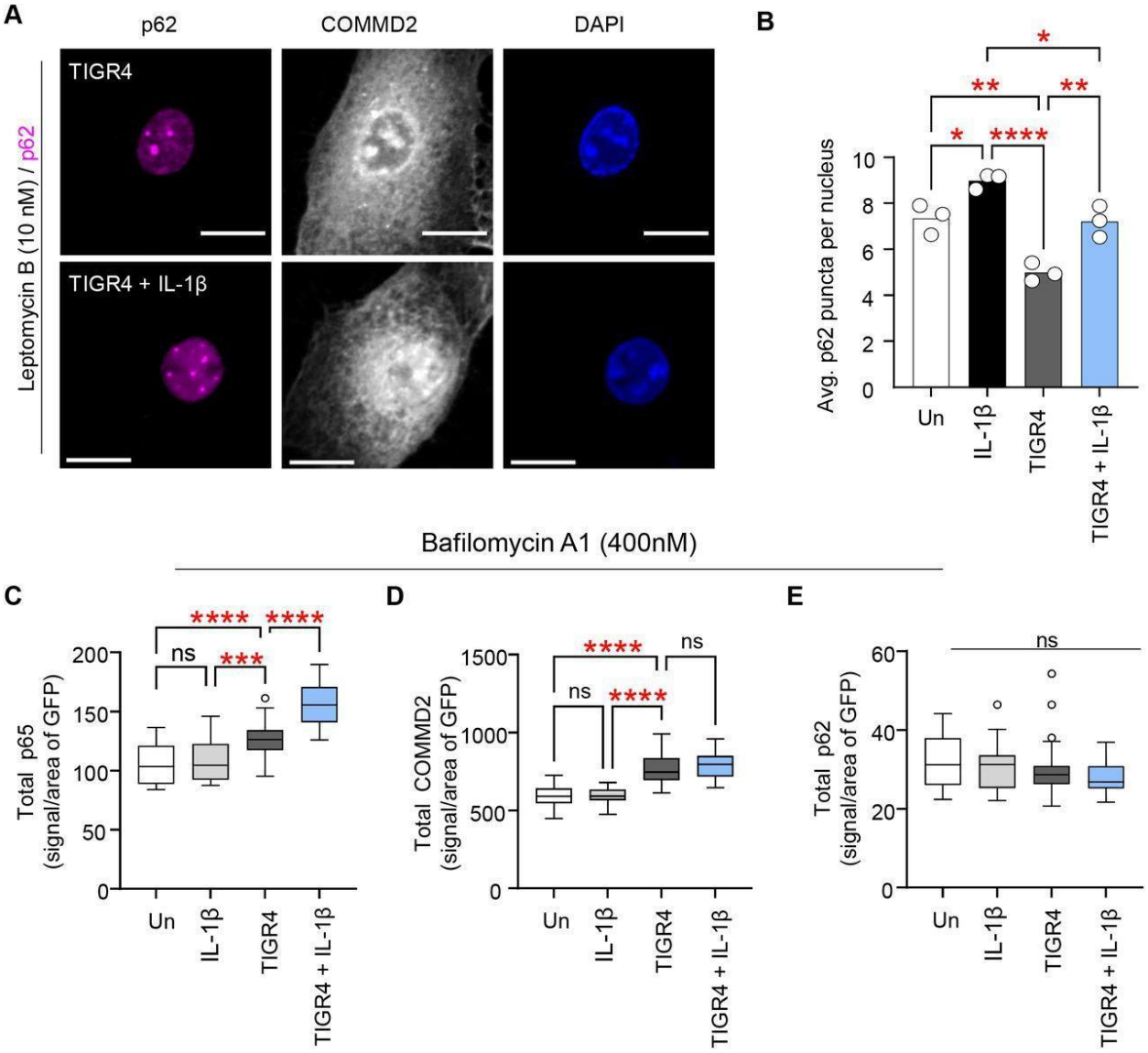

Figure 7: COMMD2-p62 export NF-kB p65 for degradation.

Representative immunofluorescence confocal microscopy of stable A549 GFP-COMMD2 pretreated for 3 hrs with Leptomycin B (10nM) prior to 2 hr challenge TIGR4 (MOI 20; +/- IL-1β; 10 ng/ml). Paraformaldehyde fixed cells stained for (A) p62 (magenta) against GFP-COMMD2 (gray) and nuclei (DAPI; blue). Scale bar = 10µm B) Nuclear p62 puncta quantification (n = 3 biological replicates with total nuclei counts for Uninfected n=1041, IL-1β n=831, TIGR4 n=1164, TIGR4 + IL-1β n=1269). Graphed as mean ± STD with dots representing individual biological replicates. One-way ANOVA comparing all means with Tukey's multiple comparison post-hoc test. *P ≤ 0.05, **P ≤ 0.01, ****P ≤ 0.0001. C) Quantified immunofluorescence confocal microscopy of A549 GFP-COMMD2 cells pretreated with Bafilomycin A1 (400nM; 3 hrs) prior to 2 hr challenge with either IL-1β (10 ng/ml) or TIGR4 (MOI 20;

+/- IL-1β; 10 ng/ml). Paraformaldehyde fixed and stained for C) p65, D) COMMD2 or E) p62. (n = 3 biological replicates with total cell count for Uninfected p62 & COMMD2 n=1648 & p65 n=1496, IL-1β p62 & COMMD2 n=2103 & p65 n=1703, TIGR4 p62 & COMMD2 n=2033 & p65 n=1597, TIGR4 + IL-1β p62 & COMMD2 n=1724 & p65 n=1759). Tukey box and whisker plot with defined box boundaries being the upper and lower interquartile range (IQR), 'whiskers' (fences) being ± 1.5 times IQR and the median depicted by the middle solid line. Dots represent outliers. Two-way ANOVA comparing all means with Tukey's multiple comparison post-hoc test. ns=not significant, ***P ≤ 0.001,****P ≤ 0.0001.

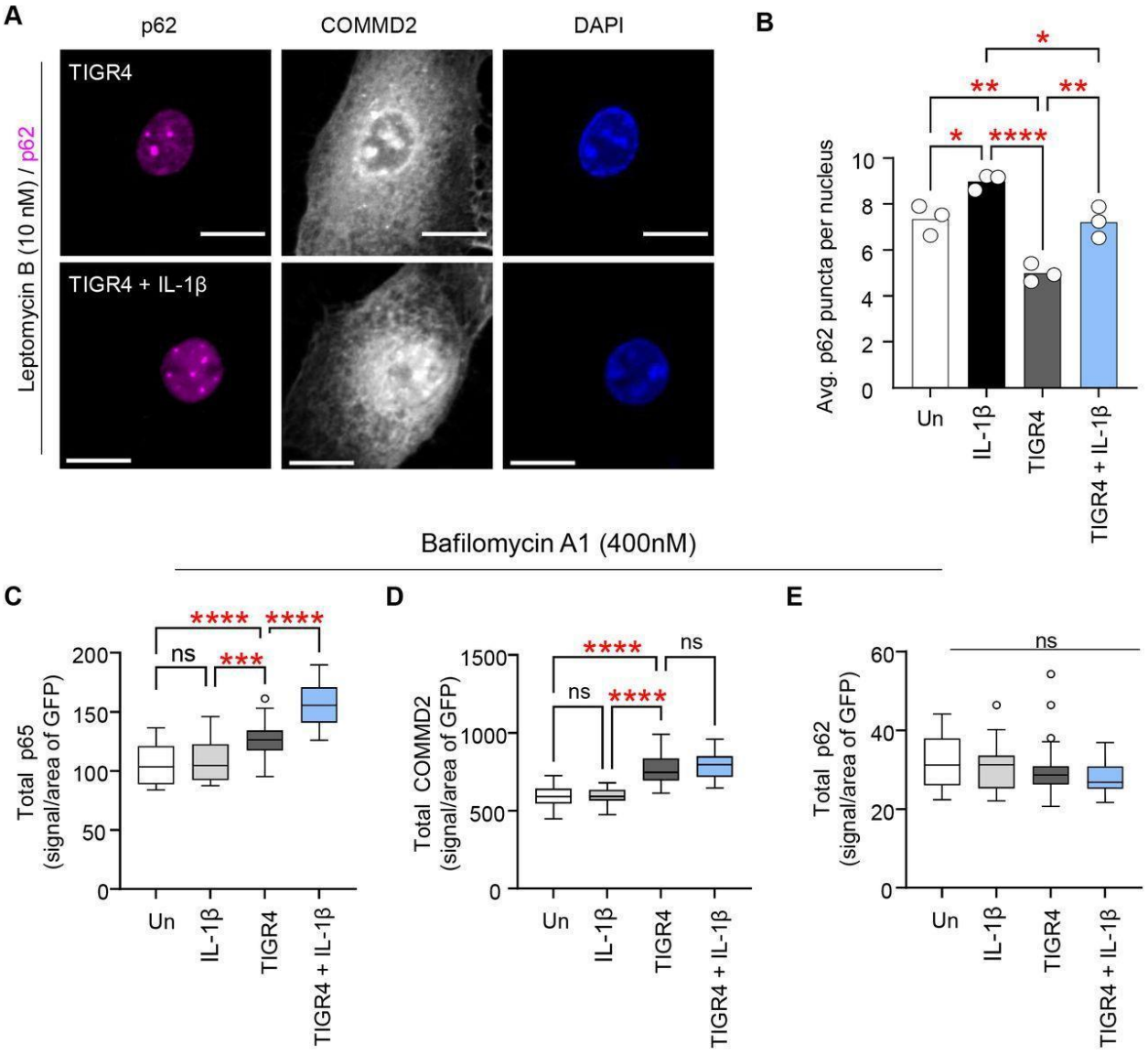

Discussion

Cellular inflammatory response is a critical component of the host defense to bacteria. Yet, the molecular processes that fine-tune NF-kB cascades across the range of colonizing to virulent bacteria is poorly understood. Herein, we show that an invasive *S. pneumoniae* TIGR4 strain, which causes symptomatic disease in murine models [24], blunts p65 activation and inflammatory gene transcription in comparison to a commensal-like asymptomatic 6B ST90 strain, that activated p65 [24]. Through mass spectrometry, interactome and post-translational modification analysis, we show these two pneumococcal isolates have diverging p65 interacting partners and phosphorylation status. We show the 6B ST90 strain upregulates RelB, a hallmark of non-canonical NF-kB signaling, whereas the p65 interactome for the invasive TIGR4 strain enriched for aggrephagy pathway components. Mechanistically, we reveal that p65 is being degraded through a unique TIGR4 induced interaction of COMMD2 with p65 and p62. Altogether, this is the first demonstration of a bacterial pathogenesis mechanism to repress inflammatory gene transcription through targeted degradation of NF-kB p65.

Negative regulation of NF-kB signaling, in contrast to the breadth of knowledge on activatory mechanisms, is poorly documented. This is in part due to the lack of identified targets and mechanisms responsible for attenuating this signaling cascade. Of the known negative regulators, A20 (TNAIP3) and COMMD1 are the better described. A20 is primarily a deubiquitinase whose transcription is NF-kB activation dependent. A20 functions in a negative feedback loop to deubiquintinate NEMO, which results in its stabilization with the IKK complex to restore NF-kB sequestration in the cytoplasm. This ultimately terminates the downstream canonical NF-kB signaling cascade of inflammatory response [5,12,51]. In contrast, COMMD1 transcription is NF-kB independent, and facilitates p65 termination by CRM1 mediated export and translocation of p65 to the proteasome for degradation via complex formation of COMMD1 with Elongins B & C, Cullin2 and SOCS1 (ECS^{SOCS1}) [14,16,17,19,21,22]. In parallel, COMMD1 contributes to repression of p65 driven gene transcription by occupying the formerly p65 bound kappa-binding site at specific gene promoters [20]. It was put forth that the diversity of potential COMMD, NF-kB and cullin assemblies and the array of physiological stimuli activating such complex formations positioned this family of proteins as potent selective negative regulators of NF-kB signaling. Our work is the first to show a role for COMMD2 in p65 turnover through p62 and aggrephagy. This new negative feedback mechanism on p65 may represent, even in a cellular state without bacterial infection, a precise mechanism to terminate or shift a given p65 dependent transcription repertoire. Additionally, by lowering the amount of p65 protein present through degradation, a lower threshold of inhibitory IKK proteins would be needed to quench this cascade within the cell. This could rapidly shift the balance in favor of IKK proteins sequestering p65, and perhaps even favor a switch in NF-kB heterodimers, leading to activation of a different transcriptional repertoire.

In essence, such inhibition would be quite potent, as inflammatory transcription, inflammatory signal sensing, and negative inflammatory feedback are all blocked simultaneously. Such a mechanism would greatly favor pathogenic infection and host cell exploitation, as we observe upon TIGR4 challenge.

To date the molecular mechanism induced by TIGR4 challenge is the only stimulus to trigger COMMD2-p62-p65 complex formation. On the other end of the virulence spectrum, the commensal like 6B ST90 strain lead to the formation of a p65-RelB complex. Therefore, such interactome studies, in combination with pro-inflammatory stimulus, will reveal new partners that govern p65 regulation. In addition, the vast array of post-translational modifications on p65 and other NF-kB subunits across differential stimulations has given rise to the "NF-κB barcode hypothesis", which suggests that distinct patterns are linked to how inflammatory gene transcription occurs [52,53]. We show here that bacterial stimuli are ideal tools to dissect the complexity of this signaling cascade and opens up the field of research in NF-kB signal termination.

Supporting this is our exploratory mass spectrometry of p65 phosphorylation, which identified serine 45 (S45) as the only enriched phosphorylated mark during TIGR4 challenge. This mark has previously been shown to negatively regulate p65, although the mechanism is unknown [54]. Lanucara et al., showed that a phosphomimetic mutant of S45 prevented IL-6 transcription and p65 binding to the promoter under TNFα stimulation [54]. It remains to be evaluated if this modification is involved in COMMD2-p62 degradation of p65 and therefore could alter the host response to pneumococcus. Interestingly, the commensal-like 6B ST90 does not induce phosphorylation of this residue. Instead, this strain leads to phosphorylation on S203 and activation of the chromatin modifier KDM6B to drive containment in the upper respiratory tract [24]. Whether differential phosphorylation of p65 is the determining factor in the ultimate host response to different strains of pneumococcus remains to be determined. In this context it is tempting to speculate that posttranslational modifications of p65 could represent markers of either host response to commensal or to invasive bacteria.

Tuning NF-kB dependent immune gene transcription is fundamental for cellular immune processes of airway epithelial cells exposed to pneumococcus [25,55]. The pro-inflammatory cytokines, TNFα and IL-1β, are major cytokines necessary for neutrophil recruitment and are found in bronchoalveolar lavage fluid of animals challenged with pneumococcal isolates [25,55,56]. However, one study showed that when isolated, murine lung epithelial cells exposed to serotypes 19 and 3 failed to induce p65 (RelA) nuclear translocation in comparison to TNFα and IL-1β [25]. Our studies directly address this paradox showing that the invasive TIGR4 pneumococcal isolate is actively engaged in repressing p65 signaling through degradation even in an environment containing pro-inflammatory stimuli. We propose that pneumococcus interaction with the 'primary' contacted host epithelial cell results in repressed NF-kB signaling with simultaneous prevention of negative feedback upon this inflammatory response. However, what has been shown during respiratory infection with other microbes [57,58], is that a balance is needed between pro-inflammatory responses and

negative regulation to ensure minimal tissue damage from the influx of neutrophils into the airway tissues [56]. Airway epithelial cells play a crucial role in both situations by regulating neutrophil recruitment and promoting epithelial repair pathways leading to tissue resilience and resolution of inflammation [55,56,59,60]. With pneumococcus actively antagonizing the ability of airway epithelial cells to both induce and respond to IL-1β we hypothesize an amplifying and runaway inflammatory cascade is created in latter stages of infection where neutrophil influx is detrimental [55,60,61]. This could lead to exacerbated and severe pneumonia with excessive tissue damage allowing pneumococcus to transmigrate through the lungs and into deeper tissues. We put forth that COMMD2, or combinations of COMMD proteins are potent modulators of bacterial driven inflammatory processes, and may represent a novel therapeutic target to avoid runaway inflammation.

In conclusion, our study shows a new regulatory role for COMMD2 in restraining p65 through aggrephagy mediated turnover triggered by bacterial interaction. We reveal this process to be specific to invasive pneumococcal challenge and partially depend on pneumolysin. Further studies charactering both the p65 and COMMD2 interactome under bacterial challenge with isolates representing divergent pneumococcal host interaction may identify new processes exploited at the microbe-host interface to regulate NF-kB signaling and identify novel negative regulators of inflammation.

Materials and methods

Bacteria strains, growth, and enumeration

Serotype 6B ST90 CC156 lineage F (ST90; CNRP# 43494) and TIGR4 were obtained from the Centre National de Référence des Pneumocoques (Emmanuelle Varon; Paris, France) and (Thomas Kohler, Universität Greifswald) respectively. Experimental starters were made from master glycerol stocks struck on 5% Columbia blood agar plates (Biomerieux Ref# 43041) and grown overnight at 37°C with 5% CO_2 prior to outgrowth in Todd-Hewitt (BD) broth supplemented with 50 mM HEPES (Sigma) (TH+H) as previously described [24]. Inocula were prepared from frozen experimental stocks grown for 3 – 4 hrs to midlog phase in TH+H at 37°C with 5% CO_2 in closed falcon tubes. Bacterial cultures were pelleted at 1,500xg for 10 mins at room temperature (RT), washed in DPBS, and concentrated in 1mL DPBS prior to dilution at desired CFU/mL using 0.6 OD_{600}/mL conversion factors in desired cell culture media [24].

Bacterial counts were determined by serial dilution plating on 5% Columbia blood agar plates and grown overnight at 37°C with 5% CO_2.

Cell culture conditions and in vitro challenge

A549 human epithelial cells (ATCC ref# CCL-185) and A549 stable cell lines were maintained in F12K media (Gibco) supplemented with 1x GlutaMax (Gibco) and 10% heat inactivated fetal calf serum (FCS) at 37°C with 5% CO_2. Detroit 562 human nasopharyngeal epithelial cells (ATCC ref# CCL-138) were maintained in DMEM supplemented with 1x sodium pyruvate (Gibco) and 1x GlutaMax (Gibco) 10% heat inactivated FCS. Primary human nasal epithelial cells (HNEpC; PromoCell ref# C-12620) were cultured and maintained in Airway Epithelial Cell Growth Medium (PromoCell ref# C-21060). All cell lines were discarded after passage 15, and HNEpC discarded after passage 4. For challenge studies cells were plated in tissue culture treated plates at 2×10^5 cells (6well; for 72 hrs), 5×10^4 cells (24well; for 48 hrs), or 1×10^4 cells (96well; for 48 hrs) [24]. Bacterial inocula (Multiplicity of infection (MOI) 20) were diluted in cell culture media, added to cells, and bacterial-epithelial cell contact synchronized by centrifugation at 200xg for 10 mins at RT. Plates were moved to 37°C with 5% CO_2 for 2 hrs and processed as desired for experiment termination. For inhibitor studies, cell culture media was aspirated, and replaced with filter sterilized culture media containing either of the inhibitors MG132 10 μM final concentration (Sigma ref# M7449), Bafilomycin A1 400 nM final concentration (Sigma ref# SML1661) or Leptomycin B 10 nM final concentration (Sigma ref# L2913) for 3 hrs prior to bacterial addition. Human IL-1β (Enzo Life Sciences ref# ALX-522-056) was used at 10 ng/mL final concentration in cell culture media.

RNA isolation and RT-qPCR

Total RNA isolated and extracted using TRIzol (Life technologies ref#15596-026) method as per manufacturer's recommendations. Recovered RNA (5 μg) was converted to cDNA with Super Script IV as per manufacturer's instructions, diluted to 20 ng/μL in molecular grade water and 1 μL used for Sybr Green reactions as per manufacturer's instructions on a BioRad CFX384 (BioRad). Relative expression was calculated by ΔΔCt method to *GapDH* [62]. RT-PCR primers listed in Sup. Table 2.

ChIP and ChIP-qPCR

Detailed ChIP buffer components and procedure were completed as previously reported [24]. Briefly, 8×10^6 A549 cells were cross-linked with 1% formaldehyde at room temperature and quenched with 130 mM

glycine. Chromatin was generated from the collected cell pellets by lysis and sonication in chromatin shearing buffer to a size of 200-900bp. ChIP grade antibody to p65 (L8F6) (CST ref #6956) was used at manufacturer's recommended concentrations and bound to DiaMag beads (diagenode ref # C03010021-150) overnight with gentle rotation. Quantified chromatin was diluted to 10 µg per immunoprecipitation and added to antibody bound DiaMag beads overnight with gentle rotation and 8% of input reserved. Beads were washed as previously described [24], and DNA purified using phenol-chloroform extraction followed by isopropanol precipitation. Recovered DNA suspended in molecular grade water was used for Sybr Green reactions (1 µL) on a BioRad CFX384 (BioRad). ChIP-qPCR primers (50-150 bp; 60 °C max melt temperature) were designed to span the NF-κB sites of interest within the promoters of *PTGS2* [63]. % recovery was calculated as 2 raised to the adjusted input Ct minus IP Ct multiplied by 100. ChIP qPCR primers listed in Sup. Table 2.

Plasmids, molecular cloning and stable cell line generation

All plasmids and primers are listed in Sup. Table 2. Routine cloning was carried out by in vivo assembly [64,65]. Briefly, primers were designed with a 15-20 bp overlap to amplify nucleic acid targets using Phusion Plus polymerase (Thermo ref# F630S). Correct sized bands were excised and nucleic acid extracted by "Freeze and squeeze" [66,67]. Herein, 0.7% - 1% agarose gel fragments were frozen for 5 mins on dry ice and centrifuged for 15 mins at >21,000 xg with the supernatant collected – the process was completed two additional times. Collected supernatant containing nucleic acid was then purified using phenol-chloroform extraction followed by isopropanol precipitation and suspension in molecular grade water. Collected nucleic acid was quantified spectrophotometrically using a NanoDrop and mixed at 3:2 (vector : insert) in 10 µl and added to chemically competent E. coli MC1061 or DH5α for transformation. After 1 hr incubation on ice bacteria outgrowth was done for 1 hr in Luria-Bertani (BD) prior to selection on LB agar containing desired antibiotic (Sup. Table 2). All plasmids were isolated with the QIAprep Spin Miniprep Kit (Qiagen ref# 27106) and eluted in molecular grade water (endotoxin free) as per manufacturer's instructions. A549 stable cell lines were generated using the transposon-based sleeping beauty system [68,69]. A549 cells were plated in tissue culture treated plates at 2×10^5 cells (6well) one day prior to transfection with 2 µg plasmid DNA + 150 ng SB100 transposase DNA. After transfection, cells were selected with 1 mg/mL Geneticin (Thermo ref# 10131035) for 7 days, with media exchanged on days 1, 3, 5 & 7. Selected cells were collected with Trypsin 0.25% EDTA (Thermo ref# 25200056) and two-way serial diluted in a 96 well tissue culture plate for monoclonal selection for another 7 – 14 days with media containing 1 mg/mL Geneticin and exchanged every 2 – 3 days. Selected colonies were expanded and FACS sorted to ensure purity, uniform expression, and comparison of intensity for selecting a robust clone for subsequent experiments.

Immunoblots and quantification

Whole cell lysates were obtained by RIPA lysis (10 mM Tris HCL pH 7.5, 150 mM EDTA, 0.1% SDS, 1% Triton X-100 & 1% Deoxycholate) supplemented with inhibitor cocktail (1X PhosSTOP, 10 mM sodium butyrate, 0.2 mM PMSF). Samples combined with 5x with Laemmli buffer [70], sonicated for 5 mins in a ultrasonic water bath, boiled at 98°C (dry bath) for 10 mins and frozen at -20°C. Whole cell lysates were ran on 4 – 20% pre-cast polyacrylamide SDS PAGE gels (BioRad), transferred to PVDF membrane (BioRad TransBlot) and blocked 1 hr in 5% BSA TBST at room temperature. Membranes were probed overnight at 4°C in 5% BSA TBST with primary antibody to p65 (CST ref #6956 or CST ref# 8242), p65 phosphorylation at serine 536 (CST ref# 3033), p65 phosphorylation at serine 276 (abcam ref# ab183559), NFkB p105 / p50 (abcam ref# ab32360), RelB (abcam ref# ab180127) or actin AC-15 monoclonal (Sigma ref# A5441) as per manufacturer's recommendations. Incubated for 1 hr at room temperature with appropriate secondary-HRP conjugated antibodies in 5% Milk TBST and developed with clarity ECL (BioRad) developing reagents with a ChemiDoc Touch (BioRad). Detroit562 immunoblots were developed using Licor Odessey using secondary antibodies at 1:7,500 - Goat anti-rabbit IgG H&L (IRDye 800CW) and goat anti-mouse IgG H&L (IRDye 680RD) from abcam. Band intensity was quantified by Image Lab (BioRad), or using Fiji [71] (Detroit 562 cells) with linear intensity values $\log_{10}$ transformed and normalized to actin prior to any additional ratio metric comparisons.

Cell fractionation

Fractionation was performed as previously described as previously described [24]. Faction lysates were combined with 5x with Laemmli buffer [70], sonicated for 5 mins in a ultrasonic water bath, boiled at 98°C (dry bath) for 10 mins and frozen at -20°C. Samples were ran on either 10% (for GFP-COMMD2) or 12% (for fraction quality controls) polyacrylamide SDS PAGE gels (BioRad), transferred to PVDF membrane (BioRad TransBlot), blocked 1 hr in 5% BSA TBST at room temperature.
Primary antibody in 5% BSA TBST to GFP (abcam ref# ab290), GapDH (abcam ref# ab8245), or histone H4 (abcam ref# ab177840) was completed overnight at 4°C. After 3x 10 min washes in TBST appropriate secondary-HRP conjugated antibodies in 5% Milk TBST were incubated for 1 hr at room temperature and developed with a ChemiDoc Touch (BioRad) as described above.

Immunofluorescence microscopy and Cellprofiler analysis

For microscopy the desired cell line were seeded on acid washed and UV treated coverslips in 24well or 96well plates as described above. Two hours post-challenge media was aspirated, cells washed in DPBS, and fixed with 2.5% PFA for 10 mins at RT. Fixed cells were blocked and permeabilized overnight in 5% BSA 0.5% Tween20 at 4°C. Primary antibody to p65 (CST ref #6956 or CST ref# 8242), COMMD2 (Sigma ref# HPA044190-25UL; only works for immunofluorescence), or p62 (SQSTM1; abcam ref# ab109012) were diluted at 1:1,000 in 5% BSA 0.5% Tween20 and incubated overnight at 4°C. Cells were washed 3x 10 mins at RT in PBS + 0.1% Tween20 prior to 1 hr incubation at 1:1,000 dilution of either Alexa Fluor 594 or Alexa Fluor 647 secondary antibody. Nuclei were stained with 10 ng/mL final concentration of Hoechst 33342 for 15 mins. Coverslips were rinsed in PBS and molecular grade water prior to mounting with Fluoromount-G Mounting Medium (INTERCHIM). Confocal microscopy images were acquired on a Nikon TiE inverted microscope with an integrated Perfect Focus System (TI-ND6-PFS Perfect Focus Unit) and a Yokogawa Confocal Spinning disk Unit (CSU-W1). Nine images per well were acquired using a 20X air objective (NA 0.75) at a step-size of 0.9µm in z-plane. Deconvoluted epifluorescent images were acquired on a Cytation 5 (BioTek) using a 20X air objective (NA 0.75) with a grid of 3 × 3 (9 images en total).

Images were processed for background using Fiji [71], and segmented using Cell Profiler [72-74]. Briefly, the pipeline for image analysis consisted of sequential modules to 'IdentifyPrimaryObjects' based on channel signal for nuclei (DAPI stain), p65 (Alexa594), or p62 (Alexa594). This was followed by 'IdentifySecondaryObjects' for the GFP-COMMD2 signal via propagation of identified nuclei. Objects were related to each other to maintain cohesion between identified nuclei, cell and cellular contents (p65 or p62). For puncta, the additional module, 'EnhanceorSupressFeatures' with 'Speckles', was used. This used a global threshold strategy with Otsu threshold method and a 2% minimum boundary to identify puncta contained within the segmented nuclei.

Immunoprecipitation

Cells were lysed in 250 µL of RIPA lysis (10 mM Tris HCL pH 7.5, 150 mM EDTA, 0.1% SDS, 1% Triton X-100 & 1% Deoxycholate) supplemented with a protease mixture inhibitor (Roche Complete, EDTA free). Lysates were either immunoprecipitated using GFP-trap agarose beads (ChromoTek ref# gta-10) or with slurry protein G beads (Sigma-Aldrich Fast Flow Protein G sepharose). For GFP-p65 and GFP-COMMD2 the samples were immunoprecipitated as per manufacturer's instructions with the elution was recovered in either 5x with Laemmli buffer [70] and boiled at 98°C (dry bath) for 10 mins, or left in Trypsin digest buffer (see LC-MS/MS Mass-spectrometry and analysis). All samples were frozen at -20°C. For endogenous samples the lysates were incubated on a rotating wheel at 4 °C for 20 min before adding 1 mL of dilution

buffer (150 mM NaCl and 50 mM Tris-HCl pH 7.5 supplemented with Protease mixture inhibitor) to reduce the detergent final concentration below 0.1%. The lysates were then centrifuged at 10,000 × g for 10 min, and the insoluble pellet was discarded. For p65 IP the lysates were then incubated with 2 µg of antibody CST ref #6956 or CST ref# 8242) at 4 °C for 2 hrs before adding 20 µL of slurry protein G beads (Sigma-Aldrich Fast Flow Protein G sepharose) for 20 min. The beads were then washed before adding 20 µL of Laemmli buffer supplemented with 2% β-mercaptoethanol and boiled for 5 min.

LC-MS/MS Mass-spectrometry and analysis

For label-free quantitative proteomic analysis of GFP-p65 and GFP-COMMD2 the respected A549 cell lines were plated in 6well tissue culture plates, and challenged with bacteria for 2hrs as described above. One plate (~5×10^7 cells) per condition was harvested using RIPA lysis and immunoperciptated with GFP-trap agarose beads (ChromoTek ref# gta-10) as per manufacturer's instructions. Three or four independent biological replicates were prepared and analyzed for each condition. Prior to on-bead Trypsin digestion, the samples were washed 3x in trypsin digest buffer (20 mM Tris.HCl pH 8.0, 2 mM $CaCl_2$). On bead digestion was performed strictly as described by Chromotek. Briefly, beads were suspended in digestion buffer (Tris 50 mM pH 7.5, urea 2 M, 1 mM DTT and 5 µg.µl of trypsin (Promega)) for 3 min at 30°C. Supernatants were transfer to new vials and beads were washed twice using (Tris 50 mM pH 7.5, urea 2 M and iodoacetamide 5 mM). All washes were pulled and incubated at 32°C for overnight digestion in the dark. Peptides were purified using C18 stage tips protocol [75].

LC-MS/SM analysis of digested peptides was performed on an Orbitrap Q Exactive Plus mass spectrometer (Thermo Fisher Scientific, Bremen) coupled to an EASY-nLC 1200 (Thermo Fisher Scientific). A home-made column was used for peptide separation (C_{18} 30 cm capillary column picotip silica emitter tip (75 µm diameter filled with 1.9 µm Reprosil-Pur Basic C_{18}-HD resin, (Dr. Maisch GmbH, Ammerbuch-Entringen, Germany)). It was equilibrated and peptide were loaded in solvent A (0.1 % FA) at 900 bars. Peptides were separated at 250 $nl.min^{-1}$. Peptides were eluted using a gradient of solvent B (80% ACN, 0.1 % FA) from 3% to 31% in 45 min, 31% to 60% in 17 min, 60% to 90% in 5 min (total length of the chromatographic run was 82 min including high ACN level step and column regeneration). Mass spectra were acquired in data-dependent acquisition mode with the XCalibur 2.2 software (Thermo Fisher Scientific, Bremen) with automatic switching between MS and MS/MS scans using a top 12 method. MS spectra were acquired at a resolution of 70000 (at *m/z* 400) with a target value of 3×10^6 ions. The scan range was limited from 300 to 1700 *m/z*. Peptide fragmentation was performed using higher-energy collision dissociation (HCD) with the energy set at 27 NCE. Intensity threshold for ions selection was set at 1×10^6 ions with charge exclusion

of z = 1 and z > 7. The MS/MS spectra were acquired at a resolution of 17500 (at *m/z* 400). Isolation window was set at 1.6 Th. Dynamic exclusion was employed within 30 s.

Data were searched using MaxQuant (version 1.5.3.8) using the Andromeda search engine[76] against a human database (74368 entries, downloaded from Uniprot the 27th of September 2019), a Streptococcus pneumoniae R6 database (2031 entries, downloaded from Uniprot the 1st of January 2020) and a Streptococcus pneumoniae serotype 4 database (2115 entries, downloaded from Uniprot 1st of January 2020).

The following search parameters were applied: carbamidomethylation of cysteines was set as a fixed modification, oxidation of methionine and protein N-terminal acetylation were set as variable modifications. The mass tolerances in MS and MS/MS were set to 5 ppm and 20 ppm respectively. Maximum peptide charge was set to 7 and 5 amino acids were required as minimum peptide length. At least 2 peptides (including 1 unique peptides) were asked to report a protein identification. A false discovery rate of 1% was set up for both protein and peptide levels. iBAQ value was calculated. The match between runs features was allowed for biological replicate only.

Data analysis for quantitative proteomics

Quantitative analysis was based on pairwise comparison of protein intensities. Values were log-transformed (log2). Reverse hits and potential contaminant were removed from the analysis. Proteins with at least 2 peptides were kept for further statistics after removing shared proteins from the uninfected GFP alone control. Intensity values were normalized by median centering within conditions (normalized function of the R package DAPAR [77]). Remaining proteins without any iBAQ value in one of both conditions have been considered as proteins quantitatively present in a condition and absent in the other. They have therefore been set aside and considered as differentially abundant proteins. Next, missing values were imputed using the impute. MLE function of the R package imp4p (https://rdrr.io/cran/imp4p/man/imp4p-package.html). Statistical testing was conducted using a limma t-test thanks to the R package limma [78]. An adaptive Benjamini-Hochberg procedure was applied on the resulting p-values thanks to the function adjust.p of R package cp4p[79] using the robust method described in ([80]) to estimate the proportion of true null hypotheses among the set of statistical tests. The proteins associated to an adjusted p-value inferior to a FDR level of 1% have been considered as significantly differentially abundant proteins.

Statistical analysis

All experiments, unless otherwise noted, were biologically repeated 3–5 times and the statistical test is reported in the figure legend. Data normality was tested by Shapiro-Wilk test, and appropriate parametric or non-parametric tests performed depending on result. P values calculated using GraphPad Prism software and the exact values are in source data. Microscopy data obtained from analysis of 3 – 5 image fields per biological replicate after being automatically acquired by the microscope software to ensure unbiased sampling with the total number of analyzed cells or nuclei noted in the figure legend.

Data Availability

All data in the present study is available upon request from the corresponding authors.

Code Availability

No custom code or software was used in the manuscript.

Author contributions

Conceived and designed all experiments: MGC and MAH. Performed and analyzed data for all experiments: MGC with specific contributions from LS (confocal microscopy imaging repeats); FC, MGE, & TC (p65 mass spectrometry data, repeats for GFP & endogenous immunoprecipitations validations, analysis…) CMW (Detroit562 immunoblot). MGC and MAH edited and reviewed the manuscript. MAH supervised the research and secured funding. All authors approved the final manuscript.

Conflict of interest statement

The authors declare no conflict of interest.

Sup. Figure 1: TIGR4 actively dampens p65 activation over time. A) Representative graph of actin normalized phosphorylated p65 S536 levels over 2 hrs quantified by immunoblot. B) Immunoblot of whole cell lysates obtained from primary human nasal epithelial cells 2 hrs post-challenge with either IL-1β (10 ng/ml), TIGR4 (MOI 20) or 6B ST90 (MOI 20) (+/- IL-1β; 10 ng/ml). PVDF membrane probed for

phosphorylated p65 Serine 536 or Actin (n=2 biological replicates). C) Immunoblot of whole cell Detroit 562 cell lysates 2 hrs post-challenge with either TIGR4 (MOI 10) or 6B ST90 (MOI 10). Nitrocellulose membrane probed for phosphorylated p65 Serine 536 or GapDH (n=2 biological replicates).

Sup. Figure 2: Proteasomal degradation is not involved in TIGR4 mediated p65 turnover. A) Quantification and representative immunoblot image of MG132 (10μM; 3 hr pretreatment) treated A549 whole cell lysates 2 hrs post-challenge with either IL-1β (10 ng/ml), TIGR4 (MOI 20) or 6B ST90 (MOI 20) (+/- IL-1β; 10 ng/ml) and probed for total p65 or actin (n=11 biological replicates). Dot blot with mean (red line). One-way ANOVA with repeated measures with mixed-effects analysis comparing all means with Tukey's multiple comparison post-hoc test. ns=not significant, ****P $\leq$ 0.0001. B) Representative immunoblot of whole cell lysates collected from primary human nasal epithelial cells treated with Bafilomycin A1 (400nM; 3 hrs) prior to 2 hr challenge with either IL-1β (10 ng/ml) or TIGR4 (MOI 20; +/- IL-1β; 10 ng/ml). PVDF membrane probed for levels of p65 and actin. C) Representative immunoblot of endogenous p65 immunoprecipitation (input & IP) from 1×10^7 A549 cells post 2 hr challenge using protein G sepharose beads. Collected lysates probed for p65, RelB or NFkB1 (p105/p50).

Sup. Figure 3: TIGR4 specifically drives COMMD2 translocation and induces aggrephagy. A) Cell fractions from a stable A549 GFP-COMMD2 cell line 2 hrs post-challenge with either IL-1β (10 ng/ml), TIGR4 (MOI 20) or 6B ST90 (MOI 20). Representative immunoblot of cell fractions and coomassie stained PVDF membranes. Blots probed for GFP (COMMD2) enrichment across cellular compartments. Representative immunoblot of A549 whole cell lysates 2 hrs post-challenge with either IL-1β (10 ng/ml) or TIGR4 (MOI 20) obtained from untreated or pretreated (3 hrs) with Bafilomycin A1 (400nM). PVDF membrane probed for p62 or actin. Table is the quantification of actin normalized p62 levels across conditions.

Acknowledgements

We would like to thank Emmanuelle Varon and Thomas Kohler for their generous gifts of *S. pneumonie* strains. We are appreciative of Pierre-Henri Commere and the Institut Pasteur, Flow Cytometry Platform (Paris, France) for sorting of the COMMD2 stable cell line. Biostatistics and R scripts generated through discussion with Sebastian Baumgarten (Plasmodium RNA Biology; Institut Pasteur) were greatly appreciated. Finally, we like to thank Daniel Hamaoui for his help processing blots during COVID-19 related work personnel restrictions. Michael G. Connor is supported by a Springboard to Independence grant (AirwayStasis) from the French Government's Investissement d'Avenir program, the Laboratoire

d'Excellence ''Integrative Biology of Emerging Infectious Diseases" (ANR-10-LABX-62-IBEID). Work in the laboratory Chromatin and infection unit (headed by Melanie A. Hamon) is supported by the Institut Pasteur, the Fondation pour la Recherche Médicale (FRM-EQU202003010152), the Fondation iXCore-iXLife and the Pasteur-Weizmann research fund. Caroline M. Weight was supported by the Medical Research Council (MR/T016329/1). We would like to thank Robert S. Heyderman (UCL) for in depth discussion on the manuscript and he is supported by the MRC (MR/T016329/1). RSH is a National Institute for Health Research (NIHR) Senior Investigator. The views expressed in this article are those of the authors and not necessarily those of the NIHR, or the Department of Health and Social Care. Jost Enninga and Lisa Sanchez, members of Dynamics of host-pathogen interactions unit (Institut Pasteur), are supported by the European Commission (ERC-CoG-Endosubvert), the ANR-HBPsensing, and are members of the IBEID and Milieu Interieur LabExes.

References

1. Ghosh, S. & Hayden, M. S. New regulators of NF-kappaB in inflammation. Nature reviews. Immunology 8, 837-848, doi:10.1038/nri2423 (2008).
2. Bhatt, D. & Ghosh, S. Regulation of the NF-kappaB-Mediated Transcription of InflammatoryGenes. Frontiers in immunology 5, 71, doi:10.3389/fimmu.2014.00071 (2014).
3. Rahman, M. M. & McFadden, G. Modulation of NF-κB signalling by microbial pathogens. Nature Reviews Microbiology 9, 291-306, doi:10.1038/nrmicro2539 (2011).
4. Brücher, B., Lang, F. & Jamall, I. NF-kB signaling and crosstalk during carcinogenesis. 4open 2,782
   1-35, doi:10.1051/fopen/2019010 (2019).
5. Hoffmann, A., Natoli, G. & Ghosh, G. Transcriptional regulation via the NF-κB signaling module. Oncogene 25, 6706-6716, doi:10.1038/sj.onc.1209933 (2006).
6. Basak, S. & Hoffmann, A. Crosstalk via the NF-kappaB signaling system. Cytokine & growth factor reviews 19, 187-197, doi:10.1016/j.cytogfr.2008.04.005 (2008).
7. Shih, V. F.-S., Tsui, R., Caldwell, A. & Hoffmann, A. A single NFκB system for both canonical and non-canonical signaling. Cell research 21, 86-102, doi:10.1038/cr.2010.161 (2011).
8. Huxford, T. & Ghosh, G. A structural guide to proteins of the NF-kappaB signaling module. Cold Spring Harbor perspectives in biology 1, a000075, doi:10.1101/cshperspect.a000075 (2009).
9. Wong, D. et al. Extensive characterization of NF-κB binding uncovers non-canonical motifs and advances the interpretation of genetic functional traits. Genome biology 12, R70-R70, doi:10.1186/gb-2011-12-7-r70 (2011).

10. Christian, F., Smith, E. L. & Carmody, R. J. The Regulation of NF-κB Subunits by795 Phosphorylation. Cells 5, 12, doi:10.3390/cells5010012 (2016).
11. Oeckinghaus, A. & Ghosh, S. The NF-κB Family of Transcription Factors and Its Regulation. Cold Spring Harbor perspectives in biology 1, a000034, doi:10.1101/cshperspect.a000034 (2009).
12. Bartuzi, P., Hofker, M. H. & van de Sluis, B. Tuning NF-κB activity: A touch of COMMD proteins. Biochimica et Biophysica Acta (BBA) - Molecular Basis of Disease 1832, 2315-2321, doi:https://doi.org/10.1016/j.bbadis.2013.09.014 (2013).
13. Newton, K. & Dixit, V. M. Signaling in innate immunity and inflammation. Cold Spring Harbor perspectives in biology 4, doi:10.1101/cshperspect.a006049 (2012).
14. Burstein, E. et al. COMMD proteins, a novel family of structural and functional homologs of MURR1. The Journal of biological chemistry 280, 22222-22232, doi:10.1074/jbc.M501928200805 (2005).
15. de Bie, P. et al. Characterization of COMMD protein-protein interactions in NF-kappaB signalling. The Biochemical journal 398, 63-71, doi:10.1042/BJ20051664 (2006).
16. Maine, G. N., Mao, X., Komarck, C. M. & Burstein, E. COMMD1 promotes the ubiquitination of NF-kappaB subunits through a cullin-containing ubiquitin ligase. Embo J 26, 436-447, doi:10.1038/sj.emboj.7601489 (2007).
17. Maine, G. N. & Burstein, E. COMMD proteins and the control of the NF kappa B pathway. CellCycle 6, 672-676, doi:10.4161/cc.6.6.3989 (2007).
18. Maine, G. N. & Burstein, E. COMMD proteins: COMMing to the scene. Cellular and molecular life sciences : CMLS 64, 1997-2005, doi:10.1007/s00018-007-7078-y (2007).
19. Riera-Romo, M. COMMD1: A Multifunctional Regulatory Protein. Journal of cellular biochemistry 119, 34-51, doi:10.1002/jcb.26151 (2018).
20. Geng, H., Wittwer, T., Dittrich-Breiholz, O., Kracht, M. & Schmitz, M. L. Phosphorylation of NF-kappaB p65 at Ser468 controls its COMMD1-dependent ubiquitination and target gene-specific proteasomal elimination. EMBO Rep 10, 381-386, doi:10.1038/embor.2009.10 (2009).
21. Thoms, H. C. et al. Nucleolar Targeting of RelA(p65) Is Regulated by COMMD1-Dependent Ubiquitination. Cancer research 70, 139-149, doi:10.1158/0008-5472.Can-09-1397 (2010).
22. Mao, X. et al. COMMD1 (copper metabolism MURR1 domain-containing protein 1) regulates Cullin RING ligases by preventing CAND1 (Cullin-associated Nedd8-dissociated protein 1) binding. The Journal of biological chemistry 286, 32355-32365, doi:10.1074/jbc.M111.278408825 (2011).

23. Johannessen, M., Askarian, F., Sangvik, M. & Sollid, J. E. Bacterial interference with canonical NFκB signalling. Microbiology (Reading, England) 159, 2001-2013, doi:10.1099/mic.0.069369-0(2013).
24. Connor, M. G. et al. The histone demethylase KDM6B fine-tunes the host response to Streptococcus pneumoniae. Nature Microbiology, doi:10.1038/s41564-020-00805-8 (2020).
25. Quinton, L. J. et al. Functions and regulation of NF-kappaB RelA during pneumococcal pneumonia. Journal of immunology (Baltimore, Md. : 1950) 178, 1896-1903, doi:10.4049/jimmunol.178.3.1896 (2007).
26. Ferreira, D. M. et al. Controlled human infection and rechallenge with Streptococcus pneumoniae reveals the protective efficacy of carriage in healthy adults. American journal of respiratory and critical care medicine 187, 855-864, doi:10.1164/rccm.201212-2277OC837(2013).
27. Henriques-Normark, B. & Tuomanen, E. I. The Pneumococcus: Epidemiology, Microbiology, and Pathogenesis. Cold Spring Harbor perspectives in medicine 3, a010215, doi:10.1101/cshperspect.a010215(2013).
28. Jochems, S. P., Weiser, J. N., Malley, R. & Ferreira, D. M. The immunological mechanisms that control pneumococcal carriage. PLoS pathogens 13, e1006665-e1006665, doi:10.1371/journal.ppat.1006665 (2017).
29. Robson, R. L., Reed, N. A. & Horvat, R. T. Differential activation of inflammatory pathways in A549 type II pneumocytes by Streptococcus pneumoniae strains with different adherence properties. BMC infectious diseases 6, 71, doi:10.1186/1471-2334-6-71 (2006).
30. Weight, C. M. et al. Microinvasion by Streptococcus pneumoniae induces epithelial innate immunity during colonisation at the human mucosal surface. Nature communications 10, 3060, doi:10.1038/s41467-019-11005-2 (2019).
31. Dong, W. et al. Streptococcus pneumoniae Infection Promotes Histone H3 Dephosphorylation by Modulating Host PP1 Phosphatase. Cell reports 30, 4016-4026.e4014, doi:https://doi.org/10.1016/j.celrep.2020.02.116 (2020).
32. Kim, S. et al. Stress-induced NEDDylation promotes cytosolic protein aggregation through HDAC6 in a p62-dependent manner. iScience 24, 102146, doi:https://doi.org/10.1016/j.isci.2021.102146 (2021).
33. Lamark, T. & Johansen, T. Aggrephagy: Selective Disposal of Protein Aggregates by Macroautophagy. International Journal of Cell Biology 2012, 736905, doi:10.1155/2012/736905 (2012).
34. Svenning, S. & Johansen, T. Selective autophagy. Essays in biochemistry 55, 79-92, doi:10.1042/bse0550079 (2013).

35. Lee, D. H. & Goldberg, A. L. Proteasome inhibitors: valuable new tools for cell biologists. Trends in cell biology 8, 397-403, doi:10.1016/s0962-8924(98)01346-4 (1998).
36. Mauvezin, C. & Neufeld, T. P. Bafilomycin A1 disrupts autophagic flux by inhibiting both V-864 ATPase-dependent acidification and Ca-P60A/SERCA-dependent autophagosome-lysosome fusion. Autophagy 11, 1437-1438, doi:10.1080/15548627.2015.1066957 (2015).
37. Dröse, S. & Altendorf, K. Bafilomycins and concanamycins as inhibitors of V-ATPases and P-ATPases. J Exp Biol 200, 1-8, doi:10.1242/jeb.200.1.1 (1997).
38. Pasquier, B. Autophagy inhibitors. Cellular and molecular life sciences : CMLS 73, 985-1001, doi:10.1007/s00018-015-2104-y (2016).
39. Pasquier, B. SAR405, a PIK3C3/VPS34 inhibitor that prevents autophagy and synergizes with MTOR inhibition in tumor cells. Autophagy 11, doi:10.1080/15548627.2015.1033601 (2015).
40. Vonk, W. I. M. et al. The Copper Metabolism MURR1 Domain Protein 1 (COMMD1) Modulates the Aggregation of Misfolded Protein Species in a Client-Specific Manner. PloS one 9, e92408, doi:10.1371/journal.pone.0092408 (2014).
41. Johansen, T. & Lamark, T. Selective autophagy mediated by autophagic adapter proteins. Autophagy 7, 279-296 (2011).
42. Johnston, J. A., Ward, C. L. & Kopito, R. R. Aggresomes: a cellular response to misfolded proteins. The Journal of cell biology 143, 1883-1898 (1998).
43. Lobb, I. T. et al. A Role for the Autophagic Receptor, SQSTM1/p62, in Trafficking NF-κB/RelA to Nucleolar Aggresomes. Molecular Cancer Research 19, 274, doi:10.1158/1541-7786.MCR-20-0336 (2021).
44. Ryu, H. W., Won, H. R., Lee, D. H. & Kwon, S. H. HDAC6 regulates sensitivity to cell death in response to stress and post-stress recovery. Cell stress & chaperones 22, 253-261, doi:10.1007/s12192-017-0763-3 (2017).
45. Wong, E. et al. Molecular determinants of selective clearance of protein inclusions by autophagy. Nature communications 3, 1240, doi:10.1038/ncomms2244 (2012).
46. Weiser, J. N., Ferreira, D. M. & Paton, J. C. Streptococcus pneumoniae: transmission, colonization and invasion. Nature reviews. Microbiology 16, 355-367, doi:10.1038/s41579-018-0001-8 (2018).
47. Kadioglu, A., Weiser, J. N., Paton, J. C. & Andrew, P. W. The role of Streptococcus pneumoniae virulence factors in host respiratory colonization and disease. Nature reviews. Microbiology 6, 288-301, doi:10.1038/nrmicro1871 (2008).
48. Bryant, J. C. et al. Pyruvate oxidase of Streptococcus pneumoniae contributes to pneumolysin release. BMC microbiology 16, 271, doi:10.1186/s12866-016-0881-6 (2016).

49. Tan, S. & Wong, E. in Methods in Enzymology Vol. 588 (eds Lorenzo Galluzzi, José Manuel Bravo-San Pedro, & Guido Kroemer) 245-281 (Academic Press, 2017).
50. Kudo, N. et al. Leptomycin B inactivates CRM1/exportin 1 by covalent modification at a cysteine residue in the central conserved region. Proceedings of the National Academy of Sciences of the United States of America 96, 9112-9117, doi:10.1073/pnas.96.16.9112 (1999).
51. Das, T., Chen, Z., Hendriks, R. W. & Kool, M. A20/Tumor Necrosis Factor α-Induced Protein 3 in Immune Cells Controls Development of Autoinflammation and Autoimmunity: Lessons from Mouse Models. Frontiers in immunology 9, doi:10.3389/fimmu.2018.00104 (2018).
52. Moreno, R., Sobotzik, J.-M., Schultz, C. & Schmitz, M. L. Specification of the NF-κB transcriptional response by p65 phosphorylation and TNF-induced nuclear translocation of IKKε. Nucleic acids research 38, 6029-6044, doi:10.1093/nar/gkq439 (2010).
53. Collins, P. E., Mitxitorena, I. & Carmody, R. J. The Ubiquitination of NF-κB Subunits in the Control of Transcription. Cells 5, 23, doi:10.3390/cells5020023 (2016).
54. Lanucara, F. et al. Dynamic phosphorylation of RelA on Ser42 and Ser45 in response to TNFalpha stimulation regulates DNA binding and transcription. Open Biol 6, doi:10.1098/rsob.160055 (2016).
55. Quinton, L. J. & Mizgerd, J. P. Dynamics of lung defense in pneumonia: resistance, resilience, and remodeling. Annual review of physiology 77, 407-430, doi:10.1146/annurev-physiol-021014-071937 (2015).
56. Pechous, R. D. With Friends Like These: The Complex Role of Neutrophils in the Progression of Severe Pneumonia. Frontiers in cellular and infection microbiology 7, 160-160, doi:10.3389/fcimb.2017.00160 (2017).
57. Liu, J. et al. Advanced Role of Neutrophils in Common Respiratory Diseases. Journal of immunology research 2017, 6710278, doi:10.1155/2017/6710278 (2017).
58. Craig, A., Mai, J., Cai, S. & Jeyaseelan, S. Neutrophil Recruitment to the Lungs during Bacterial Pneumonia. Infection and immunity 77, 568-575, doi:10.1128/IAI.00832-08 (2009).
59. Pechous, R. D., Sivaraman, V., Stasulli, N. M. & Goldman, W. E. Pneumonic Plague: The Darker Side of Yersinia pestis. Trends in microbiology, doi:10.1016/j.tim.2015.11.008 (2015).
60. Yamamoto, K. et al. Roles of lung epithelium in neutrophil recruitment during pneumococcal pneumonia. American journal of respiratory cell and molecular biology 50, 253-262, doi:10.1165/rcmb.2013-0114OC (2014).
61. Bou Ghanem, E. N. et al. Extracellular Adenosine Protects against Streptococcus pneumoniae Lung Infection by Regulating Pulmonary Neutrophil Recruitment. PLoS pathogens 11, e1005126, doi:10.1371/journal.ppat.1005126 (2015).

62. Livak, K. J. & Schmittgen, T. D. Analysis of relative gene expression data using real-time quantitative PCR and the 2(-Delta Delta C(T)) Method. Methods (San Diego, Calif.) 25, 402-408, doi:10.1006/meth.2001.1262 (2001).
63. Nguyen, L. K., Cavadas, M. A. S., Kholodenko, B. N., Frank, T. D. & Cheong, A. Species differential regulation of COX2 can be described by an NFκB-dependent logic AND gate. Cellular and molecular life sciences : CMLS 72, 2431-2443, doi:10.1007/s00018-015-1850-1 (2015).
64. Huang, F., Spangler, J. R. & Huang, A. Y. In vivo cloning of up to 16 kb plasmids in E. coli is as simple as PCR. PloS one 12, e0183974, doi:10.1371/journal.pone.0183974 (2017).
65. Watson, J. F. & García-Nafría, J. In vivo DNA assembly using common laboratory bacteria: A re-emerging tool to simplify molecular cloning. The Journal of biological chemistry 294, 15271-15281, doi:10.1074/jbc.REV119.009109 (2019).
66. Thuring, R. W., Sanders, J. P. & Borst, P. A freeze-squeeze method for recovering long DNA from agarose gels. Analytical biochemistry 66, 213-220, doi:10.1016/0003-2697(75)90739-3 (1975).
67. Tautz, D. & Renz, M. An optimized freeze-squeeze method for the recovery of DNA fragments from agarose gels. Analytical biochemistry 132, 14-19, doi:10.1016/0003-2697(83)90419-0 (1983).
68. Jin, Z. et al. The hyperactive Sleeping Beauty transposase SB100X improves the genetic modification of T cells to express a chimeric antigen receptor. Gene therapy 18, 849-856, doi:10.1038/gt.2011.40 (2011).
69. Kowarz, E., Loscher, D. & Marschalek, R. Optimized Sleeping Beauty transposons rapidly generate stable transgenic cell lines. Biotechnology journal 10, 647-653, doi:10.1002/biot.201400821 (2015).
70. Laemmli, U. K. Cleavage of Structural Proteins during the Assembly of the Head of Bacteriophage T4. Nature 227, 680-685, doi:10.1038/227680a0 (1970).
71. Schindelin, J. et al. Fiji: an open-source platform for biological-image analysis. Nature methods 9, 676-682, doi:10.1038/nmeth.2019 (2012).
72. Kamentsky, L. et al. Improved structure, function and compatibility for CellProfiler: modular high-throughput image analysis software. Bioinformatics (Oxford, England) 27, 1179-1180, doi:10.1093/bioinformatics/btr095 (2011).
73. McQuin, C. et al. CellProfiler 3.0: Next-generation image processing for biology. PLoS biology 16, e2005970, doi:10.1371/journal.pbio.2005970 (2018).
74. Stirling, D. R., Carpenter, A. E. & Cimini, B. A. CellProfiler Analyst 3.0: accessible data exploration and machine learning for image analysis. Bioinformatics (Oxford, England) 37, 3992-3994, doi:10.1093/bioinformatics/btab634 (2021).

75. Kulak, N. A., Pichler, G., Paron, I., Nagaraj, N. & Mann, M. Minimal, encapsulated proteomic-sample processing applied to copy-number estimation in eukaryotic cells. Nature methods 11, 319-324, doi:10.1038/nmeth.2834 (2014).
76. Tyanova, S., Temu, T. & Cox, J. The MaxQuant computational platform for mass spectrometry-based shotgun proteomics. Nature protocols 11, 2301-2319, doi:10.1038/nprot.2016.136 (2016).
77. Wieczorek, S. et al. DAPAR & ProStaR: software to perform statistical analyses in quantitative discovery proteomics. Bioinformatics (Oxford, England) 33, 135-136, doi:10.1093/bioinformatics/btw580 (2017).
78. Pounds, S. & Cheng, C. Robust estimation of the false discovery rate. Bioinformatics (Oxford, England) 22, 1979-1987, doi:10.1093/bioinformatics/btl328 (2006).
79. Smyth, G. K. Linear models and empirical bayes methods for assessing differential expression in microarray experiments. Statistical applications in genetics and molecular biology 3, Article3, doi:10.2202/1544-6115.1027 (2004).
80. Giai Gianetto, Q. et al. Calibration plot for proteomics: A graphical tool to visually check the assumptions underlying FDR control in quantitative experiments. Proteomics 16, 29-32, doi:10.1002/pmic.201500189 (2016).